UNIVERSITY OF CALIFORNIA
RIVERSIDE

Understanding Structure–Reactivity Relationships for Aqueous Per- and Polyfluoroalkyl Substances (PFAS) Within the UV/Sulfite System

A Dissertation submitted in partial satisfaction
of the requirements for the degree of

Doctor of Philosophy

in

Chemical and Environmental Engineering

by

Michael James Bentel

December 2020

Dissertation Committee:
Dr. Jinyong Liu, Chairperson
Dr. Haizhou Liu
Dr. Michael R. Hoffmann

The Dissertation of Michael James Bentel is approved:

_____

_____

_____

Committee Chairperson

University of California, Riverside

ACKNOWLEDGEMENTS

I would like to start by thanking my advisor, Prof. Jinyong Liu. His guidance, patience, and encouragement throughout the doctoral study was invaluable and I will forever be grateful. I would also like to thank my committee members, Prof. Michael R. Hoffmann and Prof. Haizhou Liu, for their feedback and support during this thesis study.

The support from my mother, Dorothy Bentel, and father, Matt Bentel, throughout my life is a significant reason for my success and I cannot thank them enough.

My sincerest gratitude goes to all the professors at the University of California Chemistry Department who contributed to helping me successfully earn my Master's degree in inorganic chemistry, including Prof. Gregory Beran, Prof. Matthew P. Conley, Prof. Pingyun Feng, Prof. Boniface P.T. Fokwa, Prof. W. Hill Harmon, Prof. Richard J. Hooley, and Prof. Vincet LaVallo.

I would like to thank my laboratory mates, Changxu Ren, Jinyu Gao, Tianchi Liu, and Zekun Liu for the countless nights in the lab under thoughtful discussion. I would also like to thank the following colleagues for their support throughout my doctoral studies: Dr. Christian Alcaraz, Dr. Michelle Chebeir, Dr. Ninad Kothari, Dr. Holly Mayton, Dr. Abhishek Patri, Dr. Samuel Patton, Dr. S. Drew Story, Mr. Jack Choczynski, Mr. Sergio Lovera, and Ms. Miranda Vinay.

There are a number of undergraduate students who came to be under my tutelage during my studies, and would like to thank them for the opportunity to mentor, including: Taylor Brantner, Robert Chivarilla-Vivar, Jason Cho, Vanessa Coria, Duy Dao, Andrew Delmonico, Maggy Harake, Mai Le, Ruby Ma, Berenice Munoz, Nina Nester, Vivian Ngo, Benjamin Rammelsburg, and Wenxiaoshan Sui.

I would also like to express my sincerest gratitude to Prof. Sharon Walker and Prof. Philip Christopher for this mentorship during my PhD study and guidance towards securing a postdoctoral position.

The text of this dissertation, in part, is a reprint of the material as it appears in *Defluorination of Per- and Polyfluoroalkyl Substances (PFASs) with Hydrated Electrons: Structural Dependence and Implications to PFAS Remediation and Management* (March 2, 2019), *Degradation of Perfluoroalkyl Ether Carboxylic Acids with Hydrated Electrons: Structure-Reactivity Relationships and Environmental Implications* (January 30, 2020), *and Enhanced Degradation of Perfluorocarboxylic Acids (PFCAs) by UV/Sulfite Treatment: Reaction Mechanisms and System Efficiences at pH 12* (April 23, 2020). The coauthor Dr. Jinyong Liu listed in these publications directed and supervised the research which forms the basis for this dissertation.

The work of this thesis was financially supported by NSF Integrative Graduate Education Research Traineeship (IGERT) WaterSENSE fellowship, NSF Graduate Assistance in Areas of National Need (GAANN) fellowship, American Water Works American Water scholarship, and UCR Graduate Research Mentorship Fellowship award.

DEDICATION

This dissertation is dedicated to my parents, who have given me their unconditional love and support throughout my life in order to help me achieve my goals.

ABSTRACT OF THE DISSERTATION

Understanding Structure–Reactivity Relationships for Aqueous Per- and Polyfluoroalkyl Substances (PFAS) within the UV/Sulfite System

by

Michael James Bentel

Doctor of Philosophy, Graduate Program in Chemical and Environmental Engineering
University of California, Riverside, December 2020
Dr. Jinyong Liu, Chairperson

Per- and polyfluoroalkyl substances (PFAS) comprise a large class of chemically stable compounds causing ubiquitous pollution. Their detrimental effects to humans and the environment are exacerbated by their mobility in aquatic systems. Effective and efficient methods are necessary to chemically destroy these aqueous contaminants. This thesis study focuses on understanding structure-reactivity relationships of aqueous PFAS within the UV/sulfite system, developing and optimizing this system for effective and efficient PFAS destruction, and identifying next-generation PFAS design for rapid and complete defluorination.

A photochemical system equipped with a 254 nm Hg lamp is used to irradiate an aqueous solution amended with a photosensitizer (*i.e.*, sulfite, SO_3^{2-}), spontaneously generating reactive hydrated electrons (e_{aq}^-) and sulfite radicals ($SO_3^{\bullet -}$), in order to probe the reactivity with PFAS. A systematic investigation using the UV/sulfite system reveal critical structure–reactivity relationships for legacy (*e.g.*, carboxylates, sulfonates, and telomer carboxylates) and emerging (*e.g.*, ether carboxylates) aqueous PFAS. Decay kinetics, transformation products, and defluorination (*i.e.*, percent C–F bond cleavage) results highlight distinct reaction pathways.

Quantum chemical calculations on bond dissociation energies and reaction simulations provide mechanistic interpretation of experimental results in order to elucidate destruction pathways.

System parameters, including solution pH and photosensitizer concentration, are optimized to achieve the deepest and most efficient defluorination. Kinetic studies reveal competition between reductive and oxidative defluorination mechanisms directly influencing overall system performance. Increased reactivity and deeper defluorination is achieved under increasingly basic conditions, where the reaction pathways with SO_3^{2-} are thermodynamically mediated.

Effective and efficient PFAS treatment within the UV/sulfite system is highly dependent on structure. Perfluorocaboxamides (PFCAms), containing the distinct amide functional group, can be rapidly destroyed and deeply defluorinated within the UV/sulfite system. By taking advantage of a novel defluorination mechanism upon reactivity with $SO_3^{\bullet-}$, PFCAms exhibit higher reactivity resulting in deeper defluorination in modest basic solution in the presence of UV-irradiated SO_3^{2-}. Furthermore, *N*-substituted PFCAms observe even faster reactivity and resistance to hydrolysis, demonstrating the possibility of designing future PFAS for rapid and complete defluorination.

TABLE OF CONTENTS

LIST OF FIGURES

LIST OF TABLES

LIST OF SCHEMES

CHAPTER 1: INTRODUCTION AND LITERATURE REVIEW

1.1 Introduction

Per- and polyfluoroalkyl substances (PFAS) denote a large class of fluorinated organic compounds targeted and developed for their technological and economic benefits.[1,2] PFAS benefit from containing an intrinsically stable chemical motif, the C–F bond, as demonstrated by its high bond dissociation energy (115 kcal mol^{-1}).[3] Furthermore, considering the fluorine atom possesses the greatest electronegativity of all elements, this results in a substantially polarized bond, increasing the electrostatic interaction and contributing to the overall strength of the C–F bond.[4] A consequence of this extreme electronegativity is that the fluorine atom (*i.e.*, lone pairs) resist typical interactions, such as resonance[4] and hydrogen bonding,[5] and to a lesser extent, conjugation.[6] Because of these mitigated interaction, PFAS display significantly reduced surface free energy.[2] This results in unique chemical and physical behavior, including possessing both hydrophobicity and lipophobicity and possessing inertness to chemical and thermal distress.[2] Consequently, PFAS have been utilized in broad applications, including membranes used in commodity chemical manufacturing and water treatment,[7] energy storage devices,[8–10] medical devices and supplies,[11,12] pharmaceuticals,[13] agrochemicals,[14,15] consumer products,[16–18] coatings,[19] lubricants,[20,21] refrigerants,[22,23] surfactants,[24] and suppressants (*e.g.*, aqueous film-forming foam (AFFF),[25] metal plating[26,27]). Accordingly, a global fluorochemical industry was established developing PFAS to meet the demands of emerging technology and quality of life valued at $21.4 billion per year in 2018.[28]

The broad application of PFAS for commercial and industrial interests has resulted in significant release of these chemicals into the environment.[29–31] Depending on their structure, these compounds can display high mobility in aqueous environments (*e.g.*, surface water and groundwater),[32,33] strong partitioning behavior (*e.g.*, liquid/gas and solid/liquid interface),[34–36] as

well as susceptibility to biotic[37–39] and abiotic[40–42] transformation of organic moieties for carbon centers containing C–H bonds (*i.e.*, *poly*fluoroalkyl substances). Conversely, perfluorinated moieties (*i.e.*, carbon centers containing only C–F and C–C bonds) are rigorously unreactive in the environment.[43–45] For example, microbes have been observed to degrade monofluoroaceate (MFA, $CH_2\mathbf{F}COO^-$).[46] However, the debate still persists in the literature regarding the ability for trifluoroacetate (TFA, $C\mathbf{F_3}COO^-$), the perfluorinated analog, to be naturally degraded.[47–50] In addition, it is well known that legacy chlorofluorocarbons (CFCs) and replacement hydrofluorocarbons (HFCs) undergo atmospheric degradation.[23,51] However, the transformation product is indeed the recalcitrant TFA, and is therefore an indicator of CFC and HFC use globally. Equally, due to the intrinsic strength of the C–F bond, abiotic transformation (*i.e.*, light or heat-induced transformation) of perfluorinated carbon-centers does not seem to be a significant route as evidenced by their accumulation in the environment.[50,52] Likewise, the impact of PFAS is not restricted to the environment. Indeed, significant evidence shows these compounds to be persistent and bioaccumulative,[53,54] which has been linked to PFAS toxicity.[55] Consequently, a shift has occurred globally to use short-chain (*e.g.*, perfluorobutane sulfonate, PFBS) or fluoroalkyl ether-derivatives (*e.g.*, hexafluoropropylene oxide-dimer acid, HFPO-DA), as they are considered to be less bioaccumulative,[54,56] and therefore safer. This, however is still up for debate.[57,58] Despite these efforts, *per*fluorinated compounds remain persistent in the environment, and therefore remain a threat towards human health and the environment.

Beginning in 1970 the United States (US) created the Environmental Protection Agency (EPA). This established the first regulatory body to oversee the health and safety of the natural environment within the US, including air, water, and soil systems. In that light, significant progress has been made in developing effective and economical technologies to remediate these systems from anthropogenic pollution. The aquatic system is particularly vulnerable to PFAS pollution due

in large part because of its ability to act as a *sink*.[59–61] For example, PFAS released into the atmosphere can be transformed and stripped during rain events resulting in deposition into water and soil systems.[62,63] Conversely, PFAS can be released directly into water systems, where a partition will develop between the aqueous (water) and solid (soil) phases. Over time, PFAS can leach out of solids back into water systems.[64] Current water treatment technologies, which are effective in physically removing and chemically mitigating hazardous biological species and chemical compounds, cannot address PFAS pollution. In fact, the smallest PFAS are able to evade advanced physical separation techniques (*i.e.*, filtration) including, activated carbon,[65,66] membrane separation,[67,68] and ion exchange.[69,70] Although chemical treatment techniques, so-called *advanced oxidation processes* (AOP), have been incorporated towards water treatment over the last several decades (*e.g.*, UV/H_2O_2, UV/O_3, $UV/H_2O_2/O_3$, etc.),[71–73] these strategies are not liable to cleave the incredibly strong C–F bond. This failure leads to direct exposure of PFAS to humans from drinking water sources,[74–79] as well as secondary routes through consumption of PFAS-contaminated food through agriculture practices (*e.g.*, farming,[80] dairy,[81] meat production,[82] and fish[83]), further intensified by the bioaccumulative nature of PFAS. It remains imperative that efficient and cost-effective technologies, specifically addressing chemical destruction of the C–F bond, be developed in order to mitigate further risk to humans and adverse environmental damage.

1.2 PFAS Structure and Design

The development of fluorinated organic compounds began around the 20th century as replacements for toxic refrigerants (*e.g.*, ammonia, NH_3; chloromethane, CH_3Cl; sulfur dioxide, SO_2). However, it was not until in 1938 when high molecular weight fluorinated compounds realized their potential. It was researchers at DuPont who discovered inside a pressurized cylinder of tetrafluoroethylene (TFE) that the molecules had polymerized to form perfluorooctanoic acid (PFOA), most likely catalyzed by the copper walls. This inevitably led to the development of

polytetrafluoroethylene (PTFE), commonly known by its trade name Teflon. However, it was not until research led by J. H. Simons at Pennsylvania State University that brought about the commercial development of electrochemical fluorination (ECF), often referred to as the *Simons Process*. This greatly enhanced the diversity of fluorocarbon structures available for commercial application, and consequently the fluorochemical industry greatly expanded. Although ECF has numerous advantages, there are limitations (*cf.* 1.2.1 Electrochemical Fluorination*)*. Consequently, a second process has been developed that addresses these limitations called Telomerization. The definitive advantage of this process is the ability to control chain-length and avoid undesired branching that is seen in ECF (*cf.* 1.2.2 Telomerization). The last method necessary to discuss is the polymerization of perfluoroepoxides. This method is unique due to the introduction of an ether group within the fluorocarbon backbone. The structures resulting from this method have gained recent attention as an emerging PFAS contaminant (*cf.* 1.2.3 Perfluoroexpoxide Polymerization).

1.1.1 Electrochoemical Fluorination (ECF)

The principle ECF configuration includes an electrochemical cell equipped with anhydrous hydrofluoric acid (HF) and the organic substrate of choice (*e.g.*, acyl fluoride or sulfonyl fluoride, Figure 1.1a). During operation, fluoride in solution will replace hydrogen along the carbon backbone, via a free-radical mechanism.[84] Due to the generation of free radicals, carbon chain rearrangement and breakage is inevitable. As a result, a mixture of linear and branched isomers of the starting organic substrate are generated. For example, the ratio between linear and branched is typically 70–80% linear to 20–30% branched for two legacy PFAS: PFOA and perfluorooctane sulfonate (PFOS).[85] This process has shown to be effective towards several organic substrates, including: acids,[84,86,87] alcohols,[84,86,87] amines,[86] ethers,[87] hydrocarbons.[88]

1.1.2 Telomerization

One obvious draw back with ECF is that the free-radical mechanism results in rearrangement of the fluorocarbon backbone; telomerization addresses this issue (Figure 1.1b). In brief, the starting material (*i.e.*, telogen) is perfluoroalkyl iodide ($C_mF_{2m+1}I$), typically pentafluoroethyl iodide, C_2F_5I (PFEI), and is reacted with TFE (*i.e.*, taxogen) to yield a mixture of *perfluoroalkyl iodides*, $F(CF_2)_nI$.[85] This mixture can further be reacted with ethylene ($CH_2=CH_2$) to yield *fluorotelomer iodides*, $F(CF_2)_n–CH_2CH_2I$.[85] Here lies the value of the telomerization process. The two products from this process, perfluoroalkyl iodides (*telomer A*) and fluorotelomer iodides (*telomer B*) are used as raw materials to generate a range of products (Figure 1.1c).[85] Due to the nature of how the fluorocarbon and hydrocarbon chains are built in the telomerization process, a specific nomenclature has developed in naming these compounds. This is accomplished using the *X:Y* designation, where *X* indicates the number of fluorocarbons and *Y* indicates the number of hydrocarbons (*e.g.*, 8:2 **F**luoro**T**elomer alcoh**ol**, $C_8F_{17}CH_2CH_2OH$, 8:2 FTOH).[85]

In addition to the extensive diversity that can be generated by the telomerization process, because these compounds are built using TFE and ethylene, linear telogens produce exclusively linear PFAS. Conversely, if the telogen is branched and/or has an odd number of carbon atoms (*e.g.*, $(CF_3)_2CFI$), the resulting product will contain a mixture of branched and/or an odd number of carbon atoms, despite incorporating even number of *taxogen* $–CF_2–$ units from TFE.[85]

1.1.3 Perfluoroexpoxide Oligomerization

The last PFAS manufacturing process worthy of discussion is the oligomerization of perfluoroepoxides (PFEOs). Once fluorine chemists achieved creating fluoropolymers with tunable fluorination (*i.e.*, containing all C–F bonds, or incorporating some C–H bonds), there was a desire in industry to develop perfluorinated analogs of polyethers (*i.e.*, perfluoropolyethers). In this way, the resulting fluoropolymers, with the ether group incorporated into the fluorinated backbone,

should have different properties potentially advantageous for application. One route to synthesize polyethers is through polymerization of epoxides. Indeed, once reliable methods of perfluoroolefin epoxidation was achieved, this introduced a new type of monomer unit in which fluorine chemists could use for polymerization reactions.[89] Recall in the telomerization process, the telogen (starting material) is elongated by incorporating a taxogen resulting in a hetero-oligomer (*i.e.*, molecule consisting of a few similar or identical repeating units). Indeed, PFEO oligomerization is analogous to telomerization in that there is a starting material that is elongated by incorporating repeating PFEOs (Figure 1.2). Based on the literature, the most important perfluoroepoxides are tetrafluoroethylene oxide (TFEO) and hexafluoropropylene oxide (HFPO). The use of epoxides to synthesize perfluoroalkyl ether acids (PFEAs) has further broadened the scope in PFAS application.[89]

1.3 Electron-Transfer Reactions

In order to chemically destroy PFAS (*i.e.*, cleave the C–F bond), the stability of the bond must be disrupted. One way to achieve this is through an electron-transfer (ET)-initiated bond cleavage (*i.e.*, dissociative electron transfer, DET).[90] Reactions involving DET can be either *reductive* (adding an electron) or *oxidative* (removing an electron), with regards to the species undergoing dissociation. This is demonstrated in the following two chemical equations for reductive DET (reaction **1.1**) and oxidative DET (reaction **1.2**):

$$A + BC \rightarrow A^{\bullet +} + [BC]^{\bullet -} \rightarrow A^{\bullet +} + B^{\bullet} + C^{-} \quad (1.1)$$

$$A + BC^{-} \rightarrow A^{-} + [BC]^{\bullet} \rightarrow A^{-} + B^{\bullet} + C \quad (1.2)$$

These reactions can be described as *outer sphere* ET. This is characterized by the distinct mode of electron transfer, freely moving from one redox center to another. This is not to be confused with *inner sphere* ET, which is characterized by the formation of a σ-bond enabling the transfer of

electrons (*e.g.*, bridging ligand).[91] For the UV/sulfite system, all ET events are outer sphere due to the nature of the reactive species and therefore will only be considered here.

Among DET reactions, there have been described two general pathways: (*i*) concerted (reaction **1.3**), or (*ii*) stepwise (reaction **1.4**):[92]

$$AB + e^- \rightarrow A^\bullet + B^- \qquad \textit{concerted} \qquad (1.3)$$

$$AB + e^- \rightleftarrows [AB]^{\bullet -} \rightarrow A^\bullet + B^- \qquad \textit{stepwise} \qquad (1.4)$$

$$AB + e^- \rightleftarrows [A^\bullet B^-]_{cage} \rightarrow A^\bullet + B^- \qquad \text{“}\textit{sticky}\text{”} \qquad (1.5)$$

A third intermediate pathway has been identified, in which the radical and ion form a pair through interactions in the solvent cage, known as a “sticky” DET, which are much more rare and is mentioned here for completeness (reaction **1.5**).[90] Only the first two will be discussed in detail. Despite distinct pathways, both concerted and stepwise mechanisms lead to the same products. It is noted that in the stepwise mechanism, the initial ET is reversible, whereas ET in the concerted mechanism is irreversible. Since both routes involve the transfer of a free electron (*i.e.*, no bond formation) it is appropriate to apply the Marcus theory.[93] This model can be used to relate the rate of electron transfer (*i.e.*, log *k*) to the free energy ($\Delta G°$) by using equations **1.6** and **1.7**[94] and has successfully described outer sphere ET reactions:[95]

$$k_{ET} = Z \exp\left[-\frac{\Delta G^\ddagger}{RT}\right] \qquad (1.6)$$

$$\Delta G^\ddagger = \Delta G_0^\ddagger \left(1 + \frac{\Delta G°}{4\Delta G_0^\ddagger}\right)^2 \qquad (1.7)$$

where Z is the preexponential factor, $\Delta G^\ddagger$ is the activation free energy, and $\Delta G_0^\ddagger$ is the intrinsic barrier. In doing so, it became obvious that some DET reactions possess a much weaker driving force ($\Delta G°$).[92] Later, Savéant successfully tested his model for concerted DET, thus allowing to further distinguish between the two DET reaction pathways.[96] He found that the intrinsic barrier ($\Delta G_0^\ddagger$), which is the activation free energy at $\Delta G° = 0$, is much larger for concerted DET compared

to stepwise. Indeed, the intrinsic barrier is simply the sum of the solvent ($\Delta G_{0,s}^{\ddagger}$) and inner ($\Delta G_{0,i}^{\ddagger}$) contributions, as shown in equation **1.8**:[94]

$$\Delta G_0^{\ddagger} = \Delta G_{0,s}^{\ddagger} + \Delta G_{0,i}^{\ddagger} \tag{1.8}$$

This can be rewritten by grouping the internal and solvent reorganization energies into one term (λ) and explicitly incorporating the bond dissociation energy (BDE), to generate the following equations for the intrinsic barrier towards concerted (equation **1.9**) and stepwise (equation **1.10**) reactions, respectively:[97]

$$\left(\Delta G_0^{\ddagger}\right)_{stepwise} = \frac{\lambda}{4} \tag{1.9}$$

$$\left(\Delta G_0^{\ddagger}\right)_{concerted} = \frac{\lambda+\mathrm{BDE}}{4} \tag{1.10}$$

Therefore, because $(\Delta G_0^{\ddagger})_{\text{concerted}} > (\Delta G_0^{\ddagger})_{\text{stepwise}}$, concerted DET is intrinsically slower than stepwise DET. Furthermore, when the driving force is increased (*i.e.*, using strong reductants) the initial outer sphere ET step of stepwise DETs is preferred.[92]

It has been shown, through the use of More–O'Ferrall Jencks plots, there exists a relationship between unimolecular (S_N1) and bimolecular (S_N2) reaction mechanisms in that these two represent ends of a reaction spectrum.[98] Similarly, it has been shown there exists a relationship between stepwise and concerted DET.[94] Although this can be difficult to show in homogeneous DET,[99] heterogenous DET is uniquely positioned for these experiments.[97] This is because the intrinsic barrier ($\Delta G_0^{\ddagger}$) for heterogenous DET depends essentially on the acceptor molecule. Meanwhile, the intrinsic barrier for homogeneous DET depends on both the acceptor molecule and the electron donor.[92] Furthermore, through the use of an electrochemical cell, one can explore DET over a range of applied potential for one acceptor molecule. When increasing the free energy during the reaction (*i.e.*, $-\Delta G°$), excess energy will shift the activation free energy ($\Delta G^{\ddagger}$) resulting in a competition between concerted and stepwise, $(\Delta G^{\ddagger})_{\text{concerted}} < (\Delta G^{\ddagger})_{\text{stepwise}}$. Indeed, the concerted

reaction is thermodynamically favored, specifically when the $E°$ for the formation of the radical anion is *negative*, the cleaving bond is *weak*, and the resulting anion is a *good leaving group*.[92]

The use of ET-initiated bond cleavage has been employed in several approaches towards PFAS treatment (*e.g.*, photolysis,[100] photocatalysis,[101] sonolysis,[102] radiolysis,[103] plasma,[104] and oxidation[105]). In the UV/sulfite system, the reactive species – the hydrated electron (e_{aq}^-) and the sulfite radical ($SO_3^{\bullet -}$) – will participate in ET reactions contributing to the destruction of aqueous PFAS. Therefore, understanding the properties of these reactive species can enable deeper understanding on the observations of PFAS destruction within the UV/sulfite system.

1.4 The Hydrated Electron (e_{aq}^-)

Due to the extreme electronegativity of the fluorine atom, coupled with the fact that the *per*fluorinated carbon center is fully oxidized, strong oxidants are incapable of directly cleaving the C–F bond. Consequently, it would follow that the C–F bond, and any carbon–halogen (C–X) bond, should be capable of being reductively destroyed. Furthermore, electronegative halogens bound to carbon would result in a polarized bond leaving carbon with a partial positive charge. Therefore, a reductant nucleophilic in nature could take advantage of the partial positive charge on carbon. Indeed, it has been demonstrated that halogenated species can be cleaved relatively quickly in reduction-based processes.[106,107] However, due to the relatively strong C–F bond, the reductant will need to possess a large negative reduction potential. One such reductant known to possess a high reduction potential is the solvated electron.[108] This can be thought of as a free electron in solution (*i.e.*, the smallest anion). When the solvent is water, the solvated electron is referred to as a hydrated electron (e_{aq}^-) and its formation is represented in reaction **1.11**:[109]

$$2\,H_2O \xrightarrow{h\nu} e_{aq}^- + H_3O^+ + \bullet OH \qquad (1.11)$$

In aqueous solution, the standard reduction potential is $E° = -2.87$ V against the standard hydrogen electrode (SHE).[110] Considering the large negative reduction potential and its formal negative

charge, the e_{aq}^- behaves like a nucleophile and will routinely add to chemical species with a higher reduction potential in a one-electron transfer (ET) process (reaction **1.12**):[111]

$$e_{aq}^- + S^n \rightarrow S^{n-1} \qquad (1.12)$$

where *S* is the solute and *n* is the positive charge on the solute. The reactivity of e_{aq}^- with solutes range from ~10^1 L mol^{-1} s^{-1} through to the diffusion-controlled limit.[111] This reaction is favored with unsaturated systems (*e.g.*, double bonds, aromatic systems) and is enhanced by placing electronegative moieties (*e.g.*, nitro groups, halogens) adjacent to them.[106,107] It is well established that the e_{aq}^- can react in dissociation ET (DET) processes with halogens and follow both concerted and a stepwise fashion (*cf.* 1.2 Electron–Transfer Reactions).

1.4.1 Reactivity of Acetate Derivatives

One way to investigate the reactivity of e_{aq}^- with organic species is by studying its reaction with halogenated acetate derivatives. Indeed, the rate constants provide the following trend: F<<Cl<Br<I (Table 1.2). This should be expected based on C–X bond energies.[112] For the reaction between e_{aq}^- and monohalogenated acetate, the following has been proposed (reaction **1.13**):

$$e_{aq}^- + XCH_2CO_2H \rightarrow \bullet CH_2CO_2H + X^- \qquad (1.13)$$

where the C–X bond is cleaved generating an organic radical and halide ion (X^-). This reaction is thought to proceed through an outer-sphere ET to the halogen. Notably, there is observed a drastic increase in reaction rate from fluorine (< 1.2 x 10^6 L mol^{-1} s^{-1}) to higher molecular weight halogens: chlorine (1.2 x 10^9 L mol^{-1} s^{-1}), bromine (6.2 x 10^9 L mol^{-1} s^{-1}), and iodine (1.2 x 10^{10} L mol^{-1} s^{-1}), which reaches diffusion-controlled limits. The range in reactivity for the series of halogenated acetate demonstrates that DET transitions from a concerted (–F) to a stepwise (–Cl, –Br, –I) mechanism. Furthermore, the two-order magnitude deference in rate constants between the fluoro- and chloroacetate highlight the sluggishness of concerted DET reactions, and consequentially C–F bond cleavage. To verify this, a comparison to the reaction of methane with e_{aq}^- can be made. In

this reaction, where it is assumed the C–H bond is reduced following concerted DET, the rate constant has been measured ($k < 1.0 \times 10^7$ L mol^{-1} s^{-1}) and is on the same order of magnitude as C–F bond cleavage in fluoroaceate. This provides further support demonstrating the difficulty in direct C–F bond cleavage.

Not be overlooked in the previous discussion of halogenated acetate reactivity is the role of the carbonyl group. Indeed, e_{aq}^- has been observed to be reactive with asymmetric electron deficient groups (*e.g.*, C=C, C=O).[106] This is no better demonstrated than by reaction of e_{aq}^- with acetone, where a rate constant of $k = 6.5 \times 10^9$ mol L^{-1} s^{-1} was measured.[113] Since acetone does not contain a halogen, the reactive species must either be the carbonyl group or the methyl group. Based on product formation, and considering carbon in the methyl group is fully reduced, it has been concluded the reaction proceeds as in reaction **1.14**:

$$e_{aq}^- + R_1(CO)R_2 \rightarrow R_1\dot{C}(O^-)R_2 \qquad (1.14)$$

where the electron has be inserted into the C=O π bond, generating the carbon-centered radical, or π radical anion.[113] It has been shown this reactivity is highly influenced by substitution on the carbonyl motif (*i.e.*, R groups in reaction **1.14**), as described below.

1.4.2 Influence of Substitution on Carbonyl Reactivity

Shown in Table 1.3 is a list of rate constants for compounds containing a carbonyl group, demonstrating the influence of substitution on reactivity. For example, replacing a methyl group on acetone for an alcohol group, as in acetic acid, the rate constant decreases one order of magnitude ($k = 2.0 \times 10^8$ mol L^{-1} s^{-1}). Still, upon deprotonation to form acetate, reactivity drops an additional two orders of magnitude ($k = 1.1 \times 10^6$ mol L^{-1} s^{-1}). One explanation for the decrease in reactivity between acetic acid and acetate could be due to increasing electrostatic repulsion between e_{aq}^- and reactant. Including the results from acetone and acetaldehyde ($k = 4.9 \times 10^9$ L mol^{-1}s^{-1}) the following reactivity is observed for $CH_3(C=O)$–R, where R = CH_3 > H > OH > O^-. Analysis for several series

of substituted carbonyl structures indicate that reactivity proceeds: ketone > aldehyde > carboxylic acid > amide > carboxylate (Table 1.3). Therefore, carbonyl reactivity is strongly dependent on the electronegativity of the substituted groups (*i.e.*, electron withdrawing groups disable carbonyl reactivity).

1.4.3 C–F Bond Cleavage by e_{aq}^-

Now that two reaction pathways have been identified (*i.e.*, outer sphere electron transfer to either the halogen or the carbonyl), it remains what is the competition between these two mechanisms. As mentioned earlier, the range in reactivity for the series of halogenated acetate compounds is clear evidence of the kinetic difference between concerted and stepwise DET. Furthermore, it is clear e_{aq}^- will react with carbonyl groups. However, the measured reactivity of e_{aq}^- with fluoroacetate ($<1.0 \times 10^6$ L mol^{-1} s^{-1}) and acetate (1.2×10^6 L mol^{-1} s^{-1}) does little to help distinguish if this reactivity is brought on by the presence of the halogen or the carbonyl group. As recently discussed, the electronegativity of substituted groups on the carbonyl moiety will influence reactivity. Therefore, a way to probe the mechanism is by comparing monofluoroacetate (MFA) and trifluoroacetate (TFA). If the mechanism is concerted DET, TFA should have a larger rate constant than MFA since there is three times the number of C–F bonds. However, if the mechanism is through reactivity with the carbonyl group, then the rate constant with TFA should be less than MFA. This is because the trifluoromethyl group ($–CF_3$) is more electronegative than monofluoromethyl ($–CH_2F$). Table 1.3 indicates that TFA > MFA in reactivity with the e_{aq}^-; a ~14% increase. Therefore, it appears the main mechanism for C–F bond cleavage is concerted DET, a sluggish reaction kinetically similar to the reactivity of the carboxylate group. This appears to be supported when comparing the rate constants of trichloroacetate (TCA) and monochloroacetate (MCA) with e_{aq}^-, where a ~19% increase is observed. However, since MCA follows stepwise DET,

different to that of TFA, a more comprehensive evaluation can be made by investigating the reactivity of three structures: MCA, TCA, and monochloroacetic acid (MCAA).

Based on the above discussion, two things are clear concerning e_{aq}^- reactivity: (1) number of halogen atoms leads to an increase, and (b) electron withdrawing groups substituted on the carbonyl motif results in a decrease. Therefore, as predicted: TCA > MCA (three C–Cl bonds vs one C–Cl bond); MCAA > MCA (carboxylic acid > carboxylate). However, it is not clear the influence toward reactivity when considering extent of halogenation versus carbonyl substituents. Based on the rate constants in Table 1.3, increasing the number of C–Cl bonds three times results in a ~7x increase in reactivity, or a 3.5x increase for each C–Cl bond. Meanwhile, protonating the carboxylate results in a 5.75x increase in reactivity, suggesting protonation of the carboxylate group is more influential towards increasing reactivity with e_{aq}^- than the number of halogen atoms, constrained to halogen atoms that are all the same.

The last reaction necessary for discussion when considering the e_{aq}^- as the reactant is homolytic DET. Given the electronegativity of fluorine, the C–F bond possesses an extremely low lying σ^*_{C-F} antibonding orbital. Indeed, this orbital has been observed to engage in negative hyperconjugation (*i.e.*, electrons moving from π orbital $\rightarrow \sigma^*$ orbital) with adjacent electron density containing similar symmetry and energy (*e.g.*, oxygen).[4] Although this interaction can be thought of as destabilizing, in fact it only reduces the strength of the covalent nature of the C–F bond, and instead the ionic character of the bond is increased (*i.e.*, strengthened).[4] This becomes important for C–F bonds adjacent to carbonyl groups. As discussed above, e_{aq}^- will add to the $\pi^*_{C=O}$ antibonding orbital of the carbonyl group. It has been shown in this ET reaction that the electron will migrate from $\pi^*_{C=O} \rightarrow \sigma^*_{C-F}$.[90] This results in the homolytic cleavage of the C–F bond.

1.5 Sulfur Radicals

1.5.1 UV irradiation of sulfite (SO_3^{2-})

$$SO_3^{2-} \xrightarrow{h\nu} SO_3^{\bullet-} + e_{aq}^- \quad (1.15)$$

UV light is photolytic energy (*i.e.*, photons) that can excite electrons upon irradiation. Depending on the electronic structure, this can generate radicals and electrons (*i.e.*, atoms, compounds, or ions containing an unpaired electron). There have been reported two distinct mechanisms associated with electron photodetachment: (*i*) charge-transfer-to-solvent (CTTS) state[114] and (*ii*) direct ionization.[115] An example of photodetachment is the UV irradiation of sulfite (SO_3^{2-}). At 254 nm, this energy will cause SO_3^{2-} to enter the CTTS state and eject an electron into the solvent phase, generating a solvated electron. When that medium is water this is known as a hydrated electron (e_{aq}^-), as has been discussed in the previous section. Since e_{aq}^- was generated from the stable valence shell of SO_3^{2-}, it follows that the other product in the irradiation of SO_3^{2-} would be the sulfite radical ($SO_3^{\bullet-}$). The following discussion focuses on the chemical reactivity of this and other related sulfur radicals.

1.5.2 Sulfur Radical Chemistry

Sulfur is unique considering its position on the periodic table. Located beneath oxygen, it behaves similarly to other chalcogenides (*i.e.*, oxygen, selenium). However, considering it is located one row below oxygen, sulfur can access the 3*d* orbital, allowing it to engage in bonding interactions otherwise excluded to row 2 elements (*i.e.*, engage in more than four bonding interactions). This is no better demonstrated than by the ability of sulfur to form several oxyanions (*i.e.*, SO_3^{2-}, SO_4^{2-}). While most sulfur oxyanions are relatively stable, their radical counterparts ($SO_x^{\bullet-}$) are not. Specifically, the sulfur oxyanion radicals of $SO_3^{\bullet-}$, $SO_4^{\bullet-}$, and $SO_5^{\bullet-}$ demonstrate distinct reactivities worth further investigation.[116]

As described earlier, SO_3^{2-} upon irradiation will generate $SO_3^{\bullet-}$. In an inert, pristine environment (*i.e.*, ultrapure water with no oxygen), $SO_3^{\bullet-}$ may participate in two reactions: (*i*) *dimerization*, shown in reaction **1.16**;[117] or (*ii*) *disproportionation*, shown in reaction **1.17**:[118]

$$2\ SO_3^{\bullet-} \rightarrow S_2O_6^{2-} \qquad k_{1.16} = 3.4 \times 10^8\ L\ mol^{-1}\ s^{-1}\ (pH\ 9.8) \qquad (1.16)$$

$$2\ SO_3^{\bullet-} \rightarrow SO_3 + SO_3^{2-} \qquad k_{1.17a} = 7.0 \times 10^8\ L\ mol^{-1}\ s^{-1} \qquad (1.17a)$$

$$SO_3 + H_2O \rightarrow SO_4^{2-} + 2\ H^+ \qquad (1.17b)$$

This system has been studied extensively and found the branching ratio between dimerization and disproportionation to be 1:2.[119,120] The chemistry of reaction **1.17** suggests that $SO_3^{\bullet-}$ can act as either a reductant or as an oxidant.[121] Indeed, research has shown that $SO_3^{\bullet-}$ can act as a mild oxidant (reaction **1.18**).[121] Based on reaction **1.17**, it is suggested that $SO_3^{\bullet-}$ can act as a strong reductant (reaction **1.19**).[121] However, there are no confirmed one-electron transfer reactions, instead achieving this reaction *via* O^- oxidation:[117]

$$SO_3^{\bullet-} + e^- \rightarrow SO_3^{2-} \qquad (E° = 0.63\ V) \qquad (1.18)$$

$$SO_4^{2-} + H_2O + e^- \rightarrow SO_3^{\bullet-} + 2\ OH^- \qquad (E° = -2.47\ V) \qquad (1.19)$$

When oxygen is present, $SO_3^{\bullet-}$ will react to form peroxymonosulfate radical ($SO_5^{\bullet-}$) as shown in reaction **1.23**. Peroxymonosulfate radical ($E°$ = 1.1 V at pH 7)[121] is known to be a stronger oxidant than $SO_3^{\bullet-}$, but not stronger than sulfate radical ($SO_4^{\bullet-}$, $E°$ = 2.6 V).[122,123] This is demonstrated by the reactivity of $SO_x^{\bullet-}$ with ascorbate (reaction **1.20**, **1.21** and **1.22**):[121]

$$SO_3^{\bullet-} + HA^- \rightarrow HSO_3^- + A^{\bullet-} \qquad k_{1.20} = 9.0 \times 10^6\ L\ mol^{-1}\ s^{-1} \qquad (1.20)$$

$$SO_4^{\bullet-} + HA^- \rightarrow HSO_4^- + A^{\bullet-} \qquad k_{1.21} > 10^9\ L\ mol^{-1}\ s^{-1}\ (\textit{estimated}) \qquad (1.21)$$

$$SO_5^{\bullet-} + HA^- \rightarrow HSO_5^- + A^{\bullet-} \qquad k_{1.22} = 1.4 \times 10^8\ L\ mol^{-1}\ s^{-1} \qquad (1.22)$$

Although data does not exist for the H-abstraction of ascorbate by $SO_4^{\bullet-}$, it has been estimated to be faster than either $SO_3^{\bullet-}$ or $SO_5^{\bullet-}$. Furthermore, data suggests $SO_4^{\bullet-}$ will react faster than $SO_3^{\bullet-}$

and $SO_5^{\bullet-}$ (Table 1.4). Therefore, in the presence of organic compounds with an oxidation potential between $SO_5^{\bullet-}$ and $SO_3^{\bullet-}$, a chain reaction will develop:[121,124]

$$SO_3^{\bullet-} + O_2 \rightarrow SO_5^{\bullet-} \qquad k_{1.23} = 1.5 \times 10^9 \text{ L mol}^{-1} \text{ s}^{-1} \qquad (1.23)$$

$$SO_5^{\bullet-} + R + H^+ \rightarrow HSO_5^- + R^+ \qquad E° < 1.13 \text{ V} \qquad (1.24)$$

$$R^+ + SO_3^{2-} \rightarrow R + SO_3^{\bullet-} \qquad (1.25)$$

Other reactions that might contribute to chain propagation involving $SO_x^{\bullet-}$ are the following:[117,125]

$$SO_5^{\bullet-} + SO_3^{2-} \rightarrow SO_4^{2-} + SO_4^{\bullet-} \qquad k_{1.25} = 1.3 \times 10^7 \text{ L mol}^{-1} \text{ s}^{-1} \qquad (1.25)$$

$$SO_4^{\bullet-} + SO_3^{2-} \rightarrow SO_4^{2-} + SO_3^{\bullet-} \qquad k_{1.26} > 2.0 \times 10^9 \text{ L mol}^{-1} \text{ s}^{-1} \qquad (1.26)$$

Notice that $SO_5^{\bullet-}$ in reaction **1.25** can oxidize SO_3^{2-} to generate the strong oxidant $SO_4^{\bullet-}$, which can further oxidize SO_3^{2-} to generate $SO_3^{\bullet-}$, propagating the sulfur radical chain reaction (SRCR) shown in reactions **1.23 – 1.25**. In addition, the generation of stable SO_4^{2-} is observed. It is worth noting that peroxymonosulfate (HSO_5^-), which is generated in reaction **1.24**, can form $SO_4^{\bullet-}$ and hydroxyl radical ($^{\bullet}OH$) under UV irradiation:[123]

$$HSO_5^- \xrightarrow{h\nu} SO_4^{\bullet-} + {}^{\bullet}OH \qquad (1.27)$$

Thus, demonstrating another route towards $SO_4^{\bullet-}$. Consequently, this reaction generates the strong $^{\bullet}OH$ as well.

Several termination reactions can result from this SRCR. It was shown earlier that the dimerization of $SO_3^{\bullet-}$ is possible (reaction **1.16**). Similarly, the dimerization of $SO_5^{\bullet-}$ has been proposed (reactions **1.28** and **1.29**),[121] resulting in the formation of $SO_4^{\bullet-}$ and molecular oxygen (O_2):

$$SO_5^{\bullet-} + SO_5^{\bullet-} \rightarrow 2\ SO_4^{\bullet-} + O_2 \qquad (1.28)$$

$$SO_5^{\bullet-} + SO_5^{\bullet-} \rightarrow S_2O_8^{2-} + O_2 \qquad (1.29a)$$

$$S_2O_8^{2-} \xrightarrow{h\nu} 2\ SO_4^{\bullet-} \qquad (1.29b)$$

$$SO_4^{\bullet-} + OH^- \rightarrow SO_4^{2-} + \bullet OH \qquad k_{30} = 8.3 \times 10^7 \text{ L mol}^{-1}\text{ s}^{-1}\ (\text{pH} > 11) \quad (1.30)$$

Several points should be made regarding these reactions. First, similar to $SO_3^{\bullet-}$, a branching ratio is demonstrated for $SO_5^{\bullet-}$. Interestingly, the ratio of $k_{1.28}(SO_4^{\bullet-})$ / $k_{1.29a}(S_2O_8^{2-})$ = 9, indicating a strong kinetic preference for *disproportionation* over *dimerization*,[121] similar to $SO_3^{\bullet-}$. In addition, this is considered a terminating reaction due to the high reactivity of $SO_4^{\bullet-}$ to form stable SO_4^{2-} (reaction **1.30**). Lastly, reactions **1.28** and **1.29a** demonstrate a source of O_2, necessary for the SRCR.

Considering the potential for the generation of $SO_4^{\bullet-}$ it should be briefly mentioned that $SO_4^{\bullet-}$ will also dimerize in solution, as seen in the following reaction:[117]

$$SO_4^{\bullet-} + SO_4^{\bullet-} \rightarrow S_2O_8^{2-} \qquad k_{1.31} = 8.1 \times 10^8 \text{ L mol}^{-1}\text{ s}^{-1} \quad (1.31)$$

Therefore, reactions **1.29b** and **1.31** represent a pseudo-equilibrium, similar to that of reversible reactions.

In addition to UV dissociation of HSO_5^-, it has been postulated that peroxymonosulfate (HSO_5^-) may participate in a disproportionation reaction resulting in the generation of sulfate:[126]

$$HSO_5^- + H_2O \rightarrow SO_5^{2-} + H_3O^+ \qquad p\mathit{K}a = 9.4 \quad (1.32)$$

$$HSO_5^- + SO_5^{2-} \rightarrow HSO_6^- + SO_4^{2-} \quad (1.33)$$

$$HSO_6^- + OH^- \rightarrow SO_4^{2-} + H_2O + O_2 \quad (1.34)$$

Thus, HSO_5^- can potentially behave as a terminating species.

1.6 Photochemical System Thermodynamics

As the photochemical system takes place in an aqueous environment, a discussion regarding the thermodynamics of the system (*i.e.*, pH) is necessary. This is because the physical parameter of solution pH can mediate the chemical potential of the system (*i.e.*, component speciation). It is here that the discussion will be focused.

1.6.1 Sulfite attenuation coefficient

The main active species in the UV/sulfite system is the photosensitizer SO_3^{2-}. In order to cause photodissociation, SO_3^{2-} must absorb a photon of energy.[127] The rate of absorption is known as the *attenuation coefficient* (historically known as the *extinction coefficient*).[127] The extinction coefficient quantifies how strongly a substance absorbs light at a given wavelength, either per molar concentration (ε [≡] L mol^{-1} cm^{-1}), or mass density (μ [≡] mL g^{-1} cm^{-1}).[127] This discussion hereto will be limited to molar extinction coefficient, ε. The larger this number, the more efficient the photosensitizer in absorbing photons at the specified excitation energy (*i.e.*, wavelength). Based on other photosensitizers (*e.g.*, I^-, $Fe(CN)_6^{4-}$), SO_3^{2-} is not as efficient at absorbing photons, despite its favorable electron donor abilities.[115] This is demonstrated by comparing ε and quantum yield (Φ, ratio of photons emitted to photons absorbed) of SO_3^{2-} and iodide (I^-). At 248 nm excitation energy, $\varepsilon_{sulfite}$ = 49 ± 1 L mol^{-1} cm^{-1}, whereas ε_{iodide}= 885 ± 3 L mol^{-1} cm^{-1}, demonstrating iodide absorbs photons 18x more effectively than SO_3^{2-}. However, the resulting quantum yield, Φ, which represents the efficiency of photodetachement, demonstrates the electron donor ability of sulfite ($\Phi_{sulfite}$ = 0.108 ± 0.001, while Φ_{iodide} = 0.286 ± 0.008; 2.6x increase in efficiency).[115] Due to the poor spectroscopic properties observed by SO_3^{2-}, providing a more favorable thermodynamic environment will enhance the fate of e_{aq}^- (*i.e.*, increase species lifetime). This has been shown to be effectively done by simply increasing the solution pH. Indeed, it was experimentally found that the optimal pH in order to maximize the lifetime of the e_{aq}^- is pH 12.[128] This solution pH will influence other reactions within the photochemical system as well, and are discussed below.

1.6.2 Influence of pH on UV/sulfite system

In order to understand the influence of pH in the UV/sulfite system, the attention is turned first to SO_3^{2-}. As a diprotic acid, SO_3^{2-} has two ionization constants, and therefore exist as different species depending on solution pH:

$$SO_2 + H_2O \rightarrow HSO_3^- + H^+ \qquad p\mathit{K}a = 1.8 \qquad (1.35)$$

$$HSO_3^- + OH^- \rightarrow SO_3^{2-} + H_2O \qquad pKa = 7.2 \qquad (1.36)$$

As shown in reaction **1.35**, bisulfite is not in equilibrium with sulfurous acid (H_2SO_3), but instead rapidly decomposes into sulfur dioxide gas (SO_2) and water. Therefore, the main sulfur (IV) species in solution is SO_3^{2-} and HSO_3^-. Considering SO_3^{2-} is the active photosensitize, it follows that higher solution pH will drive the sulfur (IV) distribution towards SO_3^{2-}, therefore increasing the active form.

Another issue to consider is the concentration of hydronium ion (H_3O^+). Indeed, the negatively charged e_{aq}^- is highly reactive with the positively charged H_3O^+:[111]

$$e_{aq}^- + H_3O^+ \rightarrow H\bullet + H_2O \qquad k_{1.37} = 2.8 \times 10^{10}\ L\ mol^{-1}\ s^{-1} \qquad (1.37)$$

The product of this reaction, the hydrogen atom (H•), is not nearly as strong a reductant ($E°$ = 2.1)[111] as e_{aq}^- and will negatively influence the efficiency of the UV/sulfite system. Therefore, by increasing solution pH the concentration of H_3O^+ will decrease and thus mitigate this trivial reaction. Despite this undesired reaction, it is possible to overcome and further increase the efficiency of the system. This can be done by simply increasing the solution pH > pKa of H•:[110]

$$H\bullet \rightarrow e_{aq}^- + H^+ \qquad pKa = 9.6 \qquad (1.38)$$

As shown in the above equation, H• will spontaneously dissociate into e_{aq}^- and a proton. Indeed, this is another factor that influences the lifetime of the e_{aq}^-.

Due to the presence of carbon dioxide in the atmosphere, it is necessary to briefly review the influence of carbonate species: carbonate (CO_3^{2-}) and bicarbonate (HCO_3^-) shown in equation **1.39**:

$$CO_2 + H_2O \rightleftarrows H_2CO_3 \rightleftarrows H^+ + HCO_3^- \rightleftarrows 2H^+ + CO_3^{2-} \qquad (1.39)$$

Reaction of carbonate species with e_{aq}^- is kinetically slow (Table 1.3). As discussed previously, H• possesses a lower reduction potential, and therefore is also kinetically slow in reacting with carbonate species.[111] Furthermore, carbonates do not seem kinetically reactive with strong oxidants,

based on the rate constants of OH• with CO_3^{2-} (k = 3.9 x 10^8 L mol^{-1} s^{-1}) and HCO_3^- (k = 8.5 x 10^6 L mol^{-1} s^{-1}).[111] Although the reaction of these carbonate species with reactive species in the UV/sulfite system is kinetically slow, it has been shown that bicarbonate can be reductively transformed into formate:[129]

$$HCO_3^- + 2e^- + 2H^+ \rightarrow HCOO^- + H_2O \quad E° = –0.42\ V \qquad (1.40)$$

By comparing the reduction potential of equation **1.40** with that of e_{aq}^-, this is thermodynamically available, despite it being kinetically unfavorable, and has been demonstrated electrochemically[130,131] and photochemically.[132,133]

Lastly, due to the speciation of sulfite at different solution pH, it is worth discussing here. Because H_2SO_3 does not exist stable in aqueous solution, it is only necessary to consider SO_3^{2-} and HSO_3^-. The active species in the UV/sulfite system is SO_3^{2-}, therefore by increasing pH this would provide the greatest amount of the active form of S(IV). In addition, it has been found recently that HSO_3^- can scavenge e_{aq}^-:

$$e_{aq}^- + HSO_3^- \rightarrow H• + SO_3^{2-} \qquad k_{1.41} = 1.2 \text{ x } 10^8 \text{ L mol}^{-1} \text{ s}^{-1} \qquad (1.41)$$

Therefore, increasing the pH drives the speciation towards maximizing active S(IV) form while minimizing undesired scavenging of e_{aq}^-.

1.6.3 Influence of pH on fluorine-containing organic compounds

One reaction necessary for any discussion involving fluorinated organic structures is the unimolecular conjugate base elimination ($E1_{CB}$) mechanism due to the increased acidity introduced by the C–F bond.[6] This reaction is characterized by the deprotonation α to a C–F bond via base (*e.g.*, hydroxide ion). The resulting carbanion, in order to neutralize the partial positive charge on carbon-containing C–F bond, will spontaneously, and irreversibly, eliminate fluoride:

$$CH_3CH_2–CF_2R \overset{OH^-}{\longleftrightarrow} CH_3\overline{C}H–CF_2R \overset{-F^-}{\longrightarrow} CH_3CH=CFR \qquad (1.42)$$

This reaction becomes relevant in the UV/sulfite system due to the potential presence of C–H bonds adjacent to C–F bonds in basic solution. Therefore, solution pH alone can influence the fate of fluoroorganic species within the UV/sulfite system.

1.7 Research Objectives

1) Establish structure-reactivity relationships for the chemical destruction of legacy and emerging aqueous PFAS contaminants within the UV/sulfite system (Chapter 2 and Chapter 3).
2) Understand and optimize reaction conditions within the UV/sulfite system for aqueous PFAS remediation (Chapter 4).
3) Identify alternative chemical moieties to enable deep and efficient treatment within the UV/sulfite system (Chapter 5).

1.8 Tables and Figures

Table 1.1 Hydrated electron and hydroxyl radical rate constants with select organic compounds[a]

Species	e_{aq}^- (L mol^{-1} s^{-1})	•OH (L mol^{-1}s^{-1})
$H_3C–H$	< 1 x 10^7	1.1 x 10^8
$H_3C–OH$	< 1 x 10^4	9.7 x 10^8
$H_3C–Cl$	~8 x 10^8	N/A
$H_2C=CH_2$	< 3 x 10^5	4.4 x 10^9
$H_2C=CHCl$	2.5 x 10^8	1.2 x 10^{10}
$H_2C=O$	~1 x 10^7	~1 x 10^9
$(CH_3)_2C=O$	6.5 x 10^9	1.1 x 10^8

[a]Values based on Buxton[111] unless otherwise indicated.

Table 1.2 Hydrated electron rate constants with select acetate derivatives[111,134]

Group	Acetate derivatives	Rate ($L\ mol^{-1}\ s^{-1}$)
Organic	$–CH_3$	$1.1x10^6$
	$–CH_3$ (acid)	$2.0x10^8$
Fluoro-	$–CH_2F$ (pH 10)	$<1.2x10^6$
	$–CF_3$ (pH 10)	$<1.4x10^6$
Chloro-	$–CH_2Cl$ (pH 10)	$1.2x10^9$
	$–CH_2Cl$ (acid; pH 1)	$6.9x10^9$
	$–CCl_3$ (pH 10)	$8.5x10^9$
Bromo-	$–CH_2Br$ (pH 10)	$6.2x10^9$
Iodo-	$–CH_2I$ (pH 10)	$1.2x10^{10}$

Table 1.3 Hydrated electron rate constants with select $R_1(C=O)R_2$ compounds[111]

Compound	R_1	R_2	k (L mol^{-1} s^{-1})
Formate	H	O^-	$<1.0 \times 10^6$
Formamide	H	NH_2	6.3×10^7
Formic acid	H	OH	1.4×10^8
Formaldehyde	H	H	6.3×10^7
Acetaldehyde	H	CH_3	4.9×10^9
Acetate	CH_3	O^-	1.1×10^6
Acetamide	CH_3	NH_2	3.5×10^7
Acetic acid	CH_3	OH	2.0×10^8
Acetaldehyde	CH_3	H	4.9×10^9
Acetone	CH_3	CH_3	6.5×10^9
Carbonate	O^-	O^-	3.9×10^5
Bicarbonate	OH	O^-	$<1 \times 10^6$
Carbonic acid	OH	OH	N/A
Carboxamate	NH_2	O^-	N/A
Carboxamide	NH_2	OH	N/A
Urea	NH_2	NH_2	3.0×10^5
Oxalate	O^-	COO^-	3.1×10^7
Oxalate hydrogen	OH	COO^-	3.2×10^9
Oxalic acid	OH	COOH	2.5×10^{10}
Carbon monoxide	–	–	1.7×10^9
Carbon dioxide	O	O	7.7×10^9

Table 1.4 Sulfur radical rate constants with select alcohols

# of Carbons	Alcohol	$SO_3^{\bullet-}$	$^{135}SO_4^{\bullet-}$	$SO_5^{\bullet-}$
1	Methanol	*N/A*	9.8×10^6 (N_2)	*N/A*
2	Ethanol	$\leq 2 \times 10^3$ (N_2)[116]	4.3×10^7 (N_2)	$\leq 10^3$ (N_2)[116]
3	1-propanol	*N/A*	5.9×10^7 (N_2)	*N/A*
3	2-propanol	$\leq 10^3$ (N_2)[117]	8.6×10^7 (N_2)	$\leq 10^3$ (N_2)[117]
4	1-butanol	*N/A*	8.0×10^7 (N_2)	*N/A*
4	2-methyl-1-propanol	*N/A*	1.3×10^8 (N_2)	*N/A*
4	2-methyl-2-propanol	*N/A*	8.4×10^5 (N_2)	*N/A*

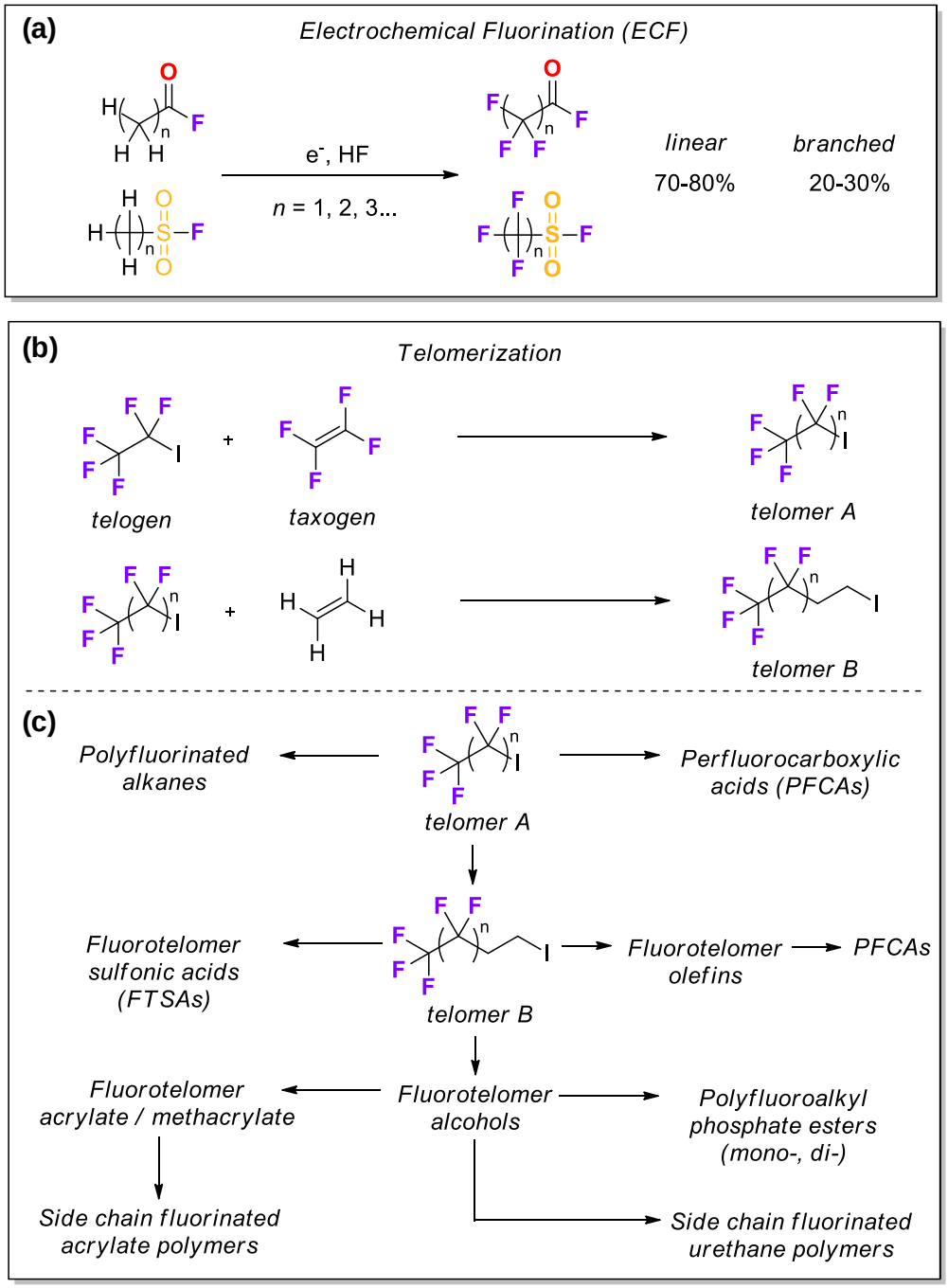

Figure 1.1 Methods to manufacture per- and polyfluoroalkyl substances (PFAS), including (a) electromchemical fluorination and (b) telomerization. (c) other classes of PFAS manufactured from telomer A and telomer B of the telomerization process.

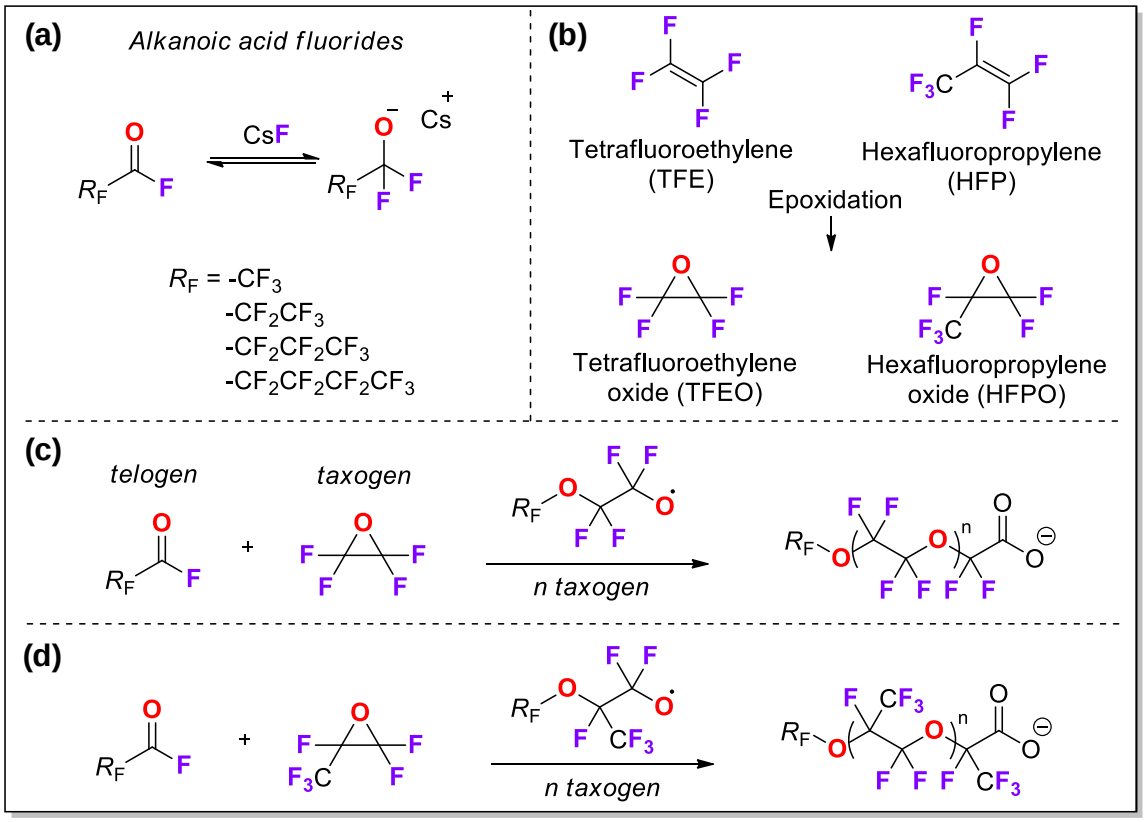

Figure 1.2 Preparation of perfluoroalkyl ether carboxylic acids (PFECAs), including (a) alkanoic acid fluoride starting material, (b) perfluoroepoxide monomer units, and examples of synthesis for (c) linear and (d) branched PFECA.

REFERENCES

(1) Wang, Z.; DeWitt, J. C.; Higgins, C. P.; Cousins, I. T. A Never-Ending Story of Per- and Polyfluoroalkyl Substances (PFASs)? *Environ. Sci. Technol.* **2017**, *51* (5), 2508–2518.

(2) Kirsh, P. *Modern Fluoroorganic Chemistry: Syntehsis, Reactivity, Applications*, 2nd ed.; Weinheim : Wiley-VCH, **2013**.

(3) Y.R. Luo. *Comprehensive Handbook of Chemical Bond Energies*; CRC Press: Boca Raton, FL, **2007**.

(4) O'Hagan, D. Understanding Organofluorine Chemistry. An Introduction to the C–F Bond. *Chem Soc Rev* **2008**, *37* (2), 308–319.

(5) Howard, J. A. K.; Hoy, V. J.; O'Hagan, D.; Smith, G. T. How Good Is Fluorine as a Hydrogen Bond Acceptor? *Tetrahedron* **1996**, *52* (38), 12613–12622.

(6) Streitwieser, A.; Holtz, David. Acidity of Hydrocarbons. XXIII. Base-Catalyzed Proton Exchange of 1H-Undecafluorobicyclo[2.2.1]Heptane and the Role of Carbon-Fluorine No-Bond Resonance. *J. Am. Chem. Soc.* **1967**, *89* (3), 692–693.

(7) Mauritz, K. A.; Moore, R. B. State of Understanding of Nafion. *Chem. Rev.* **2004**, *104* (10), 4535–4586.

(8) Yazami, R.; Shi, Q. Lithium Fluoropolymer and Fluoro-Organic Batteries. US 2008/0280191 A1, May 9, **2008**.

(9) Zhu, Y.; Casselman, M. D.; Li, Y.; Wei, A.; Abraham, D. P. Perfluoroalkyl-Substituted Ethylene Carbonates: Novel Electrolyte Additives for High-Voltage Lithium-Ion Batteries. *J. Power Sources* **2014**, *246*, 184–191.

(10) Wong, D. H. C.; Thelen, J. L.; Fu, Y.; Devaux, D.; Pandya, A. A.; Battaglia, V. S.; Balsara, N. P.; DeSimone, J. M. Nonflammable Perfluoropolyether-Based Electrolytes for Lithium Batteries. *Proc. Natl. Acad. Sci.* **2014**, *111* (9), 3327–3331.

(11) Herweck, S. A.; Gingras, P. H.; Martakos, P.; Karwoski, K. Method of Making an Expandable Fluoropolymer Device. US Patent 6395208 B1, May 28, **2002**.

(12) Grainger, D. W. Fluorinated Biomaterials. In *Biomaterials Science*; Elsevier, **2020**; pp 125–138.

(13) Ilardi, E. A.; Vitaku, E.; Njardarson, J. T. Data-Mining for Sulfur and Fluorine: An Evaluation of Pharmaceuticals To Reveal Opportunities for Drug Design and Discovery: Miniperspective. *J. Med. Chem.* **2014**, *57* (7), 2832–2842.

(14) Fujiwara, T.; O'Hagan, D. Successful Fluorine-Containing Herbicide Agrochemicals. *J. Fluor. Chem.* **2014**, *167*, 16–29.

(15) Tressaud, A. *Fluorine and the Environment: Agrochemicals, Archaeology, Green Chemistry and Water*, 1st ed.; Elsevier Science, **2006**; Vol. 2.

(16) Brown, J. F. Hydrophobic Coating Compositions and Articles Coated with Said Compositions. US Patent 8785556, July 22, **2014**.

(17) Gore, R. W. Process for Producing Porous Products. US Patent 3953566, April 27, **1976**.

(18) Plunkett, R. J. Tetrafluoroethylene Polymers. US Patent 2230654, July 1, **1939**.

(19) Bokkers, B. G. H.; van de Ven, B.; Janssen, P.; Bil, W.; van Broekhuizen, F.; Zeilmaker, M.; Oomen, A. G. *Per- and Polyfluoroalkyl Substances (PFASs) in Food Contact Materials*; RIVM Letter; 2018–0181; National Institute for Public Health and the Environment: The Netherlands, **2019**; p 112.

(20) Siegemund, G.; Schwertfeger, W.; Feiring, A.; Smart, B.; Behr, F.; Vogel, H.; McKusick, B.; Kirsch, P. Fluorine Compounds, Organic. In *Ullmann's Encyclopedia of Industrial Chemistry*; Wiley-VCH Verlag GmbH & Co. KGaA, Ed.; Wiley-VCH Verlag GmbH & Co. KGaA: Weinheim, Germany, **2016**; pp 1–56.

(21) Isobe, A.; Ishizeki, K. Fluorinated Polyether Compound, Lubricant, Liquid Composition and Article. US Patent 9598657 B2, March 21, 2017.

(22) Calm, J. M. The next Generation of Refrigerants – Historical Review, Considerations, and Outlook. *Int. J. Refrig.* **2008**, *31* (7), 1123–1133.

(23) Im, J.; Walshe-Langford, G. E.; Moon, J.-W.; Löffler, F. E. Environmental Fate of the Next Generation Refrigerant 2,3,3,3-Tetrafluoropropene (HFO-1234yf). *Environ. Sci. Technol.* **2014**, *48* (22), 13181–13187.

(24) Shen, J.; Bai, Y.; Tai, X.; Wang, W.; Wang, G. Surface Activity, Spreading, and Aggregation Behavior of Ecofriendly Perfluoropolyether Amide Propyl Betaine in Aqueous Solution. *ACS Sustain. Chem. Eng.* **2018**, *6* (5), 6183–6191.

(25) Falk, R. A. Perfluoroalkyl Anion/Perfluoroalkyl Cation Ion Pair Complexes. US Patent 4472286, September 18, **1984**.

(26) Shanghai Guangming Electroplating Plant. Jiangsu Taizhou Electrochemical Plant, Preparation of F-53 and its application in chrome mist suppression. *Shanghai Inst. Org. Chem. Chin. Acad. Sci.* **1976**, *3* (3), 27–32.

(27) Pan, Y.; Zhang, H.; Cui, Q.; Sheng, N.; Yeung, L. W. Y.; Guo, Y.; Sun, Y.; Dai, J. First Report on the Occurrence and Bioaccumulation of Hexafluoropropylene Oxide Trimer Acid: An Emerging Concern. *Environ. Sci. Technol.* **2017**, *51* (17), 9553–9560.

(28) *Fluorochemicals Market by Type (Fluorocarbons, Fluoroelastomers, Fluoropolymers, Inorganics, and Others), Application (Surfactants, Propellants, Aluminum Production, Refrigerant, Automobile, Agrochemicals, and Others), and End-Use (Electrical & Electronics, Petrochemicals, Chemicals, Aerospace, and Others): Global Opportunity Analysis and Industry Forecast, 2019–2026*; Allied Market Research: Portland, OR, **2019**; p 272.

(29) Möller, A.; Ahrens, L.; Surm, R.; Westerveld, J.; van der Wielen, F.; Ebinghaus, R.; de Voogt, P. Distribution and Sources of Polyfluoroalkyl Substances (PFAS) in the River Rhine Watershed. *Environ. Pollut.* **2010**, *158* (10), 3243–3250.

(30) Loewen, M.; Halldorson, T.; Wang, F.; Tomy, G. Fluorotelomer Carboxylic Acids and PFOS in Rainwater from an Urban Center in Canada. *Environ. Sci. Technol.* **2005**, *39* (9), 2944–2951.

(31) Björnsdotter, M. K.; Yeung, L. W. Y.; Kärrman, A.; Jogsten, I. E. Ultra-Short-Chain Perfluoroalkyl Acids Including Trifluoromethane Sulfonic Acid in Water Connected to Known and Suspected Point Sources in Sweden. *Environ. Sci. Technol.* **2019**, *53* (19), 11093–11101.

(32) Hatton, J.; Holton, C.; DiGuiseppi, B. Occurrence and Behavior of Per- and Polyfluoroalkyl Substances from Aqueous Film-Forming Foam in Groundwater Systems. *Remediat. J.* **2018**, *28* (2), 89–99.

(33) Darlington, R.; Barth, E.; McKernan, J. The Challenges of PFAS Remediation. *Mil. Eng.* **2018**, *1103* (712), 58–60.

(34) Brusseau, M. L.; Yan, N.; Van Glubt, S.; Wang, Y.; Chen, W.; Lyu, Y.; Dungan, B.; Carroll, K. C.; Holguin, F. O. Comprehensive Retention Model for PFAS Transport in Subsurface Systems. *Water Res.* **2019**, *148*, 41–50.

(35) Brusseau, M. L. Assessing the Potential Contributions of Additional Retention Processes to PFAS Retardation in the Subsurface. *Sci. Total Environ.* **2018**, 10.

(36) Munoz, G.; Budzinski, H.; Babut, M.; Lobry, J.; Selleslagh, J.; Tapie, N.; Labadie, P. Temporal Variations of Perfluoroalkyl Substances Partitioning between Surface Water, Suspended Sediment, and Biota in a Macrotidal Estuary. *Chemosphere*. **2019**, *233*, 319-326.

(37) Dasu, K.; Lee, L. S.; Turco, R. F.; Nies, L. F. Aerobic Biodegradation of 8:2 Fluorotelomer Stearate Monoester and 8:2 Fluorotelomer Citrate Triester in Forest Soil. *Chemosphere* **2013**, *91* (3), 399–405.

(38) Liu, J.; Mejia Avendaño, S. Microbial Degradation of Polyfluoroalkyl Chemicals in the Environment: A Review. *Environ. Int.* **2013**, *61*, 98–114.

(39) Shaw, D. M. J.; Munoz, G.; Bottos, E. M.; Duy, S. V.; Sauvé, S.; Liu, J.; Van Hamme, J. D. Degradation and Defluorination of 6:2 Fluorotelomer Sulfonamidoalkyl Betaine and 6:2 Fluorotelomer Sulfonate by Gordonia Sp. Strain NB4-1Y under Sulfur-Limiting Conditions. *Sci. Total Environ.* **2019**, *647*, 690–698.

(40) Gauthier, S. A.; Mabury, S. A. Aqueous Photolysis of 8:2 Fluoroteolmer Alcohol. *Environ. Toxicol. Chem.* **2005**, *24* (8), 1837.

(41) Wallington, T. J.; Hurley, M. D.; Xia, J.; Wuebbles, D. J.; Sillman, S.; Ito, A.; Penner, J. E.; Ellis, D. A.; Martin, J.; Mabury, S. A.; Nielsen, O. J.; Sulbaek Andersen, M. P. Formation of $C_7F_{15}COOH$ (PFOA) and Other Perfluorocarboxylic Acids during the Atmospheric Oxidation of 8:2 Fluorotelomer Alcohol. *Environ. Sci. Technol.* **2006**, *40* (3), 924–930.

(42) Young, C. J.; Furdui, V. I.; Franklin, J.; Koerner, R. M.; Muir, D. C. G.; Mabury, S. A. Perfluorinated Acids in Arctic Snow: New Evidence for Atmospheric Formation. *Environ. Sci. Technol.* **2007**, *41* (10), 3455–3461.

(43) Lee, H.; Mabury, S. A. Global Distribution of Polyfluoroalkyl and Perfluoroalkyl Substances and Their Transformation Products in Environmental Solids. In *Transformation Products of Emerging*

Contaminants in the Environment; Lambropoulou, D. A., Nollet, L. M. L., Eds.; John Wiley and Sons Ltd: Chichester, United Kingdom, **2014**; pp 797–826.

(44) Ahrens, L.; Bundschuh, M. Fate and Effects of Poly- and Perfluoroalkyl Substances in the Aquatic Environment: A Review: Fate and Effects of Polyfluoroalkyl and Perfluoroalkyl Substances. *Environ. Toxicol. Chem.* **2014**, *33* (9), 1921–1929.

(45) Houtz, E. F.; Higgins, C. P.; Field, J. A.; Sedlak, D. L. Persistence of Perfluoroalkyl Acid Precursors in AFFF-Impacted Groundwater and Soil. *Environ. Sci. Technol.* **2013**, *47* (15), 8187–8195.

(46) Alexandrino, D. A. M.; Ribeiro, I.; Pinto, L. M.; Cambra, R.; Oliveira, R. S.; Pereira, F.; Carvalho, M. F. Biodegradation of Mono-, Di- and Trifluoroacetate by Microbial Cultures with Different Origins. *New Biotechnol.* **2018**, *43*, 23–29.

(47) Visscher, P. T.; Culbertson, C. W.; Oremland, R. S. Degradation of Trifluoroacetate in Oxic and Anoxic Sediments. *Nature* **1994**, *369* (6483), 729–731.

(48) Kim, B. R.; Suidan, M. T.; Wallington, T. J.; Du, X. Biodegradability of Trifluoroacetic Acid. *Environ. Eng. Sci.* **2000**, *17* (6), 337–342.

(49) Key, B. D.; Howell, R. D.; Criddle, C. S. Fluorinated Organics in the Biosphere. *Environ. Sci. Technol.* **1997**, *31* (9), 2445–2454.

(50) Freeling, F.; Behringer, D.; Heydel, F.; Scheurer, M.; Ternes, T. A.; No, K. Trifluoroacetate in Precipitation: Deriving a Benchmark Data Set. *Env. Sci Technol* **2020**, 10.

(51) Burkholder, J. B.; Cox, R. A.; Ravishankara, A. R. Atmospheric Degradation of Ozone Depleting Substances, Their Substitutes, and Related Species. *Chem. Rev.* **2015**, *115* (10), 3704–3759.

(52) Wang, X.; Halsall, C.; Codling, G.; Xie, Z.; Xu, B.; Zhao, Z.; Xue, Y.; Ebinghaus, R.; Jones, K. C. Accumulation of Perfluoroalkyl Compounds in Tibetan Mountain Snow: Temporal Patterns from 1980 to 2010. *Environ. Sci. Technol.* **2014**, *48* (1), 173–181.

(53) Olsen, G. W.; Mair, D. C.; Lange, C. C.; Harrington, L. M.; Church, T. R.; Goldberg, C. L.; Herron, R. M.; Hanna, H.; Nobiletti, J. B.; Rios, J. A.; Reagen, W. K.; Ley, C. A. Per- and Polyfluoroalkyl Substances (PFAS) in American Red Cross Adult Blood Donors, 2000–2015. *Environ. Res.* **2017**, *157*, 87–95.

(54) Kudo, N.; Suzuki, E.; Katakura, M.; Ohmori, K.; Noshiro, R.; Kawashima, Y. Comparison of the Elimination between Perfluorinated Fatty Acids with Different Carbon Chain Length in Rats. *Chem. Biol. Interact.* **2001**, *134* (2), 203–216.

(55) Rappazzo, K.; Coffman, E.; Hines, E. Exposure to Perfluorinated Alkyl Substances and Health Outcomes in Children: A Systematic Review of the Epidemiologic Literature. *Int. J. Environ. Res. Public. Health* **2017**, *14* (7), 691.

(56) Zhao, S.; Zhu, L.; Liu, L.; Liu, Z.; Zhang, Y. Bioaccumulation of Perfluoroalkyl Carboxylates (PFCAs) and Perfluoroalkane Sulfonates (PFSAs) by Earthworms (*Eisenia Fetida*) in Soil. *Environ. Pollut.* **2013**, *179*, 45–52.

(57) Gomis, M. I.; Vestergren, R.; Borg, D.; Cousins, I. T. Comparing the Toxic Potency in Vivo of Long-Chain Perfluoroalkyl Acids and Fluorinated Alternatives. *Environ. Int.* **2018**, *113*, 1–9.

(58) Chen, F.; Wei, C.; Chen, Q.; Zhang, J.; Wang, L.; Zhou, Z.; Chen, M.; Liang, Y. Internal Concentrations of Perfluorobutane Sulfonate (PFBS) Comparable to Those of Perfluorooctane Sulfonate (PFOS) Induce Reproductive Toxicity in Caenorhabditis Elegans. *Ecotoxicol. Environ. Saf.* **2018**, *158*, 223–229.

(59) Yamashita, N.; Taniyasu, S.; Petrick, G.; Wei, S.; Gamo, T.; Lam, P. K. S.; Kannan, K. Perfluorinated Acids as Novel Chemical Tracers of Global Circulation of Ocean Waters. *Chemosphere*. **2008**, *70* (7), 1247–1255.

(60) Chen, H.; Reinhard, M.; Nguyen, T. V.; You, L.; He, Y.; Gin, K. Y.-H. Characterization of Occurrence, Sources and Sinks of Perfluoroalkyl and Polyfluoroalkyl Substances (PFASs) in a Tropical Urban Catchment. *Environ. Pollut.* **2017**, *227*, 397–405.

(61) González-Gaya, B.; Casal, P.; Jurado, E.; Dachs, J.; Jiménez, B. Vertical Transport and Sinks of Perfluoroalkyl Substances in the Global Open Ocean. *Environ. Sci. Process. Impacts*. **2019**, *21* (11), 1957–1969.

(62) Kwok, K. Y.; Yamazaki, E.; Yamashita, N.; Taniyasu, S.; Murphy, M. B.; Horii, Y.; Petrick, G.; Kallerborn, R.; Kannan, K.; Murano, K.; Lam, P. K. S. Transport of Perfluoroalkyl Substances (PFAS) from an Arctic Glacier to Downstream Locations: Implications for Sources. *Sci. Total Environ.* **2013**, *447*, 46–55.

(63) Taniyasu, S.; Yamashita, N.; Moon, H.-B.; Kwok, K. Y.; Lam, P. K. S.; Horii, Y.; Petrick, G.; Kannan, K. Does Wet Precipitation Represent Local and Regional Atmospheric Transportation by Perfluorinated Alkyl Substances? *Environ. Int.* **2013**, *55*, 25–32.

(64) Høisæter, Å.; Pfaff, A.; Breedveld, G. D. Leaching and Transport of PFAS from Aqueous Film-Forming Foam (AFFF) in the Unsaturated Soil at a Firefighting Training Facility under Cold Climatic Conditions. *J. Contam. Hydrol.* **2019**, *222*, 112–122.

(65) Woodard, S.; Berry, J.; Newman, B. Ion Exchange Resin for PFAS Removal and Pilot Test Comparison to GAC: WOODARD et Al. *Remediat. J.* **2017**, *27* (3), 19–27.

(66) Westreich, P.; Mimna, R.; Brewer, J.; Forrester, F. The Removal of Short-Chain and Long-Chain Perfluoroalkyl Acids and Sulfonates via Granular Activated Carbons: A Comparative Column Study. *Remediat. J.* **2018**, *29* (1), 19–26.

(67) Appleman, T. D.; Dickenson, E. R. V.; Bellona, C.; Higgins, C. P. Nanofiltration and Granular Activated Carbon Treatment of Perfluoroalkyl Acids. *J. Hazard. Mater.* **2013**, *260*, 740–746.

(68) Wang, J.; Wang, L.; Xu, C.; Zhi, R.; Miao, R.; Liang, T.; Yue, X.; Lv, Y.; Liu, T. Perfluorooctane Sulfonate and Perfluorobutane Sulfonate Removal from Water by Nanofiltration Membrane: The Roles of Solute Concentration, Ionic Strength, and Macromolecular Organic Foulants. *Chem. Eng. J.* **2018**, *332*, 787–797.

(69) Maimaiti, A.; Deng, S.; Meng, P.; Wang, W.; Wang, B.; Huang, J.; Wang, Y.; Yu, G. Competitive Adsorption of Perfluoroalkyl Substances on Anion Exchange Resins in Simulated AFFF-Impacted Groundwater. *Chem. Eng. J.* **2018**, *348*, 494–502.

(70) Ateia, M.; Alsbaiee, A.; Karanfil, T.; Dichtel, W. Efficient PFAS Removal by Amine-Functionalized Sorbents: Critical Review of the Current Literature. *Environ. Sci. Technol. Lett.* **2019**, *6* (12), 688–695.

(71) Hubbe, M. A.; Metts, J. R.; Hermosilla, D.; Blanco, M. A.; Yerushalmi, L.; Haghighat, F.; Lindholm-Lehto, P.; Khodaparast, Z.; Kamali, M.; Elliott, A. Wastewater Treatment and Reclamation: A Review of Pulp and Paper Industry Practices and Opportunities. *BioResources*. **2016**, *11* (3), 7953–8091.

(72) Xin, Z.; Rehmann, L. Application of Advanced Oxidation Process in the Food Industry. In *Advanced Oxidation Processes - Applications, Trends, and Prospects*; Bustillo-Lecompte, C., Ed.; IntechOpen, **2020**.

(73) Deng, Y.; Zhao, R. Advanced Oxidation Processes (AOPs) in Wastewater Treatment. *Curr. Pollut. Rep*. **2015**, *1* (3), 167–176.

(74) Sun, M.; Arevalo, E.; Strynar, M.; Lindstrom, A.; Richardson, M.; Kearns, B.; Pickett, A.; Smith, C.; Knappe, D. R. U. Legacy and Emerging Perfluoroalkyl Substances Are Important Drinking Water Contaminants in the Cape Fear River Watershed of North Carolina. *Environ. Sci. Technol. Lett.* **2016**, *3* (12), 415–419.

(75) Newton, S.; McMahen, R.; Stoeckel, J. A.; Chislock, M.; Lindstrom, A.; Strynar, M. Novel Polyfluorinated Compounds Identified Using High Resolution Mass Spectrometry Downstream of Manufacturing Facilities near Decatur, Alabama. *Environ. Sci. Technol.* **2017**, *51* (3), 1544–1552.

(76) Janousek, R. M.; Mayer, J.; Knepper, T. P. Is the Phase-out of Long-Chain PFASs Measurable as Fingerprint in a Defined Area? Comparison of Global PFAS Concentrations and a Monitoring Study Performed in Hesse, Germany from 2014 to 2018. *TrAC Trends Anal. Chem.* **2019**, *120*, 115393.

(77) Gebbink, W. A.; van Asseldonk, L.; van Leeuwen, S. P. J. Presence of Emerging Per- and Polyfluoroalkyl Substances (PFASs) in River and Drinking Water near a Fluorochemical Production Plant in the Netherlands. *Environ. Sci. Technol.* **2017**, *51* (19), 11057–11065.

(78) Moody, C. A.; Hebert, G. N.; Strauss, S. H.; Field, J. A. Occurrence and Persistence of Perfluorooctanesulfonate and Other Perfluorinated Surfactants in Groundwater at a Fire-Training Area at Wurtsmith Air Force Base, Michigan, USAElectronic Supplementary Information (ESI) Available: Map of Location of Wurtsmith Air Force Base, Oscoda, MI and Surrounding States. See Http://Www.Rsc.Org/Suppdata/Em/B2/B212497a/. *J. Environ. Monit.* **2003**, *5* (2), 341–345.

(79) Hu, X. C.; Andrews, D. Q.; Lindstrom, A. B.; Bruton, T. A.; Schaider, L. A.; Grandjean, P.; Lohmann, R.; Carignan, C. C.; Blum, A.; Balan, S. A.; Higgins, C. P.; Sunderland, E. M. Detection of Poly- and Perfluoroalkyl Substances (PFASs) in U.S. Drinking Water Linked to Industrial Sites, Military Fire Training Areas, and Wastewater Treatment Plants. *Environ. Sci. Technol. Lett.* **2016**, *3* (10), 344–350.

(80) Ghisi, R.; Vamerali, T.; Manzetti, S. Accumulation of Perfluorinated Alkyl Substances (PFAS) in Agricultural Plants: A Review. *Environ. Res.* **2019**, *169*, 326–341.

(81) Sznajder-Katarzyńska, K.; Surma, M.; Wiczkowski, W.; Cieślik, E. The Perfluoroalkyl Substance (PFAS) Contamination Level in Milk and Milk Products in Poland. *Int. Dairy J.* **2019**, *96*, 73–84.

(82) Tittlemier, S. A.; Pepper, K.; Seymour, C.; Moisey, J.; Bronson, R.; Cao, X.-L.; Dabeka, R. W. Dietary Exposure of Canadians to Perfluorinated Carboxylates and Perfluorooctane Sulfonate via Consumption of Meat, Fish, Fast Foods, and Food Items Prepared in Their Packaging. *J. Agric. Food Chem.* **2007**, *55* (8), 3203–3210.

(83) Christensen, K. Y.; Raymond, M.; Blackowicz, M.; Liu, Y.; Thompson, B. A.; Anderson, H. A.; Turyk, M. Perfluoroalkyl Substances and Fish Consumption. *Environ. Res.* **2017**, *154*, 145–151.

(84) Simons, J. H.; Francis, H. T.; Hogg, J. A. Production of Fluorocarbons: II. The Electrolysis of Solutions of Organic Substances in Liquid Hydrogen Fluoride. *J. Electrochem. Soc.* **1949**, *95* (2), 53–55.

(85) Buck, R. C.; Franklin, J.; Berger, U.; Conder, J. M.; Cousins, I. T.; de Voogt, P.; Jensen, A. A.; Kannan, K.; Mabury, S. A.; van Leeuwen, S. P. Perfluoroalkyl and Polyfluoroalkyl Substances in the Environment: Terminology, Classification, and Origins. *Integr. Environ. Assess. Manag.* **2011**, *7* (4), 513–541.

(86) Simons, J. H.; Habland, W. J. Production of Fluorocarbons: III. From Hydrogen Fluoride-Soluble Organic Substances. *J. Electrochem. Soc.* **1949**, *95* (2), 55–59.

(87) Simons, J. H.; Pearlson, W. H.; Brice, T. J.; Wilson, W. A.; Dresdner, R. D. Production of Fluorocarbons: IV. From Oxygen Containing Compounds. *J. Electrochem. Soc.* **1949**, *95* (2), 59–64.

(88) Brice, T. J.; Parlson, W. H.; Simons, A. H.; Simons, J. H.; Dresdner, R. D. Production of Fluorocarbons: V. From Hydrocarbons. *J. Electrochem. Soc.* **1949**, *95* (2), 64–67.

(89) Eleuterio, H. S. Polymerization of Perfluoro Epoxides. *J. Macromol. Sci. Chem.* **1972**, *6* (6), 1027–1052.

(90) Houmam, A. Electron Transfer Initiated Reactions: Bond Formation and Bond Dissociation. *Chem. Rev.* **2008**, *108* (7), 2180–2237.

(91) Taube, H.; Myers, H.; Rich, R. L. Observations on the Mechanism of Electron Transfer in Solution. *J. Am. Chem. Soc.* **1953**, *75* (16), 4118–4119.

(92) Maran, F.; Workentin, M. S. Dissociative Electron Transfer. *Electrochem. Soc. Interface.* **2002**, 6.

(93) Marcus, R. A. On the Theory of Oxidation-Reduction Reactions Involving Electron Transfer. I. *J. Chem. Phys.* **1956**, *24* (5), 966–978.

(94) Antonello, S.; Maran, F. The Role and Relevance of the Transfer Coefficient α in the Study of Dissociative Electron Transfers: Concepts and Examples from the Electroreduction of Perbenzoates. *J. Am. Chem. Soc.* **1999**, *121* (41), 9668–9676.

(95) Eberson, L. *Electron Transfer Reactions in Organic Chemistry*, 1st ed.; Springer-Verlag Berlin Heidelberg, **1987**; Vol. 25.

(96) Saveant, J. M. A Simple Model for the Kinetics of Dissociative Electron Transfer in Polar Solvents. Application to the Homogeneous and Heterogeneous Reduction of Alkyl Halides. *J. Am. Chem. Soc.* **1987**, *109* (22), 6788–6795.

(97) Antonello, S.; Maran, F. Evidence for the Transition between Concerted and Stepwise Heterogeneous Electron Transfer−Bond Fragmentation Mechanisms. *J. Am. Chem. Soc.* **1997**, *119* (51), 12595–12600.

(98) Harris, J. M.; Shafer, S. G.; Moffatt, J. R.; Becker, A. R. Prediction of SN2 Transition State Variation by the Use of More O'Ferrall Plots. *J. Am. Chem. Soc.* **1979**, *101* (12), 3295–3300.

(99) Severin, M. G.; Famia, G.; Vianello, E.; Arhalo, M. C. Competition between a Concerted and a Sequential Electron Transfer-Bond Breaking Path in Tiphenylmethyl Phenyl Sulphide Reduction. *J. Electroanal. Chem.* **1988**, *251*, 369–382.

(100) Gu, Y.; Liu, T.; Wang, H.; Han, H.; Dong, W. Hydrated Electron Based Decomposition of Perfluorooctane Sulfonate (PFOS) in the VUV/Sulfite System. *Sci. Total Environ.* **2017**, *607–608*, 541–548.

(101) Sahu, S. P.; Qanbarzadeh, M.; Ateia, M.; Torkzadeh, H.; Maroli, A. S.; Cates, E. L. Rapid Degradation and Mineralization of Perfluorooctanoic Acid by a New Petitjeanite $Bi_3O(OH)(PO_4)_2$ Microparticle Ultraviolet Photocatalyst. *Environ. Sci. Technol. Lett.* **2018**, *5* (8), 533–538.

(102) Vecitis, C. D.; Park, H.; Cheng, J.; Mader, B. T.; Hoffmann, M. R. Enhancement of Perfluorooctanoate and Perfluorooctanesulfonate Activity at Acoustic Cavitation Bubble Interfaces. *J. Phys. Chem. C.* **2008**, *112* (43), 16850–16857.

(103) Trojanowicz, M.; Bartosiewicz, I.; Bojanowska-Czajka, A.; Kulisa, K.; Szreder, T.; Bobrowski, K.; Nichipor, H.; Garcia-Reyes, J. F.; Nałęcz-Jawecki, G.; Męczyńska-Wielgosz, S.; Kisała, J. Application of Ionizing Radiation in Decomposition of Perfluorooctanoate (PFOA) in Waters. *Chem. Eng. J.* **2019**, *357*, 698–714.

(104) Singh, R. K.; Fernando, S.; Baygi, S. F.; Multari, N.; Thagard, S. M.; Holsen, T. M. Breakdown Products from Perfluorinated Alkyl Substances (PFAS) Degradation in a Plasma-Based Water Treatment Process. *Environ. Sci. Technol.* **2019**, *53* (5), 2731–2738.

(105) Dombrowski, P. M.; Kakarla, P.; Caldicott, W.; Chin, Y.; Sadeghi, V.; Bogdan, D.; Barajas-Rodriquez, F.; Chiang, S.Y. (Dora). Technology Review and Evaluation of Different Chemical Oxidation Conditions on Treatability of PFAS. *J. Environ. Cleanup Costs Technol. Tech.* **2018**, *28* (2), 135–150.

(106) Hart, E. J.; Gordon, S.; Thomas, J. K. Rate Constants of Hydrated Electron Reactions with Organic Compounds. *J. Phys. Chem.* **1964**, *68* (6), 1271–1274.

(107) Thomas, J. K. Pulse Radiolysis of Aqueous Solutions of Methyl Iodide and Methyl Bromide. The Reactions of Iodine Atoms and Methyl Radicals in Water. *J. Phys. Chem.* **1967**, *71* (6), 1919–1925.

(108) Kraus, C. A. Solutions of Metals in Non-metallic Solvents. I. General Properties of Solutions of Metals in Liquid Ammonia. *J. Am. Chem. Soc.* **1907**, *29* (11), 1557–1571.

(109) Hart, E. J. The Hydrated Electron. *Science*. **1964**, *146* (3652), 1664.

(110) Schwarz, H. A. Free Radicals Generated by Radiolysis of Aqueous Solutions. *J. Chem. Educ.* **1981**, *58* (2), 101.

(111) Buxton, G. V.; Greenstock, C. L.; Helman, W. P.; Ross, A. B. Critical Review of Rate Constants for Reactions of Hydrated Electrons, Hydrogen Atoms and Hydroxyl Radicals (·OH/·O$^-$ in Aqueous Solution. *J. Phys. Chem. Ref. Data* **1988**, *17* (2), 513–886.

(112) Anslyn, E. V.; Dougherty, D. A. *Modern Physical Organic Chemistry*; University Science Books, **2006**.

(113) Riesz, P. The Radiolysis of Acetone in Air-Free Aqueous Solutions. *J. Phys. Chem.* **1965**, *69* (4), 1366–1373.

(114) Barthel, E. R.; Martini, I. B.; Schwartz, B. J. Direct Observation of Charge-Transfer-to-Solvent (CTTS) Reactions: Ultrafast Dynamics of the Photoexcited Alkali Metal Anion Sodide (Na$^-$). *J. Chem. Phys.* **2000**, *112* (21), 9433–9444.

(115) Sauer, M. C.; Crowell, R. A.; Shkrob, I. A. Electron Photodetachment from Aqueous Anions. 1. Quantum Yields for Generation of Hydrated Electron by 193 and 248 nm Laser Photoexcitation of Miscellaneous Inorganic Anions. *J. Phys. Chem. A*. **2004**, *108* (25), 5490–5502.

(116) Hayon, E.; Treinin, A.; Wilf, J. Electronic Spectra, Photochemistry, and Autoxidation Mechanism of the Sulfite-Bisulfite-Pyrosulfite Systems. SO_2^-, SO_3^-, SO_4^-, and SO_5^- Radicals. *J. Am. Chem. Soc.* **1972**, *94* (1), 47–57.

(117) Neta, P.; Huie, R. E.; Ross, A. B. Rate Constants for Reactions of Inorganic Radicals in Aqueous Solution. *J. Phys. Chem. Ref. Data*. **1988**, *17* (3), 259.

(118) Eriksen, T. E. pH Effects on the Pulse Radiolysis of Deoxygenated Aqueous Solutions of Sulphur Dioxide. *J. Chem. Soc. Faraday Trans. 1 Phys. Chem. Condens. Phases*. **1974**, *70*, 208.

(119) Deister, Ursula.; Warneck, Peter. Photooxidation of Sulfite (SO_3^{2-}) in Aqueous Solution. *J. Phys. Chem.* **1990**, *94* (5), 2191–2198.

(120) Littlejohn, D.; Wang, Y.; Chang, S. G. Oxidation of Aqueous Sulfite Ion by Nitrogen Dioxide. *Environ. Sci. Technol.* **1993**, *27* (10), 2162–2167.

(121) Neta, P.; Huie, R. E. Free-Radical Chemistry of Sulfite. *Environ. Health Perspect.* **1985**, *64*, 209–217.

(122) Tsitonaki, A.; Petri, B.; Crimi, M.; Mosbæk, H.; Siegrist, R. L.; Bjerg, P. L. In Situ Chemical Oxidation of Contaminated Soil and Groundwater Using Persulfate: A Review. *Crit. Rev. Environ. Sci. Technol.* **2010**, *40* (1), 55–91.

(123) Guan, Y.-H.; Ma, J.; Li, X.-C.; Fang, J.-Y.; Chen, L.-W. Influence of PH on the Formation of Sulfate and Hydroxyl Radicals in the UV/Peroxymonosulfate System. *Environ. Sci. Technol.* **2011**, *45* (21), 9308–9314.

(124) Huie, R. E.; Neta, P. Chemical Behavior of Sulfur Trioxide (SO_3^-) and Sulfur Pentoxide (SO_5^-) Radicals in Aqueous Solutions. *J. Phys. Chem.* **1984**, *88* (23), 5665–5669.

(125) Karoui, H.; Hogg, N.; Fréjaville, C.; Tordo, P.; Kalyanaraman, B. Characterization of Sulfur-Centered Radical Intermediates Formed during the Oxidation of Thiols and Sulfite by Peroxynitrite: ESR-Spin Trapping and Oxygen Uptake Studies. *J. Biol. Chem.* **1996**, *271* (11), 6000–6009.

(126) Ball, D. L.; Edwards, J. O. The Kinetics and Mechanism of the Decomposition of Caro's Acid. I. *J. Am. Chem. Soc.* **1956**, *78* (6), 1125–1129.

(127) McNaught, A. D.; Wilkson, A. *IUPAC. Compendium of Chemical Terminology (the "Gold Book")*, 2nd ed.; Blackwell Scientific Publications: Oxford, 1997.

(128) Matheson, M. S.; Rabani, J. Pulse Radiolysis of Aqueous Hydrogen Solutions. I. Rate Constants for Reaction of e_{aq}^- with Itself and Other Transients. II. The Interconvertibility of e_{aq}^- and H. *J. Phys. Chem.* **1965**, *69* (4), 1324–1335.

(129) Stalder, C. J.; Chao, S.; Wrighton, M. S. Electrochemical Reduction of Aqueous Bicarbonate to Formate with High Current Efficiency near the Thermodynamic Potential at Chemically Derivatized Electrodes. *J. Am. Chem. Soc.* **1984**, *106* (12), 3673–3675.

(130) Russell, P. G.; Kovac, N.; Srinivasan, S.; Steinberg, M. The Electrochemical Reduction of Carbon Dioxide, Formic Acid, and Formaldehyde. *J. Electrochem. Soc.* **1977**, *124* (9), 1329–1338.

(131) Stalder, C. J.; Chao, S.; Summers, D. P.; Wrighton, M. S. Supported Palladium Catalysts for the Reduction of Sodium Bicarbonate to Sodium Formate in Aqueous Solution at Room Temperature and One Atmosphere of Hydrogen. *J. Am. Chem. Soc.* **1983**, *105* (20), 6318–6320.

(132) Mandler, D.; Willner, I. Effective Photoreduction of Carbon Dioxide/Bicarbonate to Formate Using Visible Light. *J. Am. Chem. Soc.* **1987**, *109* (25), 7884–7885.

(133) Goren, Z.; Willner, I.; Nelson, A. J.; Frank, A. J. Selective Photoreduction of Carbon Dioxide/Bicarbonate to Formate by Aqueous Suspensions and Colloids of Palladium-Titania. *J. Phys. Chem.* **1990**, *94* (9), 3784–3790.

(134) Anbar, M.; Hart, E. J. The Reaction of Haloaliphatic Compounds with Hydrated Electrons. *J. Phys. Chem.* **1965**, *69* (1), 271–274.

(135) Clifton, C. L.; Huie, R. E. Rate Constants for Hydrogen Abstraction Reactions of the Sulfate Radical, SO_4^-. Alcohols. *Int. J. Chem. Kinet.* **1989**, *21* (8), 677–687.

CHAPTER 2: DEFLUORINATION OF PER- AND POLYFLUOROALKYL SUBSTANCES (PFASs) WITH HYDRATED ELECTRONS: STRUCTUREAL DEPENDENCE AND IMPLICATIONS TO PFAS REMEDIATION AND MANAGEMENT

Abstract

This study investigates critical structure−reactivity relationships within 34 representative per- and polyfluoroalkyl substances (PFASs) undergoing defluorination with UV-generated hydrated electrons. While C_nF_{2n+1}−COO^- with variable fluoroalkyl chain lengths (n = 2 to 10) exhibited a similar rate and extent of parent compound decay and defluorination, the reactions of telomeric C_nF_{2n+1}−CH_2CH_2−COO^- and C_nF_{2n+1}−SO_3^- showed an apparent dependence on the length of the fluoroalkyl chain. Cross comparison of experimental results, including different rates of decay and defluorination of specific PFAS categories, the incomplete defluorination from most PFAS structures, and the surprising 100% defluorination from CF_3COO^-, leads to the elucidation of new mechanistic insights into PFAS degradation. Theoretical calculations on the C−F bond dissociation energies (BDEs) of all PFAS structures reveal strong relationships among (*i*) the rate and extent of decay and defluorination, (*ii*) head functional groups, (*iii*) fluoroalkyl chain length, and (*iv*) the position and number of C−F bonds with low BDEs. These relationships are further supported by the spontaneous cleavage of specific bonds during calculated geometry optimization of PFAS structures bearing one extra electron, and by the product analyses with high-resolution mass spectrometry. Multiple reaction pathways, including H/F exchange, dissociation of terminal functional groups, and decarboxylation-triggered HF elimination and hydrolysis, result in the formation of variable defluorination products. The selectivity and ease of C−F bond cleavage highly depends on molecular structures. These findings provide critical information for developing

PFAS treatment processes and technologies to destruct a wide scope of PFAS pollutants and for designing fluorochemical formulations to avoid releasing recalcitrant PFASs into the environment.

2.1 Introduction

The manufacturing, application, and disposal of fluorochemicals since the 1940s have led to worldwide pollution by per- and polyfluoroalkyl substances (PFASs).[1,2] The U.S. EPA listed C7, C8, and C9 perfluorinated carboxylic acids (PFCAs) and C4, C6, and C8 perfluorinated sulfonic acids (PFSAs) on the Third Unregulated Contaminant Monitoring Rule (UCMR3) in 2012,[3] and established health advisory levels for C8 perfluorooctanoic acid (PFOA) and perfluorooctanesulfonic acid (PFOS) in drinking water in 2016.[4] Very recently, the states of Vermont[5] and Massachusetts[6] have updated the health advisory for five of the six PFASs in the UCMR 3 list (except for the C4 perfluorobutanesulfonic acid PFBS). The state of New Jersey adopted the maximum contaminant level of C9 perfluorononanoic acid (PFNA),[7] and the state of North Carolina established the health advisory level for perfluoro-2-propoxypropanoic acid (GenX).[8] Regulation has triggered substantial interest and efforts in developing PFAS treatment technologies.[9,10] While physical separation (e.g., carbon adsorption, membrane filtration, and ion exchange) enables rapid PFAS removal from water,[11−13] the enriched PFASs in physical separation wastes must be destroyed. Groundwater remediation and the treatment of PFASs in obsolete products and industrial wastes also require cost-effective destruction methods. Due to the challenges in cleaving highly stable C−F bonds (i.e., defluorination),[10] novel technologies such as electrochemical,[14−17] sonochemical,[18−20] photocatalytic,[21−23] mechanochemical,[24,25] plasmatic,[26] radiolytic,[27] and other oxidative and reductive methods[9,28] have been developed for the defluorination of C8 PFOA and/or PFOS. However, PFASs have often been applied in complicated mixtures. For example, aqueous film-forming foams (AFFF) for fire-fighting contain at least hundreds of PFAS structures,[29−31] most of which contain a fluorocarbon moiety with variable

lengths and head groups connecting to highly diverse organic moieties (Figure 2.1). A large diversity of PFAS structures has been identified in water bodies polluted by fluorochemical industries,[32−35] fire-fighting practices,[29,30,36] and landfill leachates.[37] The extending list of regulated PFASs calls for the investigation into the treatment of PFASs beyond PFOA and PFOS. A fundamental and critical question is thus raised regarding the remediation of PFAS pollution: would the technologies developed for PFOA/PFOS defluorination remain effective for other PFAS structures? Alternatively, what structural factors control the rate and extent of PFAS defluorination?

Studies on the chemical destruction of other PFASs beyond PFOA/PFOS (e.g., shorter chain analogues or new structures) have been very limited. While a small number of studies has tested individual PFCAs and PFSAs in the C4−C9 range[38−40] and nonlinear structures,[41−43] there has been little information available regarding the reactivity of many common PFASs such as fluorotelomers[29,30,34,37] and short-chain acids.[36,44] It is thus imperative to obtain a thorough understanding of the structure−reactivity relationship for (1) developing and assessing technologies to treat a broad spectrum of PFASs already released into the environment and (2) designing or modifying fluorochemical formulations to prevent future release of highly recalcitrant PFASs. Hydrated electrons (e_{aq}^-) can be generated from H_2O or specific chemicals under UV irradiation.[45,46] Being highly reactive in reduction reactions, the e_{aq}^- has demonstrated excellent performance in cleaving C−F bonds. Since the pioneering work by Park *et al.*,[40] recent studies have investigated different e_{aq}^- source chemicals (e.g., iodide,[40] sulfite,[47] and indole[48]), e_{aq}^- generation strategies,[49] and UV irradiation[50,51] for the defluorination of PFOA and PFOS in aqueous solutions. At ambient temperature and in slightly basic solution (i.e., pH 9−10), a significant portion (50−90%) of C−F bonds can be cleaved from legacy PFOA[47] and PFOS[52] and the emerging GenX.[41] The dominant reactive species in the recently reported plasmatic defluorination is also e_{aq}^-.[26] Still, the feasibility

of treating a wide spectrum of PFASs with e_{aq}^- and the underlying structure−reactivity relationship remain unknown. Herein, we report on a series of unexplored but critical trends in the structural dependence for PFAS defluorination. By examining a broad collection of 34 PFAS structures with various head groups and chain lengths, this study provides comprehensive mechanistic insights, and will significantly contribute to the advancement of technologies and strategies for PFASs remediation and management.

2.2 Materials and Methods

Detailed information on chemicals and the preparation of PFAS stock solutions are described in Appendix A (AppxA). For the photochemical PFAS defluorination, a 600 mL solution containing 25 μM PFAS, 10 mM Na_2SO_3, and 5 mM $NaHCO_3$ (pH 9.5, adjusted by 1 M NaOH) was loaded in a closed-system photoreactor (cooled with 20 °C circulating water). The 18 W low-pressure mercury lamps (254 nm narrow band irradiation) were used for all reactions. Aliquots of solution were taken at time intervals for up to 48 h. Detailed reaction setup and rationales for the selected experimental conditions are described in Appx A. The concentration of fluoride ion (F^-) released from PFASs was determined by an ion selective electrode (ISE). The accuracy of F^- measurement by the ISE in the solution matrix was validated by standard calibration and ion chromatography. The concentration of PFAS parent compounds was determined with liquid chromatography−triple quadrupole mass spectrometry (LC−MS/MS). Transformation product analyses were conducted by liquid chromatography−high resolution mass spectrometry (LC−HRMS). Full details of sample analysis are described in Appx A. Theoretical calculations were performed according to the method used by Liu *et al.*[42] with details found in Appx A.

2.3 Results and Discussion

2.3.1 Decay and Defluorination of PFASs.

Perfluorocarboxylic Acids (PFCAs). Figure 2.2a shows the decay of n = 1−10 PFCAs ($C_nF_{2n+1}COO^-$). Except for CF_3COO^-, the decay of PFCAs was complete within 8 to 12 h. Based on the concentration of F^- released from the PFAS molecules into the aqueous solution, the overall defluorination ratio (deF%) is defined in Equation 2.1):

$$\textit{overall}\ \text{deF\%} = \frac{C_F}{C_0 \times N_{C\text{-}F}} \times 100\% \qquad (2.1)$$

where C_{F^-} is the molar concentration of F^- ion released in solution, C_0 is the initial molar concentration of the parent PFAS, and N_{C-F} is the number of C−F bonds in the parent PFAS molecule. The deF% for n = 2−10 PFCAs gradually leveled off to ~55% within 24 to 48 h (Figure 2.2b and Table 2.1). LC−MS/MS quantification of shorter-chain PFCAs and LC−HRMS analysis of partially defluorinated products did not fully close the mass balance with the identified charged intermediates and end products (see *PFAS Degradation Product Analysis* section). A surprising result is the 100% defluorination from trifluoroacetate (TFA, CF_3COO^-), while the rate of its degradation was slower than all $n \geq 2$ PFCAs. The contrasting results between n = 1 TFA and $n \geq 2$ PFCAs suggest new mechanistic insights (to be discussed in later sections). Transformation product analysis and discussion of degradation pathways for all PFAS categories examined in this study are presented in later sections.

Fluorotelomer Carboxylic Acids (FTCAs). We extended the investigation from PFCAs ($C_nF_{2n+1}COO^-$) to FTCAs ($C_nF_{2n+1}-CH_2CH_2-COO^-$) since a large variety of PFASs synthesized via telomerization contains one or more $-CH_2-$ groups between the fluoroalkyl chain and the headgroup (Figure 2.1).[53] In comparison to PFCAs, the presence of $-CH_2CH_2-$ in FTCAs resulted in significant persistence and dependence on C_nF_{2n+1} length for both parent compound decay

(Figure 2.2c) and F^- release (Figure 2.2d and Table 2.1). Significant degradation was observed only for $n \geq 5$ FTCAs. After 48 h, the highest *overall* deF% was 37% for $C_8F_{17}–CH_2CH_2–COO^-$. This ratio was lower than those for the PFCAs either with the same length of fluorocarbon chain, $C_8F_{17}COO^-$ (58%) or with the same length of the whole molecule, $C_8F_{17}–CF_2CF_2–COO^-$ (59%). Because a significant portion of the FTCA parent compounds still remained, the *molecular* deF% that considers the degraded portion (DG) of the parent compound is defined in Equation 2.2:

$$\textit{molecular}\ \text{deF\%} = \frac{\textit{overall}\ \text{deF\%}}{\text{DG}} \tag{2.2}$$

For the three relatively long-chain FTCAs (n = 6, 7 and 8) that showed both significant parent compound decay (15%, 37%, and 85%, respectively) and overall deF% (7.4%, 17%, and 37%, respectively) after 48 h, their corresponding molecular deF% are similar (49%, 46%, and 44% respectively). The results suggest that while FTCA parent compounds are much more recalcitrant than PFCAs, (1) longer C_nF_{2n+1} in FTCAs provide higher reactivity, and (2) the reaction intermediates from the decayed portion of FTCAs provided ~50% defluorination in a relatively fast manner, regardless of the recalcitrance of the parent FTCAs.

Per- and Polyfluoro Dicarboxylic Acids (PFdiCAs). The comparison between PFCAs and FTCAs has clearly suggested that the direct linkage between −COO− and C_nF_{2n+1} promotes defluorination. We further examined such effects in PFdiCAs ($^-OOC–C_nF_{2n}–COO^-$), which have also been detected recently in water environments.[34] As shown in Figure 2.2e, the decay of parent PFdiCA compounds (n = 3−10) were complete within 4−8 h. The rates are faster than those for PFCAs (8−12 h, Figure 2.2a). The overall deF% at 48 h (identical to the molecular deF%, since the parent compound decay was complete for all PFCAs and PFdiCAs) were ~67% regardless of C_nF_{2n} length (Figure 2.2f and Table 2.1) and deeper than those for PFCAs (~55%). Similar to the case of CF_3COO^-, for $^-OOC–CF_2CF_2–COO–$ (n = 2) where each CF_2 is directly linked to $–COO^-$, its decay

and defluorination were significantly slower than long-chain PFdiCAs. Interestingly, the rate of decay for $^{-}OOC{-}CF_2{-}COO^{-}$ (n = 1) was similar to other long-chain PFdiCAs while the deF% was higher than all other PFdiCAs. However, the deF% was limited to 81% in comparison to the 100% for CF_3COO^{-}. In comparison to perfluorinated PFdiCA structures, retarded decay and defluorination of $^{-}OOC{-}CF_2{-}CH_2{-}COO^{-}$ was observed (the "n = 1 telo*" in Figure 2.2e and f).

Perfluoroalkanesulfonic Acids (PFSAs). With the different effects of $-COO^{-}$ versus $-CH_2CH_2-COO^{-}$ on defluorination observed, it is intriguing to also probe the effect of $-SO_3^{-}$ on the treatment of $C_nF_{2n+1}SO_3^{-}$. Like the FTCAs, the decay (Figure 2.2g) and defluorination (Figure 2.2h and Table 2.1) of n =4, 6, and 8 PFSAs showed significant dependence on chain length. This trend agrees with the study by Park *et al.*,[40] where iodide was used as the source of e_{aq}^{-}. In contrast to the almost complete defluorination of CF_3COO^{-}, the n = 1 $CF_3SO_3^{-}$ showed negligible decay and defluorination. Thus, the effect of $-SO_3^{-}$ on e_{aq}^{-} mediated defluorination is vastly different from that of $-COO^{-}$. Similar with the FTCAs, n = 6 and n = 8 PFSAs that showed significant parent compound decay (50% and 96%, respectively) and *overall* deF% (32% and 57%, respectively) exhibited similar *molecular* deF% (64% and 59%, respectively) after 48 h. Similar results on PFOS degradation were found in a study by Sun *et al.*,[49] where ~50% *molecular* average deF% was observed for reactions in various experimental settings. Thus, like FTCAs, although PFSAs with different chain lengths showed varying rates of parent compound decay, the defluorination from the decayed portion was relatively fast toward a similar extent.

2.3.2 Structural Effects and Mechanism insights on PFAS degradation.

The experimental results have clearly shown that the rate of PFAS decay and defluorination highly depend on both the headgroup and the fluoroalkyl chain length. The direct linkage between the fluoroalkyl chain and $-COO^{-}$ seems critical for a fast defluorination reaction. As shown in Figure 2.2, the decay of all $n \geq 2$ $C_nF_{2n+1}COO^{-}$ proceeded at a faster pace than F^{-} release, indicating

that the degradation of reaction intermediates was slower than the transformation of parent structures. In contrast, the decay of FTCA and PFSA parent structures (e.g., n = 6/7/8 C_nF_{2n+1}−CH_2CH_2−COO^- and n = 6/8 $C_nF_{2n+1}SO_3^-$) limits the processes of F^- release, suggesting that the degradation of reaction intermediates was faster than the decay of parent structures. Results from a series of theoretical calculations and product analyses suggest deeper insights into the mechanisms and pathways for the reductive defluorination mediated by e_{aq}^-.

Theoretical Calculations of C−F Bond Dissociation Energies (BDEs). The C−F BDEs in all PFAS structures were calculated with density functional theory (DFT) in conjunction with an SDM polarizable continuum model (see App A for computational details). The full collection of BDE data is summarized in Tables A.1−A.8, and representative results are shown in Figure 2.3. As expected, BDEs of all primary C−F bonds (i.e., bonds on the terminal $-CF_3$; 117.8−123.4 kcal mol^{-1}) are higher than all secondary C−F bonds (i.e., bonds on $-CF_2-$; 106.4−113.6 kcal mol^{-1}).[42] In general, lower BDEs for both primary and secondary C−F bonds are observed in PFASs with longer fluoroalkyl chains (Figure 2.3a−c and h, i). This trend may explain why the rate of parent compound degradation was faster for longer chain FTCAs and PFSAs, where more $-CF_2-$ functional groups in the middle of the fluoroalkyl chains have low BDEs (typically ≤107.5 kcal mol^{-1}). We note that the "decay" of a parent compound only needs one bond to be cleaved. Considering our calculation results and a previous theoretical study[54] where the central $-CF_2-$ in a fluoroalkyl chain was found to have the highest affinity to the "extra" electron (i.e., e_{aq}^- in this study), we propose that the first defluorination occurs at a middle $-CF_2-$ group in long-chain (typically $n \geq 5$) FTCA and PFSA structures. As for PFCAs and PFdiCAs, the C−F BDEs for the α-position $-CF_2-$ (i.e., adjacent to $-COO^-$; 106.5−107.3 kcal mol^{-1}, Figure 2.3e and g) are all lower than those of α-position C−F bonds in FTCAs and PFSAs (109.2−113.6 kcal mol^{-1}). From the experimental results, it appears that the α-position C−F bonds may contribute to the high reactivity

of PFCAs. This is also supported by the faster decay and higher defluorination ratio from PFdiCAs rather than from PFCAs by having two $-COO^-$ head groups (Figure 2.3g vs e) and lacking primary C−F bonds. However, the similarly low BDEs for *β*-position C−F bonds in PFSAs (Figure 2.3i vs e) did not promote the reaction of short-chain $C_4F_9-SO_3^-$ structure (Figure 2.2g), indicating that the BDE of individual bonds may not be the only factor determining the rate of reaction.

Spontaneous Bond Cleavage in Electron-Added PFAS Radical Anion Structures. Since the defluorination of PFASs occurred upon the reaction with e_{aq}^-, we further conducted DFT calculations of C−F BDEs of the radical anion after the original PFAS anion received an "extra" electron:

$$C_nF_{2n+1}–COO^- + e_{aq}^- \rightarrow C_nF_{2n+1}–COO\bullet^{2-} \quad (2.3)$$

To our surprise, when a geometry optimization was applied to the radical anions of PFCAs, FTCAs, and PFSAs, a spontaneous bond stretching was observed (Figure 2.4). One *α*-position C−F bond in $C_6F_{13}-COO\bullet^{2-}$ was stretched to 4.5 Å, which indicates bond cleavage. The $C_4F_9-COO\bullet^{2-}$ and $C_8F_{17}-COO\bullet^{2-}$ analogs showed similar bond cleavage of *α*-position C−F bonds (Figure A.2). Hence, while the spontaneous bond cleavage makes it difficult to calculate BDEs in the unstable $PFAS\bullet^{2-}$, the calculation results for the original PFCA anions are informative for mechanistic interpretation or prediction of the reactions with e_{aq}^-. As for FTCA radical anions, C−F bond stretching was observed in the middle of the fluorocarbon chain in $C_6F_{13}-CH_2CH_2-COO\bullet^{2-}$ (Figure 2.4). Although $n = 4$ and $n = 8$ FTCA radical anions did not show similar C−F bond stretching, the result from the $n = 6$ structure has already suggested the possibility of middle-chain C−F bond cleavage upon the reaction between FTCA anions and e_{aq}^- (Figure A.4). The C−S bond stretching was observed for $n = 4$, 6, and 8 $C_nF_{2n+1}-SO_3\bullet^{2-}$, indicating the dissociation of the sulfonate group upon the reaction between PFSA anions and e_{aq}^- (Figure A.3). This result agrees with the previous mechanistic interpretation on PFOS degradation, where the C−S bond cleavage led to the formation

of PFOA.[50] However, we highlight that calculations of C−F and C−S bond cleavage are not the sole degradation pathways for each category of PFASs (see below).

PFAS Degradation Product Analysis. In previous studies on PFOA/PFOS defluorination with e_{aq}^-, the total concentration of all shorter-chain PFCA products contributed to <3% of the initial PFOA/PFOS concentration.[47,50] Here we used suspect screening of LC−HRMS data to identify other plausible products beyond the shorter-chain PFCAs (all results collected in Appendix Tables S9−S21). As shown in Figure 2.5a and Table A.11, the degradation of C_7F_{15}−COO^- (PFOA, initial concentration 25 μM) produced at least two partially defluorinated products, $C_7F_{14}H$−COO^- and $C_7F_{13}H_2$−COO^-, with the highest peak area of 2.42×10^8 at 4 h and 3.63×10^7 at 48 h, respectively. As analytical standards are not available for accurate quantification of those two products, the peak area is used to roughly estimate the relative abundance in comparison to the parent compound (assuming the ionization efficiencies vary within 1 order of magnitude). From the data, the max. peak intensities for $C_7F_{14}H$−COO^- (upon one H/F exchange) and $C_7F_{13}H_2$−COO^- (upon two H/F exchanges) were 1 and 2 orders of magnitude lower than the parent C_7F_{15}−COO^-, respectively. We point out that as reaction intermediates are subject to further degradation, the accumulative generation of these species could be much higher than the maximum concentration observed at a single time point. The shorter-chain PFHpA anion C_6F_{13}−COO^- was also observed with the max. concentration of 265 nM at 1 h, corresponding to 1.1% of the initial PFOA. Low-intensity peaks ($<5 \times 10^6$ but higher than the arbitrary 10^5 threshold used for product identification) for other anions were also observed (summarized in Table A.11), such as $C_7F_{12}H_3$−COO^-, $C_7F_{11}H_4$−COO^-, and $C_7F_9H_6$−COO^- (i.e., three, four, and six H/F exchanges from PFOA), as well as $C_6F_{12}H$−COO^- and $C_6F_9H_4$−COO^- (i.e., one and four H/F exchanges from the product PFHpA), and even shorter-chain $C_5F_{10}H$−COO^- (i.e., one H/F exchange from the product PFHxA). The detection of products with more than two H/F exchanges from PFOA and PFHpA suggests that,

the weak C−F bonds in the middle of the long fluoroalkyl chain in PFCAs are also susceptible to cleavage. To further understand the fate of the chain-shortened PFHpA generated from PFOA degradation, we also characterized the products from the degradation of pure PFHpA (Figure 2.5b). Very similar to the degradation of PFOA, three major products from PFHpA are single-H/F-exchange product $C_6F_{12}H{-}COO^-$ (peaked at 4 h), double-H/F-exchange product $C_6F_{11}H_2{-}COO^-$ (peaked at 12 h), and the shorter chain PFHxA (peaked at 2 h, 1.3% of the added PFHpA). Further investigations of longer (e.g., PFDA and PFNA) and shorter PFCAs (e.g., PFHxA) also revealed very similar trends (Figure A.5 and Tables A.9−A.13). From the formation curves of the three major products, the maximum intensity of shorter chain PFCAs appeared earlier than those of the two H/F exchange products. Therefore, the degradation of PFCAs have at least two independent pathways, (*i*) H/F exchange without chain-shortening and (*ii*) formation of shorter-chain PFCAs. Specifically, the $C_nF_{2n-1}H_2{-}COO^-$ built up in the reactions of all PFCAs (Figure A.5). We propose that the most probable structure for this product is $C_{n-1}F_{2n-1}{-}CH_2{-}COO^-$ (i.e., double H/F exchanges on the α-position carbon) for the following reasons. First, according to the calculated C−F BDEs in the $C_nF_{2n+1}{-}COO^-$ and the spontaneous C−F cleavage from the e_{aq}^- added $C_nF_{2n+1}{-}COO^{\bullet 2-}$, the first H/F exchange is highly likely to occur at the α-position. Second, if the first C−F bond is replaced by a C−H bond, the remaining C−F bond on the same carbon is significantly weakened (Text A.1) to become even more susceptible for the following H/F exchange. Third, as suggested by the recalcitrant decay of FTCAs, the separation of the fluoroalkyl chain and the $-COO^-$ with one $-CH_2-$ linker is the most probable structure showing recalcitrance. To further test the hypothesis regarding the slow reaction of $C_nF_{2n+1}{-}CH_2{-}COO^-$ with only one $-CH_2-$ linker, we investigated a commercially available structure, $CF_3{-}CH_2{-}COO^-$ (structural analogues with longer fluorocarbon chains were not available to test). Compared to the perfluorinated $CF_3{-}CF_2{-}COO^-$ (53% defluorination) and $CF_3{-}COO-$ (100% defluorination), the

structure with a single $-CH_2-$ linker indeed showed very sluggish reactivity with only 2.2% defluorination measured after 48 h. As for PFSAs, we analyzed the products from the reactions of PFOS and PFHxS that exhibited significant decay and defluorination. Results suggest that the calculated spontaneous C−S cleavage is one of the two reaction pathways, the other being the H/F exchange without chain shortening. For PFOS degradation, products with one ($C_8F_{16}H-SO_3^-$), two ($C_8F_{15}H_2-SO_3^-$), three ($C_8F_{14}H_3-SO_3^-$), and four H/F exchanges ($C_8F_{13}H_4-SO_3^-$) on the eight-carbon PFOS backbone were observed in significant abundance (Figure 2.5c and Table A.14). The intensity of those four peaks were 2 orders of magnitude lower than the parent PFOS. Meanwhile, a series of PFCAs (from PFOA to PFBA) were also observed with low intensities (Table A.16). However, these PFCAs showed a similar abundance in the product mixture from PFOS degradation. For comparison, in the experiments starting from individual PFCAs, the chain-shortened daughter PFCA was in much lower abundance than the parent PFCA (Figure 2.5a and b). Thus, the shorter-chain PFCAs observed in PFOS degradation were not generated from the sequential chain-shortening from PFOA. We found that the commercial PFOS reagent actually contained a small portion of shorter chain PFSAs such as PFHpS, PFHxS, and PFBS, and their corresponding H/F exchange products were also detected (Table A.15). Thus, the formation of PFCAs in relatively high abundance for all chain lengths might be attributed to the C−S cleavage of the corresponding PFSAs. Similar product profiles were observed for PFHxS degradation (Figure 2.5d and Tables A.17−19). The product analysis on the degradation of the telomeric $C_8F_{17}-CH_2CH_2-COO^-$ (Figure 2.5e and f; Tables A.20 and A.21) also suggested two reaction pathways. First, H/F exchange products were observed, for example, $C_8F_{16}H-CH_2CH_2-COO^-$ (peaked at 4 h) and $C_8F_{15}H_2-CH_2CH_2-COO^-$ (peaked at 36 h). Based on our calculation results (Figure 2.3 and Table A.6), the most probable H/F exchange should occur in the middle of the long fluoroalkyl chain. Recall that the decay of shorter-chain FTCAs was very sluggish, most probably

due to the lack of low BDE C−F bonds. However, the formation of $C_9F_{12}H_5O_2^-$, $C_8F_{10}H_5O_2^-$, and $C_7F_8H_5O_2^-$ (most probably with the structure $C_nF_{2n}H{-}CH_2CH_2{-}COO^-$) cannot be explained at this moment. Unlike PFSA reagents that contain multiple shorter-chain impurities, the shorter-chain FTCAs were not detected in t = 0 samples (Table A.20), indicating that they were indeed generated from the chain-shortening of the n = 8 FTCA. It is not yet clear how the fluorocarbon chain was shortened without losing the $-CH_2CH_2-COO^-$ headgroup. Still, low intensities of PFCAs were observed (e.g., PFBA shown in Table A.21), indicating the dissociation of $-CH_2CH_2-COO^-$ as the second mechanism for FTCA degradation.

2.3.3 Overall Reaction Mechanisms.

Based on the experimentally observed PFAS decay and defluorination, DFT calculations, and degradation product analyses, the reaction mechanisms are summarized in Scheme 2.1. PFCAs ($C_nF_{2n+1}-COO^-$) undergo two pathways upon reaction with e_{aq}^- (Scheme 2.1a). First, two H/F exchanges occur sequentially on the α-position and yield $C_{n-1}F_{2n-1}-CH_2-COO^-$, which has high recalcitrance. If the fluorocarbon chain is long, it is also possible to have additional C−F bond cleavage from middle $-CF_2-$ groups. Second, shorter-chain PFCAs are generated most probably from a decarboxylation mechanism (Scheme 2.1b), yielding an unstable perfluorinated alcohol ($C_nF_{2n+1}-OH$) that is subject to HF elimination.[55] The resulted acyl fluoride is hydrolyzed to release the second fluoride ion, and the shorter-chain PFCA ($C_{n-1}F_{2n-1}-COO^-$) thus forms and enters the next reaction cycle.[56] This decarboxylation−hydroxylation−elimination−hydrolysis (*DHEH*) pathway has been mainly inferred from prior literature[47,50,55,56] and few recent studies have provided further insights on the stability of perfluorinated alcohol. However, there is some indirect evidence to support the *DHEH* mechanism. First, perfluorinated $C_nF_{2n+1}-OH$ has been rarely reported as a bulk chemical. Instead, the widely used fluorinated alcohols are telomeric $C_nF_{2n+1}-CH_2-OH$.[57,58] This fact may reflect the instability of $C_nF_{2n+1}-OH$. Second, an analogous structure, FCH_2-OH, has

only been observed spectroscopically under low temperatures in a mixture of HCOH and HF (i.e., $FCH_2{-}OH \leftrightarrow HCOH + HF$).[59] This equilibrium supports the mechanism of HF elimination from structures with one −F and one −OH on the same carbon. We also found that the 100% defluorination of TFA ($CF_3{-}COO^-$) strongly supports this *DHEH* mechanism (Scheme 2.1c). First, TFA only has three high-BDE primary C−F bonds (Figure 2.3f) so that a direct C−F bond cleavage seems less likely. Second, our experimental results for DFA ($CF_2H{-}COO^-$) and MFA ($CFH_2{-}COO^-$) defluorination indicate that the previously proposed stepwise defluorination mechanism for TFA is less likely.[60] As shown in Figure 2.6, although complete decay of fluorinated acetates was observed, the maximum defluorination from DFA and MFA was 78% and 57%, respectively. Hence, the stepwise reaction of TFA →DFA → MFA would not lead to a 100% defluorination as observed from TFA. The incomplete defluorination from MFA and DFA might be attributed to the rapid volatilization of $FCH_2{-}OH$[59] and $F_2CH{-}OH$ prior to HF elimination. Third, the closely synchronized profiles of decay and defluorination of TFA suggest that the change of TFA parent structure triggered rapid liberation of all three F^- ions. While other reaction mechanisms have not been identified, the *DHEH* pathway is the most probable mechanism for PFCA chain-shortening and the accompanying F^- release. If the PFCA degradation followed the single pathway of chain-shortening through the *DHEH* pathway, a complete defluorination would have been observed. Thus, the ~55% max. defluorination from all $n \geq 2$ $C_nF_{2n+1}{-}COO^-$ is attributed to other reaction pathways via H/F exchange. Assuming that only these two mechanisms apply to the simple $CF_3CF_2COO^-$ structure, a *DHEH* as the first step will generate two F^- and CF_3COO^-, which can be fully defluorinated in the second *DHEH* (deF% = 100%). Meanwhile, the H/F exchange as the first step will accumulate $CF_3CH_2COO^-$ with high recalcitrance (deF% = 40%). Thus, the overall ~55% defluorination from $CF_3CF_2COO^-$ indicates a 75% probability for H/F exchange and 25% probability for *DHEH* as the first step. We also note that each shorter-chain

PFCA product will also undergo the two competing pathways, leading to the accumulation of H-containing structures with high recalcitrance. For long-chain PFCAs and intermediates H/F exchange in the middle of fluoroalkyl chain is also possible (Table A.11). The presence of one more $-COO^-$ terminal group in PFdiCAs (~67% max. defluorination) enables degradation from the other side of molecule. Either α-position H/F exchange or *DHEH* pathways from the second $-COO^-$ would lead to higher deF% than PFCAs, which have the most recalcitrant $-CF_3$ on the other end. In addition, our results do not support the previously proposed PFOA degradation mechanism, where $C_nF_{2n+1}-CH_2-COO^-$ (generated from $C_nF_{2n+1}-CF_2-COO^-$) decomposes to three pieces, $\bullet C_nF_{2n+1}$, $:CH_2$, and $\bullet COO^-$, and then the $\bullet C_nF_{2n+1}$ and $\bullet COO^-$ recombines into the shortened $C_nF_{2n+1}-COO^-$.[60] If this mechanism was dominant, the degradation of $CF_3-CH_2-COO^-$ would be fast, and the degradation of all $n \geq 2$ PFCAs would be shortened stepwise to TFA and yield 100% defluorination. We also note that even if the three-piece decomposition could occur, the chance of recombination of the two radicals in very low concentration (e.g., sub-μM level) in water would be trivial. As for PFSAs and FTCAs, the first reaction pathway is H/F exchange on relatively weak C−F bonds, which mainly occur in the middle of the long-chain structures (Scheme 2.1d). We add that if the middle-chain $-CF_2-$ is reduced to $-CH_2-$, the long fluorocarbon chain is thus divided into two short fluorocarbon chains, where most C−F bonds will have high BDEs (Figure 2.3b vs c). The other pathway is the cleavage of the head groups and the formation of PFCAs following either the H/F exchange or the *DHEH* mechanism. The similar molecular deF% values from the decayed portion of PFSAs (59−64%) and FTCAs (44−49%) in variable lengths support this speculation, which warrants further investigation. According to the MS peak areas of the parent compound and the identified degradation products (assuming they have similar ionization efficiency), the F mass balance seems not yet closed. This is probably because (1) the ionization efficiency may vary significantly for different products, leading to inaccurate estimation of product

abundances, (2) a portion of degradation products might have lost the charged headgroup and thus escaped from MS detection,[42,43] and/or (3) novel products generated from other reaction pathways were not identified by the screening of suspect products from chain shortening and H/F exchange. The mechanisms for some reactions still remain elusive. For example, FTCA chain shortening occurred with the $-CH_2CH_2-COO^-$ headgroup remaining. In the degradation of PFOS and PFHxS, high intensities of H/F exchange structures ($C_4F_8H-SO_3^-$ and $C_3F_6H-SO_3^-$) were observed (Tables A.15 and A.18) despite that PFBS and PFPrS are highly recalcitrant. These results suggest that there are still unknown degradation mechanisms involved in PFAS degradation with e_{aq}^-. However, since this treatment strategy is not very effective to short fluorocarbon chains that are not directly linked to $-COO^-$, mechanistic investigation on the unfavorable pathways goes beyond the focus of this study. Instead, priority of research should be given to further improving the rate and extent of the degradation of recalcitrant PFAS structures.

2.3.4 Critical Implications to PFASs Remediation and Management.

A series of critical environmental implications can be explicitly made from the findings of this study. First, the direct linkage between fluoroalkyl chain and −COO− is highly beneficial for reductive defluorination with e_{aq}^-. From the remediation perspective, chemical[61] and biological[62] trans- formation of telomeric structures are expected to produce PFCAs for significantly enhanced defluorination efficiency of the following treatment step with e_{aq}^-. From the management perspective, perfluorinated sulfonates with short fluoroalkyl chains[36] should be applied with caution due to their sluggish reactivity with e_{aq}^- and their recalcitrance to oxidation. We accentuate that the future design of mixed AFFF formulation should seriously consider the treatability of specific PFAS structures to avoid the recalcitrance against remediation efforts. Second, further elevated defluorination can be expected from the optimization of reaction conditions (e.g., selection of chemicals for e_{aq}^- generation,[49,63] UV energy and intensity,[50,51] and the use of heterogeneous

materials[48]) and the development of technologies with novel working principles.[24,25] Lastly, since other emerging technologies such as electrochemical and plasmatic treatment have also observed slower degradation of C6 PFHxS than C8 PFOS,[15,26] we emphasize the necessity of examining a variety of representative structures as the PFAS contamination in the real world are usually present as a mixture of diverse structures.

2.4 Tables and Figures

Table 2.1 Overall Defluorination Ratio of PFASs in Variable Fluoroalkyl Chain Lengths after 48 h of Reaction.[a]

chain length (n)	$F(CF_2)_n$− COOH	HOOC− $(CF_2)_n$− COOH	$F(CF_2)_n$− CH_2CH_2− COOH	$F(CF_2)_n$− SO_3H
1	98.2 ± 5.0	81.4 ± 4.2	0.73 ± 0.11	0.94 ± 0.18
2	53.3 ± 4.9	63.2 ± 4.3	0.94 ± 0.16	N/A[b]
3	51.1 ± 8.0	65.5 ± 4.4	1.1 ± 0.1	N/A[b]
4	56.1 ± 4.7	65.8 ± 2.1	0.71 ± 0.15	4.6 ± 0.8
5	51.0 ± 4.4	N/A[b]	4.1 ± 0.2	N/A[b]
6	55.1 ± 1.6	64.3 ± 2.2	7.4 ± 1.8	31.8 ± 0.8
7	56.5 ± 2.4	65.7 ± 3.9	17.1 ± 3.2	N/A[b]
8	58.2 ± 1.2	63.6 ± 2.7	33.4 ± 1.0	57.0 ± 1.2
9	49.1 ± 6.4	N/A[b]	N/A[b]	N/A[b]
10	59.5 ± 0.6	67.0 ± 0.5	N/A[b]	N/A[b]

[a]Reaction conditions: PFAS (0.025 mM), Na_2SO_3 (10 mM), carbonate buffer (5 mM), 254 nm irradiation (18 W low-pressure Hg lamp) at pH 9.5 and 20 °C. Errors indicate standard deviation of triplicate reactions.

[b]Data not available because the chemical was commercially unavailable, too costly to afford, or not readily soluble in water (for long-chain structures).

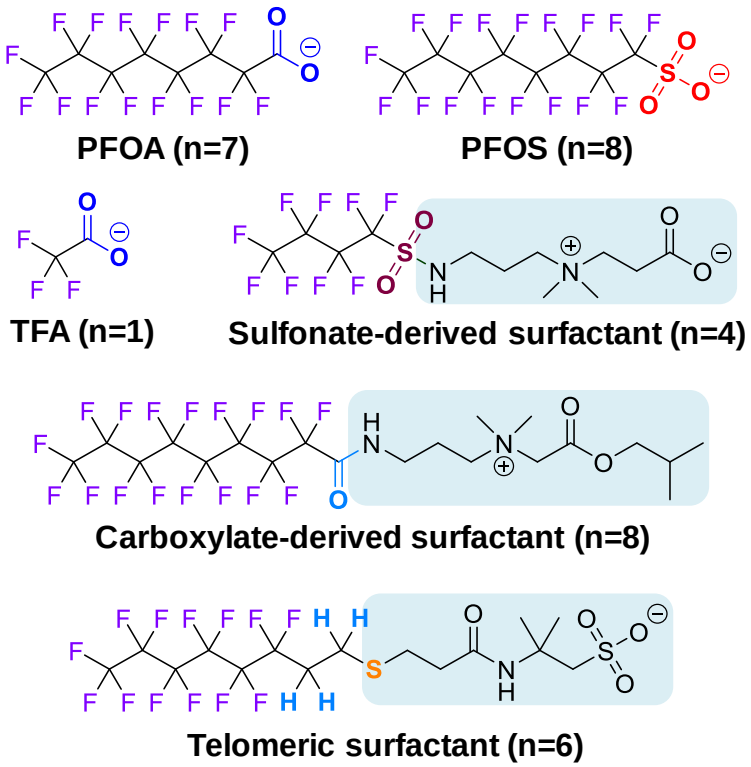

Figure 2.1 Examples of PFAS structures detected in the environment (*n* indicating the variable length of C_nF_{2n+1} shown in the figure; organic moiety in AFFF surfactants shaded in blue). Surfactant structures were taken from refs 29 and 31.

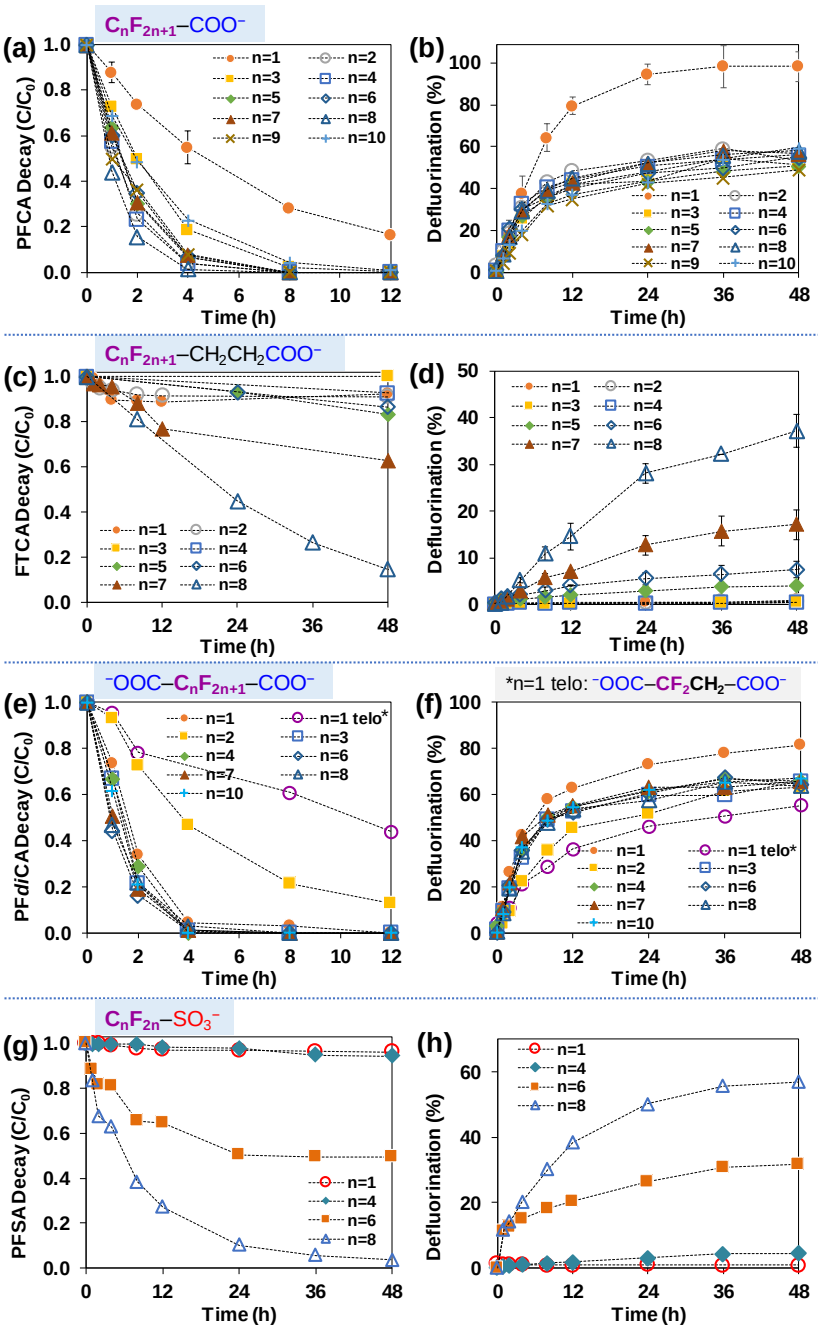

Figure 2.2 Time profiles for PFAS parent compound decay and defluorination. *Reaction conditions*: PFAS (0.025 mM), Na_2SO_3 (10 mM), carbonate buffer (5 mM), 254 nm irradiation (18 W low-pressure Hg lamp for 600 mL solution), pH 9.5 and 20 °C. Full degradation profile for TFA (*n* = 1 PFCA) is shown in Figure 2.6.

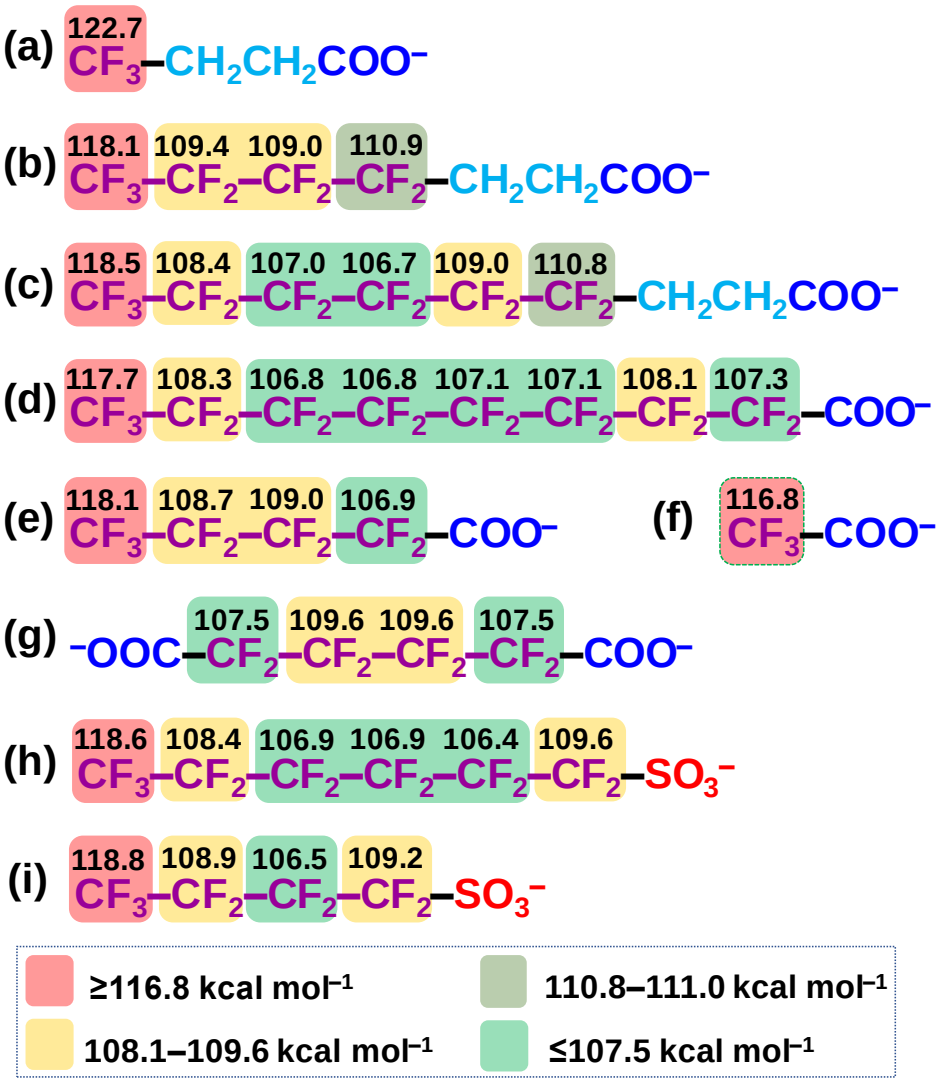

Figure 2.3 Calculated C−F BDEs (kcal mol^{-1}) of selected PFASs at the B3LYP-D3(BJ)/6-311+G(2d,2p) level of theory. Calculation results for all structures are tabulated in Tables A.1−A.5.

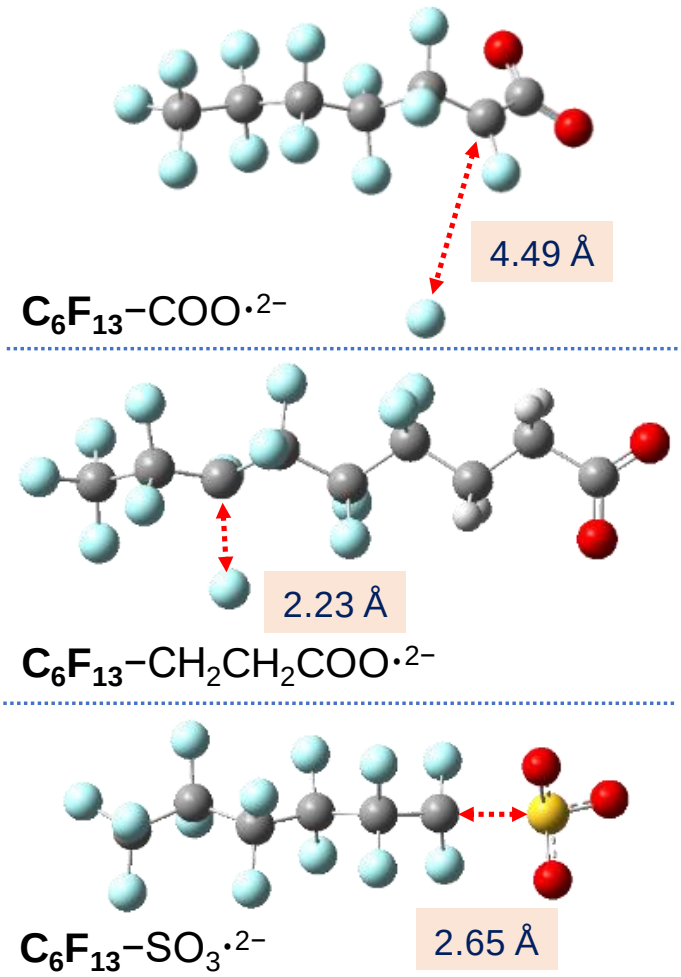

Figure 2.4 Geometry-optimized structure of the adducts of the three n = 6 PFAS anions with an e_{aq}^- ($PFAS^{\bullet 2-}$) at the B3LYP-D3(BJ)/6-311+G(2d,2p) level of theory.

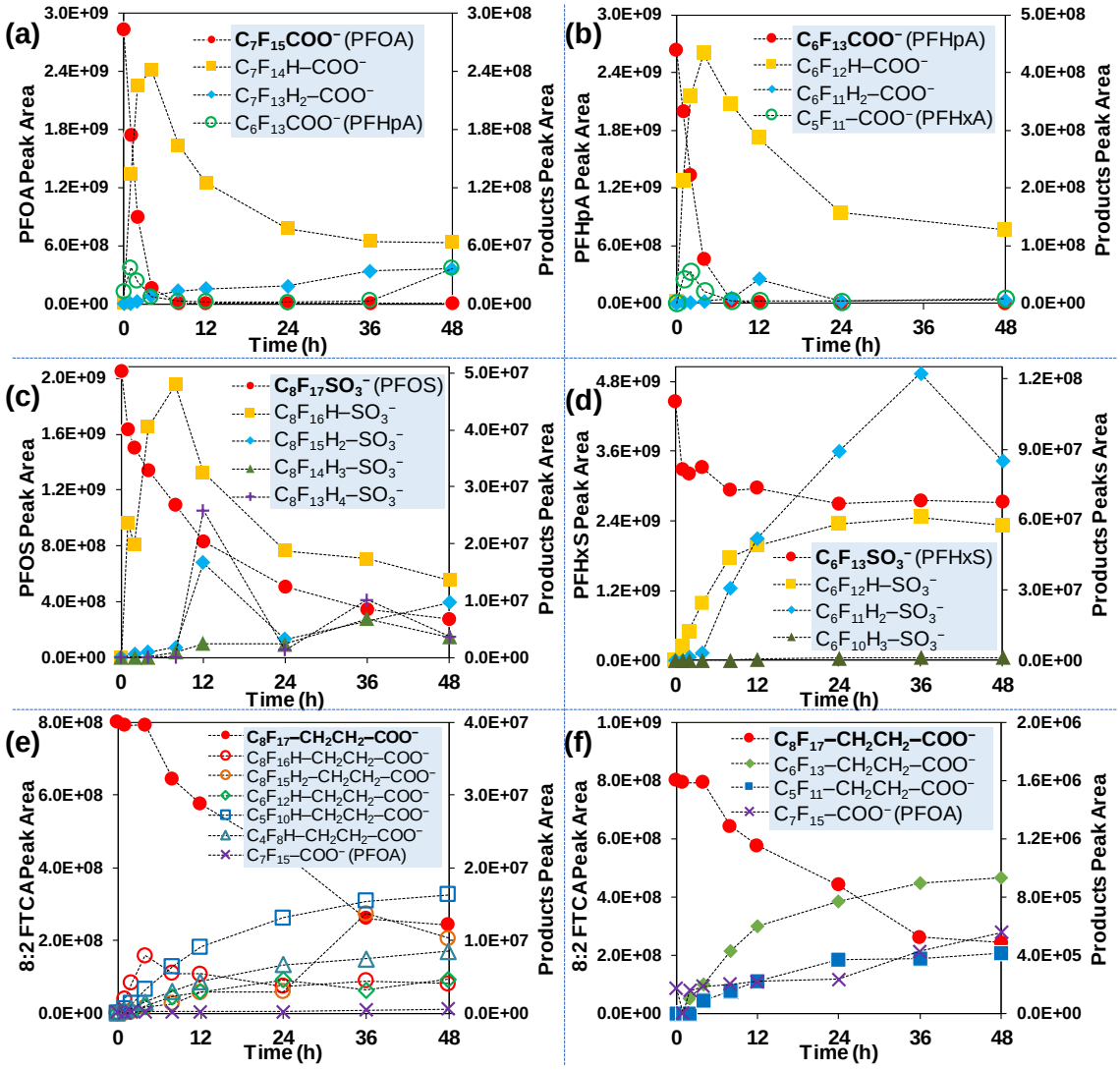

Figure 2.5 Representative degradation products from (a) PFOA, (b) PFHpA, (c) PFOS, (d) PFHxS, and (e+f) n = 8 FTCA. All detected species including those in low intensities are summarized in Tables A.6-A.18.

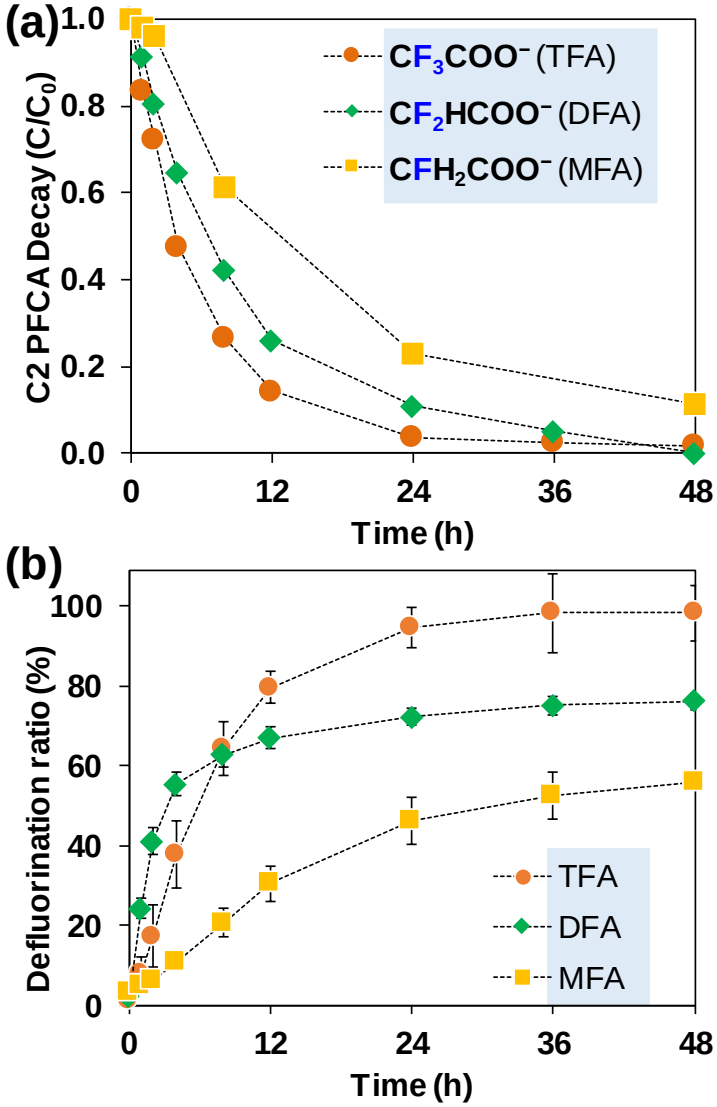

Figure 2.6 Time profiles for the (a) decay and (b) defluorination of the three fluorinated acetic acid derivatives. Reaction conditions are the same as indicated in Figure 2.2.

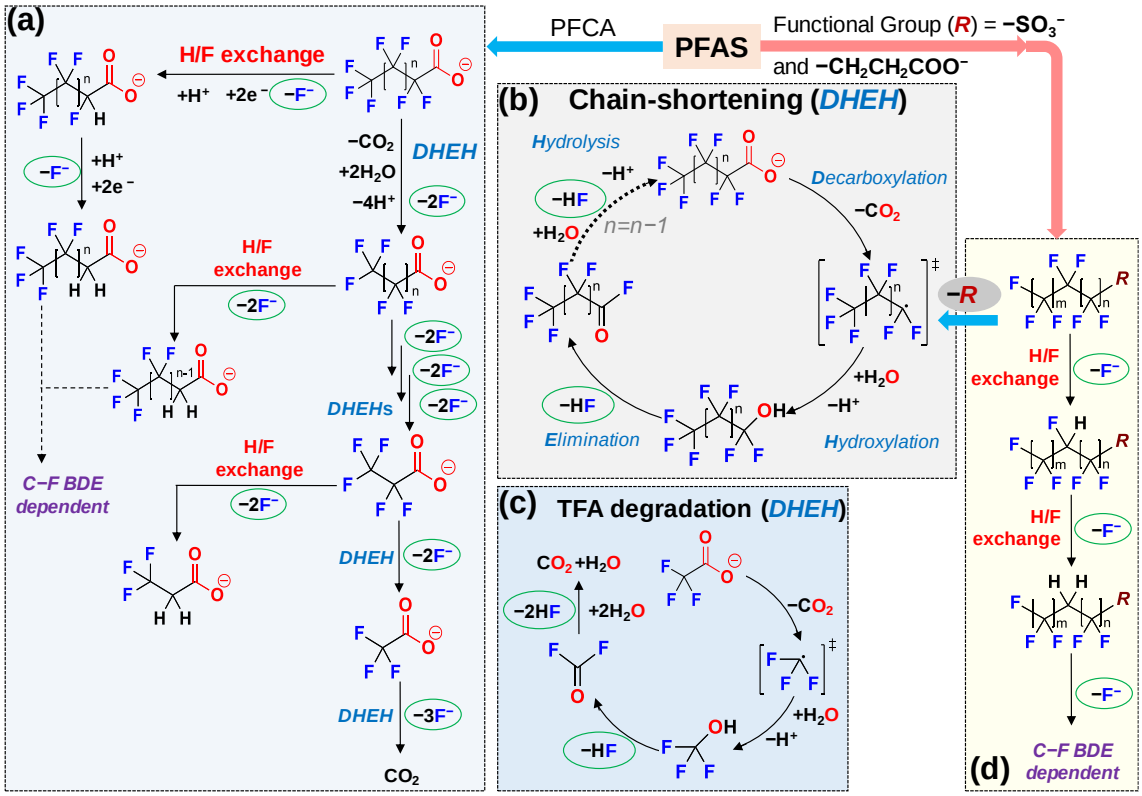

Scheme 2.1 Proposed Overall Reaction Mechanisms for PFAS Degradation and Defluorination.

REFERENCES

(1) Xiao, F. Emerging poly-and perfluoroalkyl substances in the aquatic environment: A review of current literature. *Water Res.* **2017**, *124*, 482−495.

(2) Houde, M.; De Silva, A. O.; Muir, D. C.; Letcher, R. J. Monitoring of perfluorinated compounds in aquatic biota: An updated review: PFCs in aquatic biota. *Environ. Sci. Technol.* **2011**, *45* (19), 7962−7973.

(3) U. S. Environmental Protection Agency. Revisions to the unregulated contaminant monitoring regulation (UCMR 3) for public water systems. *Fed. Reg.* **2012**, *77* (85), 26071−26101.

(4) U. S. Environmental Protection Agency. Lifetime health advisories and health effects support documents for perfluorooctanoic acid and perfluorooctane sulfonate. *Fed. Reg.* **2016**, *81* (101), 33250−33251.

(5) Vermont Department of Health. Health Department Updates Health Advisory for PFAS. http://www.healthvermont.gov/media/newsroom/updated-pfas-health-advisory-july-10-2018.

(6) Massachusetts Department of Environmental Protection. MassDEP ORS Guideline for PFAS. https://www.mass.gov/files/documents/2018/06/11/orsg-pfas-20180608.pdf.

(7) New Jersey Drinking Water Quality Institute. Maximum Contaminant Level Recommendations for Perfluorononanoic Acid in Drinking Water: Basis and Background. https://www.nj.gov/dep/watersupply/pdf/pfna-recommend-final.pdf.

(8) North Carolina Department of Environmental Quality and North Carolina Department of Health and Human Services. Secretaries' Science Advisory Board Review of the North Carolina Drinking Water Provisional Health Goal for GenX. https://files.nc.gov/ncdeq/GenX/SAB/SAB-GenX-Report-draft-08-29-2018.pdf.

(9) Trojanowicz, M.; Bojanowska-Czajka, A.; Bartosiewicz, I.; Kulisa, K. Advanced Oxidation/Reduction Processes treatment for aqueous perfluorooctanoate (PFOA) and perfluorooctanesulfonate (PFOS)−A review of recent advances. *Chem. Eng. J.* **2018**, *336*, 170−199.

(10) Merino, N.; Qu, Y.; Deeb, R. A.; Hawley, E. L.; Hoffmann, M. R.; Mahendra, S. Degradation and removal methods for perfluoroalkyl and polyfluoroalkyl substances in water. *Environ. Eng. Sci.* **2016**, *33* (9), 615−649.

(11) Rahman, M. F.; Peldszus, S.; Anderson, W. B. Behaviour and fate of perfluoroalkyl and polyfluoroalkyl substances (PFASs) in drinking water treatment: A review. *Water Res.* **2014**, *50*, 318−340.

(12) Xiao, X.; Ulrich, B. A.; Chen, B.; Higgins, C. P. Sorption of poly- and perfluoroalkyl substances (PFASs) relevant to aqueous film-forming foam (AFFF)-impacted groundwater by biochars and activated carbon. *Environ. Sci. Technol.* **2017**, *51* (11), 6342−6351.

(13) Boo, C.; Wang, Y.; Zucker, I.; Choo, Y.; Osuji, C. O.; Elimelech, M. High performance nanofiltration membrane for effective removal of perfluoroalkyl substances at high water recovery. *Environ. Sci. Technol.* **2018**, *52* (13), 7279−7288.

(14) Zhuo, Q.; Deng, S.; Yang, B.; Huang, J.; Yu, G. Efficient electrochemical oxidation of perfluorooctanoate using a Ti/SnO_2-Sb-Bi anode. *Environ. Sci. Technol.* **2011**, *45* (7), 2973−2979.

(15) Schaefer, C. E.; Andaya, C.; Burant, A.; Condee, C. W.; Urtiaga, A.; Strathmann, T. J.; Higgins, C. P. Electrochemical treatment of perfluorooctanoic acid and perfluorooctane sulfonate: Insights into mechanisms and application to groundwater treatment. *Chem. Eng. J.* **2017**, *317*, 424−432.

(16) Schaefer, C. E.; Choyke, S.; Ferguson, P. L.; Andaya, C.; Burant, A.; Maizel, A.; Strathmann, T. J.; Higgins, C. P. Electrochemical transformations of perfluoroalkyl acid (PFAA) precursors and PFAAs in groundwater impacted with aqueous film forming foams. *Environ. Sci. Technol.* **2018**, *52* (18), 10689−10697.

(17) Lin, H.; Niu, J.; Xu, J.; Huang, H.; Li, D.; Yue, Z.; Feng, C. Highly efficient and mild electrochemical mineralization of long-chain perfluorocarboxylic acids (C9−C10) by Ti/SnO_2−Sb−Ce, Ti/SnO_2−Sb/Ce−PbO_2 and Ti/BDD electrodes. *Environ. Sci. Technol.* **2013**, *47* (22), 13039−13046.

(18) Moriwaki, H.; Takagi, Y.; Tanaka, M.; Tsuruho, K.; Okitsu, K.; Maeda, Y. Sonochemical decomposition of perfluorooctane sulfonate and perfluorooctanoic acid. *Environ. Sci. Technol.* **2005**, *39* (9), 3388−3392.

(19) Vecitis, C. D.; Wang, Y.; Cheng, J.; Park, H.; Mader, B. T.; Hoffmann, M. R. Sonochemical degradation of perfluorooctanesulfonate in aqueous film-forming foams. *Environ. Sci. Technol.* **2010**, *44* (1), 432−438.

(20) Gole, V. L.; Fishgold, A.; Sierra-Alvarez, R.; Deymier, P.; Keswani, M. Treatment of perfluorooctane sulfonic acid (PFOS) using a large-scale sonochemical reactor. Sep. *Purif. Technol.* **2018**, *194*, 104−110.

(21) Sahu, S. P.; Qanbarzadeh, M.; Ateia, M.; Torkzadeh, H.; Maroli, A. S.; Cates, E. L. Rapid degradation and mineralization of perfluorooctanoic acid by a new petitjeanite $Bi_3O(OH)(PO_4)_2$ microparticle ultraviolet photocatalyst. *Environ. Sci. Technol. Lett.* **2018**, *5* (8), 533−538.

(22) Li, X.; Zhang, P.; Jin, L.; Shao, T.; Li, Z.; Cao, J. Efficient photocatalytic decomposition of perfluorooctanoic acid by indium oxide and its mechanism. *Environ. Sci. Technol.* **2012**, *46* (10), 5528−5534.

(23) Ochiai, T.; Iizuka, Y.; Nakata, K.; Murakami, T.; Tryk, D. A.; Koide, Y.; Morito, Y.; Fujishima, A. Efficient decomposition of perfluorocarboxylic acids in aqueous suspensions of a TiO_2 photocatalyst with medium-pressure ultraviolet lamp irradiation under atmospheric pressure. *Ind. Eng. Chem. Res.* **2011**, *50* (19), 10943−10947.

(24) Zhang, K.; Huang, J.; Yu, G.; Zhang, Q.; Deng, S.; Wang, B. Destruction of perfluorooctane sulfonate (PFOS) and perfluorooctanoic acid (PFOA) by ball milling. *Environ. Sci. Technol.* **2013**, *47* (12), 6471−6477.

(25) Lu, M.; Cagnetta, G.; Zhang, K.; Huang, J.; Yu, G. Mechanochemical mineralization of "very persistent" fluorocarbon surfactants−6:2 fluorotelomer sulfonate (6:2 FTS) as an example. *Sci. Rep.* **2017**, *7*, 17180.

(26) Stratton, G. R.; Dai, F.; Bellona, C. L.; Holsen, T. M.; Dickenson, E. R.; Mededovic Thagard, S. Plasma-based water treatment: efficient transformation of perfluoroalkyl substances in prepared solutions and contaminated groundwater. *Environ. Sci. Technol.* **2017**, *51* (3), 1643−1648.

(27) Zhang, Z.; Chen, J. J.; Lyu, X. J.; Yin, H.; Sheng, G. P. Complete mineralization of perfluorooctanoic acid (PFOA) by γ-irradiation in aqueous solution. *Sci. Rep.* **2015**, *4*, 7418.

(28) Dombrowski, P. M.; Kakarla, P.; Caldicott, W.; Chin, Y.; Sadeghi, V.; Bogdan, D.; Barajas Rodriguez, F.; Chiang, S. Y. Technology review and evaluation of different chemical oxidation conditions on treatability of PFAS. *Remed. J.* **2018**, *28* (2), 135−150.

(29) Barzen-Hanson, K. A.; Roberts, S. C.; Choyke, S.; Oetjen, K.; McAlees, A.; Riddell, N.; McCrindle, R.; Ferguson, P. L.; Higgins, C. P.; Field, J. A. Discovery of 40 classes of per-and polyfluoroalkyl substances in historical aqueous film-forming foams (AFFFs) and AFFF-impacted groundwater. *Environ. Sci. Technol.* **2017**, *51* (4), 2047−2057.

(30) D'Agostino, L. A.; Mabury, S. A. Certain perfluoroalkyl and polyfluoroalkyl substances associated with aqueous film forming foam are widespread in Canadian surface waters. *Environ. Sci. Technol.* **2017**, *51* (23), 13603−13613.

(31) D'Agostino, L. A.; Mabury, S. A. Identification of Novel Fluorinated Surfactants in Aqueous Film Forming Foams and Commercial Surfactant Concentrates. *Environ. Sci. Technol.* **2014**, *48* (1), 121−129.

(32) Gebbink, W. A.; van Asseldonk, L.; van Leeuwen, S. P. Presence of emerging per-and polyfluoroalkyl substances (PFASs) in river and drinking water near a fluorochemical production plant in the Netherlands. *Environ. Sci. Technol.* **2017**, *51* (19), 11057−11065.

(33) Song, X.; Vestergren, R.; Shi, Y.; Huang, J.; Cai, Y. Emissions, transport, and fate of emerging per- and polyfluoroalkyl substances from one of the major fluoropolymer manufacturing facilities in China. *Environ. Sci. Technol.* **2018**, *52* (17), 9694−9703.

(34) Wang, Y.; Yu, N.; Zhu, X.; Guo, H.; Jiang, J.; Wang, X.; Shi, W.; Wu, J.; Yu, H.; Wei, S. Suspect and nontarget screening of per- and polyfluoroalkyl substances in wastewater from a fluorochemical manufacturing park. *Environ. Sci. Technol.* **2018**, *52* (19), 11007−11016.

(35) Chen, H.; Yao, Y.; Zhao, Z.; Wang, Y.; Wang, Q.; Ren, C.; Wang, B.; Sun, H.; Alder, A. C.; Kannan, K. Multimedia distribution and transfer of per- and polyfluoroalkyl substances (PFASs) surrounding two fluorochemical manufacturing facilities in Fuxin, China. *Environ. Sci. Technol.* **2018**, *52* (15), 8263−8271.

(36) Barzen-Hanson, K. A.; Field, J. A. Discovery and implications of C2 and C3 perfluoroalkyl sulfonates in aqueous film-forming foams and groundwater. *Environ. Sci. Technol. Lett.* **2015**, *2* (4), 95−99.

(37) Lang, J. R.; Allred, B. M.; Peaslee, G. F.; Field, J. A.; Barlaz, M. A. Release of per- and polyfluoroalkyl substances (PFASs) from carpet and clothing in model anaerobic landfill reactors. *Environ. Sci. Technol.* **2016**, *50* (10), 5024−5032.

(38) Niu, J.; Lin, H.; Xu, J.; Wu, H.; Li, Y. Electrochemical mineralization of perfluorocarboxylic acids (PFCAs) by Ce-doped modified porous nanocrystalline PbO_2 film electrode. *Environ. Sci. Technol.* **2012**, *46* (18), 10191−10198.

(39) Campbell, T. Y.; Vecitis, C. D.; Mader, B. T.; Hoffmann, M. R. Perfluorinated surfactant chain-length effects on sonochemical kinetics. *J. Phys. Chem. A.* **2009**, *113* (36), 9834−9842.

(40) Park, H.; Vecitis, C. D.; Cheng, J.; Choi, W.; Mader, B. T.; Hoffmann, M. R. Reductive defluorination of aqueous perfluorinated alkyl surfactants: Effects of ionic headgroup and chain length. *J. Phys. Chem. A.* **2009**, *113* (4), 690−696.

(41) Bao, Y.; Deng, S.; Jiang, X.; Qu, Y.; He, Y.; Liu, L.; Chai, Q.; Mumtaz, M.; Huang, J.; Cagnetta, G.; Yu, G. Degradation of PFOA substitute: GenX (HFPO−DA ammonium salt): Oxidation with UV/persulfate or reduction with UV/sulfite? *Environ. Sci. Technol.* **2018**, *52* (20), 11728−11734.

(42) Liu, J.; Van Hoomissen, D. J.; Liu, T.; Maizel, A.; Huo, X.; Fernández, S. R.; Ren, C.; Xiao, X.; Fang, Y.; Schaefer, C. E. Reductive defluorination of branched per-and polyfluoroalkyl substances with cobalt complex catalysts. *Environ. Sci. Technol. Lett.* **2018**, *5* (5), 289−294.

(43) Park, S.; de Perre, C.; Lee, L. S. Alternate reductants with VB12 to transform C8 and C6 perfluoroalkyl sulfonates: Limitations and insights into isomer-specific transformation rates, products and pathways. *Environ. Sci. Technol.* **2017**, *51* (23), 13869−13877.

(44) Wang, Z.; Wang, Y.; Li, J.; Henne, S.; Zhang, B.; Hu, J.; Zhang, J. Impacts of the degradation of 2,3,3,3-tetrafluoropropene into trifluoroacetic acid from its application in automobile air conditioners in China, the United States, and Europe. *Environ. Sci. Technol.* **2018**, *52* (5), 2819−2826.

(45) Grossweiner, L. I.; Swenson, G. W.; Zwicker, E. F. Photochemical generation of the hydrated electron. *Science*. **1963**, *141* (3583), 805−806.

(46) Fischer, M.; Warneck, P. Photodecomposition and photooxidation of hydrogen sulfite in aqueous solution. *J. Phys. Chem.* **1996**, *100* (37), 15111−15117.

(47) Song, Z.; Tang, H.; Wang, N.; Zhu, L. Reductive defluorination of perfluorooctanoic acid by hydrated electrons in a sulfite-mediated UV photochemical system. *J. Hazard. Mater.* **2013**, *262*, 332−338.

(48) Tian, H.; Gao, J.; Li, H.; Boyd, S. A.; Gu, C. Complete defluorination of perfluorinated compounds by hydrated electrons generated from 3-indole-acetic-acid in organomodified montmorillonite. *Sci. Rep.* **2016**, *6*, 32949.

(49) Sun, Z.; Zhang, C.; Xing, L.; Zhou, Q.; Dong, W.; Hoffmann, M. R. UV/nitrilotriacetic acid process as a novel strategy for efficient photoreductive degradation of perfluorooctanesulfonate. *Environ. Sci. Technol.* **2018**, *52* (5), 2953−2962.

(50) Gu, Y.; Dong, W.; Luo, C.; Liu, T. Efficient reductive decomposition of perfluorooctanesulfonate in a high photon flux UV/sulfite system. *Environ. Sci. Technol.* **2016**, *50* (19), 10554−10561.

(51) Gu, Y.; Liu, T.; Wang, H.; Han, H.; Dong, W. Hydrated electron based decomposition of perfluorooctane sulfonate (PFOS) in the VUV/sulfite system. *Sci. Total Environ.* **2017**, *607*, 541−548.

(52) Gu, Y.; Liu, T.; Zhang, Q.; Dong, W. Efficient decomposition of perfluorooctanoic acid by a high photon flux UV/sulfite process: Kinetics and associated toxicity. *Chem. Eng. J.* **2017**, *326*, 1125−1133.

(53) Banks, R. E.; Smart, B. E.; Tatlow, *J. Organofluorine Chemistry: Principles and Commercial Applications*; Springer Science & Business Media, **2013**.

(54) Paul, A.; Wannere, C. S.; Schaefer, H. F. Do linear-chain perfluoroalkanes bind an electron*? J. Phys. Chem. A*. **2004**, *108* (43), 9428−9434.

(55) Nohara, K.; Toma, M.; Kutsuna, S.; Takeuchi, K.; Ibusuki, T. Cl atom-initiated oxidation of three homologous methyl perfluoroalkyl ethers. *Environ. Sci. Technol.* **2001**, *35* (1), 114−120.

(56) Hori, H.; Hayakawa, E.; Einaga, H.; Kutsuna, S.; Koike, K.; Ibusuki, T.; Kiatagawa, H.; Arakawa, R. Decomposition of environmentally persistent perfluorooctanoic acid in water by photochemical approaches. *Environ. Sci. Technol.* **2004**, *38* (22), 6118−6124.

(57) Vandamme, M.; Bouchard, L.; Gilbert, A.; Keita, M.; Paquin, J.-F. Direct esterification of carboxylic acids with perfluorinated alcohols mediated by XtalFluor-E. *Org. Lett.* **2016**, *18* (24), 6468−6471.

(58) Yuan, G.; Peng, H.; Huang, C.; Hu, J. Ubiquitous occurrence of fluorotelomer alcohols in eco-friendly paper-made food-contact materials and their implication for human exposure. *Environ. Sci. Technol.* **2016**, *50* (2), 942−950.

(59) Suenram, R.; Lovas, F.; Pickett, H. Fluoromethanol: Synthesis, microwave spectrum, and dipole moment. *J. Mol. Spectrosc.* **1986**, *119* (2), 446−455.

(60) Qu, Y.; Zhang, C.; Li, F.; Chen, J.; Zhou, Q. Photo-reductive defluorination of perfluorooctanoic acid in water. *Water Res.* **2010**, *44* (9), 2939−2947.

(61) Houtz, E. F.; Sedlak, D. L. Oxidative conversion as a means of detecting precursors to perfluoroalkyl acids in urban runoff. *Environ. Sci. Technol.* **2012**, *46* (17), 9342−9349.

(62) Harding-Marjanovic, K. C.; Houtz, E. F.; Yi, S.; Field, J. A.; Sedlak, D. L.; Alvarez-Cohen, L. Aerobic biotransformation of fluorotelomer thioether amido sulfonate (Lodyne) in AFFF-amended microcosms. *Environ. Sci. Technol.* **2015**, *49* (13), 7666−7674.

(63) Tian, H.; Gu, C. Effects of different factors on photodefluorination of perfluorinated compounds by hydrated electrons in organo-montmorillonite system. *Chemosphere*. **2018**, *191*, 280−287.

CHAPTER 3: DEGRADATION OF PERFLUOROALKYL ETHER CARBOYXLIC ACIDS WITH HYDRATED ELECTRONS: STRUCTURE-REACTIVITY RELATIONSHIPS AND ENVIRONMENTAL IMPLICATIONS

Abstract

This study explores structure−reactivity relationships for the degradation of emerging perfluoroalkyl ether carboxylic acid (PFECA) pollutants with ultraviolet-generated hydrated electrons (e_{aq}^-). The rate and extent of PFECA degradation depend on both the branching extent and the chain length of oxygen-segregated fluoroalkyl moieties. Kinetic measurements, theoretical calculations, and transformation product analyses provide a comprehensive understanding of the PFECA degradation mechanisms and pathways. In comparison to traditional full-carbon-chain perfluorocarboxylic acids, the distinct degradation behavior of PFECAs is attributed to their ether structures. The ether oxygen atoms increase the bond dissociation energy of the C−F bonds on the adjacent $-CF_2-$ moieties. This impact reduces the formation of H/F-exchanged polyfluorinated products that are recalcitrant to reductive defluorination. Instead, the cleavage of ether C−O bonds generates unstable perfluoroalcohols and thus promotes deep defluorination of short fluoroalkyl moieties. In comparison to linear PFECAs, branched PFECAs have a higher tendency of H/F exchange on the tertiary carbon and thus lower percentages of defluorination. These findings provide mechanistic insights for an improved design and efficient degradation of fluorochemicals.

3.1 Introduction

Since the 1940s, per- and polyfluoroalkyl substances (PFASs) have been extensively used in a wide range of applications because of their unique properties (e.g., hydrophobicity, lipophobicity, and thermal stability) as well as their relative ease in chemical design and synthesis.[1−5] The highly stable C−F bond makes PFAS molecules recalcitrant to natural and engineered degradation,[6] leading to global PFAS pollution[7] and worldwide efforts on PFAS

regulation.[8–11] Fluorochemical industries have been phasing out the production and use of some legacy PFASs [e.g., perfluorooctanoic acid (PFOA)][2,12] because of their heavy pollution of the environment and high toxicities to humans.[13,14] Perfluoroalkyl ether carboxylic acids (PFECAs) that contain ether C−O bonds in molecules have been developed as "less bioaccumulative alternatives" to full-carbon-chain predecessor PFASs.[15] However, toxicological studies have revealed an even higher bioaccumulation potential and toxicity of some PFECAs than PFOA,[16–19] and PFECAs have been recognized as a new class of contaminants of emerging concern (Figure 3.1).[20–23] At some sites in North America and in Europe, PFECAs have been detected in much higher concentrations than legacy PFASs.[24,25] Furthermore, because of the facile synthesis of PFECAs from flexible choices of fluoroalkene oxide building blocks (e.g., Figure B.1)[26] and the formation of byproducts,[27] the diversity of PFECA contaminants identified in the environment has been rapidly increasing.[27–29] While physical separation methods (e.g., carbon adsorption, ion exchange, and membrane filtration) enable rapid PFAS removal from contaminated water,[30] concentrated PFASs in carbon/resin regeneration waste and membrane rejects still require degradation treatment. Various novel methods, such as electrochemical,[31] sonochemical,[32] radiolytic,[33] plasmatic,[34] and other oxidative and reductive approaches,[30,35] have been primarily developed for the degradation of PFOA and perfluorooctane sulfonic acid. A few studies have investigated the destruction of selected PFECAs, including sonochemicaloxidation with persulfate,[36] photocatalytic oxidation with phosphotungstic acid under pressurized O_2,[37] and reduction with ultraviolet (UV)-generated hydrated electrons (e_{aq}^-).[38,39] These early studies have revealed a variety of mechanistic insights on PFECA degradation. In particular, reductive degradation of branched PFECAs (e.g., GenX in Figure 3.1) using e_{aq}^- is much more effective than oxidative degradation using sulfate radicals.[38,39] However, a systematic understanding of reaction pathways and structure−reactivity relationships has not yet been established. Recently, our research

team has systematically studied the reductive defluorination of full-carbon-chain PFASs by e_{aq}^- produced from aqueous sulfite under UV irradiation.[40] The degradation mechanisms for perfluorocarboxylic acids (PFCAs) and fluorotelomer carboxylic acids (FTCAs) are significantly different. FTCAs ($\mathbf{R_F}$−CH_2CH_2−COO^-, where $\mathbf{R_F}$ represents the fluorocarbon moiety) are much more recalcitrant than PFCAs ($\mathbf{R_F}$−COO^-), especially when the chain length of $\mathbf{R_F}$ is short. The incomplete defluorination of PFCAs can also be attributed to the formation of polyfluorinated $\mathbf{R_F}$−CH_2−COO^- products.[40] These findings indicate the importance of a direct linkage between $\mathbf{R_F}$ and $-COO^-$ to allow an effective degradation of full-carbon-chain PFASs using e_{aq}^-. In comparison, the flexible incorporation of ether linkages in PFECAs generates various oxygen-segregated fluoroalkyl moieties, which can be either branched or linear in variable lengths. This novel structural diversity raises fundamental questions regarding mechanistic understanding and pollution control: (1) Mechanistically, what roles do the ether C−O bond and other structural features play in PFECA degradation using e_{aq}^-? (2) Practically, in comparison to full-carbon-chain PFCAs, can PFECAs be treated with a higher effectivity by these promising reductive technologies? To answer these questions, we investigated the reductive defluorination of 10 PFECAs with (*i*) varying numbers of ether C−O bonds, (*ii*) varying chain lengths of oxygen-segregated fluoroalkyl moieties, and (*iii*) branched versus linear fluoroalkyl structures. To achieve a comprehensive understanding, we conducted kinetic measurements on parent compound decay and fluoride ion (F^-) release, theoretical calculations on C−F/C−O bond dissociation energies, spontaneous bond cleavage upon reaction with e_{aq}^-, and transformation product (TP) analyses with high-resolution mass spectrometry. These results collectively reveal and confirm novel mechanistic insights into PFECA degradation. These findings will advance treatment technologies for existing PFECA pollutants and facilitate the molecular design of fluorochemicals with enhanced degradability.

3.2 Materials and Methods

This study utilized 10 PFECAs with fine-tuned structural variability in 4 categories (**A1** through **D2** in Table 3.1) and 2 special compounds [trifluoropyruvate (TFPy) $CF_3{-}CO{-}COO^-$ and trifluoromethoxyacetate (TFMOA) $CF_3{-}O{-}CH_2{-}COO^-$] for mechanistic investigations. Detailed information on these chemicals is included in the Appendix B (App B). Preparation of PFECA stock solutions, photochemical reaction settings, sample analysis, and theoretical calculations have been fully described in our previous work (open access).[40] We used consistent reaction conditions to compare the degradation behavior between PFECAs and traditional full-carbon-chain PFCAs. Briefly, the photochemical degradation of individual PFECAs was carried out in 600 mL closed-system batch reactors equipped with a low-pressure mercury lamp (254 nm, 18 W, enclosed in a quartz immersion well). Both the reactor and immersion well were connected to circulating cooling water at 20 °C. The reaction mixture contained 25 μM PFECA, 10 mM Na_2SO_3, and 5 mM $NaHCO_3$, and the pH was adjusted to 9.5 with NaOH. The released F^- was measured with an ion-selective electrode, which has been validated for quantification accuracy by ion chromatography (IC). All reactions were conducted in triplicates of operations from the preparation of stock solution to the quantification of the defluorination percentage (deF %), which is defined as

$$\text{deF \%} = \frac{C_{F^-}}{C_0 \times N_{C-F}} \times 100\% \tag{3.1}$$

where C_{F^-} is the molar concentration of F^- released in solution, C_0 is the initial molar concentration of parent PFECAs, and N_{C-F} is the number of C−F bonds in the parent PFECA molecule. Reaction samples were analyzed with a liquid chromatography−triple quadrupole mass spectrometer (LC−MS/MS) for the quantification of parent compounds and TPs that have pure chemicals available as analytical standards. A liquid chromatography−high-resolution mass spectrometer (LC-HRMS) was also used for the screening of TPs without analytical standards. The quality assurance and quality control of our MS analyses have been addressed previously,[40] with new

details provided in the App B for the PFECA degradation samples. Small ionic species including trifluoroacetate, TFPy, oxalate, perfluoromethoxyacetate (PFMOA, $CF_3{-}O{-}CF_2{-}COO^-$), and TFMOA ($CF_3{-}O{-}CH_2{-}COO^-$) were analyzed by an ion chromatograph equipped with a conductivity detector (specific separation conditions are described in the App B).

3.3 Results and Discussion

3.3.1 Degradation of PFECAs.

Different Degradability between PFECAs and Traditional PFCAs. Figure 3.2 shows the decay and defluorination of four PFASs representing full carbon-chain PFCAs, linear PFECAs, and branched PFECAs. The parent compound decay is the fastest for the two traditional PFCAs and the slowest for the branched PFECA (Figure 3.2a). The order of parent compound decay rates for these structures does not match the order of their defluorination percentages. Figure 3.2b shows the distinct defluorination profiles between PFECAs and traditional PFCAs as well as between linear and branched PFECAs. All four PFASs showed an initial period of rapid F^- release, followed by slower F^- release before reaching a plateau. However, the initial rates of defluorination from the two PFECAs are slower than those from the two PFCAs. In particular, the linear PFECA showed a slower initial rate but a significantly deeper defluorination than perfluoroheptanoic acid (i.e., 75 vs 55% of the 13 F atoms in each molecule). In contrast, the branched PFECA showed both a slower rate and a lower extent of defluorination than perfluorononanoic acid (i.e., 40 vs 58% of the 17 F atoms in each molecule). These results suggest new structure−reactivity relationships governing PFECA degradation. To systematically understand these mechanisms, we extended our study to 10 individual PFECAs, which exhibited structure-specific profiles of parent compound decay and defluorination (Table 3.1 and Figure 3.3).

Different Degradability of Four PFECA Structure Categories. Category **A** includes structures **A1−A3** with branched $-CF_3$ groups, which are the acid forms of hexafluoropropylene

oxide dimer, trimer, and tetramer (HFPO−DA, HFPO−TrA, and HFPO−TeA), respectively. The initial rates of parent compound decay were similar (Figure 3.3a), but longer structures showed a lower deF % (Figure 3.3b). The defluorination percentages of these branched PFECAs (31−45%) were significantly lower than those of traditional PFCAs (~55%) under the same reaction conditions.[40] Category **B** includes monoether structures **B1−B3** with the CF_3O- head group and linear $-(CF_2)_n-$ moieties (n = 1, 2, and 3, respectively) before the terminal $-COO^-$ group. The decay of **B2** and **B3** finished within 12 h (Figure 3.3c), and the time profiles for their parent compound decay were similar to full carbon-chain PFCAs (Figure 3.2a).[40] The final defluorination percentages are also similar (61 and 52% for **B2** and **B3**, respectively, vs 55% for PFCAs). In stark contrast, whereas the decay of **B1** (n = 1) was much slower than those of **B2** and **B3**, the deF % was substantially higher (91%). From the kinetic data, it seems that these $CF_3-O-(CF_2)_n-COO^-$ structures behave similarly to $F(CF_2)_n-COO^-$ under reductive treatment. In our previous study,[40] the decay of CF_3-COO^- took 24 h to complete while the deF % was almost 100%, whereas the decay of all longer PFCAs took 8−12 h to complete, but the maximal deF % was ~55% (Table 3.1, entry **E1** vs **E2**). We further tested two linear multiether PFECA categories, **C** and **D**. Both categories contain tetrafluoroethylene oxide (TFEO) building blocks, but the head groups are CF_3O^- and $C_4F_9O^-$, respectively. With $-O-CF_2-COO^-$ as the end group, the parent compound decay became slow again (cf. Figure 3.3e,g). Like the decay profile for the long-molecule **A3** (Figure 3.3a), the decay of the long-molecule **D2** was also incomplete within 48 h. The other three structures **C1**, **C2**, and **D1** showed profiles similar to the decay of **B1**. The notable difference between these two PFECA categories is that **C1** and **C2** with their short CF_3O^- head groups yielded a significantly higher deF % (82 and 75%, respectively) than **D1** and **D2** with their long $C_4F_9O^-$ head groups (58 and 65%, respectively) (cf. Figure 3.3f vs 3h).

3.3.2 Structural Effects on PFECA Degradation.

The kinetic data shown above indicates the following characteristics of PFECA degradation in comparison to traditional PFCAs: (1) branched PFECAs show slower decay and lower defluorination; (2) linear PFECAs exhibit slower decay if they contain $-O-CF_2-COO^-$ end groups or a very similar rate of decay if more than one $-CF_2-$ linker is present in the $-O-(CF_2)_n-COO^-$ functional group; (3) linear PFECAs containing shorter oxygen-segregated fluoroalkyl moieties showed a higher deF % To interpret these interesting results on the molecular level, we conducted theoretical calculations and TP analyses.

Theoretical Calculations of C−F and C−O BDEs. The bond dissociation energies (BDEs) of C−F and ether C−O bonds in all PFECA structures were calculated with density functional theory. Representative results are shown in Figure 3.4, and the full data sets are collected in Figures B.2−B.5. We identified new trends for C−F BDEs in PFECAs compared to full-carbon-chain PFCAs. First, the ether oxygen increases the BDE of C−F on the adjacent fluorocarbons. While the terminal $-CF_3$ in long fluoroalkyl chains has a typical C−F BDE < 119 kcal mol^{-1} (Figure 3.4d,f,h,i), the inclusion of ether oxygen atoms increased the C−F BDE to 120−123 kcal mol^{-1} (Figure 3.4a−c,g). In fluorinated molecules, the ether oxygen acts as an electron-donating group like the $-CH_2-$ group in FTCAs (Figure 3.4e). With multiple oxygen atoms in the chain, the relatively weak C−F bonds in long-chain PFCAs were not found in linear PFECAs (cf. Figure 3.4f vs 4g,h). In particular, the typically weak C−F bond at the α-position of PFCAs (i.e., BDE < 108 kcal mol^{-1}, Figure 3.4d,f) does not exist in linear PFECAs with an ether oxygen at the β-position (i.e., $\mathbf{R_F}-O-CF_2-COO^-$, BDE > 111 kcal mol^{-1}, Figure 3.4a,g,h). However, when the fluoroalkyl chain adjacent to $-COO^-$ is longer (i.e., n = 2 or 3 in $\mathbf{R_F}-O-(CF_2)_n-COO^-$), the weak C−F bond at the α-position appears again (Figure 3.4b,c). These novel trends on C−F BDEs in linear PFECAs corroborate the different rates of parent compound decay. The two structures with the weak α-

position C−F bonds (**B2** and **B3** in Figure 3.3c) showed a rate of decay similar to the full-carbon-chain PFCAs (Figure 3.2a), whereas the other $\mathbf{R_F}$−O−CF_2−COO^- structures showed slower parent compound decay (**B1**, **C1**, and **C2** in Figure 3.3c,e).

As for the branched PFECAs, the inclusion of ether oxygen atoms showed a similar effect on increasing the C−F BDEs. In comparison to a full-carbon-chain branched PFCA that contains very weak tertiary C−F bonds,[41] the oxygen atoms in HFPO−TrA significantly strengthen all secondary and tertiary C−F bonds (cf. Figure 3.4i vs 4j). Although the HFPO oligomer acids contain distinctly weak tertiary C−F bonds (i.e., BDE < 104 kcal mol^{-1}), the rates of the parent compound decay were slower than those of most of the linear PFECAs (Figure 3.3). Thus, other mechanisms and considerations beyond the cleavage of weak C−F bonds are likely responsible for the degradation of branched PFECAs. As the cleavage of ether C−O bonds has been proposed for the degradation of HFPO−DA,[38,39] we further examined the BDEs of C−O bonds in all PFECAs. A very interesting phenomenon is the "asymmetric" strength of the two C−O bonds on the first ether linkage counted from the terminal $-COO^-$ (Figure 3.4k−n). On this ether oxygen atom, the C−O bond away from $-COO^-$ has a considerably lower BDE (63−73 kcal mol^{-1}) than the other one closer to $-COO^-$ (78−94 kcal mol^{-1}). This phenomenon was observed in all PFECAs regardless of the total number of ether linkages, branched versus linear molecular backbone, or the distance between $-COO^-$ and the first ether linkage (cf. Figure 3.4k vs 4l). The BDE difference between those two C−O bonds in the three branched PFECAs ranges from 14.7 to 18.3 kcal mol^{-1}, and the difference in linear PFECAs is even greater, from 19.8 to 23.3 kcal mol^{-1} (see Figures B.2−B.5 for full data sets). However, if the PFECA molecule contains multiple ether oxygens, the pairs of C−O bonds in the remaining ether linkages have similar BDEs (i.e., only with small differences ranging from 0.1 to 3.4 kcal mol^{-1}, Figure 3.4m,n). In addition, because of the electron-withdrawing effect

by the $-CF_3$ branches, the BDEs of these "normal" C−O bonds in branched multiether structures (82−84 kcal mol^{-1}) are lower than those in linear multiether structures (89−97 kcal mol−1).

Spontaneous Bond Cleavage in Electron-Added PFECA Radical Anion Structures. The distinctly weak C−O bond in all PFECAs and the relatively weak tertiary C−F bonds in branched PFECAs imply the potential cleavage of these bonds during the reaction. To verify this hypothesis, we further conducted geometry optimization of the radical anion $[\mathbf{R_F}-COO]^{\bullet 2-}$ upon adding an extra electron (which simulates an e_{aq}^-) to the original PFECA anion ($\mathbf{R_F}-COO^-$).[40] As expected, the spontaneous stretching of the α-position C−F bonds (Figure 3.5a,b) and ether C−O bonds (Figure 3.5c,d) was observed. The distance between the two atoms stretched considerably longer than the normal length for C−O and C−F bonds (i.e., bond cleavage). The results for all PFECA structures are collected in Figures B.6 and B.7. Interestingly, although the calculated C−O bond cleavage in $[\mathbf{R_F}-COO]^{\bullet 2-}$ structures indeed occurred at the first ether linkage counted from the $-COO^-$ group, the cleaved C−O bond was not the "significantly weaker one" as calculated in the original $\mathbf{R_F}-COO^-$ (e.g., Figure 3.5c vs 3.4n). This discrepancy could be due to the addition of the extra electron, which altered the bonding structure of PFECA anions. More importantly, the calculation shows that C−O bond cleavage can be a major pathway for PFECA degradation by e_{aq}^-. The previously elucidated cleavage of weak C−F bonds[40] was also observed both from branched PFECAs (with very weak tertiary C−F bonds) and from the linear structure **B1** $CF_3-O-CF_2-COO^-$ where the *α*-position C−F BDE is relatively high (112 kcal mol^{-1}). These results suggest that C−F bond cleavage can be another degradation pathway, even if the inclusion of ether oxygen atoms causes many C−F bonds to be more recalcitrant than those in full-carbon-chain PFCAs.

PFECA Degradation Product Analysis. The above theoretical calculations have indicated the possibility of C−F and C−O bond cleavage. On the basis of our previous study, the decarboxylation−hydroxylation−HF elimination−hydrolysis (*DHEH*) is another major degradation

pathway for structures with the fluoroalkyl moiety directly linked with $-COO^-$.[40] Hence, we hypothesized that the degradation of PFECAs takes place via at least three pathways: (*i*) cleavage of weak C−F bonds and the formation of C−H bonds (i.e., H/F exchange), (*ii*) *DHEH*, and (*iii*) characteristic cleavage of ether C−O bonds. To detect the TPs and confirm the degradation pathways, we used both targeted analysis with triple quadruple mass spectrometry and suspect screening with high-resolution mass spectrometry data (all results are collected in Tables B.3−B.9). A series of TPs was detected, which supports all three proposed degradation pathways. The overall TP detection and the corresponding degradation pathways from the longest PFECA in each of the four structure categories are discussed below (Figure 3.6, and Schemes 3.1 and 3.2). The reaction schemes proposed for individual PFECAs are provided in Schemes B.1−B.10. As shown in Figure 3.6a, the degradation of **A3** HFPO−TeA generated **A2** HFPO−TrA and **A1** HFPO−DA daughter products. The maximum concentrations of **A2** (7.9 μM) and **A1** (3.7 μM) were detected at 8 and 12 h, respectively. We attribute this transformation to the cleavage of the first C−O bond counted from the terminal $-COO^-$ group. The two fragments reacted with H_2O to form two perfluorinated alcohols, which were not stable and subject to HF elimination to acyl fluoride.[42,43] The subsequent hydrolysis generated carboxylic acid, resulting in the net conversion from $\mathbf{R_F}-CF_2OH$ into R_F-COO^- and two F^-. The C−O cleavage on the first ether linkage counted from $-COO^-$ shortens HFPO−TeA into HFPO−TrA and then into HFPO−DA, which can be further degraded into $CF_3CF_2-COO^-$ via another C−O cleavage (Scheme 3.1). Each round of C−O cleavage also generated the same product $CF_3CF(OH)-COO^-$, which underwent further HF elimination into $CF_3-CO-COO^-$ (TFPy), as structures with F and OH on the same carbon (e.g., FCH_2OH) are generally unstable.[44] We confirmed the formation of TFPy during the degradation of HFPO−DA with IC detection (Figure B.8). Like CF_3-COO^- (trifluoroacetic acid, TFA), pure TFPy also showed near complete defluorination (Figure B.9), and TFA is a possible degradation intermediate

(Figure B.10). Although TFA was not detected in our samples from HFPO−DA degradation, we have elucidated that TFA can be generated from both CF_3CF_2−COO^- and TFPy and then completely mineralized via the *DHEH* pathway (Scheme 3.1b).[40] Suspect screening using the HRMS data identified a series of H/F exchange products from the HFPO oligomer acids. On the basis of our calculations, we assign the C−H bonds to the branched carbons (particularly the *α*-position branched carbon) where weak tertiary C−F bonds are located (Figure 3.6b and Scheme 3.1a). We also observed products missing one or more $-CF_3$ groups (i.e., H/CF_3 exchange). By comparing the results with those for linear PFECAs, such TP structures missing $-CF_3$ groups are specific for branched PFECAs. Therefore, we interpret the transformation pathway to be the cleavage of the branching $-CF_3$ rather than the terminal $-CF_3$. In addition, the degradation products and reaction schemes from pure HFPO−DA and HFPO−TrA (Tables B.3 and B.4 and Schemes B.1 and B.2) further corroborate the mechanistic insights obtained from HFPO−TeA degradation. For the degradation of **B3** (CF_3−O−$CF_2CF_2CF_2$−COO^-), the C−O bond cleavage mechanism was confirmed by the detection of ^-OOC−CF_2CF_2−COO^- (Figure 3.6c and Scheme 3.2a). The head CF_3− group was thus believed to be fully defluorinated via the formation of unstable CF_3−OH. The *DHEH* mechanism was also confirmed by the generation of **B2** CF_3−O−CF_2CF_2−COO^-. The HRMS detection of two products with one and two H/F exchanges on the parent compound (most probably at the *α*-position) is not surprising (Figure 3.6d). The degradation of the two multiether linear PFECAs **C2** and **D2** also followed the three reaction pathways, which are supported by the TPs identified (Figure 3.6e−h). Although the C−F BDEs of the *α*-position $-CF_2-$ in these structures are higher than those in full-carbon-chain PFCAs (Figure 3.4g vs 3.4f), the H/F-exchanged TPs were detected, thus corroborating the spontaneous C−F bond stretching by theoretical calculations (Figure 3.5a). Additionally, the C−O bond cleavage in **B1** (also in category **C** and **D** structures that contain $-O-CF_2-COO^-$) was supposed to generate $HO-CF_2-COO^-$, which should further

decompose into oxalate ($^{-}OOC-COO^{-}$). IC detection confirmed the formation of oxalate (Figure B.11), thus further consolidating this C−O bond cleavage mechanism.

3.3.3 Overall Mechanistic Insights into Reductive PFECA Degradation.

On the basis of the degradation kinetics, theoretical calculations, and TP analyses, we have confirmed that the PFECAs have three pathways for the reductive degradation by e_{aq}^{-}: (1) ether C−O bond cleavage, (2) C−C bond cleavage, including the decarboxylation step of *DHEH* and the cleavage of $-CF_3$ from branched PFECAs, and (3) direct C−F bond cleavage followed by H/F exchange. Here, we categorize the first two as indirect pathways for defluorination and the third one as a direct pathway for defluorination. It is worth noting here that all three independent pathways are enabled upon PFECAs interacting with e_{aq}^{-}. First, control experiments with UV irradiation without adding sulfite showed very slow and limited degradation (Figure B.12). Second, spontaneous C−O bond cleavage was observed after the PFECA anion received an extra electron (Figure 3.5). Third, the generation of e_{aq}^{-} from sulfite has been confirmed by spectroscopic observations,[45,46] and other chemicals such as iodide[47] and indole[48] have also been used as the source of e_{aq}^{-}, which have achieved similar results for PFOA defluorination. The cleavage of the C−O or C−C bond in PFECAs will generate perfluoroalcohols, which will undergo HF elimination and the following hydrolysis to yield two F^{-} and the corresponding carboxylic acids. This mechanism has been collectively supported by (1) the decay of HFPO and TFEO oligomer acids into shorter analogues (Figure 3.6a,e,g, supporting C−O cleavage) and the decay of **B3** into **B2** (Figure 3.6c, supporting C−C cleavage), (2) the generation of $^{-}OOC-CF_2CF_2-COO^{-}$ from **B3** ($CF_3-O-CF_2CF_2CF_2-COO^{-}$) and the generation of $^{-}OOC-COO^{-}$ from $\mathbf{R_F}-O-CF_2-COO^{-}$ structures, and most importantly (3) the high deF% of linear PFECAs with short oxygen-segregated fluorocarbon moieties. The results in Figure 3.3d,f,h show a clear trend that PFECAs containing longer fluorocarbon moieties (rather than a longer length of the molecule) yielded a lower deF %.

Because the perfluoroalcohol decomposition can only ensure the liberation of two F^- ions, if this step yields a full-carbon chain PFCA containing two or more fluorocarbons, a relatively easy H/F exchange on the *α*-position will occur, yielding $\mathbf{R_F}{-}CH_2{-}COO^-$. As previously elucidated, the reductive defluorination of this product is very sluggish, especially when the $\mathbf{R_F}$ moiety is short (i.e., lack of weak C−F bonds).[40] Among all PFECAs, **B1** ($CF_3{-}O{-}CF_2{-}COO^-$) allowed an outstanding deF % at 91% because either C−O cleavage or decarboxylation will trigger the perfluoroalcohol decomposition mechanism to liberate all five F− from the two oxygen-segregated single fluorocarbons. We hypothesized that the incomplete defluorination was attributed to the minor chance of H/F exchange on the α-position (Figure 3.5a). To verify this hypothesis, we examined the degradation of polyfluorinated $CF_3{-}O{-}CH_2{-}COO^-$ under the same reaction conditions (Figure 3.7). As expected, the $-CH_2-$ group at the *α*-position leads to a high recalcitrance in comparison with B1 (Figure 3.3c,d). However, to our surprise, the degradation at 24 h (30%) was much higher than the full-carbon-chain counterpart $CF_3CH_2{-}COO^-$ (<2%).[40] The overall deF % of 28% indicates near-complete defluorination of the decayed 30% fraction of the parent compound, and the time profiles of the parent compound decay and defluorination are highly symmetric. These results support the degradation mechanism of C−O bond cleavage rather than a stepwise H/F exchange. Therefore, C−O bond cleavage can still occur in a polyfluorinated ether structure, with a hydrocarbon moiety segregating the $-COO^-$ group from the fluorinated moiety. The rate is faster than in a polyfluorinated full-carbon-chain structure, but slower than in a perfluorinated ether structure. For comparison, under the same reaction conditions, the deF % for the full-carbon $CF_3CF_2{-}COO^-$ was 53%.[40] In our previous study, by assuming that $CF_3CF_2{-}COO^-$ will take either H/F exchange (forming the highly recalcitrant $CF_3CH_2{-}COO^-$ with negligible further degradation, with an overall deF % of 40%) or *DHEH* (leading to 100% defluorination via forming $CF_3{-}COO{-}$), we estimated that the probability of $CF_3CF_2{-}COO^-$ undergoing the H/F

exchange versus *DHEH* is 75 versus 25%.[40] Similarly, if all **B1** CF_3−O−CF_2−COO− first undergoes C−O or C−C bond cleavage, 100% defluorination would be achieved. If all **B1** first undergoes H/F exchange to yield CF_3−O−CH_2−COO− (deF % = 40% at this step), which then undergoes slow degradation for up to 30%, this would result in 40% + 60% × 30% = 58% defluorination. Hence, to yield an overall defluorination of 91% through the two competing pathways, the probability for **B1** to undergo H/F exchange is only 21%. This significantly decreased probability of H/F exchange from 75 to 21% should be attributed to the increased α-position C−F BDE in the $\mathbf{R_F}$−O−CF_2−COO^- structures (Figure 3.4a,g,h). This mechanistic insight also explains the low deF % for **B2** CF_3−O−CF_2CF_2−COO^- and **B3** CF_3−O−$CF_2CF_2CF_2$−COO^-, as the lower α-position C−F BDEs (Figure 3.4b,c) enabled easier H/F exchange. In Figure 3.3, the parent compound decays of **B2** and **B3** were faster than those of all $\mathbf{R_F}$−O−CF_2−COO− compounds. The formation of −CH_2− at the α-position significantly slowed down further degradation. In contrast, all PFECAs that allowed higher deF % than PFCAs (~55%)[40] contain only short (**C1** or **C2**) fluorocarbon moieties, which suppress the direct defluorination via H/F exchange (an unfavorable pathway, typically breaking weak C−F bonds) and enhance the indirect defluorination via C−O or C−C bond cleavage (a favorable pathway, breaking all C−F bonds on the carbon bearing −OH, regardless of the BDEs). The above mechanistic insights also explain the degradation pattern of branched PFECAs. The branching −CF_3 generates distinctly weak tertiary C−F bonds, especially at the α-position (Figures 3.4i and B.2). As shown in Figures 3.5b and 3.6b, these structures have a high tendency to undergo H/F exchange. The following cleavage of the branching −CF_3 leads to the formation of −CH_2− at the α-position, thus retarding further degradation. The longest structure **A3** has three tertiary C−F bonds; thus, the parent **A3** and the C−O cleavage products **A2** and **A1** all have a high probability of an unfavorable H/F exchange. Therefore, **A3** showed the lowest deF % among the three branched PFECAs. From the HRMS data for all PFECAs (Tables S3−S11), in general, the TPs with one H/F

exchange increased at the beginning of the reaction and then slowly decreased. In contrast, the two H/F exchange TPs slowly accumulated throughout the reaction, indicating high recalcitrance. In comparison to linear PFECAs and full-carbon-chain PFCAs, the slower parent compound decay of branched PFECAs is probably attributed to the kinetic hindrance by the branching $-CF_3$. We note that earlier studies by Bao *et al.*[38,39] on the degradation of HFPO oligomer acids (**A1**, **A2**, and **A3**) observed a significantly faster parent compound decay and higher deF % than our observations. In comparison to our reaction settings (one UV lamp for a 600 mL solution, pH 9.5, and 10 mM sulfite), Bao *et al.* used considerably more favorable conditions, including intense UV irradiation (16 similar UV lamps for a 45 mL solution), tripled basicity (pH 10), and a doubled sulfite concentration (20 mM). Because the duplication of using 20 mM sulfite at pH 10 in our photoreactors (one UV lamp for a 600 mL solution) achieved limited improvements on deF % (Figure B.13), the significantly higher defluorination observed by Bao *et al.*[38,39] should be attributed to the higher intensity of the 254 nm UV irradiation. Nonetheless, by comparing all PFECA compounds, we have identified new structural features allowing much deeper defluorination than HFPO oligomers. We expect that further enhanced degradation of PFECA structures can be achieved under energy−efficient reaction conditions, which are under optimization in our lab.

3.3.4 Implications for Fluorochemical Design and Environmental Remediation.

As seen from the diverse PFECA structures involved in this study, the design of PFECA is highly flexible as multiple fluorinated building blocks can be integrated into the molecule in various sequences. Although the design rationale of individual PFECAs (e.g., branched vs linear and the length of oxygen-segregated fluorocarbon moieties) and their targeted properties for specific industrial applications remain largely unknown to the environmental chemistry community, we are able to identify critical molecular features that can lead to enhanced PFECA degradation using reductive approaches. UV irradiation (on sulfite, iodide, indole, or hydroxyl radical

scavengers),[46–49] plasma treatment,[34] and high-energy irradiation[33] all involve e_{aq}^- as a primary reactive species. In general, the switch from full-carbon-chain PFCAs to PFECAs has indeed brought in unique advantages that enable deeper defluorination, including (1) spontaneous defluorination from alcohol intermediates upon C−O cleavage and (2) suppressed H/F exchange due to the strong C−F bonds. To minimize the incomplete defluorination caused by the conversion into recalcitrant products (e.g., with $-CH_2-$ separating the fluoroalkyl moiety and $-COO^-$), a desirable structural feature is $\mathbf{R_F}-O-CF_2-COO^-$. In other words, the last building block of the PFECA molecule can be a TFEO; after the epoxide ring opens, the alcohol product $\mathbf{R_F}-O-CF_2CF_2OH$ will transform to $\mathbf{R_F}-O-CF_2-COO^-$. As elucidated in earlier sections, the relatively high BDE of the α-position C−F favors indirect defluorination through C−O cleavage and decarboxylation. The other desirable structural feature is to limit the length of other fluorocarbon moieties segregated by ether oxygen atoms. If the chain length is **C1** (either CF_3-O- or $-O-CF_2-O-$), the C−O cleavage is expected to provide complete defluorination of that fluorocarbon moiety. This prediction, which is based on model PFECAs studied in this work, can be further examined when chemicals containing $-O-CF_2-O-$ moieties [e.g., $CF_3-(O-CF_2)_n-O-CF_2-COO^-$, n = 1 to 3][24,27] become available for experimental tests. Because the oxygen atoms substantially increase C−F BDEs (Figure 3.4), direct H/F exchange on **C1** or **C2** fluorocarbon moieties (not linked with $-COO^-$) is less likely. However, for **C2** fluorocarbon moieties (e.g., $-O-CF_2CF_2-O-$), the formation of $-O-CF_2-COO^-$ will still induce a low probability of H/F exchange. On the other hand, the mechanistic insights from this study will guide the development of PFECA degradation technologies. In particular, if direct defluorination cannot be fully avoided, effective degradation of the recalcitrant polyfluorinated products will be necessary to ensure deep or complete defluorination. Although we observed poor defluorination from the branched PFECAs that contain very weak tertiary C−F bonds and a long C3 fluorocarbon moiety,

studies by Bao *et al.*[38,39] have achieved deep defluorination of those structures by applying a high UV intensity. Therefore, coordinated efforts from both fluorochemical design (e.g., developing PFECAs with high degradability) and environmental remediation (e.g., optimizing the consumption of energy and chemicals) can be expected to transform the development, use, and treatment of fluorinated chemicals, with minimal adverse impact on the environment.

3.4 Tables and Figures

Table 3.1 Overall Defluorination Percentages of PFECAs after 48 Hours of Reaction.[a]

Entry	Structure	*n*	deF%
	A. *Branched (HFPO oligomers)*		
A1	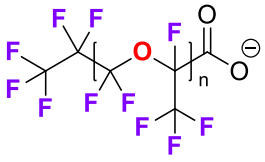	1	44.9 ± 5.3
A2		2	36.5 ± 2.9
A3		3	30.8 ± 4.2
	B. *Mono-ether with head CF_3O–*		
B1	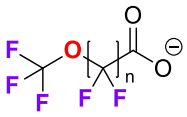	1	90.5 ± 2.1
B2		2	61.2 ± 7.5
B3		3	52.3 ± 3.1
	C. *TFEO oligomers with head CF_3O–*		
C1	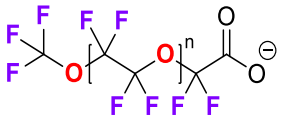	1	82.3 ± 4.4
C2		2	75.0 ± 3.8
	D. *TFEO oligomers with head C_4F_9O–*		
D1	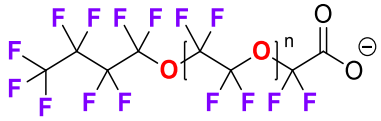	1	58.0 ± 4.0
D2		2	65.4 ± 6.3
	E. *Full-carbon-chain PFCAs*[b]		
E1		1	98.2 ± 5.0
E2		2-10	54.5 ± 3.5

[a]Reaction condition: PFAS (0.025 mM), Na_2SO_3 (10 mM), carbonate buffer (5 mM), 254 nm irradiation (a 18 W low-pressure Hg lamp for 600 mL solution) at pH 9.5 and 20°C.

[b]Data from Ref. 39 for comparison. The average and standard deviation of the deF% value for n = 2−10 is based on 27 data points (nine PFCA structures with triplicates).

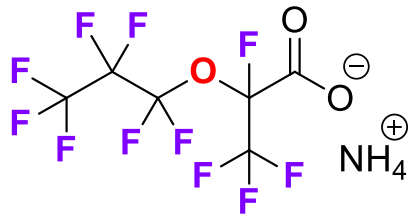

Perfluoro(2-methyl-3-oxahexanoate)
(GenX® – CAS No. 62037-80-3)

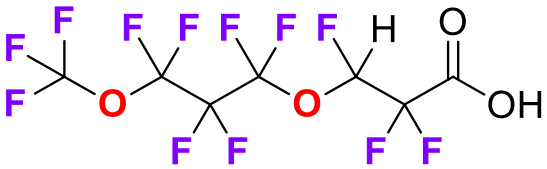

3H-perfluoro-3-[(3-methoxy-propoxy)propionic acid)
(ADONA® – CAS No. 958445-44-8)

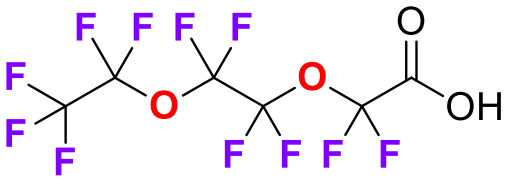

Perfluoro[(2-ethyloxy-ethoxy)acetic acid]
(EEA – CAS No. 908020-52-0)

Figure 3.1 Examples of commercial perfluorinated (GenX and EEA) and polyfluorinated (ADONA) ether carboxylic acids detected in the environment.

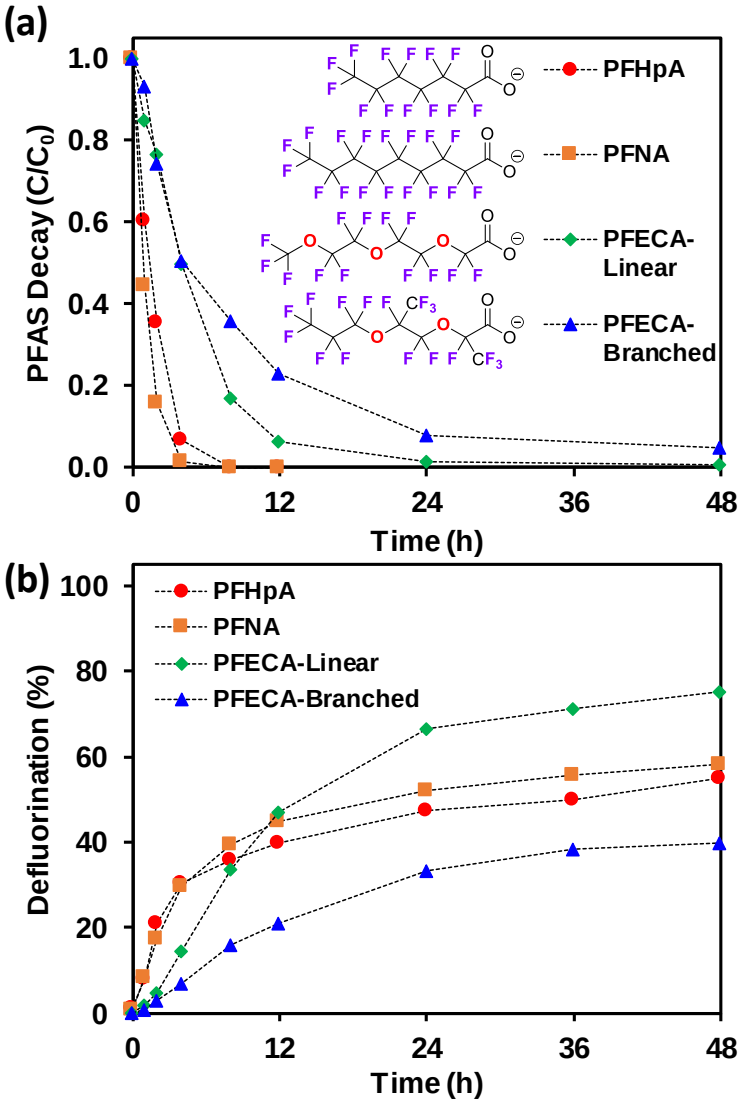

Figure 3.2 Time profiles for (a) parent compound decay and (b) defluorination percentages for two full-carbon-chain PFCAs with 13 and 17 F atoms, a linear PFECA with 13 F atoms, and a branched PFECA with 17 F atoms. *Reaction conditions*: PFAS (0.025 mM), Na_2SO_3 (10 mM), carbonate buffer (5 mM), 254 nm irradiation (18 W low-pressure Hg lamp for 600 mL solution) at pH 9.5 and 20 °C.

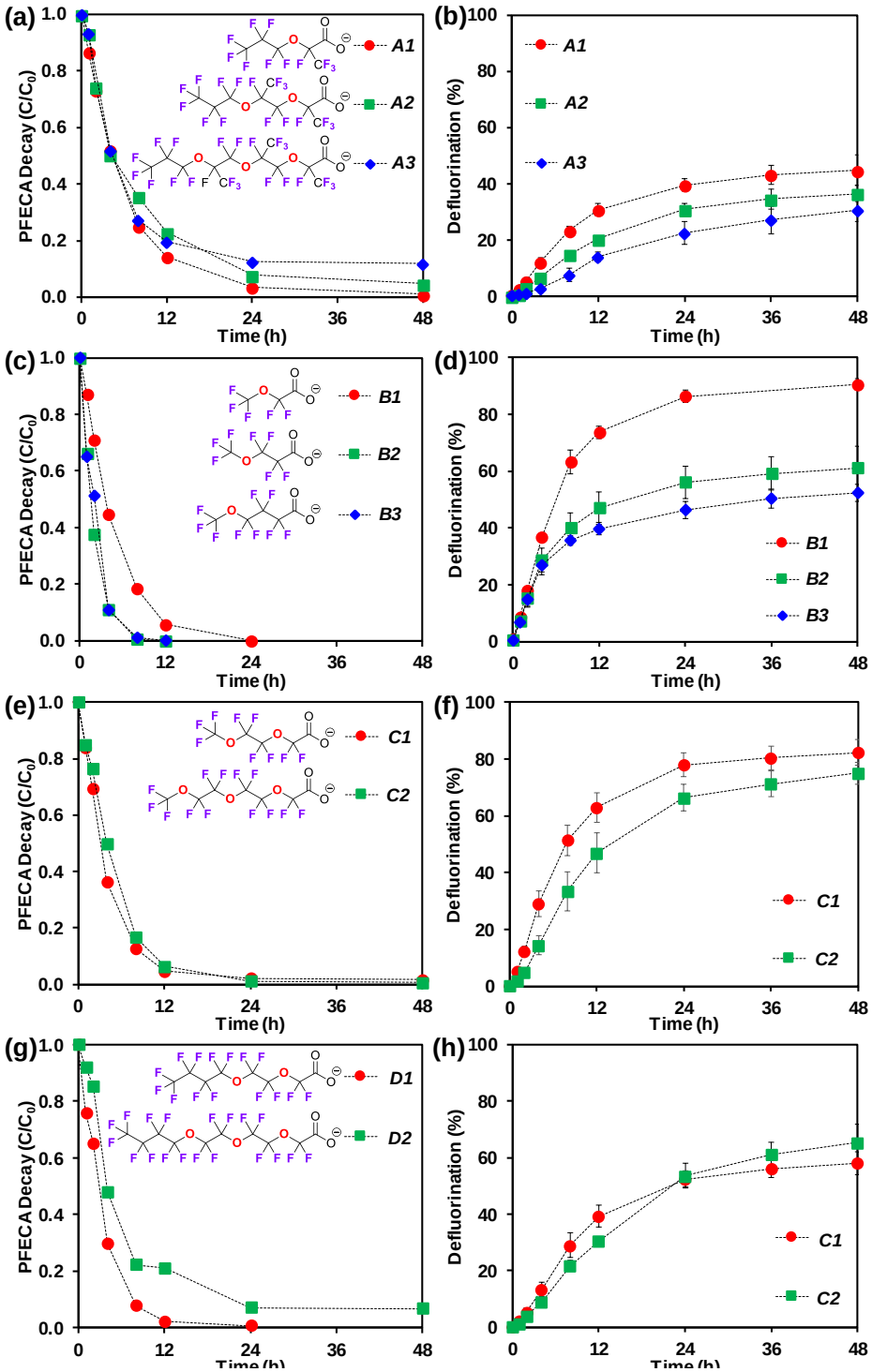

Figure 3.3 Time profiles of parent compound decay and defluorination for the four PFECA structure categories. Reaction conditions are described in the title of Figure 3.2.

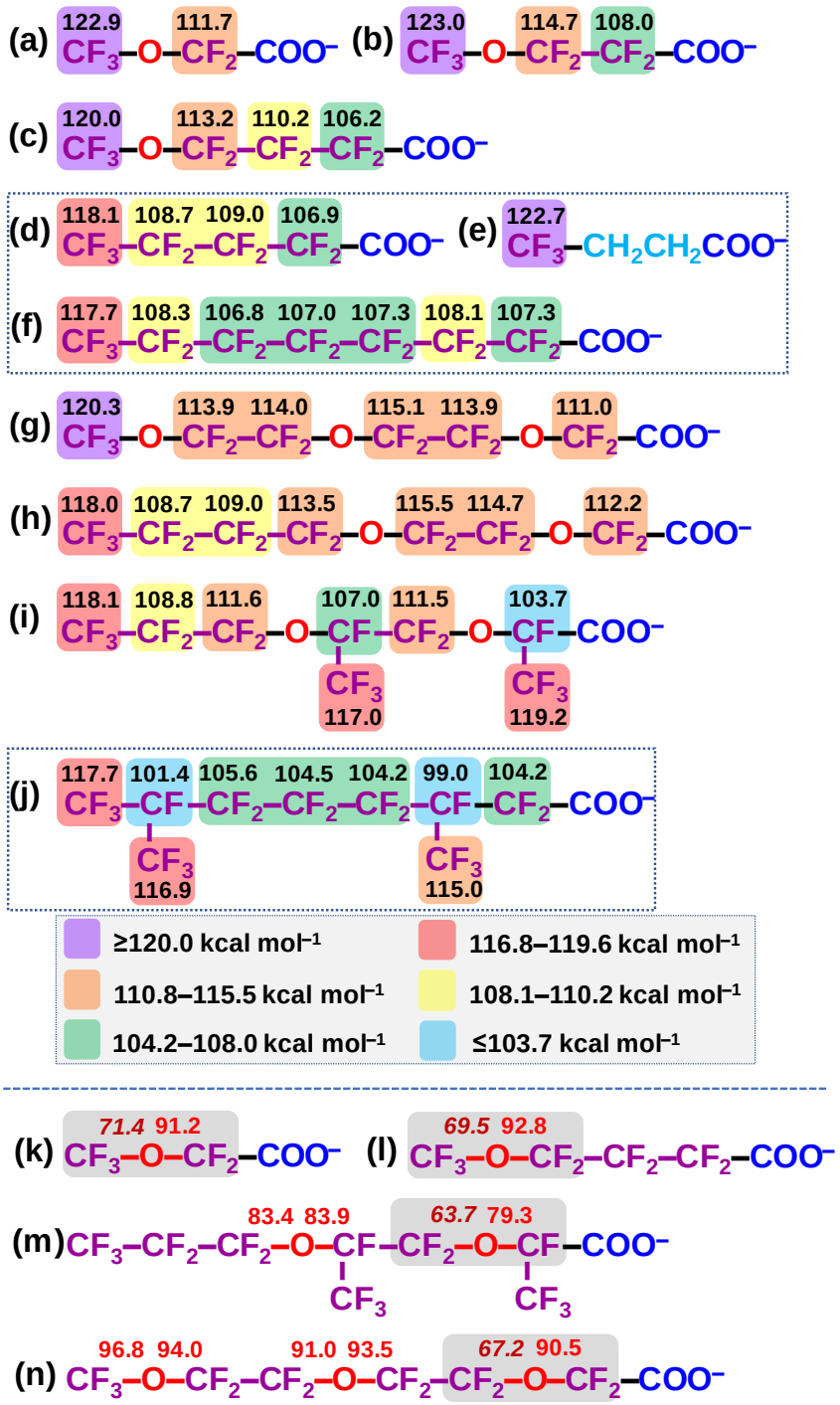

Figure 3.4 Calculated C−F BDEs (a–j) and C−O BDEs (k–n) (in kcal mol^{-1}) of selected PFASs at the B3LYP-D3(BJ)/6-311+G-(2d,2p) level of theory. Results for all PFECA structures are collected in Figures B.2−B.5. Data for (d−f,j) are from refs 40 and 41.

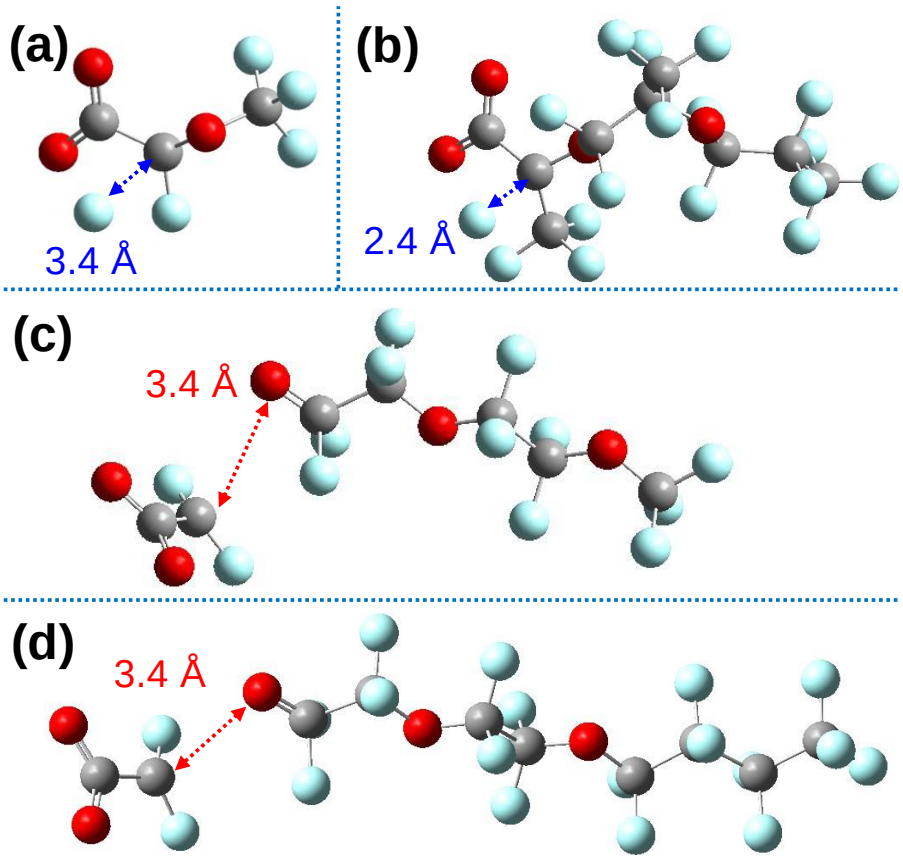

Figure 3.5 Geometry-optimized structure of the adducts of PFECA anions with an e_{aq}^- ($PFECA^{\bullet 2-}$) at the B3LYP-D3(BJ)/6-311+G-(2d,2p) level of theory, showing the stretching of C−F (blue) and C−O (red) bonds. Results for all PFECA structures are collected in Figures B.6 and B.7.

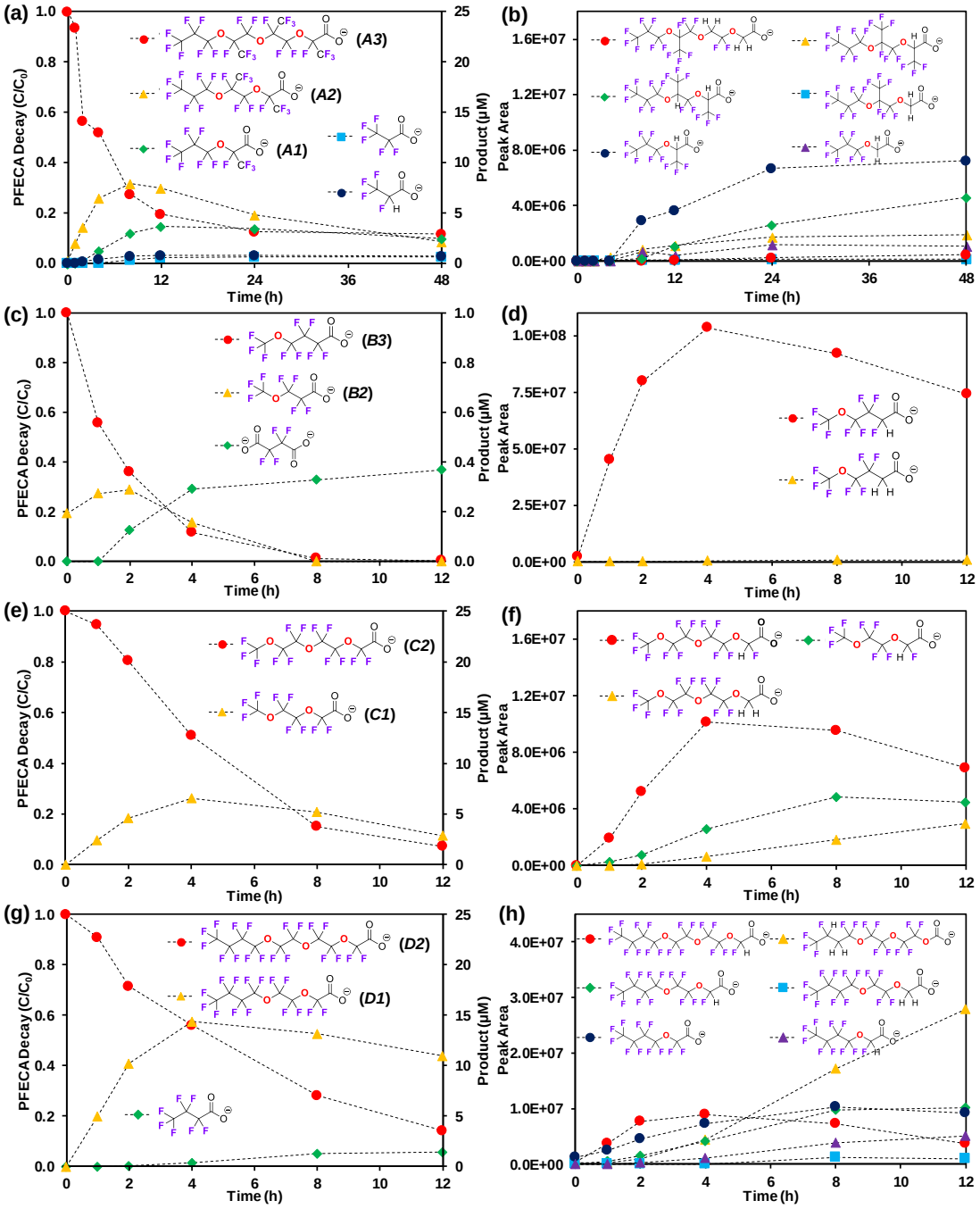

Figure 3.6 Representative degradation products of the longest compound in each structure category (**A3**, **B2**, **C2**, and **D2**, C_0 = 25 μM). Reaction conditions are described in the title of Figure 3.2. For each structure, quantified products with standard compounds are shown in the left panel, and species without standard compounds are presented in peak areas in the right panel. All detected species are listed in Tables B.3–B.11

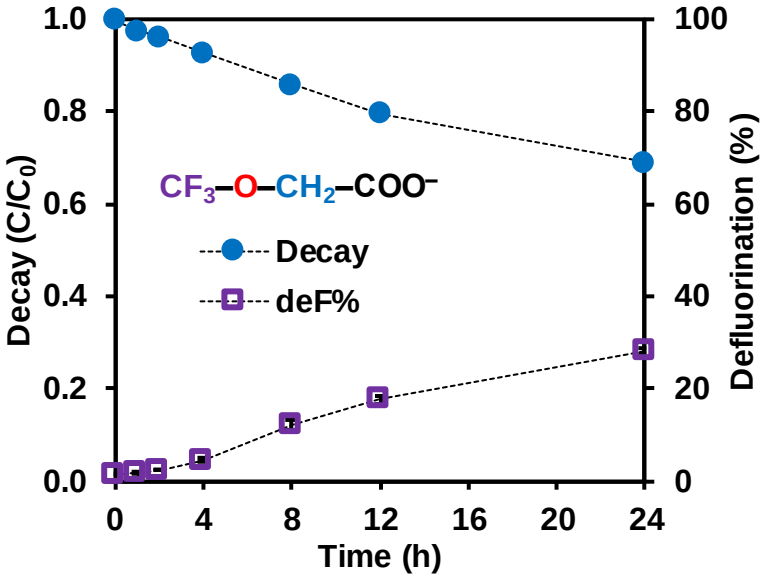

Figure 3.7 Time profiles of parent compound decay and defluorination for polyfluorinated CF_3–O–CH_2–COO^- under the same reaction conditions for all other PFECAs (described in the title of Figure 3.2).

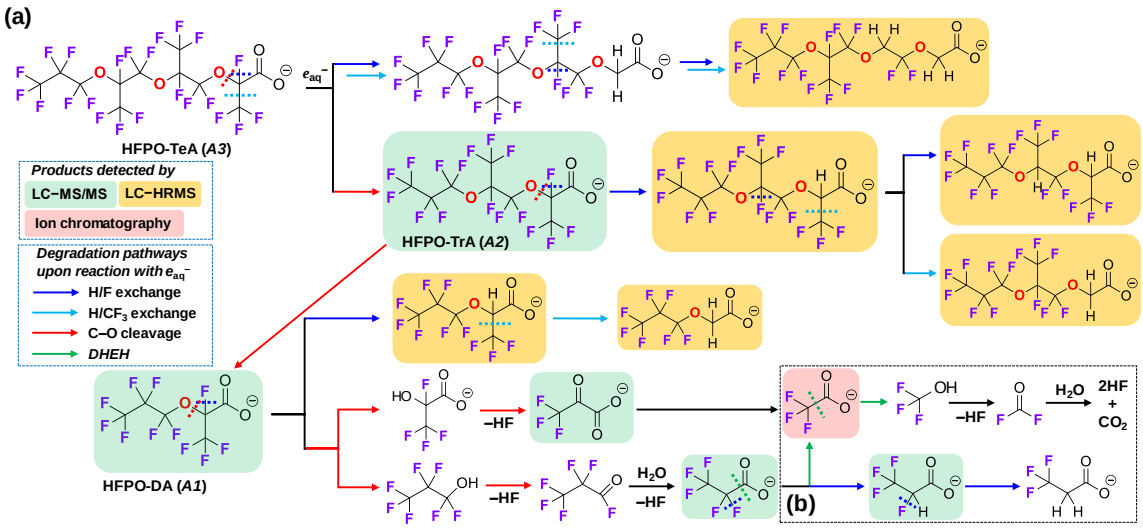

Scheme 3.1 Degradation Pathways for (a) HFPO Oligomer Acids Starting from the Longest Compound A3 and (b) the Daughter Product PFPrA; Detected TPs are Highlighted.

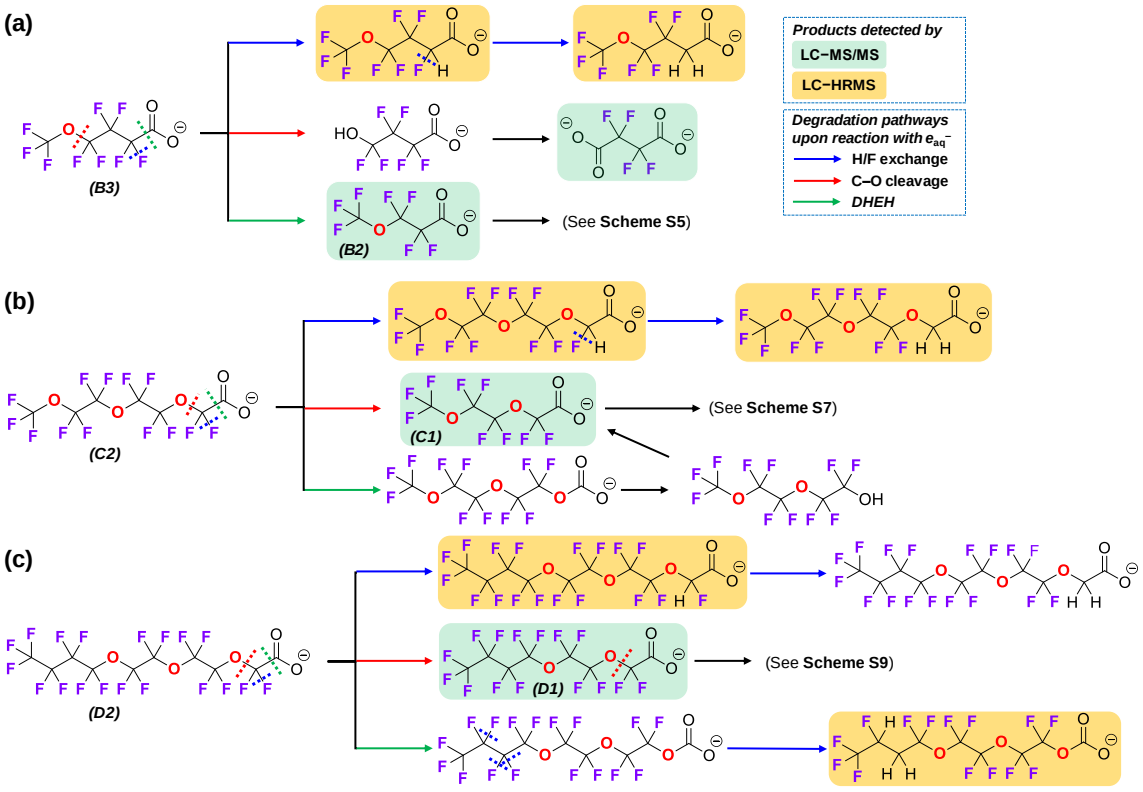

Scheme 3.2 Degradation Pathways for the Three PFECA Structure Categories Starting from the Longest Compound (a) ***B3***, (b) ***C2***, and (c) ***D2***; Detected TPs are highlighted.

REFERENCES

(1) Banks, R. E.; Smart, B. E.; Tatlow, J. Organofluorine Chemistry: Principles and Commercial Applications; Springer Science & Business Media, **2013**.

(2) Wang, Z.; DeWitt, J. C.; Higgins, C. P.; Cousins, I. T. A never-ending story of per-and polyfluoroalkyl substances (PFASs)? *Environ. Sci. Technol.* **2017**, *51*, 2508−2518.

(3) Buck, R. C.; Franklin, J.; Berger, U.; Conder, J. M.; Cousins, I. T.; De Voogt, P.; Jensen, A. A.; Kannan, K.; Mabury, S. A.; van Leeuwen, S. P. Perfluoroalkyl and polyfluoroalkyl substances in the environment: terminology, classification, and origins. *Integr. Environ. Assess. Manage.* **2011**, *7*, 513−541.

(4) Meshri, D. T. The modern inorganic fluorochemical industry. *J. Fluorine Chem.* **1986**, *33*, 195−226.

(5) Xiao, F. Emerging poly-and perfluoroalkyl substances in the aquatic environment: a review of current literature. *Water Res.* **2017**, *124*, 482−495.

(6) Liu, J.; Mejia Avendaño, S. Microbial degradation of polyfluoroalkyl chemicals in the environment: A review. *Environ. Int.* **2013**, *61*, 98−114.

(7) Kelly, B. C.; Ikonomou, M. G.; Blair, J. D.; Surridge, B.; Hoover, D.; Grace, R.; Gobas, F. A. P. C. Perfluoroalkyl contaminants in an Arctic marine food web: trophic magnification and wildlife exposure. *Environ. Sci. Technol.* **2009**, *43*, 4037−4043.

(8) United States Environmental Protection Agency. Revisions to the unregulated contaminant monitoring regulation (UCMR 3) for public water systems. *Fed. Reg.* **2012**, *77*, 26071−26101.

(9) United States Environmental Protection Agency. Lifetime health advisories and health effects support documents for perfluorooctanoic acid and perfluorooctane sulfonate. *Fed. Reg.* **2016**, *81*, 33250−33251.

(10) COMMISSION REGULATION (EU) 2017/1000 of 13 June 2017 amending Annex XVII to Regulation (EC) No. 1907/2006 of the European Parliament and of the Council concerning the Registration, Evaluation, Authorisation and Restriction of Chemicals (REACH) as regards perfluorooctanoic acid (PFOA), its salts and PFOA-related substances. Off. *J. Eur. Union*. **2017**, 14.6.2017, L 150/14-L 150/18.

(11) Post, G. B.; Gleason, J. A.; Cooper, K. R. Key scientific issues in developing drinking water guidelines for perfluoroalkyl acids: Contaminants of emerging concern. *PLoS Biol.* **2017**, *15* (12), No. e2002855.

(12) U.S. EPA. 2010/15 PFOA Stewardship Program. https://www.epa.gov/assessing-and-managing-chemicals-under-tsca/riskmanagement-and-polyfluoroalkyl-substances-pfass#tab-3 (accessed January 27, 2020).

(13) Wang, J.; Pan, Y.; Cui, Q.; Yao, B.; Wang, J.; Dai, J. Penetration of PFASs across the blood cerebrospinal fluid barrier and its determinants in humans. *Environ. Sci. Technol.* **2018**, *52*, 13553−13561.

(14) Rappazzo, K.; Coffman, E.; Hines, E. Exposure to perfluorinated alkyl substances and health outcomes in children: a systematic review of the epidemiologic literature. *Int. J. Environ. Res. Public Health*. **2017**, *14*, 691.

(15) Brandsma, S.; Koekkoek, J.; van Velzen, M.; de Boer, J. The PFOA substitute GenX detected in the environment near a fluoropolymer manufacturing plant in the Netherlands. *Chemosphere*. **2019**, *220*, 493−500.

(16) Wang, Z.; Cousins, I. T.; Scheringer, M.; Hungerbühler, K. Fluorinated alternatives to long-chain perfluoroalkyl carboxylic acids (PFCAs), perfluoroalkane sulfonic acids (PFSAs) and their potential precursors. *Environ. Int.* **2013**, *60*, 242−248.

(17) Strynar, M.; Dagnino, S.; McMahen, R.; Liang, S.; Lindstrom, A.; Andersen, E.; McMillan, L.; Thurman, M.; Ferrer, I.; Ball, C. Identification of novel perfluoroalkyl ether carboxylic acids (PFECAs) and sulfonic acids (PFESAs) in natural waters using accurate mass time-of-flight mass spectrometry (TOFMS). *Environ. Sci. Technol.* **2015**, *49*, 11622−11630.

(18) Pan, Y.; Zhang, H.; Cui, Q.; Sheng, N.; Yeung, L. W. Y.; Guo, Y.; Sun, Y.; Dai, J. First report on the occurrence and bioaccumulation of hexafluoropropylene oxide trimer acid: An emerging concern. *Environ. Sci. Technol*. **2017**, *51*, 9553−9560.

(19) Pan, Y.; Zhang, H.; Cui, Q.; Sheng, N.; Yeung, L. W. Y.; Sun, Y.; Guo, Y.; Dai, J. Worldwide distribution of novel perfluoroether carboxylic and sulfonic acids in surface water. *Environ. Sci. Technol.* **2018**, *52*, 7621−7629.

(20) Sun, M.; Arevalo, E.; Strynar, M.; Lindstrom, A.; Richardson, M.; Kearns, B.; Pickett, A.; Smith, C.; Knappe, D. R. U. Legacy and emerging perfluoroalkyl substances are important drinking water contaminants in the Cape Fear River Watershed of North Carolina. *Environ. Sci. Technol. Lett.* **2016**, *3*, 415−419.

(21) Gebbink, W. A.; van Asseldonk, L.; van Leeuwen, S. P. J. Presence of emerging per-and polyfluoroalkyl substances (PFASs) in river and drinking water near a fluorochemical production plant in the Netherlands. *Environ. Sci. Technol.* **2017**, *51*, 11057−11065.

(22) Conley, J. M.; Lambright, C. S.; Evans, N.; Strynar, M. J.; McCord, J.; McIntyre, B. S.; Travlos, G. S.; Cardon, M. C.; Medlock- Kakaley, E.; Hartig, P. C.; Wilson, V. S.; Gray, L. E. Adverse Maternal, Fetal, and Postnatal Effects of Hexafluoropropylene Oxide Dimer Acid (GenX) from Oral Gestational Exposure in Sprague-Dawley Rats. *Environ. Health Perspect.* **2019**, *127*, 037008.

(23) Sheng, N.; Pan, Y.; Guo, Y.; Sun, Y.; Dai, J. Hepatotoxic effects of hexafluoropropylene oxide trimer acid (HFPO-TA), a novel perfluorooctanoic acid (PFOA) alternative, on mice. *Environ. Sci. Technol.* **2018**, *52*, 8005−8015.

(24) Cui, Q.; Pan, Y.; Zhang, H.; Sheng, N.; Wang, J.; Guo, Y.; Dai, J. Occurrence and tissue distribution of novel perfluoroether carboxylic and sulfonic acids and legacy per/polyfluoroalkyl substances in black-spotted frog (Pelophylax nigromaculatus). *Environ. Sci. Technol.* **2018**, *52*, 982−990.

(25) Sheng, N.; Cui, R.; Wang, J.; Guo, Y.; Wang, J.; Dai, J. Cytotoxicity of novel fluorinated alternatives to long-chain perfluoroalkyl substances to human liver cell line and their binding capacity to human liver fatty acid binding protein. *Arch. Toxicol.* **2018**, *92*, 359−369.

(26) Hill, J. T. Polymers from hexafluoropropylene oxide (HFPO). *J. Macromol. Sci. A.* **1974**, *8*, 499−520.

(27) McCord, J.; Strynar, M. Identification of per-and polyfluoroalkyl substances in the Cape Fear River by high resolution mass spectrometry and nontargeted screening. *Environ. Sci. Technol.* **2019**, *53*, 4717−4727.

(28) McCord, J.; Newton, S.; Strynar, M. Validation of quantitative measurements and semi-quantitative estimates of emerging perfluoroethercarboxylic acids (PFECAs) and hexfluoroprolyene oxide acids (HFPOAs). *J. Chromatogr. A.* **2018**, *1551*, 52−58.

(29) Wang, Y.; Yu, N.; Zhu, X.; Guo, H.; Jiang, J.; Wang, X.; Shi, W.; Wu, J.; Yu, H.; Wei, S. Suspect and nontarget screening of per-and polyfluoroalkyl substances in wastewater from a fluorochemical manufacturing park. *Environ. Sci. Technol.* **2018**, *52*, 11007−11016.

(30) Merino, N.; Qu, Y.; Deeb, R. A.; Hawley, E. L.; Hoffmann, M. R.; Mahendra, S. Degradation and removal methods for perfluoroalkyl and polyfluoroalkyl substances in water. *Environ. Eng. Sci.* **2016**, *33*, 615−649.

(31) Schaefer, C. E.; Andaya, C.; Burant, A.; Condee, C. W.; Urtiaga, A.; Strathmann, T. J.; Higgins, C. P. Electrochemical treatment of perfluorooctanoic acid and perfluorooctane sulfonate: Insights into mechanisms and application to groundwater treatment. *Chem. Eng. J.* **2017**, *317*, 424−432.

(32) Gole, V. L.; Fishgold, A.; Sierra-Alvarez, R.; Deymier, P.; Keswani, M. Treatment of perfluorooctane sulfonic acid (PFOS) using a large-scale sonochemical reactor. *Sep. Purif. Technol.* **2018**, *194*, 104−110.

(33) Zhang, Z.; Chen, J.-J.; Lyu, X.-J.; Yin, H.; Sheng, G.-P. Complete mineralization of perfluorooctanoic acid (PFOA) by γ-irradiation in aqueous solution. *Sci. Rep.* **2015**, *4*, 7418.

(34) Stratton, G. R.; Dai, F.; Bellona, C. L.; Holsen, T. M.; Dickenson, E. R. V.; Mededovic Thagard, S. Plasma-based water treatment: Efficient transformation of perfluoroalkyl substances in prepared solutions and contaminated groundwater. *Environ. Sci. Technol.* **2017**, *51*, 1643−1648.

(35) Trojanowicz, M.; Bojanowska-Czajka, A.; Bartosiewicz, I.; Kulisa, K. Advanced oxidation/reduction processes treatment for aqueous perfluorooctanoate (PFOA) and perfluorooctanesulfonate (PFOS)−A review of recent advances. *Chem. Eng. J.* **2018**, *336*, 170−199.

(36) Hori, H.; Nagano, Y.; Murayama, M.; Koike, K.; Kutsuna, S. Efficient decomposition of perfluoroether carboxylic acids in water with a combination of persulfate oxidant and ultrasonic irradiation. *J. Fluorine Chem.* **2012**, *141*, 5−10.

(37) Hori, H.; Yamamoto, A.; Koike, K.; Kutsuna, S.; Murayama, M.; Yoshimoto, A.; Arakawa, R. Photocatalytic decomposition of a perfluoroether carboxylic acid by tungstic heteropolyacids in water. *Appl. Catal., B.* **2008**, *82*, 58−66.

(38) Bao, Y.; Deng, S.; Jiang, X.; Qu, Y.; He, Y.; Liu, L.; Chai, Q.; Mumtaz, M.; Huang, J.; Cagnetta, G. Degradation of PFOA substitute: GenX (HFPO−DA ammonium salt): Oxidation with UV/persulfate or reduction with UV/sulfite? *Environ. Sci. Technol.* **2018**, *52*, 11728−11734.

(39) Bao, Y.; Cagnetta, G.; Huang, J.; Yu, G. Degradation of hexafluoropropylene oxide oligomer acids as PFOA alternatives in simulated nanofiltration concentrate: Effect of molecular structure. *Chem. Eng. J.* **2020**, *382*, 122866.

(40) Bentel, M. J.; Yu, Y.; Xu, L.; Li, Z.; Wong, B. M.; Men, Y.; Liu, J. Defluorination of per- and polyfluoroalkyl substances (PFASs) with hydrated electrons: Structural dependence and implications to PFAS remediation and management. *Environ. Sci. Technol.* **2019**, *53*, 3718−3728.

(41) Liu, J.; Van Hoomissen, D. J.; Liu, T.; Maizel, A.; Huo, X.; Fernández, S. R.; Ren, C.; Xiao, X.; Fang, Y.; Schaefer, C. E.; Higgins, C. P.; Vyas, S.; Strathmann, T. J. Reductive defluorination of branched

per- and polyfluoroalkyl substances with cobalt complex catalysts. *Environ. Sci. Technol. Lett.* **2018**, *5*, 289−294.

(42) Seppelt, K. Trifluoromethanol, CF_3OH. *Angew. Chem., Int. Ed.* **1977**, *16*, 322−323.

(43) Christe, K. O.; Hegge, J.; Hoge, B.; Haiges, R. Convenient access to trifluoromethanol. *Angew. Chem., Int. Ed.* **2007**, *46*, 6155−6158.

(44) Suenram, R. D.; Lovas, F. J.; Pickett, H. M. Fluoromethanol: Synthesis, microwave spectrum, and dipole moment. *J. Mol. Spectrosc.* **1986**, *119*, 446−455.

(45) Maza, W. A.; Breslin, V. M.; Plymale, N. T.; DeSario, P. A.; Epshteyn, A.; Owrutsky, J. C.; Pate, B. B. Nanosecond transient absorption studies of the pH-dependent hydrated electron quenching by HSO_3^-. *Photochem. Photobiol. Sci.* **2019**, *18*, 1526−1532.

(46) Sun, Z.; Zhang, C.; Xing, L.; Zhou, Q.; Dong, W.; Hoffmann, M. R. UV/nitrilotriacetic acid process as a novel strategy for efficient photoreductive degradation of perfluorooctanesulfonate. *Environ. Sci. Technol.* **2018**, *52*, 2953−2962.

(47) Park, H.; Vecitis, C. D.; Cheng, J.; Dalleska, N. F.; Mader, B. T.; Hoffmann, M. R. Reductive degradation of perfluoroalkyl compounds with aquated electrons generated from iodide photolysis at 254 nm. *Photochem. Photobiol. Sci.* **2011**, *10*, 1945−1953.

(48) Tian, H.; Gao, J.; Li, H.; Boyd, S. A.; Gu, C. Complete defluorination of perfluorinated compounds by hydrated electrons generated from 3-indole-acetic-acid in organomodified montmorillonite. *Sci. Rep.* **2016**, *6*, 32949.

(49) Song, Z.; Tang, H.; Wang, N.; Zhu, L. Reductive defluorination of perfluorooctanoic acid by hydrated electrons in a sulfite-mediated UV photochemical system. *J. Hazard. Mater.* **2013**, *262*, 332−338.

CHAPTER 4: ENHANCED DEGRADATION OF PERFLUOROCARBOXYLIC ACIDS (PFCAs) BY UV/SULFITE TREATMENT: REACTION MECHANISMS AND SYSTEM EFFICIENCES AT PH 12

Abstract

Reductive defluorination with UV-generated hydrated electrons (e_{aq}^-) is a promising technology for the destruction of perfluorocarboxylic acids (PFCAs, $C_nF_{2n+1}COO^-$). However, prior studies using pH 9−10 observed a slow reaction rate, limited defluorination percentage (deF%), and thus high energy consumption. Herein, we report on the substantially enhanced rate and extent of PFCA defluorination by operating the UV/sulfite system at the optimized pH 12. Degradation kinetics and transformation products show that at pH 12 the e_{aq}^- cleaved multiple strong C−F bonds that could not be cleaved at pH 9.5. The high pH condition also significantly favored the preferred decarboxylation pathway toward a deep defluorination. In comparison to the reactions at pH 9.5, the increase in solution pH to 12 improved the UV lamp energy efficiency by 5−22 folds, enhanced the deF% of C3−C9 PFCAs to 73%−93%, and reduced the overall consumption of chemicals.

4.1 Introduction

The global environmental pollution by per- and polyfluoroalkyl substances (PFAS)[1–3] requires remediation technologies to be both effective and efficient. While separation methods (e.g., carbon adsorption, ion exchange, and membrane filtration) provide rapid PFAS removal from polluted water,[4–6] concentrated PFAS compounds in the wastewaters from sorbent regeneration or membrane rejection must be destructed. As the biological degradation of PFAS is sluggish,[7,8] a variety of physicochemical approaches (e.g., electrochemical,[9,10] photochemical,[11,12] plasmatic,[13–15] sonochemical,[16–18] and radiolytic[19]) for PFAS destruction have been under development.[20,21] These technologies utilize reductive and oxidative species to cleave the highly stable C−F bonds[22] from

PFAS molecules (i.e., defluorination). Currently, most approaches are challenged by (1) slow parent compound decay, (2) limited extent of defluorination, and (3) high energy consumption.

Reductive defluorination using UV-generated hydrated electrons (e_{aq}^-)[23−25] is a homogeneous process in aqueous solution. The reaction of dissolved PFAS molecules, especially the short-chain structures, is not limited by the mass transfer from the bulk solution to the water−solid (e.g., electrode surface or photocatalyst particle) or water−gas (e.g., in plasma or sonochemical systems) heterogeneous interfaces.[10,14,18] Among the e_{aq}^- source chemicals (e.g., sulfite,[26] iodide,[27] amino acids,[28] and indoles[29]) used for PFAS destruction, sulfite has already been applied in various wastewater treatment processes,[30−32] and the final product is the nontoxic sulfate. Despite the advantages, the UV/sulfite approach has been challenged by the high energy consumption of UV lamps.[25,33] In our previous study using a low-pressure 254 nm mercury lamp at pH 9.5, the decay of $n \geq 2$ perfluorocarboxylic acid (PFCAs, $C_nF_{2n+1}COO^-$) parent compounds took 8−12 h. The completion of a partial defluorination from those PFCAs required an even longer time of 24−48 h.[25] Higher intensity (e.g., using multiple 254 nm lamps)[34] or higher energy UV irradiation (e.g., using medium-pressure lamps with a wide emission spectrum)[35] could accelerate the reaction, but the energy consumption became even higher. Earlier studies on UV/iodide[36] and UV/amino acid[28] systems had observed better performance at higher pH; however, most studies using e_{aq}^- for PFAS destruction chose the pH at 9−10,[34,35,37−40] probably for consistency with earlier reported conditions.

In this Letter, by raising the pH from 9.5 to 12, we observed substantially enhanced rates and extents of defluorination from PFCAs. PFCAs are not only a major category of PFAS pollutants but also the degradation intermediates from fluorotelomers (upon oxidation of hydrocarbon moieties)[7,41] and perfluorosulfonic acids (upon C−S bond cleavage).[25,33] Transformation product (TP) analyses and tests using model structures reveal new mechanistic insights into the effects of

pH elevation. Further optimization of the UV/sulfite reaction conditions demonstrates that a simple pH adjustment will significantly save both electrical energy and chemical reagents needed for a deep destruction of PFCA pollutants.

4.2 Materials and Methods

Details of chemicals and experimental procedures are described in Appendix C (App C). To compare the effects of pH and other key parameters of the UV/sulfite system, the photoreactor settings and reaction conditions closely followed our previous work (open access).[25] Briefly, an aqueous solution (600 mL) containing 25 μM of individual PFCA compounds, 5 mM of $NaHCO_3$, and 10 mM of Na_2SO_3 was treated by an 18 W low-pressure mercury UV lamp at 20°C (with water bath cooling). Control experiments have excluded direct photolysis of PFCAs by the minor 185 nm VUV emission[42] (Figure C.2). The initial pH was adjusted to 9.5−12.0 by NaOH and monitored with a Radiometer Analytical PHC2401−8 pH electrode, which has a working range of pH 0−12. The pH of 12.3 (equivalent to 20 mM OH^-) was achieved by adding another 10 mM NaOH after the solution pH was adjusted to 12.0. The pH drifts after all reactions were less than 0.3. Sulfite slowly decayed during the reaction, with at least 20% remaining by 8 h at pH 12.0 and by 24 h at pH 9.5 (Figure C.3). Sample analyses of the released fluoride ion (F^-), PFCA parent compounds, and TPs have been described in our previous work,[25] and the details for pH 12 experiments are described in App C. The defluorination percentage (deF%) is defined as the concentration ratio between the released F^- in solution and the total F in the parent PFCA molecule prior to the reaction.

4.3 Results and Discussion

When the solution pH was increased from 9.5, the UV/sulfite treatment of the probe compound, PFOA, showed faster rates and higher percentages (Figure 4.1a). We identified pH 12.0 as the optimal condition after comparing the kinetics data measured at multiple pH values between 11.0 (equivalent to 1 mM of OH^-) and 12.3 (equivalent to 20 mM of OH^-). At pH 12, the optimal

Na_2SO_3 concentration was 10 mM (Figure 4.1b). The use of pH 12 and 10 mM sulfite enhanced PFCA destruction in multiple aspects. The $n \geq 2$ $C_nF_{2n+1}COO^-$ structures showed similar degradation kinetics regardless of the chain length. From pH 9.5 to 12, a greater than 99.9% decay of 25 μM parent compounds was substantially accelerated from 8−12 h to less than 1 h (Figure 4.1c), and the time to reach the deF% plateau was shortened from greater than 24 h to 4−8 h (Figure 4.1d). Most importantly, the maximum deF% values were significantly enhanced to 73%−93% (Table 4.1). The $n = 1$ CF_3COO^- (trifluoroacetate, TFA) is much more recalcitrant than $n \geq 2$ PFCAs. At pH 9.5, the completion of both decay and defluorination of TFA required more than 24 h.[25] In stark contrast, at pH 12, the parent compound decay and 100% defluorination were completed within 1 and 4 h, respectively.

To quantitatively demonstrate the energy saving by pH control, we calculated the electrical energy per order (EE/O),[43,44] which is defined as the number of kilowatt-hours (kWh) of electrical energy required to reduce the pollutant concentration by 1 order of magnitude per m^3 of water. At pH 9.5, the EE/O for $n = 1$ TFA and $n \geq 2$ PFCAs were 457 and 77−174 kWh m^{-3}, respectively (Table 4.1). At pH 12, as the reactions became much faster, the corresponding EE/O was substantially reduced to 20 kWh m^{-3} for TFA and 10−16 kWhm^{-3} for $n \geq 2$ PFCAs.

Previous studies have provided initial mechanistic insights, on the effects of pH, from the perspectives in the concentration and lifetime of e_{aq}^-. Song *et al.*[26] correlated the initial deF% from PFOA to the pseudosteady-state concentration of e_{aq}^-, which is generated from SO_3^{2-} but quenched by HSO^{3-}, $S_2O_6^{2-}$, and H^+. Later on, using laser flash photolysis experiments, Maza *et al.*[45] and Qu *et al.*[36] observed higher absorbance and longer lifetime of e_{aq}^- at higher pH (up to 10) in UV/sulfite and UV/iodide systems, respectively. We note that the p*K*a of HSO_3^-/SO_3^{2-} is 7.17,[46] and most sulfite should be SO_3^{2-} at pH > 9. At pH 7.5 and above, the aqueous sulfite solution shows the same level of absorption at 254 nm.[47] Thus, the further enhancement of PFCA degradation from pH 9.5

to 12 can be attributed to the lowered concentration of H^+ (see App C for the thermodynamic estimation that a lowered redox potential of e_{aq}^- allows the cleavage of more recalcitrant C−F bonds) and probably additional unknown pathways involving other reactive species.[23,48] We aimed at elucidating the molecular transformations corresponding to the enhanced availability of e_{aq}^- at pH 12.

First, the degradation kinetics of TFA at pH 12 revealed a different mechanism from that at pH 9.5. In comparison to $n \geq 2$ PFCAs, TFA is distinctively recalcitrant because the calculated bond dissociation energy (BDE) of the C−F bond in CF_3−COO^- is 116.8 kcal mol^{-1},[25] which is significantly stronger than the weak α-position C−F bonds in $n \geq 2$ PFCAs ($C_{n-1}F_{2n-1}$−CF_2−COO^-, with BDEs of 106.8−107.3 kcal mol^{-1}).[25] At pH 9.5, the profiles of TFA decay and F^- release are nearly symmetric (Figure 3.2a), indicating that the transformation of the CF_3−COO^- parent structure triggers a rapid cleavage of all three C−F bonds through the *DHEH* pathway[25,49,50]

CF_3−$COO^- + e_{aq}^- \rightarrow ? \rightarrow CF_3$−$OH$ (***D***ecarboxylation and ***H***ydroxylation)

CF_3−$OH + OH^- \rightarrow FC(O)F + F^- + H_2O$ (HF ***E***limination)

$FC(O)F + 4OH^- \rightarrow CO_3^{2-} + 2F^- + 2\ H_2O$ (***H***ydrolysis)

We note that the mechanism for the decarboxylation−hydroxylation step remains elusive[49] because the role of e_{aq}^- is unclear, while direct photolysis of PFCA by 254 nm UV did not occur (Figure C.2). At pH 9.5, difluoroacetate (DFA, CF_2H−COO^-), monofluoroacetate (MFA, CFH_2−COO^-), and acetate (CH_3−COO^-) were not detected throughout TFA degradation, suggesting that H/F exchange from TFA was not allowed. In contrast, at pH 12, while greater than 99% decay of the TFA parent compound was already achieved within 1 h, the complete defluorination required 4 h (Figure 4.2a), and we identified DFA, MFA, and acetic acid as major TPs from TFA degradation (Figure 4.2b). From the initial 25 μM of TFA, the maximum concentrations for these products were 2.4 μM at 8 min for DFA, 3.5 μM at 45 min for MFA, and

15.4 μM at 4 h for acetate. Experiments using DFA and MFA as the starting compounds (Figure C.4) further consolidated the stepwise degradation pathway of TFA → DFA → MFA → acetate (Figure 4.2c). Because the final concentration of acetate was lower than the starting fluorinated precursors, *DHEH* is still another major pathway for the degradation of TFA, DFA, and MFA.[25] Thus, at pH 12, the increased concentration, lifetime, and lowered redox potential of e_{aq}^- enable the H/F exchange pathway by directly cleaving the relatively strong C−F bonds. Still, these C−F BDEs are lower than those in CF_3−CH_2−COO^- (121.5 kcal mol^{-1}) and CF_3−CH_2CH_2−COO^- (122.7 kcal mol^{-1}).[25] At pH 12, the deF% values from these two polyfluorinated structures at 24 h were merely 8.8% and 10.3%, respectively, although higher than the deF% values achieved at pH 9.5 (2.2% and 0.7%).[25] Therefore, the capability of e_{aq}^- in directly cleaving very strong C−F bonds is still limited even at pH 12.

We further extended the mechanistic investigation to $n \geq 2$ PFCAs. The shortest $n = 2$ CF_3CF_2−COO^- (PFPrA) was chosen as the probe. According to our proposed PFCA degradation mechanism,[25] PFPrA will undergo either (1) *DHEH* to yield TFA, leading to complete defluorination, or (2) stepwise H/F exchange of the weak α-position C−F bonds to sequentially yield CF_3CFH−COO^- and CF_3CH_2−COO^- (Figure 4.2f). As mentioned above, CF_3CH_2−COO^- is still recalcitrant at pH 12. The monitoring of TPs from 250 μM PFPrA (Figure 4.2d versus e) shows that the high pH significantly accelerated H/F exchange reactions. At pH 9.5, the maximum concentrations of CF_3CFH−COO^- (27.3 μM) and CF_3CH_2−COO^- (41.0 μM) were reached at 4 and 24 h, respectively (Table C.3). At pH 12, the maximum concentrations of these two intermediates (22.9 μM and 33.2 μM) were reached at 1 and 8 h, respectively. At both pH conditions, the concentrations of TFA were maintained at a relatively constant level (2.8−3.1 μM at pH 9.5 and 4.3−5.8 μM at pH 12). However, we note that this "steady-state" presence of TFA is a balance between formation and degradation. Since TFA degradation at pH 12 was much faster than at pH

9.5 (Table 4.1), it follows that much more TFA should have formed during the PFPrA degradation at pH 12 than at pH 9.5. In other words, the probability of taking the *DHEH* pathway is significantly increased at high pH.

This mechanistic insight is further corroborated by the results of longer-chain n = 5−8 PFCAs. At pH 12, the maximum molar concentrations of the chain-shortened PFCA products (e.g., n = 7 PFOA generated from n = 8 PFNA) were 3.1%−5.7% of the initial parent PFCAs (Table C.4; detailed degradation data shown in Tables C.5−C.10). These ratios are 6−10 times of those at pH 9.5 (0.5−1.0%). Still, as all PFCAs can be rapidly degraded at pH 12, the total amount of chain shortened PFCA intermediates should be higher than the measured concentrations, which results from the balance between formation and degradation.

If *DHEH* was the only degradation pathway, each *DHEH* step would remove the α-position CF_2 and eventually yield TFA, thus achieving 100% defluorination. Therefore, the incomplete defluorination from $n \geq 2$ PFCAs can be attributed to the undesirable H/F exchange, which generates recalcitrant products such as $C_{n-1}F_{2n-1}-CH_2-COO^-$.[25] If the $C_{n-1}F_{2n-1}$ chain is long (i.e., containing relatively weak C−F bonds on the middle carbons),[25] further H/F exchange reactions can occur and get enhanced at the high pH. Indeed, we observed TPs with up to eight H/F exchanges on the PFNA skeleton (i.e., $C_8F_9H_8-CO_2^-$ from $C_8F_{17}-CO_2^-$) at pH 12 (Figure 4.3a). For TPs with up to five H/F exchanges, their intensity reached the maximum at 1 h and then decreased. Only the two TPs with six and eight H/F exchanges showed slowly increasing or plateaued concentrations (Figure 4.3b). In contrast, we only detected TPs with up to three H/F exchanges on PFNA at pH 9.5 (Figure 4.3c).[25] Only the TP with one H/F exchange reached the maximum at 2 h and then decreased. The TPs with two and three H/F exchanges kept the increasing trend (Figure 4.3d). The increased number of CH_2 moieties in the molecular skeleton will strengthen the remaining C−F bonds by generating isolated fluorocarbons (e.g., $-CH_2-CF_2-CH_2-$).[25] Therefore, the comparison

of H/F exchange TP profiles further confirms the significantly enhanced capability of e_{aq}^- in directly cleaving relatively strong C−F bonds at high pH.

We note that other reaction pathways are also possible, as the mass balance of the F element during the PFCA degradation cannot be fully closed by the sum of the F^- and C−F bonds in all quantifiable fluorinated acids (e.g., Figures 4.2d and e). This should be caused by the formation of nonionizable or small TPs that cannot be detected by the detection method used in this study. Nevertheless, we have elucidated two distinct effects of the high solution pH on the molecular transformation of PFCAs by the UV/sulfite treatment. First, the probability of the favorable *DHEH* pathway is significantly increased. Second, the H/F exchange of stronger C−F bonds that cannot be cleaved at a lower pH is enabled. While both improvements could be attributed to the enhanced reaction kinetics and thermodynamics at high pH, more spectroscopic and theoretical investigations are warranted for a deeper understanding.

Rather than directly treating drinking water containing ppt levels of PFAS, this energy- and chemical-intensive UV/sulfite technology is suitable for treating concentrated PFAS (e.g., at ppm levels) in sorbent regeneration waste brines. The concentrated 5.6% NaCl only slightly lowered the PFOA treatment performance in brine (Figure C.5). We emphasize that because the wastes from sorbent regeneration and membrane rejection already contain concentrated salts or bases (e.g., 1% NaCl or 10 mM NaOH),[51,52] the destruction of PFAS does not have to be restricted at a circumneutral pH condition. It is also worth noting that an elevated pH can reduce the overall consumption of chemicals. At pH 9.5, raising the concentration of Na_2SO_3 from 10 to 50 mM could only slightly enhance defluorination (Figure C.6). In comparison, the use of 10 mM Na_2SO_3 at pH 12 (equivalent to 10 mM OH^-) achieved a much higher rate and extent of defluorination. Therefore, operating the UV/sulfite system at pH 12 not only significantly enhances PFCA degradation but also greatly reduces the consumption of both electrical energy and chemicals. Our lab is examining

the application of UV/sulfite at pH 12 for treating PFAS-containing waste streams from separation processes.

4.4 Tables and Figures

Table 4.1 Defluorination Ratio, Rate Constant, and EE/O[a] of PFCAs at pH 9.5 and 12[b]

PFCA $C_nF_{2n+1}COO^-$	C_nF_{2n+1} chain length (n)	deF%		k (h^{-1})		EE/O (kWh m^{-3})[b]	
		pH 9.5 (24 h)	pH 12 (8 h)	pH 9.5[c]	pH 12[c]	pH 9.5[c]	pH 12[c]
TFA	1	94 ± 3.8[c]	100 ± 2.0	0.15	3.44	457	20.1
PFPrA	2	54 ± 6.3	73 ± 2.0	0.66	5.14	105	13.4
PFBA	3	48 ± 5.2	92 ± 2.8	0.40	7.16	174	9.6
PFPeA	4	51 ± 2.7	79 ± 7.7	0.70	6.63	99	10.4
PFHxA	5	49 ± 6.4	89 ± 2.4	0.57	5.78	121	12.0
PFHpA	6	49 ± 2.9	83 ± 0.8	0.52	5.69	132	12.1
PFOA	7	52 ± 5.6	93 ± 1.6	0.56	4.38	122	15.8
PFNA	8	52 ± 1.8	82 ± 0.6	0.89	5.05	77	13.7

[a]EE/O: number of kilowatt-hours of electrical energy required to reduce the parent PFCA concentration by 1 order of magnitude per m^3 of water.
[b]Reaction conditions: individual PFCA (0.025 mM), Na_2SO_3 (10 mM), carbonate (5 mM), 254 nm irradiation (18 W low-pressure Hg lamp for 600 mL solution) at 20 °C. Errors indicate standard deviation of triplicate reactions.
[c]We note that the data for $n \geq 2$ PFCAs demonstrate high similarities other than significant differences between individual structures (cf. Figure 4.1c).
[d]At pH 9.5, deF% of TFA reached 100% after 48 h.[25]

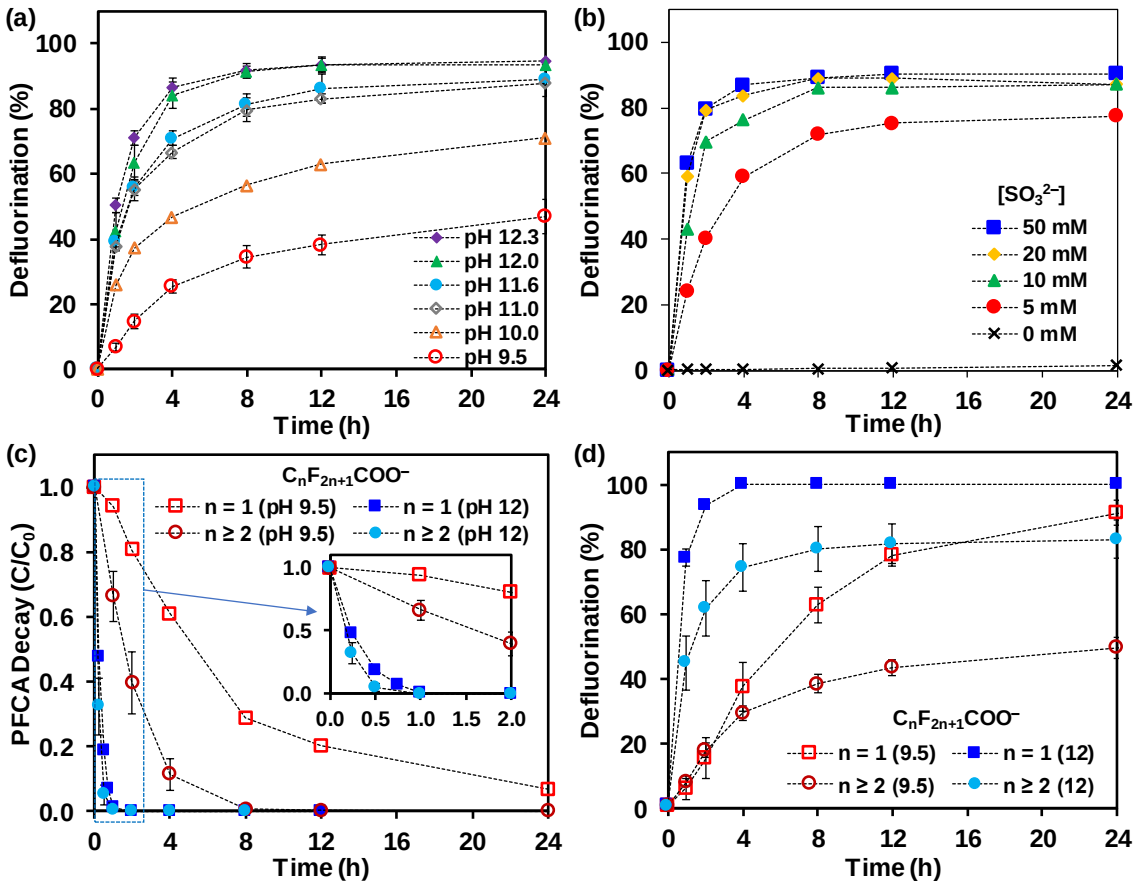

Figure 4.1 Defluorination profiles from n = 7 PFOA using (a) 10 mM Na_2SO_3 at various solution pH and (b) various sulfite concentrations at pH 12. Profiles for (c) parent compound decay and (d) defluorination of trifluoroacetic acid (n = 1) and longer-chain PFCAs (n = 2−8, averaged) at pH 9.5 and pH 12 with 10 mM Na_2SO_3. *Reaction conditions*: individual PFCA (0.025 mM), carbonate (5 mM), and 254 nm irradiation (18 W low-pressure Hg lamp for 600 mL solution) at 20 °C.

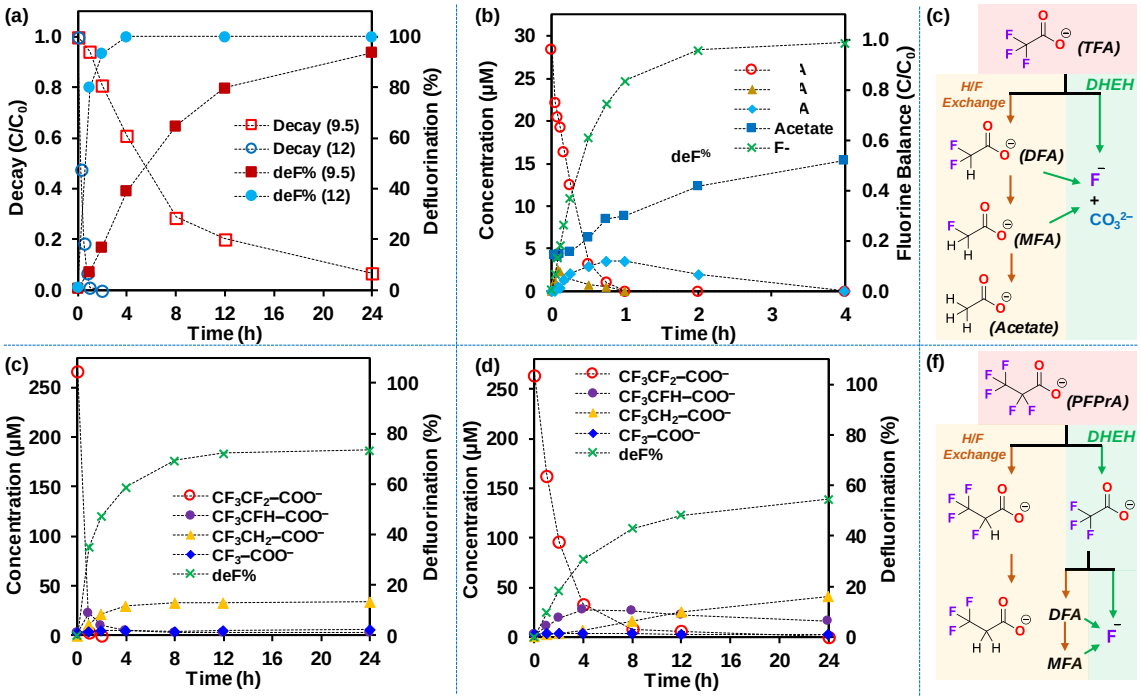

Figure 4.2 Time profiles for (a) parent compound decay and defluorination of *n* = 1 TFA at pH 9.5 and 12. (b) TPs and defluorination from TFA at pH 12. Comparison of parent compound decay, TP formation, and defluorination of n = 2 PFPrA at (d) pH 12 and (e) pH 9.5. Reaction schemes are shown in panels (c) and (f). *Reaction conditions*: carbonate (5 mM) and 254 nm irradiation (18 W low-pressure Hg lamp for 600 mL solution) at 20 °C.

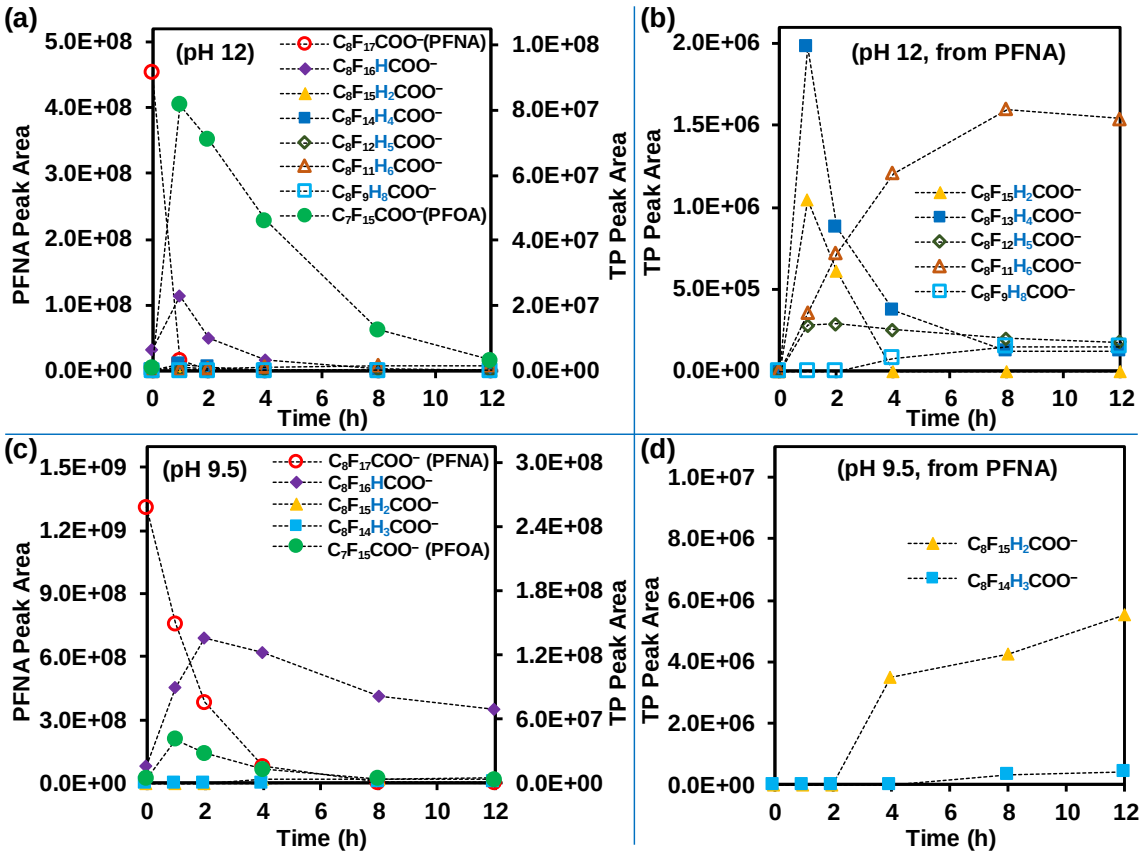

Figure 4.3 Time profiles for the decay of *n* = 8 PFNA and TP formation at pH 9.5 and 12. In panels (a) and (c), the scale for the TP peak area (right side) is 20% of the scale for the parent PFNA peak area (left side). Panels (b) and (d) are magnified displays for TPs with relatively low peak areas. *Reaction conditions*: PFNA (0.025 mM), carbonate (5 mM), and 254 nm irradiation (18 W low-pressure Hg lamp for 600 mL solution) at 20 °C.

REFERENCES

(1) Wang, Z.; DeWitt, J. C.; Higgins, C. P.; Cousins, I. T. A never ending story of per-and polyfluoroalkyl substances (PFASs)? *Environ. Sci. Technol.* **2017**, *51*, 2508−2518.

(2) Xiao, F. Emerging poly-and perfluoroalkyl substances in the aquatic environment: A review of current literature. *Water Res.* **2017**, *124*, 482−495.

(3) Sunderland, E. M.; Hu, X. C.; Dassuncao, C.; Tokranov, A. K.; Wagner, C. C.; Allen, J. G. A review of the pathways of human exposure to poly-and perfluoroalkyl substances (PFASs) and present understanding of health effects. *J. Exposure Sci. Environ. Epidemiol.* **2019**, *29*, 131−147.

(4) Rahman, M. F.; Peldszus, S.; Anderson, W. B. Behaviour and fate of perfluoroalkyl and polyfluoroalkyl substances (PFASs) in drinking water treatment: A review. *Water Res.* **2014**, *50*, 318−340.

(5) Xiao, X.; Ulrich, B. A.; Chen, B.; Higgins, C. P. Sorption of poly and perfluoroalkyl substances (PFASs) relevant to aqueous film forming foam (AFFF)-impacted groundwater by biochars and activated carbon. *Environ. Sci. Technol.* **2017**, *51*, 6342−6351.

(6) Boo, C.; Wang, Y.; Zucker, I.; Choo, Y.; Osuji, C. O.; Elimelech, M. High performance nanofiltration membrane for effective removal of perfluoroalkyl substances at high water recovery. *Environ. Sci. Technol.* **2018**, *52*, 7279−7288.

(7) Liu, J.; Avendaño, S. M. Microbial degradation of polyfluoroalkyl chemicals in the environment: A review. *Environ. Int.* **2013**, *61*, 98−114.

(8) Huang, S.; Jaffé, P. R. Defluorination of perfluorooctanoic acid (PFOA) and perfluorooctane sulfonate (PFOS) by *Acidimicrobium sp.* Strain A6. *Environ. Sci. Technol.* **2019**, *53*, 11410−11419.

(9) Yang, S.; Fernando, S.; Holsen, T. M.; Yang, Y. Inhibition of perchlorate formation during the electrochemical oxidation of perfluoroalkyl acid in groundwater. *Environ. Sci. Technol. Lett.* **2019**, *6*, 775−780.

(10) Schaefer, C. E.; Andaya, C.; Urtiaga, A.; McKenzie, E. R.; Higgins, C. P. Electrochemical treatment of perfluorooctanoic acid (PFOA) and perfluorooctane sulfonic acid (PFOS) in groundwater impacted by aqueous film forming foams (AFFFs). *J. Hazard. Mater.* **2015**, *295*, 170−175.

(11) Sahu, S. P.; Qanbarzadeh, M.; Ateia, M.; Torkzadeh, H.; Maroli, A. S.; Cates, E. L. Rapid degradation and mineralization of perfluorooctanoic acid by a new petit jeanite $Bi_3O(OH)(PO_4)_2$ microparticle ultraviolet photocatalyst. *Environ. Sci. Technol. Lett.* **2018**, *5*, 533−538.

(12) Shao, T.; Zhang, P.; Jin, L.; Li, Z. Photocatalytic decomposition of perfluorooctanoic acid in pure water and sewage water by nanostructured gallium oxide. *Appl. Catal., B.* **2013**, *142*, 654−661.

(13) Stratton, G. R.; Dai, F.; Bellona, C. L.; Holsen, T. M.; Dickenson, E. R.; Mededovic Thagard, S. Plasma-based water treatment: efficient transformation of perfluoroalkyl substances in prepared solutions and contaminated groundwater. *Environ. Sci. Technol.* **2017**, *51*, 1643−1648.

(14) Singh, R. K.; Multari, N.; Nau-Hix, C.; Anderson, R. H.; Richardson, S. D.; Holsen, T. M.; Mededovic Thagard, S. Rapid removal of poly-and perfluorinated compounds from investigation derived waste (IDW) in a pilot-scale plasma reactor. *Environ. Sci. Technol.* **2019**, *53*, 11375−11382.

(15) Saleem, M.; Biondo, O.; Sretenović, G.; Tomei, G.; Magarotto, M.; Pavarin, D.; Marotta, E.; Paradisi, C. Comparative performance assessment of plasma reactors for the treatment of PFOA; reactor design, kinetics, mineralization and energy yield. *Chem. Eng. J.* **2020**, *382*, 123031.

(16) Moriwaki, H.; Takagi, Y.; Tanaka, M.; Tsuruho, K.; Okitsu, K.; Maeda, Y. Sonochemical decomposition of perfluorooctane sulfonate and perfluorooctanoic acid. *Environ. Sci. Technol.* **2005**, *39*, 3388−3392.

(17) Vecitis, C. D.; Park, H.; Cheng, J.; Mader, B. T.; Hoffmann, M. R. Kinetics and mechanism of the sonolytic conversion of the aqueous perfluorinated surfactants, perfluorooctanoate (PFOA), and perfluorooctane sulfonate (PFOS) into inorganic products. *J. Phys. Chem. A.* **2008**, *112*, 4261−4270.

(18) Campbell, T. Y.; Vecitis, C. D.; Mader, B. T.; Hoffmann, M. R. Perfluorinated surfactant chain-length effects on sonochemical kinetics. *J. Phys. Chem. A.* **2009**, *113*, 9834−9842.

(19) Zhang, Z.; Chen, J.-J.; Lyu, X.-J.; Yin, H.; Sheng, G.-P. Complete mineralization of perfluorooctanoic acid (PFOA) by γ-irradiation in aqueous solution. *Sci. Rep.* **2015**, *4*, 7418.

(20) Nzeribe, B. N.; Crimi, M.; Mededovic Thagard, S.; Holsen, T. M. Physico-chemical processes for the treatment of per- and polyfluoroalkyl substances (PFAS): A review. *Crit. Rev. Environ. Sci. Technol.* **2019**, *49*, 866−915.

(21) Merino, N.; Qu, Y.; Deeb, R. A.; Hawley, E. L.; Hoffmann, M. R.; Mahendra, S. Degradation and removal methods for perfluoroalkyl and polyfluoroalkyl substances in water. *Environ. Eng. Sci.* **2016**, *33* (9), 615−649.

(22) O'Hagan, D. Understanding organofluorine chemistry. An introduction to the C−F bond. *Chem. Soc. Rev.* **2008**, *37*, 308−319.

(23) Buxton, G. V.; Greenstock, C. L.; Helman, W. P.; Ross, A. B. Critical review of rate constants for reactions of hydrated electrons, hydrogen atoms and hydroxyl radicals (·OH/·O^-) in aqueous solution. *J. Phys. Chem. Ref. Data*. **1988**, *17*, 513−886.

(24) Park, H.; Vecitis, C. D.; Cheng, J.; Choi, W.; Mader, B. T.; Hoffmann, M. R. Reductive defluorination of aqueous perfluorinated alkyl surfactants: Effects of ionic headgroup and chain length. *J. Phys. Chem. A.* **2009**, *113*, 690−696.

(25) Bentel, M. J.; Yu, Y.; Xu, L.; Li, Z.; Wong, B. M.; Men, Y.; Liu, J. Defluorination of per- and polyfluoroalkyl substances (PFASs) with hydrated electrons: Structural dependence and implications to PFAS remediation and management. *Environ. Sci. Technol.* **2019**, *53*, 3718−3728.

(26) Song, Z.; Tang, H.; Wang, N.; Zhu, L. Reductive defluorination of perfluorooctanoic acid by hydrated electrons in a sulfite-mediated UV photochemical system. *J. Hazard. Mater.* **2013**, *262*, 332−338.

(27) Qu, Y.; Zhang, C.; Li, F.; Chen, J.; Zhou, Q. Photo-reductive defluorination of perfluorooctanoic acid in water. *Water Res.* **2010**, *44*, 2939−2947.

(28) Sun, Z.; Zhang, C.; Xing, L.; Zhou, Q.; Dong, W.; Hoffmann, M. R. UV/nitrilotriacetic acid process as a novel strategy for efficient photoreductive degradation of perfluorooctanesulfonate. *Environ. Sci. Technol.* **2018**, *52*, 2953−2962.

(29) Tian, H.; Gao, J.; Li, H.; Boyd, S. A.; Gu, C. Complete defluorination of perfluorinated compounds by hydrated electrons generated from 3-indole-acetic-acid in organomodified montmorillonite. *Sci. Rep.* **2016**, *6*, 32949.

(30) Kulkarni, U. S.; Dixit, S. G. Destruction of phenol from wastewater by oxidation with sulfite-oxygen. *Ind. Eng. Chem. Res.* **1991**, *30*, 1916−1920.

(31) MacCrehan, W. A.; Jensen, J. S.; Helz, G. R. Detection of sewage organic chlorination products that are resistant to dichlorination with sulfite. *Environ. Sci. Technol.* **1998**, *32*, 3640−3645.

(32) Sun, B.; Guan, X.; Fang, J.; Tratnyek, P. G. Activation of manganese oxidants with bisulfite for enhanced oxidation of organic contaminants: The involvement of Mn (III). *Environ. Sci. Technol.* **2015**, *49*, 12414−12421.

(33) Gu, Y.; Dong, W.; Luo, C.; Liu, T. Efficient reductive decomposition of perfluorooctanesulfonate in a high photon flux UV/sulfite system. *Environ. Sci. Technol.* **2016**, *50*, 10554−10561.

(34) Bao, Y.; Deng, S.; Jiang, X.; Qu, Y.; He, Y.; Liu, L.; Chai, Q.; Mumtaz, M.; Huang, J.; Cagnetta, G.; Yu, G. Degradation of PFOA substitute: GenX (HFPO−DA ammonium salt): oxidation with UV/persulfate or reduction with UV/sulfite? *Environ. Sci. Technol.* **2018**, *52*, 11728−11734.

(35) Gu, Y.; Liu, T.; Zhang, Q.; Dong, W. Efficient decomposition of perfluorooctanoic acid by a high photon flux UV/sulfite process: Kinetics and associated toxicity. *Chem. Eng. J.* **2017**, *326*, 1125−1133.

(36) Qu, Y.; Zhang, C.-J.; Chen, P.; Zhou, Q.; Zhang, W.-X. Effect of initial solution pH on photo-induced reductive decomposition of perfluorooctanoic acid. *Chemosphere*. **2014**, *107*, 218−223.

(37) Bao, Y.; Huang, J.; Cagnetta, G.; Yu, G. Removal of F−53B as PFOS alternative in chrome plating wastewater by UV/Sulfite reduction. *Water Res.* **2019**, *163*, 114907.

(38) Gu, P.; Zhang, C.; Sun, Z.; Zhang, H.; Zhou, Q.; Lin, S.; Rong, J.; Hoffmann, M. R. Enhanced photoreductive degradation of perfluorooctanesulfonate by UV irradiation in the presence of ethylenediaminetetraacetic acid. *Chem. Eng. J.* **2020**, *379*, 122338.

(39) Bao, Y.; Cagnetta, G.; Huang, J.; Yu, G. Degradation of hexafluoropropylene oxide oligomer acids as PFOA alternatives in simulated nanofiltration concentrate: Effect of molecular structure. *Chem. Eng. J.* **2020**, *382*, 122866.

(40) Bentel, M. J.; Yu, Y.; Xu, L.; Kwon, H.; Li, Z.; Wong, B. M.; Men, Y.; Liu, J. Degradation of perfluoroalkyl ether carboxylic acids with hydrated electrons: Structure−reactivity relationships and environmental implications. *Environ. Sci. Technol.* **2020**, *54*, 2489−2499.

(41) Houtz, E. F.; Sedlak, D. L. Oxidative conversion as a means of detecting precursors to perfluoroalkyl acids in urban runoff. *Environ. Sci. Technol.* **2012**, *46*, 9342−9349.

(42) Giri, R. R.; Ozaki, H.; Okada, T.; Taniguchi, S.; Takanami, R. Factors influencing UV photodecomposition of perfluorooctanoic acid in water. *Chem. Eng. J.* **2012**, *180*, 197−203.

(43) Bolton, J. R.; Bircher, K. G.; Tumas, W.; Tolman, C. A. Figures of merit for the technical development and application of advanced oxidation processes. *J. Adv. Oxid. Technol.* **1996**, *1*, 13−17.

(44) U.S. Environmental Protection Agency. Drinking Water Treatability Database: Ultraviolet Irradiation +HydrogenPeroxide.

https://iaspub.epa.gov/tdb/pages/treatment/treatmentOverviewdo?treatmentProcessId=-300168699 = (accessed April 20, 2020).

(45) Maza, W. A.; Breslin, V. M.; Plymale, N. T.; DeSario, P. A.; Epshteyn, A.; Owrutsky, J. C.; Pate, B. B. Nanosecond transient absorption studies of the pH-dependent hydrated electron quenching by HSO_3^-. *Photoch. Photobio Sci.* **2019**, *18*, 1526−1532.

(46) Goldberg, R. N.; Kishore, N.; Lennen, R. M. Thermodynamic quantities for the ionization reactions of buffers. *J. Phys. Chem. Ref. Data* **2002**, *31* (2), 231−370.

(47) Vellanki, B. P.; Batchelor, B. Perchlorate reduction by the sulfite/ultraviolet light advanced reduction process. *J. Hazard. Mater.* **2013**, *262*, 348−356.

(48) Hayon, E.; Treinin, A.; Wilf, J. Electronic spectra, photochemistry, and autoxidation mechanism of the sulfite-bisulfitepyrosulfite systems. SO_2^-, SO_3^-, SO_4^-, and SO_5^- radicals. *J. Am. Chem. Soc.* **1972**, *94*, 47−57.

(49) Cui, J.; Gao, P.; Deng, Y. Destruction of per- and polyfluoroalkyl substances (PFAS) with advanced reduction processes (ARPs): A critical review. *Environ. Sci. Technol.* **2020**, *54*, 3752−3766.

(50) Zhang, Y.; Moores, A.; Liu, J.; Ghoshal, S. New insights into the degradation mechanism of perfluorooctanoic acid by persulfate from density functional theory and experimental data. *Environ. Sci. Technol.* **2019**, *53*, 8672−8681.

(51) Deng, S.; Yu, Q.; Huang, J.; Yu, G. Removal of perfluorooctane sulfonate from wastewater by anion exchange resins: Effects of resin properties and solution chemistry. *Water Res.* **2010**, *44*, 5188−5195.

(52) Du, Z.; Deng, S.; Chen, Y.; Wang, B.; Huang, J.; Wang, Y.; Yu, G. Removal of perfluorinated carboxylates from washing wastewater of perfluorooctanesulfonyl fluoride using activated carbons and resins. *J. Hazard. Mater.* **2015**, *286*, 136−143.

CHAPTER 5: RAPID PHOTOCHEMICAL DEGRADATION OF PERFLUORINATED CARBOXAMIDES

Abstract

This study investigates the reactivity of perfluorocarboxamides (PFCAms) in a UV/sulfite photochemical system. Utilizing PFCAms with the structure $C_nF_{2n+1}CONH_2$ (n = 1−5, 7, 9) a novel defluorination mechanism was identified that resembles the well-known Hofmann Rearrangement. This new reaction mechanism allows for the rapid destruction of linear PFCAms while recovering significant amount of organic fluorine as inorganic fluoride. The decay kinetics of the reaction appear dependent on fluoroalkyl chain length, with n = 1−5 showing faster kinetics than n = 7, and still, n = 9. For n = 3−7, defluorination reached 70% within 1 h. The short n = 1 and n = 2 PFCAms displayed high reactivity, but displayed lower defluorination compared to n = 3−7 after 1 h. Subsequent experiments identified two reactivity trends dependent on chain-length: (1) rate of hydrolysis and (2) rate of H/F exchange. Thus, the lower defluorination observed within 1 h of reaction is attributed to the increased rate of hydrolysis for n = 1 and increased rate of H/F exchange for n = 2 (H/F exchange was not observed for n = 1). Scavenging experiments were executed in order to identify the reactive species responsible. Based on results from solutions amended with various alcohols (oxidant scavenger) and nitrogen oxyanions (reductant scavenger) it has been determined the sulfite radical is responsible. Subsequent experiments investigating substitution of the terminal amine group found to inhibit undesired hydrolysis to the perfluorocarboxylic analog, most likely due to steric effects. Substitution of a primary C−F bond with the carboxamide functional group [$H_2N-(CF_2)_n-NH_2$] resulted in rapid and complete defluorination for n = 1−4. This novel reaction mechanism demonstrates the potential for per- and polyfluoroalkyl substances to be strategically designed to meet performance demands while

mitigating detrimental human and environmental affects due to their high recalcitrance to current treatment technologies.

5.1 Introduction

The manufacturing, application, and disposal of fluorochemicals have led to worldwide pollution by per- and polyfluoroalkyl substances (PFAS).[1–3] Recent research efforts have substantially advanced the knowledge of detection,[4–6] toxicity,[7,8] removal,[9–11] and destruction of PFAS pollutants.[12,13] Perfluorocarboxylates (PFCAs, $C_nF_{2n+1}{-}COO^-$), perfluoroalkanesulfonates (PFSAs, $C_nF_{2n+1}{-}SO_3^-$), and fluorotelomers ($C_nF_{2n+1}{-}(CH_2)_m{-}R$) have received the most attention (Figure 5.1a) because they are either building blocks or natural degradation products of the highly diverse fluoro-organo conjugates used in fire-fighting foams,[14] consumer products,[15,16] batteries,[17–19] semiconductor production,[20] and medical application.[21] The fluoro and organo alkyl moieties are usually integrated by carboxamide, sulfonamide, or telomer hydrocarbon linkers.[22] Natural degradation and conventional water treatment methods can hydrolyze or oxidize those linkers, yielding PFCAs and PFSAs as the highly recalcitrant end products.[23–25]

Accordingly, a variety of chemical and materials approaches (e.g., photochemical,[26] electrochemical,[27] sonochemical,[28] photocatalytic,[29] plasmatic,[30] radiolytic,[31] hydrothermal,[32] and other novel materials approaches[33]) have been developed to cleave C−F bonds in PFCAs and PFSAs. Those methods utilize strong reducing species (e.g., hydrated electron e_{aq}^-),[34] oxidizing species (e.g., hydroxyl radical HO• and sulfate radical $SO_4^{\bullet-}$), or a combination of both. In particular, e_{aq}^- can be generated from specific chemicals (e.g., sulfite[35] and iodide[26]) under UV irradiation and ***directly*** cleave weak C−F bonds (i.e., bond dissociation energy BDE <117 kcal mol^{-1}).[36] However, direct cleavage of relatively strong C−F bonds by e_{aq}^- is challenging, yielding partially defluorinated and potentially harmful products (Figure 5.1b).[37,38] Instead, a deep defluorination of PFCAs and PFSAs relies on the cleavage of C−C and C–S bonds in $\boldsymbol{R_F}CF_2{-}COO^-$

and $\boldsymbol{R_F}CF_2{-}SO_3^-$, respectively.[37] The unstable intermediate, perfluorinated $\boldsymbol{R_F}CF_2{-}OH$,[39–41] spontaneously loses two F atoms to yield chain-shortened $\boldsymbol{R_F}COO^-$ (Figure 5.1c).[37] Because all C−F bonds can be cleaved regardless of the BDE, this ***indirect*** defluorination pathway is desirable for PFAS destruction.[38] Nevertheless, the slow kinetics still indicate high energy consumption. Therefore, there remains an imperative need for both fluorochemical industries and environmental practitioners to identify alternative structures, which should have similar application properties but much higher degradability than conventional PFCAs and PFSAs.

In this contribution, we report on the unexpected rapid defluorination of a series of perfluorocarboxamides (PFCAms, $C_nF_{2n+1}{-}CONH_2$). PFCAm structures have been used as a large class of surfactants,[42–44] bioactive and electronic materials,[45–48] or generated as a byproduct from historical sulfonamide production.[49,50] In comparison to other PFAS compounds, PFCAms exhibit much higher reactivity by the photochemical degradation using e_{aq}^-. The findings not only reveal a distinct degradation mechanism via intramolecular fluoroalkyl chain migration, but also indicates substantially enhanced energy efficiency for environmental remediation. We anticipate a transformative impact of this work on the future design and management of fluorochemicals for industrial sustainability and environmental protection.

5.2 Materials and Methods

Details of chemical and experiment procedures are described in Appendix D (App D). Briefly, aqueous solutions of individual PFCAms, previously dissolved in methanol, were prepared and amended with 10 mM Na_2SO_3, 5 mM $NaHCO_3$ and pH adjusted to 9.5 by 1 N NaOH. Immediately after dissolution the aqueous solutions were irradiated with an 18 W low-pressure mercury UV lamp at 20°C (with water bath cooling). Samples were taken at predetermined intervals and analyzed for PFCAm decay, generated transformation products, inorganic fluoride, and ammonia.

Theoretical calculations were performed to simulate reaction of PFCAms with hydrated electron and provide C−F bond dissociation energy with the details described in our previous work.[37]

5.3 Results and Discussion

In the UV/sulfite photochemical system, aqueous perfluoroocatamide (PFOAm, C_7F_{15}−$CONH_2$) exhibited substantially faster and deeper defluorination than its carboxylate counterpart, perfluorooctanate (PFOA, C_7F_{15}−COO^-). Within only 1 h, the rapid degradation cleaved 70% of the C−F bonds in PFOAm into F^- (Figure 5.2a). The following degradation became slower, with the defluorination percentage of 81%, 85%, and 88% after 2 h, 4 h, and 8 h, respectively. In sharp contrast, under the same reaction conditions the defluorination of PFOA was merely 8% after 1 h and gradually reached 50% at 24 h. The highly rapid degradation behavior is unique to PFOAm, as the defluorination of perfluoroocatane sulfonamide (PFOSAm, C_8F_{17}−SO_2NH_2) and sulfonate (PFOS, C_8F_{17}−SO_3^-) were both slightly slower than PFOA, without showing a significant difference between each other (Figure 5.2a). Control experiments using only 254 nm irradiation did not degrade either PFOAm (Figure D.1a) or PFOA.[37] The defluorination required the use of more than 0.5 mM Na_2SO_3 because the solution contained dissolved oxygen (Figure 5.2c). Higher concentrations of Na_2SO_3 led to faster and deeper defluorination. Comparison of defluorination between two solutions containing the same amount of sulfite and different PFOAm concentrations demonstrate the efficient use of sulfite in the degradation reaction (Figure D.2). The highest defluorination efficiency for PFOAm was achieved under a mild basic condition at pH 9−10 (Figure 5.2d). For comparison, the defluorination of PFOA became faster and deeper when the pH was raised from 9.5 to 12.[36]

PFCAms are not readily ionizable for the detection by electrospray ionization high-resolution mass spectrometry (ESI–HRMS) but are subject to alkaline hydrolysis (see *Appendix D, App D*). Therefore, all aqueous PFCAm degradation samples were treated with excess base (20 mM KOH)

for at least 3 d to allow for complete hydrolysis into PFCAs. During the degradation of PFOAm, an apparent "turning point" at 1 h, from rapid to slow, was observed for both the PFOA concentration profile and the defluorination profile (Figure 5.2e). The pseudo-first-order rate constant for the rapid PFOA decay in the first hour was 22.9 h^{-1}, whereas the rate constant for the following decay between 1 h and 8 h was merely 0.21 h^{-1}. For comparison, the degradation of pure PFOA under the same reaction condition showed a rate constant of 0.56 h^{-1}.[37] Therefore, the distinct kinetics within the first hour is attributed to the rapid degradation of PFOAm, and the slow kinetics after 1 h reflected the degradation of PFOA, most of which was generated during the first hour of reaction.

Moreover, multiple short-chain PFCAs (n = 1−6 C_nF_{2n+1}−COO^-) were detected within the first hour (Figure 5.2f), in molar ratios of 0.2−1.9% of the parent n = 7 PFOAm. This pattern of transformation product formation is vastly different from the degradation of n = 7 PFOA, where the only chain-shortened PFCA product was n = 6 PFHpA and shorter $n \leq 5$ PFCAs were negligible throughout the reaction. Therefore, the detection of multiple shorter-chain PFCAms from PFOAm degradation within the first hour is attributed to the rapid formation of shorter-chain PFCAms. After 1 h, all the shorter-chain PFCAs slowly degraded within 4−8 h. The rate constants for these PFCAs after 1 h were at the same order of magnitude as measured in our previous study on pure PFCAs.[37] Hence, a novel degradation mechanism leads to the rapid degradation of PFOAm and shorter-chain PFCAm products at the beginning. Most PFCAms were rapidly converted into PFCAs within 1 h so that the subsequent degradation followed the previously elucidated mechanisms for PFCAs.[37]

It has been established that the degradation of PFOA involves an "unzipping" mechanism via decarboxylation and the formation of an unstable perfluoroalcohol intermediate (C_nF_{2n+1}−OH, Scheme 5.1b). For the rapid degradation of PFOAm, we first assumed that the dissociation and re-association of an amino-containing moiety might be responsible for the enhanced defluorination.

However, addition of various small molecules containing the carboxamide moiety (e.g., $HO{-}CONH_2$, $H{-}CONH_2$, $H_3C{-}CONH_2$, and $H_2N{-}CONH_2$) did not enhance the defluorination of PFOA at all (Figure 5.2b). Moreover, a 1:1 mixture of PFOAm and PFOA produced a defluorination profile exactly the average of those for the two individual compounds. Therefore, the amino group must have been conserved within the molecule throughout the rapid and deep defluorination of PFOAm and the shorter-chain PFCAm intermediates.

The migration of fluoroalkyl chains from the carbonyl to the nitrogen atom has been reported in early literature. Perfluoroalkyl isocyanates ($C_nF_{2n+1}{-}N{=}C{=}O$) can be prepared from acyl azide $C_nF_{2n+1}{-}CO{-}N{=}N^{+}{=}N^{-}$ (Curtis rearrangement, in refluxed toluene at 110 °C)[51] or from hydroxamic acid $C_nF_{2n+1}{-}CO{-}NH{-}OH$ (Lossen rearrangement, under pyrolysis at 375 °C).[52] We propose a similar reaction pathway for the conversion of $C_nF_{2n+1}{-}CONH_2$ into $C_nF_{2n+1}{-}N{=}C{=}O$, (Scheme 5.1a) which further reacts with H_2O to yield $C_nF_{2n+1}{-}NH_2$ (Scheme 5.1e). At 20°C, the α-position $-CF_2-$ is not stable and undergoes defluorination, yielding the chain-shortened $C_{n-1}F_{2n-1}{-}CONH_2$ (Scheme 5.1d).

Under UV irradiation, aqueous SO_3^{2-} is converted into sulfite radical ($SO_3^{\bullet-}$) and e_{aq}^{-}:

$$SO_3^{2-} \xrightarrow{h\nu} SO_3^{\bullet-} + e_{aq}^{-} \qquad (5.1)$$

In order to implicate the reactive species responsible for PFOAm degradation, several scavenging experiments were conducted targeting both $SO_3^{\bullet-}$ and e_{aq}^{-}. It is established that e_{aq}^{-} is rigorously unreactive towards alcohols.[53] Therefore, a series of experiments using alcohol as the oxidant scavenger were conducted with the results demonstrating a clear influence on defluorination early in the reaction (i.e., < 2 h). Furthermore, defluorination resumes normal performance (compared to control experiments) after 2 h for all alcohol scavenging experiments (Figure D.3). Despite the poor reactivity of $SO_3^{\bullet-}$ with alcohol,[54,55] these results combined implicate an oxidative mode of reaction. The trend for inhibition by each alcohol (i.e., *iso*propanol (most reactive) > *n*-propanol > ethanol >

methanol (lease reactive)) appears correlated to C−H bond strength. Due to the presence of oxygen, $SO_3^{\bullet-}$ will react to form peroxymonosulfate radical ($SO_5^{\bullet-}$),[56] which participates in the sulfur radical chain reaction to form sulfate radical ($SO_4^{\bullet-}$), a strong oxidant ($E°$ = 2.6 V).[56] Photochemical experiments using $K_2S_2O_8$ as the photosensitizer, which will undergo homolytic cleavage under 254 nm UV light to generate $SO_4^{\bullet-}$, resulted in no defluorination (Figure D.4). An additional experiment using the photochemically active $KHSO_5$ to generate $SO_5^{\bullet-}$ resulted in no defluorination (Figure D.4). This result implies $SO_3^{\bullet-}$ is necessary for defluorination. Additional experiments using $NaNO_2$ and $NaNO_3$, known e_{aq}^- scavengers,[57] resulted in no observable defluorination (Figure D.3). However, NO_2^- is known to reduce $SO_4^{\bullet-}$ and therefore is able to scavenge oxidants in solution.[54] Furthermore, nitrate radical ($NO_3^{\bullet-}$) has been shown through *ab initio* approaches to possess strong reducing abilities, demonstrated by the calculated reduction potential ($E°$ = –1.1 V).[58] Therefore, additional experiments are necessary to determine precisely the role of e_{aq}^-.

The rapid but incomplete defluorination (up to 90% after 48 h) of PFOAm prompted us to identify other degradation pathways that prevent a small fraction of C−F bonds from defluorination. The degradation of n = 3–5 C_nF_{2n+1}−$CONH_2$ (PFBAm, PFPeAm, and PFHxAm) was even faster than n = 7 PFOAm. The decay of the parent PFCAms reached 81−90% within the first 5 min, followed by a much slower decay of the corresponding PFCAs to non-detectable in the next 4−8 h (Figure 5.3a). The rapid defluorination reached 65−80% within the first 30 min (Figure 5.3b). Similar to the profile of transformation products from PFOAm (Figure 5.2f), shorter-chain PFCAm intermediates were detected from n = 3–5 parent PFCAms (Figure D.5). Nevertheless, despite even faster kinetics than PFOAm, the defluorination of the three shorter-chain PFCAms were still incomplete (82−87% after 48 h). Interestingly, the n = 9 PFDAm defluorinated much slower than n = 7 PFOAm (n = 6 PFHpAm and n = 8 PFNAm were not commercially available for comparison). The defluorination of PFDAm after 1 h was only 2% but slowly increased to 81% after 48 h. The

relatively slow reaction of n = 7 and 9 PFCAms is probably due to the low mobility of long fluoroalkyl chains during the rearrangement or due to the high tendency of aggregation as micelles in the aqueous environment. In comparison, the defluorination of pure PFDA under the same reaction condition was only 55% after 48 h.[37]

Similar to n = 3–5 PFCAms, 84% decay of n = 2 PFPrAm was achieved within 5 min (Figure 5.2c). Despite rapid defluorination within the first 30 min, the ~60% maximum achieved (Figure 5.2d) is distinctively low in comparison to the longer-chain PFCAms (81−90%). Thus, we assume that the degradation of $n \geq 3$ PFCAms primarily follows the chain-shortening pathway via fluoroalkyl migration (Scheme 5.1f) until yielding n = 2 PFPrAm. From here, if PFPrAm decay only took the chain-shortening pathway to n = 1 TFAm, the defluorination would reach 100%. Results from TFAm degradation experiments display almost symmetric profiles of decay and defluorination (Figure D.9). Furthermore, the 62 ± 0.2% decay with 57 ± 1.4% defluorination within the first 15 minutes indicates rapid and complete defluorination of all three C−F bonds in TFAm. Following Scheme 5.1a, the final defluorination product would be carbamate, which further hydrolyzes into carbonate and ammonia. Despite TFAm being susceptible to hydrolysis into TFA, our previous study has shown that defluorination of TFA is 100% within 48 h via decarboxylation mechanim.[37] Hence, the incomplete defluorination of PFPrAm is due to other degradation pathways.

Two polyfluorinated products, $CF_3CF\mathbf{H}{-}COO^-$ and $CF_3C\mathbf{H}_2{-}COO^-$, were detected from the degradation of 25 μM PFPrAm (Figure D.10a). At 8 h the accumulated $CF_3CF\mathbf{H}{-}COO^-$ and $CF_3C\mathbf{H}_2{-}COO^-$ accounted for 38 ± 1.6% of the total organic F in the original PFPrAm, complimentary to the overall defluorination of 61 ± 0.6% and closing the fluorine mass balance. Therefore, these two products represent the other significant reaction pathway. The transformation of C−F into C−H is reductive and involves two e_{aq}^- (Figure 5.1b). However, the rate of generation

for these two products is distinctly faster than the carboxylic analog (Figure D.10b). Density Functional Theory (DFT) calculations for PFPrAm C−F bond dissociation energy reveal similar, or slightly lower, values compared to PFPrA (Figure D.12). Reaction of e_{aq}^- with acetone to form isopropanol has been postulated to proceed through a radical intermediate where the extra electron is localized to the π* orbital of the carbonyl group.[59] For PFCAs, the lowest unoccupied molecular orbital (LUMO) has been identified to be delocalized across the $\pi^*_{C=O}$ and σ^*_{C-F}.[60] Therefore, reaction of PFCAs with e_{aq}^- would result in populating the LUMO π* orbital to generate a singly occupied molecular orbital (SOMO). The intramolecular dissociation of carbon−halogen bonds has been identified to occur via transfer of an electron from the SOMO π* orbital to the carbon−halogen σ* orbital.[61] In order to simulate the reaction between the fluorochemical and the e_{aq}^-, we added an extra electron onto the neutral PFPrAm and the anionic PFPrA. Spontaneous sequential cleavage of the two α-position C−F bonds in both structures were observed (Figure D.15) and thus support the reductive defluorination mechanism. Therefore, the carboxamide structure significantly accelerates the H/F exchange reaction. In literature, the second-order rate constants for the reaction between e_{aq}^- and carboxamides are generally 1−2 orders of magnitude higher than that between e_{aq}^- and the corresponding anionic carboxylate, further supporting this observation.[57]

To further probe the competition between reductive H/F exchange and oxidative chain-shortening defluorination, additional experiments were conducted with *poly*fluorinated structures of the form R−CF_2−FG, where R = −CH_3, −H and FG = −$CONH_2$ or −COO^-. Starting with pure C**H**$_3CF_2$−$CONH_2$ resulted in 100% defluorination within 1 h (Figure 5.4a). The rapid sequential formation of C**H**$_3$CF**H**−COO^- and C**H**$_3$C**H**$_2$−COO^- during C**H**$_3CF_2$−$CONH_2$ decay suggest substantially enhanced H/F exchange of the polyfluorinated carboxamide (Figure 5.4b) and is supported by calculated BDE (Figure D.13) and simulation (Figure D.16). Notably, defluorination of pure C**H**$_3CF_2$−COO^- and C**H**$_3$CF**H**−COO^- over 24 h were only 29% and 23%, respectively

(Figure 5.4a). Therefore, the complete defluorination of the mono-fluorinated alkyl chain must come from the C**H**$_3$CF**H**−CONH$_2$ intermediate before the hydrolysis into C**H**$_3$CF**H**−COO$^-$. In addition, C**H**$_3$−COO$^-$ also showed up within 5 min, indicating the parallel chain-shortening mechanism (Figure 5.4e). Another experiment using **H**CF$_2$−CONH$_2$ (DFAm) achieved 88% and 98% defluorination at 10 min and 2 h, respectively (Figure 5.4c). About half of the parent compound was converted into C**H**$_3$−COO$^-$ within 10 min, indicating substantially enhanced H/F exchange of the amide (Figure 5.4d); again, supported by calculation (Figure D.14) and simulation (Figure D.17). The other half of the parent DFAm was most probably degraded by the chain-shortening mechanism to generate formamide. Due to challenges separating formate (generated by hydrolysis of formamide) from the UV/sulfite solution matrix, quantification of this compound is difficult. For comparison, the degradation of **H**CF$_2$−COO$^-$ reached 72% after 24 h (Figure 5.4c). These results point to the unique advantage of the terminal carboxamide moiety for the rapid photochemical defluorination.

The incomplete defluorination of PFCAms is also attributed to the rapid hydrolysis of carboxamide into carboxylate. At any specific pH between 8 and 12, the hydrolysis of CF$_3$−CONH$_2$ is 4−5 orders of magnitude faster than CH$_3$−CONH$_2$ (e.g., $10^{-0.35}$ min^{-1} vs. $10^{-5.00}$ min^{-1} at pH 11).[62] We used the salicylate method (see AppD *Ammonia Analysis*) to quantify the NH$_3$ released from freshly added n = 1−7 PFCAms, and observed significantly faster hydrolysis of shorter-chain PFCAms (Figure D.7). The storage of all PFCAms at pH 12.3 (20 mM KOH) for two days led to complete hydrolysis into corresponding PFCAs (Figure D.8). This also explained why a high pH is not favorable for PFCAm degradation (Figure 5.2d). The n = 1 TFAm and n = 2 PFPrAm are highly susceptible, even at pH 9.5. To minimize the hydrolysis before photochemical degradation, we prepared stock solutions of all PFCAms with methanol immediately before use. Notably, although the majority of n = 7 PFOAm could be preserved at pH 9.5 for two days, the hydrolysis

was complete within 1 h during the UV/sulfite reaction (Figure 5.2e). However, the 254 nm irradiation at pH 9.5, without adding sulfite, did not accelerate PFCAm hydrolysis (Figure D.1b). The higher susceptibility to alkaline hydrolysis of the shorter-chain PFCAms is consistent with the narrower time window where rapid defluorination could be observed: <15 min for TFAm and PFPrAm versus >1 h for PFOAm.

Based on the above results, we propose the overall PFCAm degradation pathways as shown in Scheme 5.2f. For $n \geq 3$ PFCAms, as the sum of all PFCAs (generated from the hydrolysis of PFCAm intermediates) and released F^- accounts for 80−95% of the total F balance (Figures 5.2e,f and 5.3c,d), the chain-shortening via fluoroalkyl chain migration is the dominant degradation pathway. Shorter-chain PFCAms also have faster hydrolysis into PFCAs, which are much more recalcitrant than PFCAms under the same reaction condition. Because the carboxamide moiety significantly enhances reductive defluorination from the α-position $-CF_2-$, minor probabilities of H/F exchange also exist. The greatest likelihood of H/F exchange is observed on n = 2 PFPrAm. The residual C−F bonds are found in short-chain polyfluorinated carboxylates, such as $CF_3C\mathbf{H}_2-COO^-$.

Implications to fluorochemical design and environmental protection. Our extended examination on an carboxamide-based ammonium salt surfactant ($C_nF_{2n+1}-CONH-(CH_2)_3-NMe_3^+$, PFOAAmS) observed significantly faster degradation kinetics than PFOAm ($C_nF_{2n+1}-CONH_2$) despite both structures generating similar maximum defluorination (Figure 5.5). This is attributed to the increased solubility due to the positive charge located on the ammonium group. Therefore, the use of carboxamide linkers in surfactant design can substantially increase the degradability of the fluoroalkyl moiety. We also note that the introduction of alkyl substitutions on the amide nitrogen can decrease the rate of hydrolysis for two or more orders of magnitude.[38] Alkaline pretreatment of this surfactant at various pH confirmed its higher resistance against hydrolysis than

PFOAm (Figure D.8d). Therefore, the design of perfluorocarboxamide-based surfactants for storage or application in non-aqueous or neutral aqueous environments will bring substantial benefits in saving energy and chemical during the following degradation (e.g., treatment of in-plant wastewater or remediation of contaminated sites).

Additional defluorination reactions with perfluorodicarboxamide (PFdiCAm) structures ($H_2N{-}(CF_2)_n{-}NH_2$) from n = 1−4 demonstrated enhanced kinetics (Figure D.6) and overall defluorination (Table 5.1) compared to their PFCAm analog. These results further highlight the enhanced reactivity of the carboxamide functional group. Furthermore, the replacement of the terminal $-CF_3$ group with the carboxamide functional group not only removes strong primary C−F bonds, but appears to mitigate the generation of recalcitrant $-CF_3$ products.

5.4 Tables and Figures

Table 5.1 Defluorination of PFCAms and PFCAs in the UV/sulfite system

		1 h defluorination				*Maximum Defluorination*		
n	C_nF_{2n+1} Abbreviation	R_F–$CONH_2$	NH_2CO–R_F–$CONH_2$	R_F–COO^-	^-OOC–R_F–COO^-	[a]R_F–$CONH_2$ (1 h, pH 9.5)	R_F–COO^- (24 h, pH 9.5)	R_F–COO^- (8 h, pH 12)
1	TFA(m)	69 ± 3.3	99 ± 1.6	8.2 ± 1.9	11 ± 0.6	76	94	100
2	PFPrA(m)	54 ± 1.4	94 ± 6.5	9.1 ± 3.0	3.9 ± 0.5	86	54	73
3	PFBA(m)	81 ± 2.8	96 ± 1.4	7.1 ± 4.8	9.4 ± 1.3	93	48	92
4	PFPeA(m)	75 ± 2.2	88 ± 7.6	9.6 ± 0.4	9.7 ± 1.5	91	51	79
5	PFHxA(m)	71 ± 3.2	*N/A*	8.9 ± 2.6	*N/A*	86	49	89
6	PFHpA(m)	N/A	*N/A*	8.7 ± 1.7	9.0 ± 1.4	*N/A*	49	83
7	PFOA(m)	70 ± 5.1	*N/A*	8.5 ± 1.6	11 ± 1.8	78	52	93
8	PFNA(m)	N/A	*N/A*	8.4 ± 1.1	8.4 ± 1.7	*N/A*	*N/A*	*N/A*
9	PFDA(m)	2.1 ± 0.1	*N/A*	4.0 ± 3.7	*N/A*	*N/A*	*N/A*	*N/A*

[a]Calculated as percent of overall defluorination at 1 h

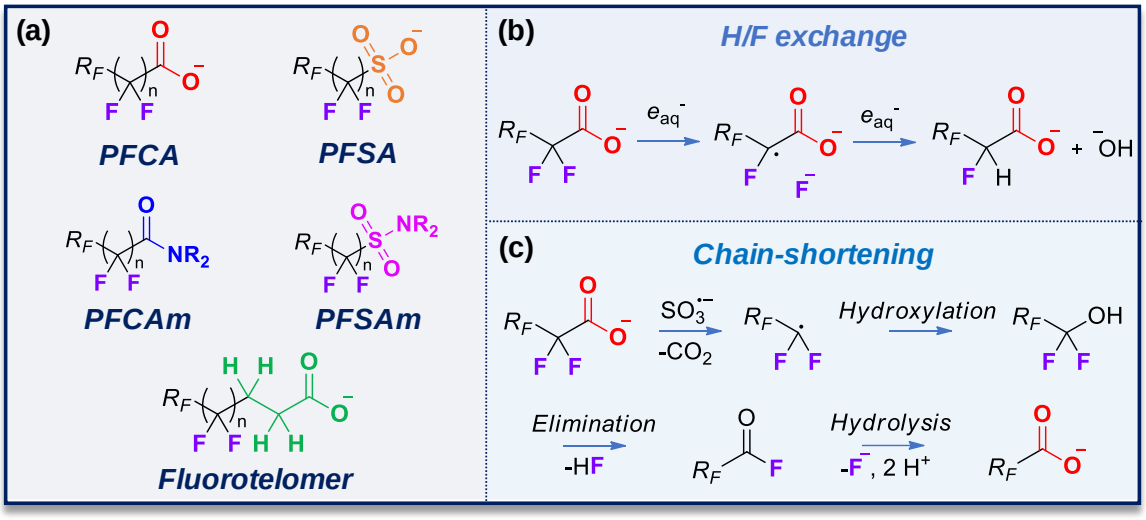

Figure 5.1(a) Commonly detected PFAS in the environment; (b) direct and (c) indirect C–F bond cleavage reactions in the UV/sulfite system.

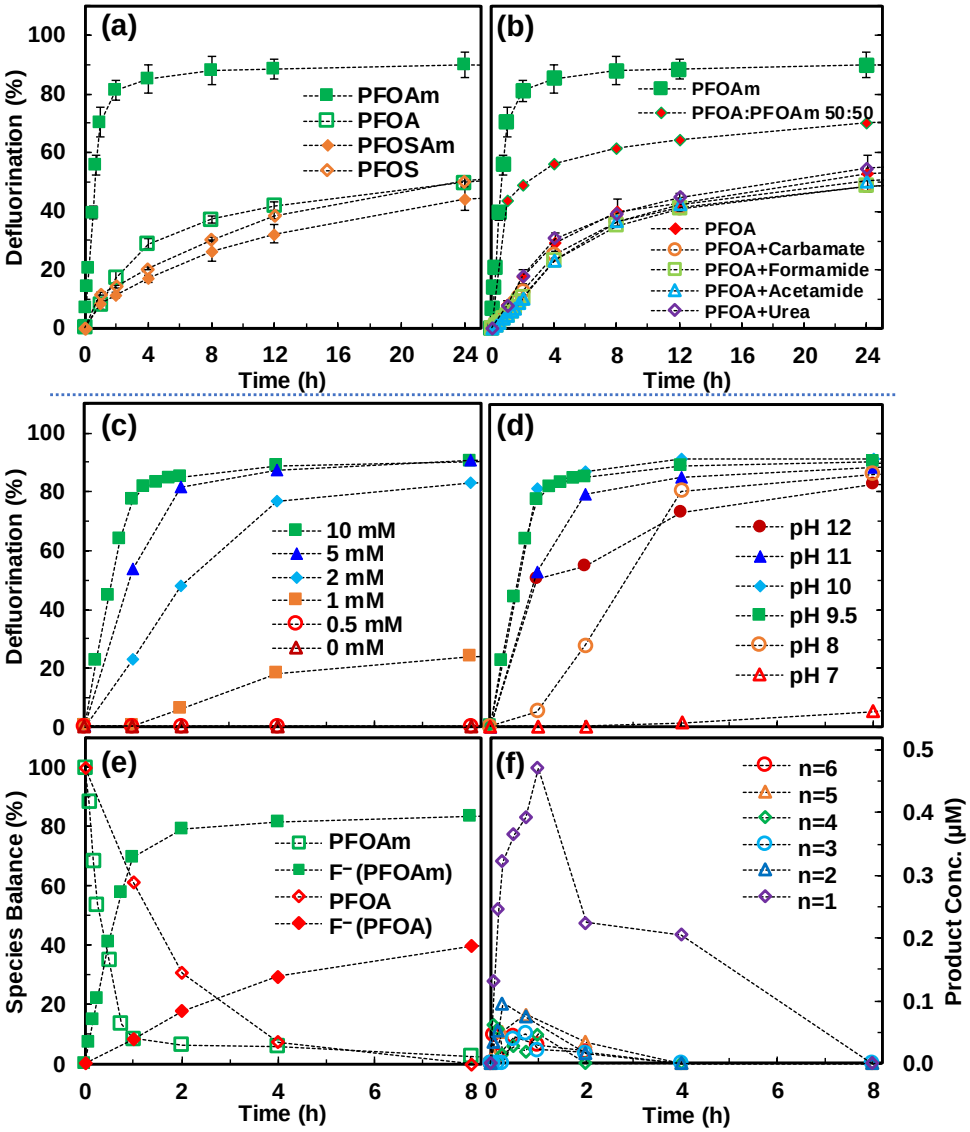

Figure 5.2 (a) Defluorination profiles of *n*=7 perfluorinated amide (PFOAm) and carboxylate (PFOA), *n*=8 perfluorinated sulfonamide (PFOSAm) and sulfonate (PFOS). (b) Defluorination profiles of *n*=7 carboxylate with addition of small molecules containing carboxamide moiety. (c) Defluorination profiles of *n*=7 PFOAm under various SO_3^{2-} concentration. (d) Defluorination profiles of *n*=7 PFOAm under various solution pH. (e) Decay and defluorination profiles of *n*=7 PFOAm and PFOA. (f) Transformation products from reaction of *n*=7 PFOAm within the UV/sulfite system. *Reaction conditions*: PFAS (0.025 mM), Na_2SO_3 (10 mM, unless specified otherwise), carbonate buffer (5 mM), 254 nm irradiation (18 W low-pressure Hg lamp for 600 mL solution) at pH 9.5 (unless specified otherwise) and 20 °C.

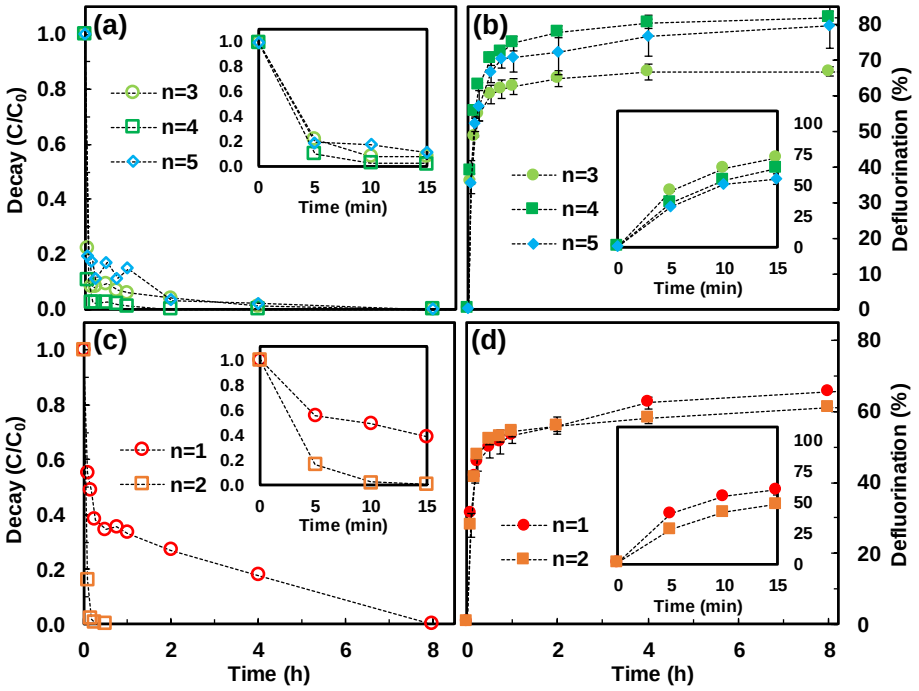

Figure 5.3 (a) Decay profiles for *n*=3–5 PFCAms. (b) Defluorination profiles for *n*=3–5 PFCAms. (c) Decay profiles for *n*=1–2 PFCAms. (d) Defluorination profiles for *n*=1–2 PFCAms. *Reaction conditions*: PFCAm (0.025 mM), Na_2SO_3 (10 mM), carbonate buffer (5 mM), 254 nm irradiation (18 W low-pressure Hg lamp for 600 mL solution) at pH 9.5 and 20 °C.

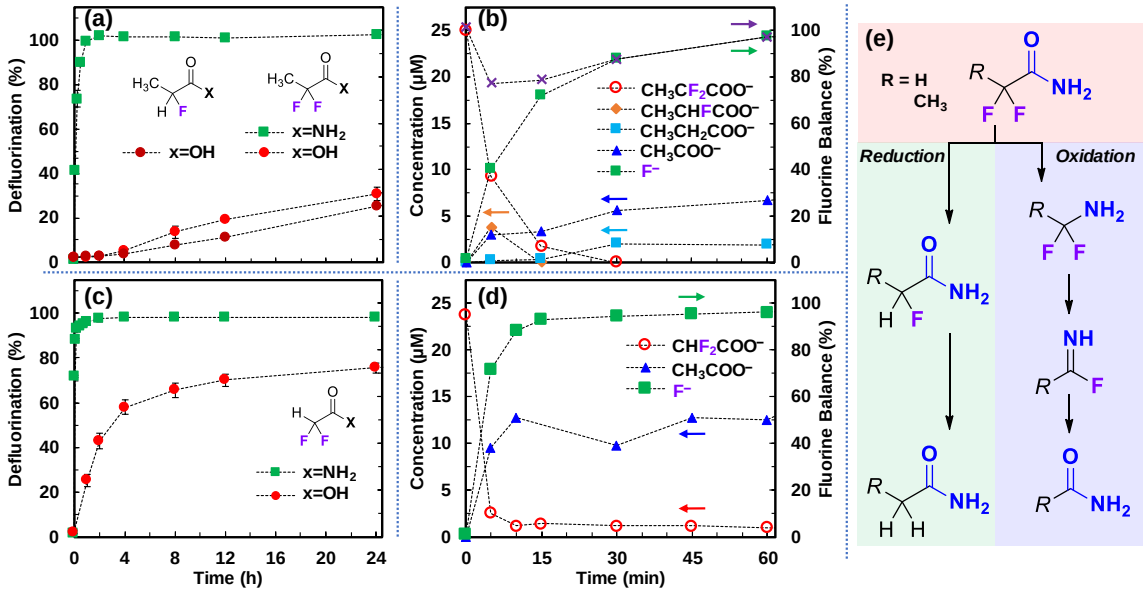

Figure 5.4 (a) Defluorination profiles for polyfluorinated C3 PFCAms and PFCAs. (b) Decay and transformation products for 2,2-difluoropropranamide [$CH_3{-}CF_2{-}CONH_2$]. (c) Defluorination profiles for difluoroacetamide (DFAm) and difluoroacetate (DFA). (d) Decay and transformation products for DFAm [$H{-}CF_2{-}CONH_2$]. (e) Reductive and oxidative defluorination reaction schemes. *Reaction conditions*: PFAS (0.025 mM), Na_2SO_3 (10 mM), carbonate buffer (5 mM), 254 nm irradiation (18 W low-pressure Hg lamp for 600 mL solution) at pH 9.5 and 20 °C.

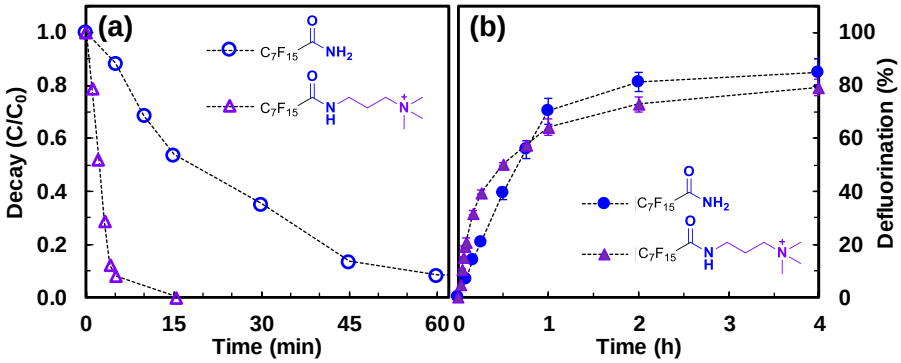

Figure 5.5 (a) Decay and (b) defluorination profiles for *n*=7 PFOAAmS and *n*=7 PFOAm. *Reaction conditions*: PFCAm (0.025 mM), Na_2SO_3 (10 mM), carbonate buffer (5 mM), 254 nm irradiation (an 18 W low-pressure Hg lamp for 600 mL solution), pH 9.5 and 20 °C.

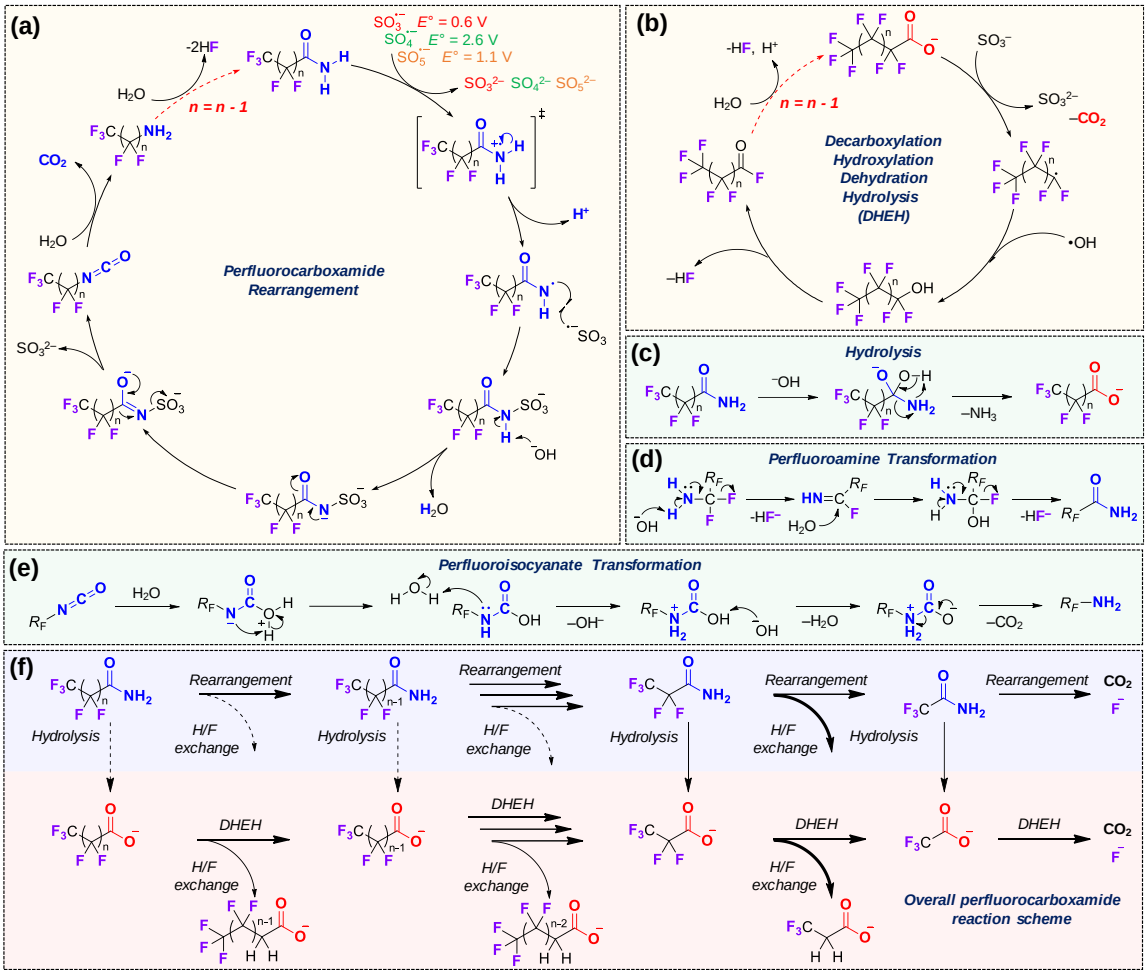

Scheme 5.1 (a) Perfluorocarboxamide (PFCAm) rearrangement mechanism; (b) perfluorocarboxylate (PFCA) chain-shortening mechanism; (c) PFCAm hydrolysis reaction; (d) perfluoroamine transformation; (e) perfluoroisocyanate transformation; and (f) overall PFCAm defluorination mechanism within the UV/sulfite system.

REFERENCES

(1) Wang, Z.; DeWitt, J. C.; Higgins, C. P.; Cousins, I. T. A Never-Ending Story of Per- and Polyfluoroalkyl Substances (PFASs)? *Environ. Sci. Technol.* **2017**, *51* (5), 2508–2518.

(2) Wang, Z.; Cousins, I. T.; Scheringer, M.; Buck, R. C.; Hungerbühler, K. Global Emission Inventories for C4–C14 Perfluoroalkyl Carboxylic Acid (PFCA) Homologues from 1951 to 2030, Part I: Production and Emissions from Quantifiable Sources. *Environment International* **2014**, *70*, 62–75.

(3) Wang, Z.; Cousins, I. T.; Scheringer, M.; Buck, R. C.; Hungerbühler, K. Global Emission Inventories for C4–C14 Perfluoroalkyl Carboxylic Acid (PFCA) Homologues from 1951 to 2030, Part II: The Remaining Pieces of the Puzzle. *Environment International* **2014**, *69*, 166–176.

(4) Jamari, N. L. A.; Dohmann, J. F.; Raab, A.; Krupp, E. M.; Feldmann, J. Novel Non-Targeted Analysis of Perfluorinated Compounds Using Fluorine-Specific Detection Regardless of Their Ionisability (HPLC-ICPMS/MS-ESI-MS). *Analytica Chimica Acta* **2019**, *1053*, 22–31.

(5) Rodriguez, K. L.; Hwang, J.-H.; Esfahani, A. R.; Sadmani, A. H. M. A.; Lee, W. H. Recent Developments of PFAS-Detecting Sensors and Future Direction: A Review. *Micromachines* **2020**, *11* (7), 667.

(6) Brase, R. A.; Spink, D. C. Enhanced Sensitivity for the Analysis of Perfluoroethercarboxylic Acids Using LC–ESI–MS/MS: Effects of Probe Position, Mobile Phase Additive, and Capillary Voltage. *J. Am. Soc. Mass Spectrom.* **2020**, *31* (10), 2124–2132.

(7) Fenton, S. E.; Ducatman, A.; Boobis, A.; DeWitt, J. C.; Lau, C.; Ng, C.; Smith, J. S.; Roberts, S. M. Per- and Polyfluoroalkyl Substance Toxicity and Human Health Review: Current State of Knowledge and Strategies for Informing Future Research. *Environ Toxicol Chem.* **2020**, etc.4890.

(8) Patlewicz, G.; Richard, A. M.; Williams, A. J.; Grulke, C. M.; Sams, R.; Lambert, J.; Noyes, P. D.; DeVito, M. J.; Hines, R. N.; Strynar, M.; Guiseppi-Elie, A.; Thomas, R. S. A Chemical Category-Based Prioritization Approach for Selecting 75 Per- and Polyfluoroalkyl Substances (PFAS) for Tiered Toxicity and Toxicokinetic Testing. *Environ Health Perspect.* **2019**, *127* (1), 014501.

(9) Kumarasamy, E.; Manning, I. M.; Collins, L. B.; Coronell, O.; Leibfarth, F. A. Ionic Fluorogels for Remediation of Per- and Polyfluorinated Alkyl Substances from Water. *ACS Cent. Sci.* **2020**, *6* (4), 487–492.

(10) Van den Bergh, M.; Krajnc, A.; Voorspoels, S.; Tavares, S. R.; Mullens, S.; Beurroies, I.; Maurin, G.; Mali, G.; De Vos, D. E. Highly Selective Removal of Perfluorinated Contaminants by Adsorption on All-Silica Zeolite Beta. *Angew. Chem. Int. Ed.* **2020**, *59*, 14086–14090.

(11) Ji, W.; Xiao, L.; Ling, Y.; Ching, C.; Matsumoto, M.; Bisbey, R. P.; Helbling, D. E.; Dichtel, W. R. Removal of GenX and Perfluorinated Alkyl Substances from Water by Amine-Functionalized Covalent Organic Frameworks. *J. Am. Chem. Soc.* **2018**, *140* (40), 12677–12681.

(12) Merino, N.; Qu, Y.; Deeb, R. A.; Hawley, E. L.; Hoffmann, M. R.; Mahendra, S. Degradation and Removal Methods for Perfluoroalkyl and Polyfluoroalkyl Substances in Water. *Environ. Eng. Sci.* **2016**, *33* (9), 615–649.

(13) Cui, J.; Gao, P.; Deng, Y. Destruction of Per- and Polyfluoroalkyl Substances (PFAS) with Advanced Reduction Processes (ARPs): A Critical Review. *Environ. Sci. Technol.* **2020**, *54* (7), 3752–3766.

(14) Barzen-Hanson, K. A.; Roberts, S. C.; Choyke, S.; Oetjen, K.; McAlees, A.; Riddell, N.; McCrindle, R.; Ferguson, P. L.; Higgins, C. P.; Field, J. A. Discovery of 40 Classes of Per- and Polyfluoroalkyl Substances in Historical Aqueous Film-Forming Foams (AFFFs) and AFFF-Impacted Groundwater. *Environ. Sci. Technol.* **2017**, *51* (4), 2047–2057.

(15) Haniff, M.; John, J.; Jennings, J.; Mueller, K. F. Perfluoroalkyl-Substituted Amines, Acids, Amino Acids and Thioether Acids. US 2003/0153780 A1, August 15, **2003**.

(16) Bokkers, B. G. H.; van de Ven, B.; Janssen, P.; Bil, W.; van Broekhuizen, F.; Zeilmaker, M.; Oomen, A. G. *Per- and Polyfluoroalkyl Substances (PFASs) in Food Contact Materials*; RIVM Letter; 2018–0181; National Institute for Public Health and the Environment: The Netherlands, **2019**; p 112.

(17) Zhu, Y.; Casselman, M. D.; Li, Y.; Wei, A.; Abraham, D. P. Perfluoroalkyl-Substituted Ethylene Carbonates: Novel Electrolyte Additives for High-Voltage Lithium-Ion Batteries. *J. Power Sources.* **2014**, *246*, 184–191.

(18) Wong, D. H. C.; Thelen, J. L.; Fu, Y.; Devaux, D.; Pandya, A. A.; Battaglia, V. S.; Balsara, N. P.; DeSimone, J. M. Nonflammable Perfluoropolyether-Based Electrolytes for Lithium Batteries. *PNAS* **2014**, *111* (9), 3327–3331.

(19) Teran, A.; Rupert, B.; Nasybulin, E.; Burdynska, J. Functionalized Perfluoroalkanes and Electrolyte Compositions. US 2016/0301107 A1, October 13, **2016**.

(20) Wang, S.; Huang, J.; Yang, Y.; Hui, Y.; Ge, Y.; Larssen, T.; Yu, G.; Deng, S.; Wang, B.; Harman, C. First Report of a Chinese PFOS Alternative Overlooked for 30 Years: Its Toxicity, Persistence, and Presence in the Environment. *Environ. Sci. Technol.* **2013**, *47* (18), 10163–10170.

(21) Herweck, S. A.; Gingras, P. H.; Martakos, P.; Karwoski, K. Method of Making an Expandable Fluoropolymer Device. US Patent 6395208 B1, May 28, **2002**.

(22) Buck, R. C.; Franklin, J.; Berger, U.; Conder, J. M.; Cousins, I. T.; de Voogt, P.; Jensen, A. A.; Kannan, K.; Mabury, S. A.; van Leeuwen, S. P. Perfluoroalkyl and Polyfluoroalkyl Substances in the Environment: Terminology, Classification, and Origins. *Integr. Environ. Assess. Manag.* **2011**, *7* (4), 513–541.

(23) Harding-Marjanovic, K. C.; Houtz, E. F.; Yi, S.; Field, J. A.; Sedlak, D. L.; Alvarez-Cohen, L. Aerobic Biotransformation of Fluorotelomer Thioether Amido Sulfonate (Lodyne) in AFFF-Amended Microcosms. *Environ. Sci. Technol.* **2015**, *49* (13), 7666–7674.

(24) Chen, H.; Liu, M.; Munoz, G.; Duy, S. V.; Sauvé, S.; Yao, Y.; Sun, H.; Liu, J. Fast Generation of Perfluoroalkyl Acids from Polyfluoroalkyl Amine Oxides in Aerobic Soils. *Environ. Sci. Technol. Lett.* **2020**, *7* (10), 714–720.

(25) Houtz, E. F.; Sedlak, D. L. Oxidative Conversion as a Means of Detecting Precursors to Perfluoroalkyl Acids in Urban Runoff. *Environ. Sci. Technol.* **2012**, *46* (17), 9342–9349.

(26) Park, H.; Vecitis, C. D.; Cheng, J.; Choi, W.; Mader, B. T.; Hoffmann, M. R. Reductive Defluorination of Aqueous Perfluorinated Alkyl Surfactants: Effects of Ionic Headgroup and Chain Length. *J. Phys. Chem. A.* **2009**, *113* (4), 690–696.

(27) Carter, K. E.; Farrell, J. Oxidative Destruction of Perfluorooctane Sulfonate Using Boron-Doped Diamond Film Electrodes. *Environ. Sci. Technol.* **2008**, *42* (16), 6111–6115.

(28) Vecitis, C. D.; Park, H.; Cheng, J.; Mader, B. T.; Hoffmann, M. R. Kinetics and Mechanism of the Sonolytic Conversion of the Aqueous Perfluorinated Surfactants, Perfluorooctanoate (PFOA), and Perfluorooctane Sulfonate (PFOS) into Inorganic Products. *J. Phys. Chem. A.* **2008**, *112* (18), 4261–4270.

(29) Hori, H.; Hayakawa, E.; Einaga, H.; Kutsuna, S.; Koike, K.; Ibusuki, T.; Kiatagawa, H.; Arakawa, R. Decomposition of Environmentally Persistent Perfluorooctanoic Acid in Water by Photochemical Approaches. *Environ. Sci. Technol.* **2004**, *38* (22), 6118–6124.

(30) Stratton, G. R.; Dai, F.; Bellona, C. L.; Holsen, T. M.; Dickenson, E. R. V.; Mededovic Thagard, S. Plasma-Based Water Treatment: Efficient Transformation of Perfluoroalkyl Substances in Prepared Solutions and Contaminated Groundwater. *Environ. Sci. Technol.* **2017**, *51* (3), 1643–1648.

(31) Zhang, Z.; Chen, J.-J.; Lyu, X.-J.; Yin, H.; Sheng, G.-P. Complete Mineralization of Perfluorooctanoic Acid (PFOA) by γ-Irradiation in Aqueous Solution. *Sci Rep* **2015**, *4* (1), 7418.

(32) Wu, B.; Hao, S.; Choi, Y.; Higgins, C. P.; Deeb, R.; Strathmann, T. J. Rapid Destruction and Defluorination of Perfluorooctanesulfonate by Alkaline Hydrothermal Reaction. *Environ. Sci. Technol. Lett.* **2019**, *6* (10), 630–636.

(33) Huang, D.; de Vera, G. A.; Chu, C.; Zhu, Q.; Stavitski, E.; Mao, J.; Xin, H.; Spies, J. A.; Schmuttenmaer, C. A.; Niu, J.; Haller, G. L.; Kim, J.-H. Single-Atom Pt Catalyst for Effective C–F Bond Activation via Hydrodefluorination. *ACS Catal.* **2018**, *8* (10), 9353–9358.

(34) Hart, E. J.; Boag, J. W. Absorption Spectrum of the Hydrated Electron in Water and in Aqueous Solutions. *J. Am. Chem. Soc.* **1962**, *84* (21), 4090–4095.

(35) Song, Z.; Tang, H.; Wang, N.; Zhu, L. Reductive Defluorination of Perfluorooctanoic Acid by Hydrated Electrons in a Sulfite-Mediated UV Photochemical System. *J. Hazard. Mat.* **2013**, *262*, 332–338.

(36) Bentel, M. J.; Liu, Z.; Yu, Y.; Gao, J.; Men, Y.; Liu, J. Enhanced Degradation of Perfluorocarboxylic Acids (PFCAs) by UV/Sulfite Treatment: Reaction Mechanisms and System Efficiencies at PH 12. *Environ. Sci. Technol. Lett.* **2020**, *7* (5), 351–357.

(37) Bentel, M. J.; Yu, Y.; Xu, L.; Li, Z.; Wong, B. M.; Men, Y.; Liu, J. Defluorination of Per- and Polyfluoroalkyl Substances (PFASs) with Hydrated Electrons: Structural Dependence and Implications to PFAS Remediation and Management. *Environ. Sci. Technol.* **2019**, *53* (7), 3718–3728.

(38) Bentel, M. J.; Yu, Y.; Xu, L.; Kwon, H.; Li, Z.; Wong, B. M.; Men, Y.; Liu, J. Degradation of Perfluoroalkyl Ether Carboxylic Acids with Hydrated Electrons: Structure–Reactivity Relationships and Environmental Implications. *Environ. Sci. Technol.* **2020**, *54* (4), 2489–2499.

(39) Kloeter, G.; Seppelt, K. Trifluoromethanol (CF_3OH) and Trifluoromethylamine (CF_3NH_2). *J. Am. Chem. Soc.* **1979**, *101* (2), 347–349.

(40) Cheburkov, Y.; Lillquist, G. J. Perfluoroalcohols. *J. Fluor. Chem.* **2002**, *118* (1–2), 123–126.

(41) Nguyen, M. T.; Matus, M. H.; Ngan, V. T.; Haiges, R.; Christe, K. O.; Dixon, D. A. Energetics and Mechanism of the Decomposition of Trifluoromethanol. *J. Phys. Chem. A.* **2008**, *112* (6), 1298–1312.

(42) Shen, J.; Bai, Y.; Tai, X.; Wang, W.; Wang, G. Surface Activity, Spreading, and Aggregation Behavior of Ecofriendly Perfluoropolyether Amide Propyl Betaine in Aqueous Solution. *ACS Sustain. Chem. Eng.* **2018**, *6* (5), 6183–6191.

(43) D'Agostino, L. A.; Mabury, S. A. Identification of Novel Fluorinated Surfactants in Aqueous Film Forming Foams and Commercial Surfactant Concentrates. *Environ. Sci. Technol.* **2014**, *48* (1), 121–129.

(44) Kimura, C.; Kashiwaya, K.; Kobayashi, M.; Nishiyama, T.; Kudoh, M.; Kusuyama, T.; Yamaguchi, S.; Fudano, S. Preparation and Surface-Active Properties of Sulfopropylated N-Alkylperfluorooctanamides. *J. Am. Oil Chem.' Soc.* **1984**, *61* (1), 3.

(45) Cheng, W.; Ng, C. A. Using Machine Learning to Classify Bioactivity for 3486 Per- and Polyfluoroalkyl Substances (PFASs) from the OECD List. *Environ. Sci. Technol.* **2019**, *53* (23), 13970–13980.

(46) Bahmanjah, S.; Zhang, N.; Davis, J. T. Monoacylglycerols as Transmembrane Cl^- Anion Transporters. *Chem. Commun.* **2012**, *48* (37), 4432.

(47) Rota, P.; Allevi, P.; Agnolin, I. S.; Mattina, R.; Papini, N.; Anastasia, M. A Simple Synthesis of N-Perfluoroacylated and N-Acylated Glycals of Neuraminic Acid with a Cyclic Aminic Substituent at the 4α Position as Possible Inhibitors of Sialidases. *Org. Biomol. Chem.* **2012**, *10* (14), 2885.

(48) Masanori, T.; Akira, S. The Thin Film of a Fluorine-Containing Polymer with Cyclodextrin Prepared by the Langmuir–Blodgett Technique and Its Application to Photochromic Thin Films. *Bull.Chem. Soc. Jpn.* **1993**, *66* (5), 1356–1360.

(49) Jackson, D. A.; Mabury, S. A. Polyfluorinated Amides as a Historical PFCA Source by Electrochemical Fluorination of Alkyl Sulfonyl Fluorides. *Environ. Sci. Technol.* **2013**, *47* (1), 382–389.

(50) Jackson, D. A.; Wallington, T. J.; Mabury, S. A. Atmospheric Oxidation of Polyfluorinated Amides: Historical Source of Perfluorinated Carboxylic Acids to the Environment. *Environ. Sci. Technol.* **2013**, *47* (9), 4317–4324.

(51) Ahlbrecht, A. H.; Husted, D. R. Perfluoroalkyl Isocyanates. US Patent 2617817, November, 11 **1952**.

(52) Middleton, W. J. Perfluoroalkyl Isocyanates: General Synthesis by the Pyrolysis of Disilyl Esters of Hydroxamic Acids. *J. Org. Chem.* **1984**, *49* (23), 4541–4543.

(53) Matheson, M. S.; Rabani, J. Pulse Radiolysis of Aqueous Hydrogen Solutions. I. Rate Constants for Reaction of e_{aq}^- with Itself and Other Transients. II. The Interconvertibility of e_{aq}^- and H. *J. Phys. Chem.* **1965**, *69* (4), 1324–1335.

(54) Neta, P.; Huie, R. E.; Ross, A. B. Rate Constants for Reactions of Inorganic Radicals in Aqueous Solution. *J. Phys. Chem. Ref. Data.* **1988**, *17* (3), 259.

(55) Hayon, E.; Treinin, A.; Wilf, J. Electronic Spectra, Photochemistry, and Autoxidation Mechanism of the Sulfite-Bisulfite-Pyrosulfite Systems. SO_2^-, SO_3^-, SO_4^-, and SO_5^- Radicals. *J. Am. Chem. Soc.* **1972**, *94* (1), 47–57.

(56) Neta, P.; Huie, R. E. Free-Radical Chemistry of Sulfite. *Environ. Health Perspect.* **1985**, *64*, 209–217.

(57) Buxton, G. V.; Greenstock, C. L.; Helman, W. P.; Ross, A. B. Critical Review of Rate Constants for Reactions of Hydrated Electrons, Hydrogen Atoms and Hydroxyl Radicals (·OH/·O $^-$ in Aqueous Solution. *Journal of Physical and Chemical Reference Data* **1988**, *17* (2), 513–886.

(58) Cook, A. R.; Dimitrijevic, N.; Dreyfus, B. W.; Meisel, D.; Curtiss, L. A.; Camaioni, D. M. Reducing Radicals in Nitrate Solutions. The NO_3^{2-} System Revisited. *J. Phys. Chem. A.* **2001**, *105* (14), 3658–3666.

(59) Riesz, P. The Radiolysis of Acetone in Air-Free Aqueous Solutions. *J. Phys. Chem.* **1965**, *69* (4), 1366–1373.

(60) Van Hoomissen, D. J.; Vyas, S. Early Events in the Reductive Dehalogenation of Linear Perfluoroalkyl Substances. *Environ. Sci. Technol. Lett.* **2019**, *6* (6), 365–371.

(61) Houmam, A. Electron Transfer Initiated Reactions: Bond Formation and Bond Dissociation. *Chem. Rev.* **2008**, *108* (7), 2180–2237.

(62) Meresaar, U.; Bratt, L. Hydrolysis of Amides. Alkaline and General Acid Catalyzed Alkaline Hydrolysis of Some Substituted Acetamides and Benzamides. *Acta Chem. Scand., Ser. A* **1974**, *28*, 715–722.

CHAPTER 6: CONCLUSIONS AND FUTURE WORK

A photochemical system applying UV (i.e., 254 nm) light and a photosensitizer was used to establish structure-reactivity relationships for several legacy and emerging PFAS within the UV/sulfite system, known to generate the strong reductant, hydrated electron (e_{aq}^-). Experimental observations from PFAS decay kinetics, transformation production analysis, fluorine recovery, and reactions of model PFAS structures, with the aid of theoretical results from quantum chemical calculations and simulations, have provided strong evidence for critical reaction mechanisms of PFAS within the UV/sulfite system. PFAS reactivity is significantly enhanced by functional head group (e.g., carboxylate > sulfonate) and fluoroalkyl carbon chain length (e.g., $n \geq 4$). Although both chain-shortening and H/F exchange reactions occur within the UV/sulfite system for several PFAS structures, carboxylates are more labile to chain-shortening, while PFAS with fluorocarbon chains not directly bonded to a carboxylate (e.g., fluorotelomer carboxylic acids, FTCAs) favor H/F exchange. Competition between chain-shortening and H/F exchange reactions determine the extent of defluorination. Defluorination ceases when all labile C–F bonds have been cleaved, resulting in a mixture of polyfluorinated organic compounds unreactive in the UV/sulfite system.

Incorporation of the ether group within the carbon backbone chain results in overall slower reaction kinetics. The integration of the ether linkage generates small fluoroalkyl segments segregated by oxygen atoms, which influence the overall defluorination mechanism. This is primarily due to the increased stability of C–F bonds adjacent to ether linkages, consequently reducing the probability for H/F exchange along the fluorocarbon backbone. For linear fluoroalkyl segments, high defluorination can be achieved. Conversely, branched fluoroalkyl segments inhibit the overall defluorination. This is due to the increased probability towards H/F exchange for labile tertiary C–F bonds and trifluoromethyl groups, generating recalcitrant polyfluorinated species. Furthermore, the presence of the ether linkage introduces a new reaction pathway involving the

cleavage of the C–O bond within the fluoroalkyl ether chain. This design allows the UV/sulfite system to overcome adverse H/F exchange products that inhibit defluorination of legacy PFAS.

System parameters were found to be significantly influential in mediating defluorination mechanisms. Elevated pH provides a more effective system as demonstrated by the increased overall defluorination, while achieving greater efficiency as evidenced by shorter treatment times. This is attributed to the (*i*) increased lifetime of the e_{aq}^- and (*ii*) thermodynamic influence on kinetically controlled reaction mechanisms. Enhanced reactivity with PFAS was observed, where a noticeable shift in transformation product distribution provides evidence of competing reactions. For example, early in the reaction, chain-shortened transformation products increased upon increase of solution pH, indicating a preference for oxidative chain-shortening mechanism. Meanwhile, transformation products exhibiting extensive C–F bond substitution for C–H bonds late in the reaction further supports the increased lifetime of the e_{aq}^-, thus improving the effectiveness of the photochemical system at elevated pH towards C–F bond cleavage.

Treatment of a series of perfluorocarboxamides (PFCAms) within the UV/sulfite system has revealed a novel defluorination mechanism exhibiting substantially higher rates of reaction, deeper defluorination, while minimizing undesired side reactions (e.g., H/F exchange). Notably, this new reaction mechanism enables defluorination at substantially lower (*i*) solution pH (9.5 vs 12 for PFCAs), (*ii*) sulfite concentration (5 mM vs 10 mM for PFCAs), and (*iii*) treatment time (2 h vs 8 h for PFCAs) to achieve maximum defluorination. Furthermore, undesired H/F exchange reactions are minimized resulting in decreased formation of recalcitrant transformation products, thus preventing the arrest of defluorination. These results are contributed to the enhanced reactivity of the carboxamide group towards reduction by e_{aq}^- and oxidation by sulfite radicals ($SO_x^{\bullet -}$). Although carboxamides are susceptible to hydrolysis, the slightly basic (pH 9.5) reaction condition does not influence long-chain PFCAms. However, short chain (i.e., $n \leq 2$) PFCAms will hydrolyze

to the acid relatively quickly. Overall, this novel reaction mechanism enables substantial defluorination (80–90%) with the remaining C–F bonds trapped in small polyfluorinated compounds (i.e., CF_3–C**H**$_2$–COO). Although this product is recalcitrant in the UV/sulfite system, it is easily transformed into CO_2 and F^- by oxidation, enabling 100% recovery of F^-. Lastly, strategic design of PFCAms can enable faster decay and achieve complete (>99%) F^- recovery while mitigating unfavorable hydrolysis towards recalcitrant PFCAs.

Outcomes of this work highlight critical aspects towards identifying promising technologies in the search for global PFAS remediation, providing a general outline regarding how to approach this complex issue. In addition, reaction mechanisms have provided key insights on structure leading to predictive treatment outcomes. First, extensive structure-reactivity relationships clearly demonstrate the need for engineered solutions to consider entire classes of PFAS structures (e.g., carboxylates, sulfonates, etc.) and not to target specific compounds (e.g., PFOA, PFOS, HFPO-DA). This is due to the broad, and sometimes unpredictable, physical and chemical properties exhibited across each class of PFAS. Therefore, treatment efforts that address specific PFAS structures, and not classes, will undoubtedly result in generating misleading conclusions and potentially misguiding the scientific community at large. Furthermore, undesired reaction products will likely possess altered physical (e.g., adsorption) and chemical (i.e., reactivity) properties than targeted compounds. Therefore, to evaluate future PFAS remediation technologies, it is necessary to not only address target pollutants, but secondary transformation products, in order to achieve complete treatment and mitigate adverse effects.

Furthermore, key structural components have been identified that directly influence performance of treatment strategies. Indeed, these features provide insights on identifying promising approaches to initiate bond cleavage events. Due to the strength and stability of the C–F bond, it appears highly advantageous (i.e., achieve faster and deeper defluorination) to target

transforming the stability of PFAS compounds rather than targeting direct C–F bond cleavage. Information based on observed reaction mechanisms can inform future PFAS design in order to enable highly efficient, and complete, treatment of compounds. This strategy will mitigate the need for extended treatment times, reduce generation of harmful reaction products, and minimize overall remediation costs.

As extensive work has been dedicated to (*i*) determining structure-reactivity relationships across several classes of PFAS and (*ii*) optimizing the thermodynamic conditions within the UV/sulfite system, strategies to continue improving this system to achieve a realized solution must be identified. For example, are there other known photosensitizers that can mediate both oxidative and reductive reaction pathways? And if so, what – if any – kinetic preference do they exhibit for oxidative (*chain-shortening*) over reductive (*H/F exchange*) reactivity? Furthermore, is it possible to design photosensitizers that preferentially facilitate chain-shortening over H/F exchange reactions? Also, to what extent can the energy source (i.e., UV lamp) influence the kinetics of the UV/photosensitizer system? Can emerging UV light-emitting diodes (UV LED), which do not contain harmful mercury or produce carcinogenic ozone, while consuming significantly less energy, be used as a replacement, further driving down expense costs? Lastly, is it possible to design a system that can separate oxidative and reductive processes to enable a single-pass continuous flow treatment scheme?

This thesis research provides a general approach for developing a facile aqueous chemical treatment method (i.e., UV light with inexpensive photosensitizers) in order to elucidate reactivity across a broad class of chemically recalcitrant compounds, highlighting the simplicity in optimizing performance and ability to control reaction pathways, and identifies a novel defluorination reaction pathway enabling the rapid and complete destruction of PFAS compounds.

APPENDIX A: APPENDICES FOR CHAPTER 2

Detailed Information on Materials and Methods

Chemicals and the Preparation of PFAS Stock Solutions. All PFAS chemicals were purchased from Acros Organics, Alfa-Aesar, MP Biomedicals, Oakwood Chemicals, Sigma-Aldrich, and SynQuest Laboratories. Table A.1 (next page) summarizes the name, purity, and CAS number of all PFASs included in this study. All other chemicals and solvents were purchased from Fisher Chemical. Individual PFASs were dissolved in either deionized (DI, produced by Milli-Q system) water as 10 mM stock solutions. For carboxylic acids, the addition of 20 mM NaOH (for PFCAs) or 40 mM NaOH (for PFdiCAs) effectively facilitated the dissolution of long chain structures in water and prevented the volatilization of short chain structures. For long chain FTCAs (more than 8 carbons in the molecule), methanol was used as the solvent. Methanol does not interfere with the PFAS defluorination with hydrated electrons. For example, preliminary experiments with 25 μM PFOA introduced with the water stock solution (1.5 mL into 600 mL final volume) and with the methanol stock solution (0.3 mL into 600 mL final volume, resulting in ~12 mM methanol in water) gave the same rate and extent of defluorination. All PFAS stock solutions were stored at 4°C.

Table A.1 Information of PFASs Used in This Study.

Entry	Chemical Name	Fluoroalkyl Length (n)	Purity	CAS#
	$F(CF_2)_n$−COOH (or salt)			
1	Sodium trifluoroacetate	1	98%	2923-18-4
2	Perfluoropropionic acid	2	97%	422-64-0
3	Perfluorobutyric acid	3	98%	375-22-4
4	Perfluoropentanoic acid	4	97%	2706-90-3
5	Perfluorohexanoic acid	5	97%	307-24-4
6	Perfluoroheptanoic acid	6	98%	375-85-9
7	Perfluorooctanoic acid	7	96%	335-67-1
8	Perfluorononanoic acid	8	97%	375-95-1
9	Perfluorodecanoic acid	9	97%	335-76-2
10	Perfluoroundecanoic acid	10	96%	2058-94-8
	HOOC−$(CF_2)_n$−COOH			
11	Difluoromalonic acid	1	98%	1514-85-8
12	Tetrafluorosuccinic acid	2	98%	377-38-8
13	Hexafluoroglutaric acid	3	98%	376-73-8
14	Octafluoroadipic acid	4	97%	336-08-3
15	Dodecafluorosuberic acid	6	98%	678-45-5
16	Tetradecafluoroazelaic acid	7	90%	23453-64-7
17	Hexdecafluorosebacic acid	8	95%	307-78-8
18	Perfluoro-1,10-decanedicarboxylic acid	10	96%	865-85-0
	$F(CF_2)_n$−CH_2CH_2−COOH			
19	4,4,4-Trifluorobutyric acid	1	99%	406-93-9
20	2H,2H,3H,3H-Perfluoropentanoic acid	2	N/A	3637-31-8
21	2H,2H,3H,3H-Perfluorohexanoic acid	3	97%	356-02-5
22	2H,2H,3H,3H-Perfluoroheptanoic acid	4	97%	80705-13-1
23	2H,2H,3H,3H-Perfluorooctanoic acid	5	N/A	914637-49-3
24	2H,2H,3H,3H-Perfluorononanoic acid	6	97%	27854-30-4
25	2H,2H,3H,3H-Perfluorodecanoic acid	7	97%	812-70-4
26	2H,2H,3H,3H-Perfluoroundecanoic acid	8	97%	34598-33-9
	$F(CF_2)_n$−SO_3H (or salt)			
27	Sodium trifluoromethanesulfonate	1	98%	2926-30-9
28	Potassium nonafluorobutanesulfonate	4	98%	29420-49-3
29	Potassium perfluorohexane-1-sulfonate	6	95%	3871-99-6
30	Perfluorooctanesulfonic acid	8	97%	1763-23-1
	Special structures			
31	2,2-difluorosuccinic acid **HOOC−CF_2CH_2−COOH**		97%	665-31-6
32	3,3,3-Trifluoropropionic acid **CF_3−CH_2−COOH**		97%	2516-99-6
33	Difluoroacetic acid **CF_2H−COOH**		98%	381-73-7
34	Sodium fluoroacetate **CFH_2−COONa**		98%	62-74-8

Defluorination Reaction Settings. A 600-mL solution containing 25 μM PFAS, 10 mM Na_2SO_3, and 5 mM $NaHCO_3$ (pH 9.5, adjusted by 0.5 mL of 1 M NaOH) was prepared with DI water. Powders of Na_2SO_3 (756 mg) and $NaHCO_3$ (252 mg) were used to prepare each fresh solution without on-shelf storage in solution. The closed-system cylindrical photochemical reactor consisted of a borosilicate glass shell and a quartz immersion well, both of which are double-layered for cooling with circulated water (20°C) in the jacket. The space between the glass shell and immersion well (~2 cm thickness ring column) was loaded with the 600-mL reaction solution. A magnetic stir bar was placed at the bottom of the reactor, and the stirring speed was set at 360 rpm. An 18 W low-pressure mercury lamp (GPH212T5L/4P/HO, "High Output") in the immersion well delivered 254 nm UV irradiation to the surrounding solution. A previous report[1] has described the photochemical parameters of a system with the same key dimension of both the photoreactor and the UV lamp (except that the power of GPH212T5L/4P lamp in that report was 10 W). The reactor assembly was wrapped in heavy-duty aluminum foil to prevent UV irradiation leaking. After the UV lamp was turned on, aliquots of solution (5 mL each) were taken at time intervals through a 16-gauge stainless steel needle that penetrated the rubber-sealed sampling port. The samples were stored in 7-mL glass scintillation vials at 4°C prior to analysis.

Two reasons for choosing sulfite as the e_{aq}^- source are (1) the resulting sulfate is a ubiquitous natural water mineral, and (2) sulfite can be economically obtained from coal combustion flue gas scrubbing.[2] The reason for choosing carbonate as the buffer/additive is that carbonate is ubiquitous in all natural waters, especially in groundwater. Reaction conditions tested in this study and reported in the literature on PFOA/PFOS defluorination are summarized in Table A.2 (next page). During the preliminary tests, the N_2 sparging step prior to the photochemical reaction did not show significant enhancement to the defluorination from PFOA (e.g., **entry 1** vs. **2**, and **entry 3** vs. **4** although other parameters were slightly different) probably because the added

10 mM Na_2SO_3 far exceeded the dissolved oxygen (the saturated DO level at 20°C is 9.0 mg L^{-1} or 0.28 mM). Thus, most reactions in this study did not have the N_2 sparging step for DO removal. During the preliminary tests, the $NaHCO_3$ buffer and NH_4Cl buffer at pH 9.2−9.5 showed no significant influence on the defluorination of PFOA (e.g., **entry 3** vs. **7**). When 10 mM Na_2SO_3 was used, the maximum defluorination ratio of PFOA and PFOS were also similar to (or even slightly higher than) the previous reports that used a high-pressure UV lamp (250 W, high photon flux with a wide irradiation spectrum of 200–600 nm),[3, 4] Na_2SO_3 or potassium iodide (KI) as the electron source chemical,[5, 6] or nitrilotriacetic acid (NTA) as the hydroxyl radical scavenger.[7] Thus, the experimental setting of this study can be representative for the reported systems using variable hydrated electron source chemicals and UV lamps.

Table A.2 Summary of Experimental Conditions for PFOA/PFOS Defluorination

Entry	Reaction Condition	Buffer Chemical[a]	pH	N_2 Sparge	Reaction Time	DeF Ratio	Reference
	PFOA defluorination reactions						
1	25 μM PFOA; 254 nm (18W); 10 mM Na_2SO_3; 20°C	$NaHCO_3$ (5mM)	9.5	1 h	12 h	49%	This study
2	25 μM PFOA; 254 nm (18W); 10 mM Na_2SO_3; 20°C	$NaHCO_3$ (5mM)	9.5	No sparge	12 h	48%	This study
3	25 μM PFOA; 254 nm (18W); 10 mM Na_2SO_3; 20°C	$NaHCO_3$ (5mM)	9.5	No sparge	48 h	57%	This study
4	20 μM PFOA; 254 nm (10W); 10 mM Na_2SO_3; 25°C	NH_4OH	9.3	30 min	24 h	63%	[6]
5	39 μM PFOA; 200− 400 nm (<250 W);[b] 10 mM Na_2SO_3; 25°C	Not added	9.2	No sparge	10 min	46%	[4]
6	25 μM PFOA; 254 nm (18 W); 0.3 mM KI; 20°C	NH_4Cl (5 mM)	9.3	1 h	8 h	34%	This study
7	25 μM PFOA; 254 nm (18 W); 1.0 mM KI; 20°C	NH_4Cl (5 mM)	9.3	1 h	22 h	58%	This study
8	25 μM PFOA; 254 nm (15 W); 0.3 mM KI; room temperature	NH_4Cl	9.0	30 min	14 h	99%[c]	[5]
9	25 μM PFOA; 254 nm (15 W); 0.3 mM KI; room temperature	NH_4Cl	9.0	30 min	8 h	85%[c]	[5]
	PFOS defluorination reactions						
10	25 μM PFOS; 254 nm (18W); 10 mM Na_2SO_3; 20°C	$NaHCO_3$ (5mM)	9.5	No sparge	48 h	56%	This study
11	25 μM PFOS; 254 nm (18W); 10 mM Na_2SO_3; 20°C	$NaHCO_3$ (5mM)	9.5	No sparge	12 h	38%	This study
12	32 μM PFOS; 200− 400 nm (<250 W);[b] 10 mM Na_2SO_3; 25°C	Not added	9.2	No sparge	30 min	56%	[3]
13	10 μM PFOS; 254 nm (14W); 2 mM NTA; 30°C	NH_4Cl	10.0	20 min	10 h	47%	[7]
14	10 μM PFOS; 254 nm (14W); 2 mM Na_2SO_3; 30°C	NH_4Cl	10.0	20 min	10 h	30%	[7]

[a]NaOH and NH_4OH were used to raise the pH of solutions added with $NaHCO_3$ and NH_4Cl, respectively.
[b]The 400−600 nm portion was blocked so the effective irradiation power to the solution was reduced.
[c]Results are questionable because 99% and 85% defluorination of 0.025 mM PFOA ($C_7F_{15}COOH$) would require cleaving 0.37 mM and 0.32 mM C−F bonds, respectively. However, the KI concentration was only 0.30 mM. The maximum C−F cleavage, assuming 100% reaction efficiency of e_{aq}^- excited from KI, could be only 0.15 mM based on the theoretical 2:1 stoichiometry,[8] where both C and F need one electron after the bond cleavage.

Measurement of PFAS Parent Compound Decay. Concentrations of ionic PFAS parent compounds were analyzed by a high-performance liquid chromatography–triple quadrupole mass spectrometry system (HPLC−MS/MS, Agilent 1200 HPLC, and Sciex 5500 QTRAP MS) in the Metabolomics Lab of Roy J. Carver Biotechnology Center at UIUC. The Analyst 1.6.2 software was used for data acquisition and analysis. For HPLC separation, a 10-μL sample was loaded onto a Zorbax SB-Aq column (particle size 5μm, 4.6×50 mm, Agilent) eluted with 350 μL min^{-1} of 10 mM ammonia formate (A) and methanol (B). The linear gradient was as follows: 100% A for 0−1 min, 2% A for 2−15 min, and 100% A for 16−21 min. The mass spectra were acquired under negative ionization (ESI) mode. The ion spray voltage was set to −4500 V, and the source temperature was set to 450 °C. The curtain gas, ion source gas 1, and ion source gas 2 flow were set to 30, 50, and 60 psi, respectively. Multiple reaction monitoring (MRM) was used for quantification, and the MRM transition was listed in Table A.3. The limit of quantification (LOQ) for each compound was determined as the lowest concentration with a detection variation < 20%, which was listed in Table A.3. An ion chromatography system (see below) was used for the quantification of short-chain PFASs ($CF_3CO_2^-$, $CF_2HCO_2^-$, $CFH_2CO_2^-$, and $CF_3SO_3^-$).

PFAS Transformation Product analysis. PFAS transformation products were measured by liquid chromatography coupled with a high-resolution quadrupole orbitrap mass spectrometer (LC-HRMS/MS) (Q Exactive, Thermo Fisher Scientific). The LC analysis was the same as above described. The transformation products were detected in full scan negative ionization mode on HRMS at a resolution of 70,000 at m/z 200 and a scan range of m/z 50−750. The software Xcalibur (Thermo Fisher Scientific) was used for data acquisition and analysis.

Suspect screening was carried out to identify transformation products as previously described, but with slightly modification.[9, 10] Briefly, suspect screening was done by TraceFinder 4.1 EFS (Thermo Fisher Scientific). The transformation product suspect lists were generated by a

self-written automatic product mass prediction script, which includes all possible products from the mechanisms of both chain shortening and H/F exchange. Plausible transformation products were identified based on the following criteria: (*i*) mass tolerance < 5 ppm; (*ii*) isotopic pattern score > 70%; (*iii*) peak area > 10^5; (*iv*) peak area showing increasing or first increase then followed by a decrease trend over time. The limit of quantification (LOQ) of known compounds are 100 nM for PFCAs and PFSAs, and 10 nM for FTCAs.

Quality Assurance and Quality Control (QA/QC). To take into account the matrix effect on the LC-MS/MS quantification of various PFASs investigated in this study, a PFAS-free solution from the photoreactor (i.e., all inorganic chemicals added and treated under the same UV irradiation) was used to prepare the calibration standards. The matrix-match standard series included nine points from 1 nM to 5 µM. MilliQ water and matrix blank controls were included, where no PFASs were detected on LC-MS/MS. MilliQ water blanks were also ran between each group of batch experiment samples and checked for PFASs detection in the blanks, to avoid PFAS carry over. The storage time for all samples was less than three weeks at 4°C.

Table A.3 MRM Transition and LOQ.

Entry	Chemical Name	Chain Length (n)	MRM Transition (m/z)	LOQ (nM)
	$F(CF_2)_n$−COOH (or salt)			
1	Sodium trifluoroacetate	1	113.0/69.0	200
2	Perfluoropropionic acid	2	163.0/119.0	200
3	Perfluorobutyric acid	3	213.0/169.0	100
4	Perfluoropentanoic acid	4	263.0/219.0	25
5	Perfluorohexanoic acid	5	313.0/269.0	2
6	Perfluoroheptanoic acid	6	363.0/319.0	1
7	Perfluorooctanoic acid	7	413.0/369.0	2
8	Perfluorononanoic acid	8	463.0/419.0	1
9	Perfluorodecanoic acid	9	513.0/469.0	2
10	Perfluoroundecanoic acid	10	563.0/519.0	10
	HOOC−$(CF_2)_n$−COOH			
11	Difluoromalonic acid	1	139.0/95.0	200
12	Tetrafluorosuccinic acid	2	189.0/101.0	50
13	Hexafluoroglutaric acid	3	239.0/131.0	5
14	Octafluoroadipic acid	4	289.0/181.0	1
15	Dodecafluorosuberic acid	6	389.0/281.0	20
16	Tetradecafluoroazelaic acid	7	439.0/331.0	50
17	Hexdecafluorosebacic acid	8	489.0/381.0	50
18	Perfluoro-1,10-decanedicarboxylic acid	10	589.0/481.0	1
	$F(CF_2)_n$−CH_2CH_2−COOH			
19	4,4,4-Trifluorobutyric acid	1	141.0/121.0	50
20	2H,2H,3H,3H-Perfluoropentanoic acid	2	191.0/127.0	50
21	2H,2H,3H,3H-Perfluorohexanoic acid	3	241.0/177.0	50
22	2H,2H,3H,3H-Perfluoroheptanoic acid	4	291.0/167.0	20
23	2H,2H,3H,3H-Perfluorooctanoic acid	5	341.0 /237.0	5
24	2H,2H,3H,3H-Perfluorononanoic acid	6	391.0/287.0	5
25	2H,2H,3H,3H-Perfluorodecanoic acid	7	441.0/337.0	2
26	2H,2H,3H,3H-Perfluoroundecanoic acid	8	491.0/387.0	2
	$F(CF_2)_n$−SO_3H (or salt)			
27	Sodium trifluoromethanesulfonate	1	149.0/80.0	1
28	Potassium nonafluorobutanesulfonate	4	299.0/80.0	5
29	Potassium perfluorohexane-1-sulfonate	6	399.0/80.0	1
30	Perfluorooctanesulfonic acid	8	499.0/80.0	2
	Special structures			
31	2,2-difluorosuccinic acid **HOOC−CF_2CH_2−COOH**		153.0/89.0	50

Measurement of Fluoride Ion Release. The concentration of fluoride ion (F^-) released from PFASs was primarily determined by an ion selective electrode (ISE, Fisherbrand accumet solidstate) connected to a Thermo Scientific Orion Versa Star Pro meter. A 2-mL aliquot of reaction sample was added in the equal volume of the total ionic strength adjustment buffer (TISAB for fluoride electrode, Thermo Scientific), and the F^- concentration was determined with the ISE. The accuracy of F^- measurement by the ISE in the solution matrix was validated by the measurement of representative reaction samples using ion chromatography (Figure A.1). A Dionex ICS-5000 ion chromatography system equipped with a conductivity detector and a Dionex IonPac AS11-HC column (4×250 mm) with an AG11-HC guard column (4×50 mm) was used for the ISE validation and the quantification of C2 short-chain PFASs. The samples were diluted for 10 fold with DI water. The column was used at 30°C, with a 20 mM NaOH isocratic eluent at 1.5 mL min^{-1}, and a suppressor current at 75 mA.

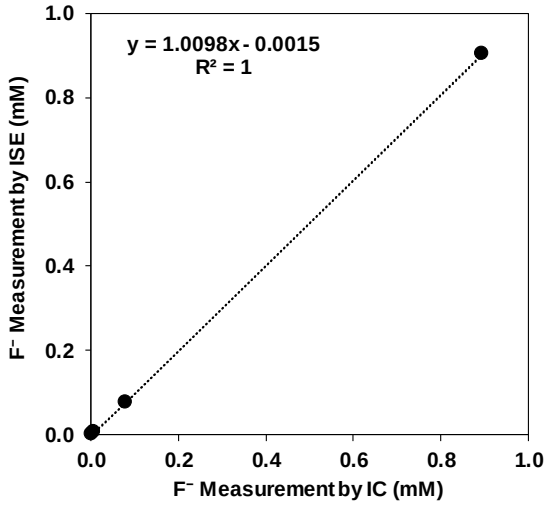

Figure A.1 Fluoride measurement comparison between the ion chromatography (IC) and the fluoride ion-selective electrode (ISE) in samples with the reaction solution matrix.

DFT Calculation of C−F Bond Dissociation Energies (BDEs). The C−F BDEs for all PFASs examined in this study were calculated using the GAUSSIAN 09 software package.[11] All molecular geometries were fully optimized with the Grimme empirical dispersion correction with

the Becke-Johnson damping term (D3-BJ)[12] added to the B3LYP/6-311+G(2d,2p) hybrid functional energies.[13-16] We have specifically chosen this level of theory to allow for a straightforward comparison with previous studies on similar compounds.[17] Truhlar's SMD solvation model was chosen to implicitly simulate the aqueous environment.[18] Harmonic frequency calculations were carried out to confirm that all of the structures were local minima on the potential energy surface. The BDE for each bond was calculated through the following expression:

$$E_{\mathrm{BDE}} = \left(H^{*}_{\text{radical[PFAS minus F]}} + H^{*}_{\text{radical F}}\right) - H^{*}_{\text{parent PFAS}}$$

where H^{*} represents the enthalpy of formation.[17] Calculation results are summarized in Tables A.4−A.8.

Because a detailed defluorination mechanism remains elusive, in this study we still chose to calculate the energy for C−F bond dissociation to investigate a simplified correlation with the rate and extent of defluorination. We point out that since the reactions with e_{aq}^{-} will involve radical structures from the parent PFAS compounds and the release of fluoride ion, neither homolytic (i.e., forming a C radical and an F radical) nor heterolytic dissociation (i.e., forming a C cation and an F anion) of the ideal structures could reflect the exact reactions. However, the C−F BDEs can be used as a predictive descriptor because (1) the calculation results agree well with experimental findings, and (2) it provides a quick tool to predict the susceptibility to defluorination in an engineered treatment system using e_{aq}^{-}.

Tables A.4 to A.21 Referred in the Main Text

Table A.4 Calculated C−F BDEs (kcal mol^{-1}) for Perfluorocarboxylate Anions (PFCAs).

Numbering: $^{2}CF_3–^{1}COO^-$

$^{12}CF_3–^{11}CF_2–^{10}CF_2–^{9}CF_2–^{8}CF_2–^{7}CF_2–^{6}CF_2–^{5}CF_2–^{4}CF_2–^{3}CF_2–^{2}CF_2–^{1}COO^-$

Position	2	3	4	5	6	7	8	9	10	11	12
$CF_3CO_2^-$	116.8										
$C_2F_5CO_2^-$	106.9	119.2									
$C_3F_7CO_2^-$	106.8	110.5	119.2								
$C_4F_9CO_2^-$	106.9	109.0	108.6	118.1							
$C_5F_{11}CO_2^-$	107.2	107.8	107.2	108.4	117.9						
$C_6F_{13}CO_2^-$	107.3	108.8	106.9	107.0	108.4	118.6					
$C_7F_{15}CO_2^-$	107.3	108.1	107.3	107.0	106.8	108.3	117.7				
$C_8F_{17}CO_2^-$	107.3	108.1	107.1	107.1	106.8	106.8	108.3	117.7			
$C_9F_{19}CO_2^-$	107.3	108.0	107.3	107.1	106.9	106.6	106.7	108.3	118.5		
$C_{10}F_{21}CO_2^-$	107.3	108.9	107.3	106.0	106.9	106.8	106.6	106.8	108.1	118.8	
$C_{11}F_{23}CO_2^-$	107.3	107.8	107.3	106.9	106.8	106.7	106.7	106.6	106.8	108.1	117.7

Table A.5 Calculated C−F BDEs (kcal mol^{-1}) for Perfluorodicarboxylate Anions (PFdiCAs).

Numbering:

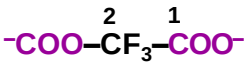

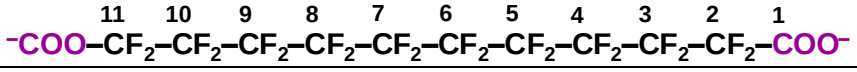

Position	2	3	4	5	6	7	8	9	10	11
$^{-}O_2CCF_2CO_2^{-}$	107.3									
$^{-}O_2CCF_2CH_2CO_2^{-}$	107.5									
$^{-}O_2CC_2F_4CO_2^{-}$	106.7	106.6								
$^{-}O_2CC_3F_6CO_2^{-}$	106.9	110.5	106.9							
$^{-}O_2CC_4F_8CO_2^{-}$	107.5	109.6	109.6	107.5						
$^{-}O_2CC_6F_{12}CO_2^{-}$	107.4	108.4	107.5	107.5	108.4	107.4				
$^{-}O_2CC_7F_{14}CO_2^{-}$	107.4	108.3	107.5	107.3	107.5	108.3	107.4			
$^{-}O_2CC_8F_{16}CO_2^{-}$	107.3	108.5	107.4	107.3	107.3	107.4	108.5	107.3		
$^{-}O_2CC_{10}F_{20}CO_2^{-}$	107.3	107.8	107.3	107.0	107.0	107.0	107.0	107.3	107.8	107.3

Table A.6 Calculated C−F BDEs (kcal mol^{-1}) for Fluorotelomer Carboxylate Anions (FTCAs).

Numbering: $^{4}CF_3–^{3}CH_2^{2}CH_2^{1}COO^-$

$^{11}CF_3–^{10}CF_2–^{9}CF_2–^{8}CF_2–^{7}CF_2–^{6}CF_2–^{5}CF_2–^{4}CF_2–^{3}CH_2^{2}CH_2^{1}COO^-$

Position	4	5	6	7	8	9	10	11
$CF_3CH_2CH_2CO_2^-$	122.68							
$C_2F_5CH_2CH_2CO_2^-$	113.34	120.59						
$C_3F_7CH_2CH_2CO_2^-$	112.18	110.99	118.82					
$C_4F_9CH_2CH_2CO_2^-$	110.91	109.00	109.43	118.10				
$C_5F_{11}CH_2CH_2CO_2^-$	111.02	110.12	107.02	108.48	118.73			
$C_6F_{13}CH_2CH_2CO_2^-$	110.82	108.97	106.71	106.99	108.37	118.56		
$C_7F_{15}CH_2CH_2CO_2^-$	110.76	108.79	107.19	106.79	106.86	108.17	117.76	
$C_8F_{17}CH_2CH_2CO_2^-$	110.72	108.95	107.11	106.89	106.42	106.78	108.09	118.55

Table A.7 Calculated C−F BDEs (kcal mol^{-1}) for Perfluorosulfonate Anions (PFSAs).

Numbering:

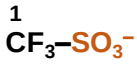

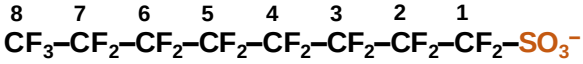

Position	1	2	3	4	5	6	7	8
$CF_3SO_3^-$	119.57							
$C_4F_9SO_3^-$	109.18	106.54	108.85	118.77				
$C_6F_{13}SO_3^-$	109.57	106.38	106.85	106.90	108.41	118.58		
$C_8F_{17}SO_3^-$	112.06	106.73	106.96	106.67	106.67	106.67	108.38	118.80

Table A.8 Calculated C−F BDEs (kcal mol^{-1}) for the Three Fluorinated Acetate Anions.

$CF_3CO_2^-$	116.81
$CF_2HCO_2^-$	109.70
$CFH_2CO_2^-$	108.61

Table A.9 Peak Areas and Quantification of Transformation Products (TPs) from PFDA Degradation.

(**Note:** only the species (*i*) with peak areas above the quantification limit and (*ii*) having standard chemicals are quantified into the molar concentration.)

	PFDA[a]			
Time(h)	**$C_{10}F_{19}O_2^-$**	$C_{10}F_{18}HO_2^-$	$C_{10}F_{17}H_2O_2^-$	$C_{10}F_{16}H_3O_2^-$
0	1.60E+09	1.49E+06	ND	ND
1	1.47E+09	5.08E+07	ND	ND
2	1.11E+09	1.08E+08	3.53E+05	ND
4	6.52E+08	1.90E+08	3.34E+06	ND
8	8.81E+07	1.94E+08	1.11E+07	1.42E+06
12	1.07E+07	1.33E+08	4.70E+06	3.32E+05

	PFNA			**PFOA**	
Time(h)	**$C_9F_{17}O_2^-$**		$C_9F_{16}HO_2^-$	**$C_8F_{15}O_2^-$**	$C_8F_{14}HO_2^-$
0	1.70E+06	<LOQ	ND	1.61E+06	1.11E+05
1	4.81E+07	327 nM	3.48E+05	2.78E+06	9.27E+05
2	5.69E+07	387 nM	1.08E+06	3.51E+06	1.23E+06
4	5.79E+07	394 nM	2.85E+06	3.68E+06	1.72E+06
8	2.32E+07	158 nM	4.48E+06	3.25E+06	8.41E+05
12	1.45E+07	98.4 nM	3.88E+06	3.39E+06	4.45E+05

	PFHpA			**PFHxA**			**PFPeA**		**PFBA**
Time(h)	**$C_7F_{13}O_2^-$**	$C_7F_{12}HO_2^-$	$C_7F_{11}H_2O_2^-$	**$C_6F_{11}O_2^-$**	$C_6F_{10}HO_2^-$	$C_6F_9H_2O_2^-$	**$C_5F_9O_2^-$**	$C_5F_8HO_2^-$	**$C_4F_7O_2^-$**
0	1.90E+05	4.11E+05	ND	7.52E+04	4.28E+05	ND	ND	ND	ND
1	1.95E+06	2.63E+06	ND	8.64E+05	1.80E+06	ND	1.12E+06	4.76E+05	5.36E+05
2	1.85E+06	4.81E+06	2.09E+05	1.70E+06	3.21E+06	7.28E+04	2.15E+06	4.69E+05	7.49E+05
4	1.87E+06	6.77E+06	1.05E+06	2.40E+06	4.22E+06	4.76E+05	3.09E+06	1.20E+06	1.15E+06
8	1.58E+06	2.83E+06	2.97E+06	2.21E+06	1.98E+06	1.45E+06	2.25E+06	6.09E+05	1.11E+06
12	1.47E+06	7.47E+05	3.08E+06	1.72E+06	7.84E+05	1.51E+06	2.15E+06	2.75E+05	7.27E+05

[a]Products with the same chain length are assumed to be H/F exchange derivatives from the corresponding PFCA.

Table A.10 Peak Areas and Quantification of TPs from PFNA Degradation.

	PFNA[a]				**PFOA**		
Time(h)	**$C_9F_{17}O_2^-$**	$C_9F_{16}HO_2^-$	$C_9F_{15}H_2O_2^-$	$C_9F_{14}H_3O_2^-$	**$C_8F_{15}O_2^-$**		$C_8F_{14}HO_2^-$
0	1.31E+09	1.59E+07	0.00E+00	0.00E+00	3.76E+06	<LOQ	0.00E+00
1	7.56E+08	8.91E+07	0.00E+00	0.00E+00	4.10E+07	222 nM	0.00E+00
2	3.83E+08	1.36E+08	0.00E+00	0.00E+00	2.79E+07	151 nM	4.50E+05
4	7.97E+07	1.22E+08	3.47E+06	0.00E+00	1.26E+07	<LOQ	1.05E+06
8	2.19E+06	8.07E+07	4.25E+06	3.19E+05	4.09E+06	<LOQ	5.53E+05
12	7.34E+05	6.90E+07	5.52E+06	4.13E+05	3.34E+06	<LOQ	4.44E+05

	PFHpA			**PFHxA**			**PFPeA**		**PFBA**
Time(h)	**$C_7F_{13}O_2^-$**	$C_7F_{12}HO_2^-$	$C_7F_{11}H_2O_2^-$	**$C_6F_{11}O_2^-$**	$C_6F_{10}HO_2^-$	$C_6F_9H_2O_2^-$	**$C_5F_9O_2^-$**	$C_5F_8HO_2^-$	**$C_4F_7O_2^-$**
0	1.02E+07	2.45E+06	0.00E+00	1.01E+06	1.84E+05	0.00E+00	3.97E+05	0.00E+00	0.00E+00
1	5.01E+06	3.16E+06	0.00E+00	8.04E+05	4.44E+06	1.84E+05	1.25E+06	1.67E+06	1.08E+06
2	2.31E+06	2.33E+06	3.98E+05	5.79E+05	4.50E+06	7.60E+05	1.32E+06	1.81E+06	1.34E+06
4	5.44E+05	1.16E+06	1.03E+06	3.19E+05	1.95E+06	1.77E+06	8.44E+05	7.29E+05	9.78E+05
8	3.24E+05	0.00E+00	1.25E+06	2.00E+05	2.07E+05	2.16E+06	4.96E+05	0.00E+00	5.78E+05
12	8.12E+05	0.00E+00	1.24E+06	1.68E+05	1.60E+05	2.00E+06	4.08E+05	0.00E+00	0.00E+00

[a]Products with the same chain length are assumed to be H/F exchange derivatives from the corresponding PFCA.

Table A.11 Peak Areas and Quantification of TPs from PFOA Degradation.

	PFOA[a]					
Time(h)	**$C_8F_{15}O_2^-$**	$C_8F_{14}HO_2^-$	$C_8F_{13}H_2O_2^-$	$C_8F_{12}H_3O_2^-$	$C_8F_{11}H_4O_2^-$	$C_8F_9H_6O_2^-$
0	2.84E+09	1.19E+06	6.44E+04	ND	5.17E+05	ND
1	1.74E+09	1.34E+08	5.78E+05	ND	6.53E+05	ND
2	8.99E+08	2.26E+08	2.63E+06	ND	8.66E+05	ND
4	1.61E+08	2.42E+08	8.12E+06	ND	1.37E+06	1.03E+05
8	1.09E+07	1.64E+08	1.31E+07	6.84E+05	1.56E+06	3.90E+05
12	4.79E+06	1.25E+08	1.55E+07	6.85E+05	2.16E+06	5.57E+05
24	4.43E+06	7.79E+07	1.84E+07	8.42E+05	2.69E+06	1.01E+06
36	4.83E+06	6.47E+07	3.40E+07	1.89E+06	4.24E+06	1.07E+06
48	4.91E+06	6.34E+07	3.63E+07	2.12E+06	7.55E+06	8.78E+05

	PFHpA				**PFHxA**
Time(h)	**$C_7F_{13}O_2^-$**		$C_7F_{12}HO_2^-$	$C_7F_9H_4O_2^-$	$C_6F_{10}HO_2^-$
0	1.27E+07	<LOQ	ND	ND	ND
1	3.74E+07	265 nM	4.57E+05	ND	9.66E+05
2	2.36E+07	167 nM	1.07E+06	ND	8.01E+05
4	7.44E+06	<LOQ	1.15E+06	ND	6.54E+05
8	2.68E+06	<LOQ	8.86E+05	ND	1.58E+05
12	2.25E+06	<LOQ	7.37E+05	1.01E+06	ND
24	1.88E+06	<LOQ	6.33E+05	9.74E+05	ND
36	3.49E+06	<LOQ	8.45E+05	1.93E+06	ND
48	3.66E+06	<LOQ	1.96E+06	2.71E+06	ND

[a]Products with the same chain length are assumed to be H/F exchange derivatives from the corresponding PFCA.

Table A.12 Peak Areas and Quantification of TPs from PFHpA Degradation.

	PFHpA[a]			
Time (h)	**$C_7F_{13}O_2^-$**	$C_7F_{12}HO_2^-$	$C_7F_{11}H_2O_2^-$	$C_7F_{10}H_3O_2^-$
0	2.63E+09	3.39E+06	ND	ND
1	1.99E+09	2.13E+08	3.66E+05	ND
2	1.33E+09	3.59E+08	8.87E+05	ND
4	4.52E+08	4.32E+08	3.39E+06	9.87E+04
8	2.14E+07	3.45E+08	8.53E+06	1.96E+05
12	8.79E+05	2.86E+08	4.16E+07	8.76E+05
24	2.05E+05	1.57E+08	3.15E+06	1.84E+05
48	1.43E+05	1.26E+08	4.96E+06	2.61E+05

	PFHxA				**PFPeA**	
Time (h)	**$C_6F_{11}O_2^-$**		$C_6F_{10}HO_2^-$	$C_6F_9H_2O_2^-$	**$C_5F_9O_2^-$**	$C_5F_8HO_2^-$
0	3.29E+05	<LOQ	1.11E+07	ND	1.57E+05	ND
1	4.29E+07	250 nM	6.95E+06	2.09E+05	2.62E+05	1.72E+05
2	5.44E+07	317 nM	4.04E+06	4.07E+05	3.41E+05	7.90E+05
4	2.09E+07	122 nM	1.45E+06	6.10E+05	6.09E+05	8.40E+05
8	4.70E+06	<LOQ	1.04E+06	4.80E+05	7.66E+05	2.04E+05
12	4.63E+06	<LOQ	8.88E+05	7.34E+05	6.18E+05	ND
24	3.55E+06	<LOQ	5.62E+05	4.05E+05	3.38E+05	ND
48	7.73E+06	<LOQ	8.00E+05	3.08E+05	6.84E+05	ND

[a]Products with the same chain length are assumed to be H/F exchange derivatives from the corresponding PFCA.

Table A.13 Peak Areas of TPs from PFHxA Degradation.

	PFHxA[a]			**PFPeA**	
Time (h)	**$C_6F_{11}O_2^-$**	$C_6F_{10}HO_2^-$	$C_6F_9H_2O_2^-$	**$C_5F_9O_2^-$**	$C_5F_8HO_2^-$
0	2.65E+09	3.27E+07	1.86E+06	3.76E+06	1.06E+05
1	2.01E+09	1.84E+08	2.20E+06	2.97E+07	1.66E+05
2	1.37E+09	3.06E+08	3.67E+06	1.08E+07	2.49E+05
4	4.42E+08	3.62E+08	3.11E+06	8.90E+06	3.59E+05
8	1.78E+07	2.74E+08	1.35E+07	1.27E+06	4.03E+05
12	1.48E+06	2.31E+08	1.68E+07	1.46E+06	3.69E+05

[a]Products with the same chain length are assumed to be H/F exchange derivatives from the corresponding PFCA.

Table A.14 Peak Areas of C8 Sulfonate TPs from PFOS Degradation.

	PFOS[a]							
Time(h)	**$C_8F_{17}SO_3^-$**	$C_8F_{16}HSO_3^-$	$C_8F_{15}H_2SO_3^-$	$C_8F_{14}H_3SO_3^-$	$C_8F_{13}H_4SO_3^-$	$C_8F_{12}H_5SO_3^-$	$C_8F_{11}H_6SO_3^-$	$C_8F_9H_8SO_3^-$
0	2.05E+09	ND	ND	ND	ND	ND	ND	ND
1	1.64E+09	2.37E+07	ND	ND	ND	ND	ND	ND
2	1.51E+09	1.99E+07	6.93E+05	9.17E+04	ND	ND	ND	ND
4	1.34E+09	4.05E+07	9.66E+05	1.13E+05	1.17E+05	ND	ND	ND
8	1.09E+09	4.79E+07	1.79E+06	9.36E+05	1.07E+05	ND	5.69E+04	5.56E+04
12	8.29E+08	3.25E+07	1.67E+07	2.50E+06	2.58E+07	ND	ND	1.22E+05
24	5.11E+08	1.87E+07	3.17E+06	2.40E+06	1.28E+06	ND	1.42E+05	2.81E+05
36	3.43E+08	1.73E+07	9.15E+07	6.80E+06	1.02E+07	2.49E+05	ND	2.85E+05
48	2.78E+08	1.36E+07	9.63E+06	3.59E+06	3.68E+06	3.15E+05	1.53E+05	2.70E+05

	PFOS						
Time(h)	$C_8F_8H_9SO_3^-$	$C_8F_7H_{10}SO_3^-$	$C_8F_6H_{11}SO_3^-$	$C_8F_5H_{12}SO_3^-$	$C_8F_4H_{13}SO_3^-$	$C_8F_3H_{14}SO_3^-$	$C_8FH_{16}SO_3^-$
0	ND	ND	ND	ND	ND	ND	ND
1	ND	ND	ND	ND	ND	ND	1.48E+05
2	ND	ND	ND	ND	ND	ND	1.70E+05
4	ND	ND	ND	ND	ND	ND	ND
8	ND	ND	ND	ND	6.77E+04	ND	ND
12	ND	ND	ND	ND	1.27E+05	ND	ND
24	1.43E+05	6.19E+04	8.67E+04	ND	1.38E+05	ND	1.66E+05
36	1.54E+05	5.72E+04	1.63E+05	4.74E+04	1.38E+05	ND	ND
48	1.42E+05	ND	ND	ND	1.13E+05	8.62E+04	ND

[a]Products with the same chain length are assumed to be H/F exchange derivatives from the corresponding PFSA.

Table A.15 Peak Areas and Quantification of C7, C6, and C4 Sulfonate TPs from PFOS Degradation.

	PFHpS[a]				
Time(h)	**$C_7F_{15}SO_3^-$**	$C_7F_{14}HSO_3^-$	$C_7F_{13}H_2SO_3^-$	$C_7F_{12}H_3SO_3^-$	$C_7F_{11}H_4SO_3^-$
0	2.84E+08	ND	ND	ND	ND
1	2.37E+08	4.77E+05	ND	ND	ND
2	2.12E+08	9.13E+05	ND	ND	ND
4	1.94E+08	1.34E+06	ND	ND	ND
8	1.53E+08	1.84E+06	1.31E+05	ND	ND
12	1.30E+08	1.65E+06	9.10E+05	ND	ND
24	7.93E+07	1.22E+06	3.10E+05	ND	ND
36	6.71E+07	1.35E+06	5.34E+06	1.33E+05	1.02E+05
48	5.73E+07	1.56E+06	9.16E+05	ND	ND

	PFHxS				PFBS		
Time(h)	**$C_6F_{13}SO_3^-$**		$C_6F_{12}HSO_3^-$	$C_6F_{11}H_2SO_3^-$	**$C_4F_9SO_3^-$**	$C_4F_8HSO_3^-$[b]	$C_4F_7H_2SO_3^-$
0	4.50E+07	335 nM	ND	2.72E+05	1.08E+07	1.83E+05	ND
1	1.74E+07	130 nM	2.18E+06	ND	1.05E+07	8.33E+06	ND
2	2.13E+07	158 nM	7.23E+06	ND	1.04E+07	2.12E+07	ND
4	1.63E+07	121 nM	1.45E+07	ND	1.03E+07	4.38E+07	ND
8	1.38E+07	102 nM	2.47E+07	ND	1.01E+07	8.15E+07	ND
12	1.22E+07	<LOQ	3.14E+07	1.59E+05	1.04E+07	1.03E+08	ND
24	9.60E+06	<LOQ	3.76E+07	ND	9.81E+06	1.32E+08	ND
36	8.48E+06	<LOQ	3.23E+07	4.40E+05	9.36E+06	1.37E+08	2.48E+05
48	7.60E+06	<LOQ	3.90E+07	2.50E+05	9.44E+06	1.43E+08	2.25E+05

[a]The C7 PFSA (PFHpS), C6 PFSA (PFHxS) and C4 PFSA (PFBS) in the PFOS reagent have significant peak areas in the t=0 sample, and are thus believed to be impurities from PFOS production. Degradation products with the same chain length are assumed to be H/F exchange derivatives from the corresponding PFSA.

[b]The large peak areas of products with one H/F exchange at 48 h is higher than the perfluorinated sulfonate in the same chain length, probably indicating other mechanisms of formation from longer-chain precursors.

Table A.16 Peak Areas of Carboxylate TPs from PFOS Degradation.

	PFOA[a]		**PFHpA**[b]		**PFHxA**[b]		**PFPeA**[b]		**PFBA**[b]
Time(h)	$\mathbf{C_8F_{15}O_2^-}$	$C_8F_{14}HO_2^-$	$\mathbf{C_7F_{13}O_2^-}$	$C_7F_{12}HO_2^-$	$\mathbf{C_6F_{11}O_2^-}$	$C_6F_{10}HO_2^-$	$\mathbf{C_5F_9O_2^-}$	$C_5F_8HO_2^-$	$\mathbf{C_4F_7O_2^-}$
0	1.79E+06	ND	7.75E+04	ND	ND	ND	ND	ND	ND
1	1.77E+06	6.92E+04	1.61E+06	ND	5.83E+05	ND	1.60E+06	ND	1.89E+06
2	1.57E+06	1.95E+05	3.28E+06	ND	1.37E+06	ND	3.35E+06	ND	4.03E+06
4	1.23E+06	3.81E+05	3.76E+06	3.81E+05	1.96E+06	1.78E+05	4.17E+06	3.74E+05	5.26E+06
8	6.81E+05	4.77E+05	2.14E+06	8.77E+05	1.30E+06	4.91E+05	2.70E+06	8.50E+05	3.68E+06
12	5.82E+05	5.19E+05	1.56E+06	9.65E+05	1.25E+06	5.47E+05	2.10E+06	9.65E+05	2.70E+06
24	2.73E+05	2.73E+05	6.46E+05	5.33E+05	4.42E+05	4.92E+05	1.24E+06	6.41E+05	1.64E+06
36	1.79E+05	2.16E+05	3.27E+05	3.71E+05	2.24E+05	2.60E+05	8.06E+05	4.75E+05	7.51E+05
48	1.82E+05	2.01E+05	3.82E+05	3.14E+05	3.19E+05	3.12E+05	8.75E+05	4.10E+05	4.82E+05

[a]Products with the same chain length are assumed to be H/F exchange derivatives from the corresponding PFCA.
[b]The ratios of shorter-chain PFCAs to PFOA in this table are much higher than the ratios observed in PFCA degradation reactions (Tables A.9-A.13). This indicates that a significant portion of the shorter-chain PFCAs are from the degradation of shorter-chain PFSA impurities in the PFOS reagent (e.g., PFHpS, PFHxS, and PFBS; see Table A.15).

Table A.17 Peak Areas of C6 Sulfonate TPs from PFHxS Degradation.

	PFHxS[a]					
Time(h)	**$C_6F_{13}SO_3^-$**	$C_6F_{12}HSO_3^-$	$C_6F_{11}H_2SO_3^-$	$C_6F_{10}H_3SO_3^-$	$C_6F_9H_4SO_3^-$	$C_6F_6H_7SO_3^-$
0	4.45E+09	ND	ND	ND	ND	ND
1	3.29E+09	5.84E+06	ND	ND	ND	ND
2	3.22E+09	1.25E+07	1.38E+06	ND	1.00E+05	ND
4	3.31E+09	2.43E+07	3.24E+06	ND	1.53E+05	ND
8	2.93E+09	4.36E+07	3.05E+07	8.48E+04	1.65E+05	3.85E+05
12	2.97E+09	4.90E+07	5.20E+07	3.43E+05	1.54E+05	3.99E+05
24	2.69E+09	5.82E+07	8.90E+07	8.30E+05	1.83E+05	4.48E+05
36	2.75E+09	6.10E+07	1.22E+08	1.19E+06	2.39E+05	4.24E+05
48	2.72E+09	5.74E+07	8.50E+07	1.19E+06	ND	5.85E+05

[a]Products with the same chain length are assumed to be H/F exchange derivatives from the corresponding PFSA.

Table A.18 Peak Areas of C5, C4, and C3 Sulfonate TPs from PFHxS Degradation.

	PFPeS[a]		**PFBS**		**PFPrS**
Time(h)	**$C_5F_{11}SO_3^-$**	$C_5F_{10}HSO_3^-$	**$C_4F_9SO_3^-$**	$C_4F_8HSO_3^-$[b]	$C_3F_6HSO_3^-$
0	2.20E+07	ND	1.18E+07	0.00E+00	0.00E+00
1	2.09E+07	ND	1.12E+07	1.47E+06	7.72E+05
2	2.03E+07	ND	1.10E+07	3.28E+06	2.72E+06
4	2.13E+07	ND	1.20E+07	1.50E+07	4.08E+06
8	1.90E+07	2.05E+05	1.13E+07	1.44E+07	9.08E+06
12	1.99E+07	4.12E+05	1.19E+07	2.13E+07	2.42E+07
24	1.64E+07	5.01E+05	1.09E+07	2.99E+07	2.07E+07
36	1.85E+07	6.09E+05	1.17E+07	3.51E+07	4.12E+07
48	1.72E+07	6.71E+05	1.14E+07	4.83E+07	2.37E+07

[a]Products with the same chain length are assumed to be H/F exchange derivatives from the corresponding PFSA.

[b]The peak areas of products with one H/F exchange at 48 h are higher than the perfluorinated sulfonate in the same chain length, probably indicating other mechanisms of formation from longer-chain precursors.

Table A.19 Peak Areas of Carboxylate TPs from PFHxS Degradation.

	PFHxA[a]			**PFPeA**[b]		**PFBA**[b]
Time(h)	**$C_6F_{11}O_2^-$**	$C_6F_{10}HO_2^-$	$C_6F_9H_2O_2^-$	**$C_5F_9O_2^-$**	$C_5F_8HO_2^-$	**$C_4F_7O_2^-$**
0	1.32E+05	3.63E+05	ND	ND	ND	ND
1	2.04E+06	1.83E+05	ND	2.16E+06	ND	ND
2	2.68E+06	3.98E+05	ND	4.24E+06	ND	3.54E+05
4	3.09E+06	1.01E+06	ND	5.51E+06	3.07E+05	5.65E+05
8	2.26E+06	1.67E+06	7.49E+04	3.58E+06	6.88E+05	5.95E+05
12	2.00E+06	2.05E+06	1.12E+05	3.24E+06	9.48E+05	8.58E+05
24	1.84E+06	2.17E+06	2.31E+05	2.55E+06	9.50E+05	3.64E+05
36	2.01E+06	2.58E+06	3.30E+05	2.43E+06	9.58E+05	3.15E+05
48	2.23E+06	2.32E+06	2.75E+05	2.97E+06	9.38E+05	3.51E+05

[a]Products with the same chain length are assumed to be H/F exchange derivatives from the corresponding PFCA.

[b]The ratios of shorter-chain PFCAs to PFOA in this table are much higher than the ratios observed in PFCA degradation reactions (Tables A.9-A.13). This indicates that a significant portion of the shorter-chain PFCAs are from the degradation of shorter-chain PFSA impurities in the PFHxS reagent (e.g., PFPeS and PFBS; see Table A.18).

Table A.20 Peak Areas and Quantification of Telomeric Carboxylate TPs from n=8 FTCA Degradation.

	n=8 FTCA ($C_8F_{17}CH_2CH_2COO^-$)[a]			**n=6 FTCA[b]**		
Time (h)	**$C_{11}F_{17}H_4O_2^-$**	$C_{11}F_{16}H_5O_2^-$	$C_{11}F_{15}H_6O_2^-$	**$C_9F_{13}H_4O_2^-$**		$C_9F_{12}H_5O_2^-$
0	7.99E+08	ND	ND	ND	<LOQ	ND
1	7.91E+08	1.93E+06	ND	ND	<LOQ	9.51E+04
2	7.37E+08	4.22E+06	1.54E+05	1.04E+05	<LOQ	2.48E+05
4	7.92E+08	7.93E+06	7.71E+05	1.96E+05	<LOQ	9.04E+05
8	6.42E+08	5.46E+06	1.32E+06	4.28E+05	10.5 nM	2.27E+06
12	5.75E+08	5.42E+06	2.86E+06	5.94E+05	14.6 nM	2.97E+06
24	4.40E+08	3.71E+06	2.92E+06	7.68E+05	18.9 nM	4.58E+06
36	2.61E+08	4.46E+06	1.37E+07	8.96E+05	22.0 nM	3.17E+06
48	2.42E+08	4.03E+06	1.03E+07	9.31E+05	22.9 nM	4.63E+06

	n=5 FTCA[b]	**n=5 FTCA[b]**	**n=4 FTCA**
Time (h)	**$C_8F_{11}H_4O_2^-$**	**$C_8F_{11}H_4O_2^-$**	$C_7F_8H_5O_2^-$
0	ND	ND	ND
1	ND	ND	2.73E+05
2	ND	ND	6.19E+05
4	8.84E+04	8.84E+04	1.50E+06
8	1.55E+05	1.55E+05	3.01E+06
12	2.23E+05	2.23E+05	4.37E+06
24	3.67E+05	3.67E+05	6.65E+06
36	3.74E+05	3.74E+05	7.47E+06
48	4.09E+05	4.09E+05	8.49E+06

[a]Products with the same chain length and containing more than 5 hydrogens are assumed to be H/F exchange derivatives from the corresponding FTCA. Note that perfluorinated carboxylates did not yield detectable products with more than 4 H/F exchanges.
[b]Unlike shorter-chain PFSAs in PFOS and PFHxS degradation samples, these shorter-chain FTCAs are not impurities in the $n = 8$ FTCA reagent because they were not detected in the $t = 0$ sample.

Table A.21 Peak Areas and Quantification of Carboxylate TPs from n=8 FTCA Degradation.

	PFOA[a]	**PFHpA**	**PFHxA**	**PFPeA**	**PFBA**
Time(h)	**$C_8F_{15}O_2^-$**	**$C_7F_{13}O_2^-$**	**$C_6F_{11}O_2^-$**	**$C_5F_9O_2^-$**	**$C_4F_7O_2^-$**
0	1.71E+05	ND	ND	ND	ND
1	ND	ND	ND	ND	6.60E+05
2	1.54E+05	ND	ND	ND	1.40E+06
4	1.84E+05	ND	ND	1.24E+05	2.23E+06
8	1.98E+05	ND	ND	1.30E+05	1.96E+06
12	2.17E+05	ND	ND	9.90E+04	1.58E+06
24	2.31E+05	6.09E+04	ND	1.05E+05	9.88E+05
36	4.23E+05	1.05E+05	7.68E+04	8.23E+04	7.17E+05
48	5.54E+05	1.84E+05	1.78E+05	1.48E+05	6.54E+05

[a]Products with H/F exchanges from perfluorinated carboxylates were not detected.

Figures A.2 to A.5 Referred in the Main Text

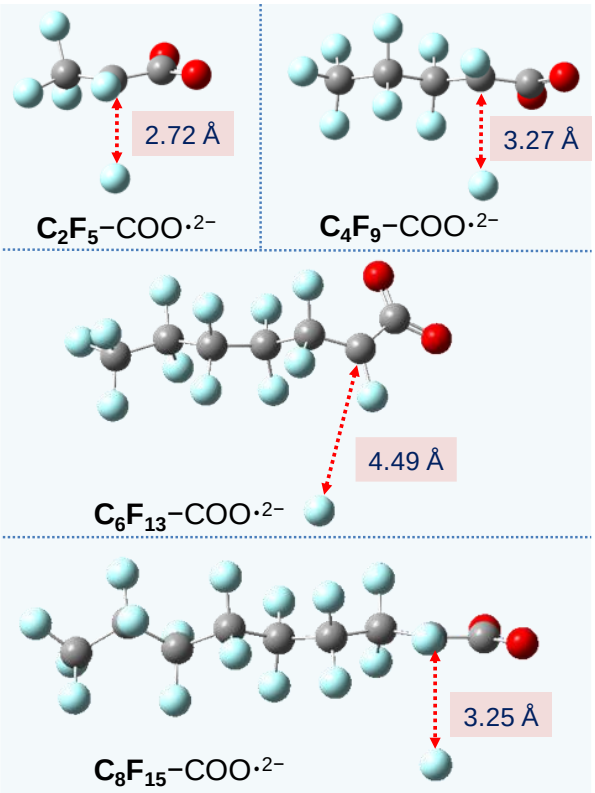

Figure A.2 Geometry-optimized structure of n = 2, 4, 6, and 8 PFCA$^{\bullet 2-}$ at the B3LYP-D3(BJ)/6-311+G(2d,2p) level of theory.

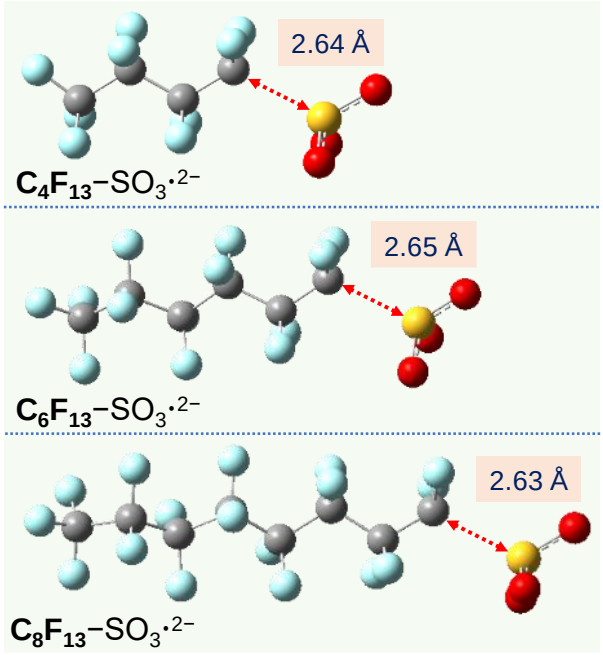

Figure A.3 Geometry-optimized structure of n = 4, 6, and 8 $PFSA^{\bullet 2-}$ at the B3LYP-D3(BJ)/6-311+G(2d,2p) level of theory.

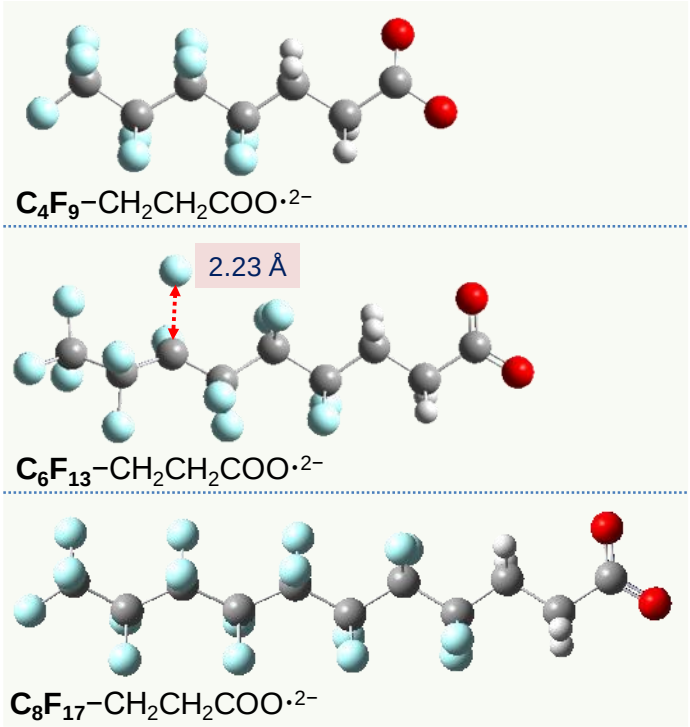

Figure A.4 Geometry-optimized structure of n = 4, 6, and 8 FTCA$^{\bullet 2-}$ at the B3LYP-D3(BJ)/6-311+G(2d,2p) level of theory.

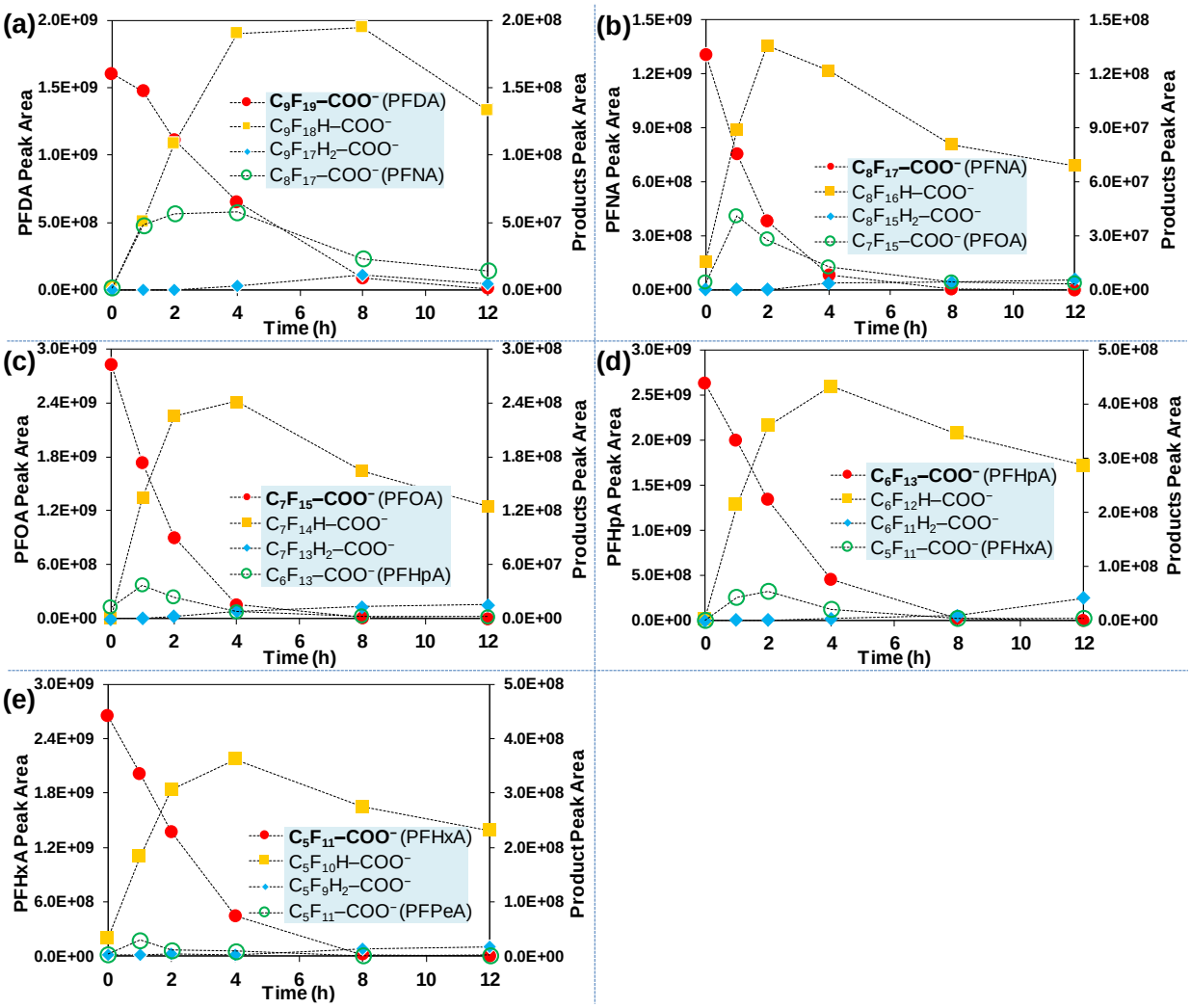

Figure A.5 Representative degradation products from (a) PFDA, (b) PFNA, (c) PFOA, (d) PFHpA, and (e) PFHxA. All detected species including those in low intensities are summarized in Tables A9−A21.

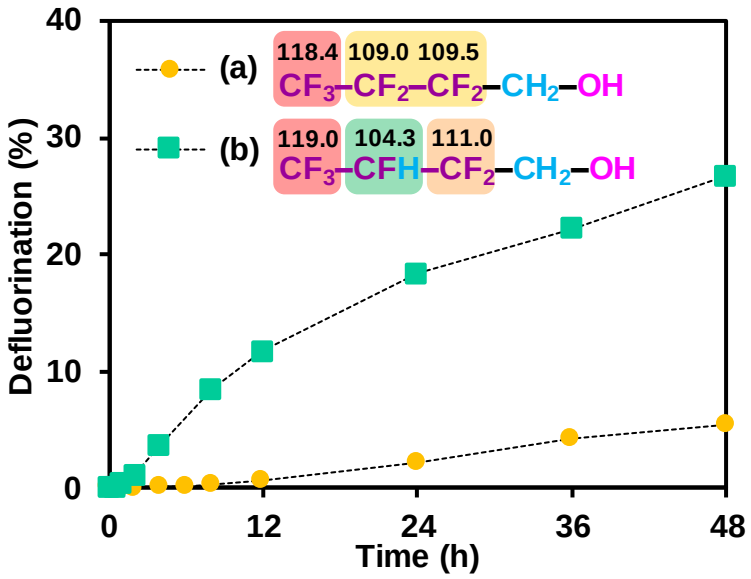

Figure A.6 Time profiles for the defluorination of two probing fluorinated alcohols. *Reaction conditions*: PFAS (0.025 mM), Na_2SO_3 (10 mM), carbonate buffer (5 mM), 254 nm irradiation (18 W low-pressure Hg lamp for 600 mL solutions), pH 9.5 and 20 °C. Numbers on the top of each molecule show the calculated C–F BDEs (kcal mol^{-1}) at the B3LYP-D3(BJ)/6-311+G(2d,2p) level of theory.

Text A.1 Referred in the Main Text

Text A.1 In general, the C−F BDE for −CH*F*− is lower than that of –CF_2–, whereas the C−F BDE for –CF_2−CH_2– is higher than that of –CF_2−CF_2–.

For the former case, the increasing number of F atoms on the same (geminal) C atom will increase the positive partial charge on the C atom. This would increase the ionic character of the C−F bond, leading to an elevated BDE.[19] This theory is supported by comparing C−F BDEs among CF_4, CF_3H, CF_2H_2, and CFH_3,[19] and between CF_3CF_3 and CH_3CH_2F.[20]

For the latter case, the fluorocarbon group −CF_2– or –CF_3 is a strong electron-withdrawing group to weaken the C−F bonds on the neighboring –CF_2− group. The hydrocarbon group does not have such an effect to weaken the C−F bonds on the neighboring –CF_2− group. This theory is supported by the calculated C−F BDEs of PFCAs and FTCAs in this study. More examples can be found from Liu *et al.*[17] where a variety of branched PFASs structures were calculated.

We examined two polyfluorinated alcohols (Figure A.6) as the probe compounds. The structure (**structure b**) with −CH*F*− in the middle of the fluorocarbon chain indeed showed (*i*) lower C−F BDE and (*ii*) much faster defluorination in comparison to the one with –CF_2− in the middle of the fluorocarbon chain (**structure a**).

REFERENCES

(1) Li, X.; Ma, J.; Liu, G.; Fang, J.; Yue, S.; Guan, Y.; Chen, L.; Liu, X., Efficient reductive dechlorination of monochloroacetic acid by sulfite/UV process. *Environ. Sci. Technol.* **2012,** *46*, (13), 7342-7349.

(2) Srivastava, R. K.; Jozewicz, W., Flue gas desulfurization: the state of the art. *J. Air Waste Manag. Assoc.* **2001,** *51*, (12), 1676-1688.

(3) Gu, Y.; Dong, W.; Luo, C.; Liu, T., Efficient reductive decomposition of perfluorooctanesulfonate in a high photon flux UV/sulfite system. *Environ. Sci. Technol.* **2016,** *50*, (19), 10554-10561.

(4) Gu, Y.; Liu, T.; Zhang, Q.; Dong, W., Efficient decomposition of perfluorooctanoic acid by a high photon flux UV/sulfite process: Kinetics and associated toxicity. *Chem. Eng. J.* **2017,** *326*, 1125-1133.

(5) Qu, Y.; Zhang, C.; Li, F.; Chen, J.; Zhou, Q., Photo-reductive defluorination of perfluorooctanoic acid in water. *Water Res.* **2010,** *44*, (9), 2939-2947.

(6) Song, Z.; Tang, H.; Wang, N.; Zhu, L., Reductive defluorination of perfluorooctanoic acid by hydrated electrons in a sulfite-mediated UV photochemical system. *J. Hazard. Mater.* **2013,** *262*, 332-338.

(7) Sun, Z.; Zhang, C.; Xing, L.; Zhou, Q.; Dong, W.; Hoffmann, M. R., UV/Nitrilotriacetic Acid Process as a Novel Strategy for Efficient Photoreductive Degradation of Perfluorooctanesulfonate. *Environ. Sci. Technol.* **2018,** *52*, (5), 2953-2962.

(8) Park, H.; Vecitis, C. D.; Cheng, J.; Choi, W.; Mader, B. T.; Hoffmann, M. R., Reductive defluorination of aqueous perfluorinated alkyl surfactants: effects of ionic headgroup and chain length. *J. Phys. Chem. A.* **2009,** *113*, (4), 690-696.

(9) Yu, Y.; Han, P.; Zhou, L.-J.; Li, Z.; Wagner, M.; Men, Y., Ammonia monooxygenase-mediated cometabolic biotransformation and hydroxylamine-mediated abiotic transformation of micropollutants in an AOB/NOB coculture. *Environ. Sci. Technol.* **2018,** *52*, (16), 9196-9205.

(10) Men, Y.; Han, P.; Helbling, D. E.; Jehmlich, N.; Herbold, C.; Gulde, R.; Onnis-Hayden, A.; Gu, A. Z.; Johnson, D. R.; Wagner, M.; Fenner, K., Biotransformation of two pharmaceuticals by the ammonia-oxidizing archaeon *Nitrososphaera gargensis*. *Environ. Sci. Technol.* **2016,** *50*, (9), 4682-4692.

(11) Frisch, M. J.; Trucks, G. W.; Schlegel, H. B.; Scuseria, G. E.; Robb, M. A.; Cheeseman, J. R.; Scalmani, G.; Barone, V.; Petersson, G. A.; Nakatsuji, H.; Li, X.; Caricato, M.; Marenich, A. V.; Bloino, J.; Janesko, B. G.; Gomperts, R.; Mennucci, B.; Hratchian, H. P.; Ortiz, J. V.; Izmaylov, A. F.; Sonnenberg, J. L.; Williams; Ding, F.; Lipparini, F.; Egidi, F.; Goings, J.; Peng, B.; Petrone, A.; Henderson, T.; Ranasinghe, D.; Zakrzewski, V. G.; Gao, J.; Rega, N.; Zheng, G.; Liang, W.; Hada, M.; Ehara, M.; Toyota, K.; Fukuda, R.; Hasegawa, J.; Ishida, M.; Nakajima, T.; Honda, Y.; Kitao, O.; Nakai, H.; Vreven, T.; Throssell, K.; Montgomery Jr., J. A.; Peralta, J. E.; Ogliaro, F.; Bearpark, M. J.; Heyd, J. J.; Brothers, E. N.; Kudin, K. N.; Staroverov, V. N.; Keith, T. A.; Kobayashi, R.; Normand, J.; Raghavachari, K.; Rendell, A. P.; Burant, J. C.; Iyengar, S. S.; Tomasi, J.; Cossi, M.; Millam, J. M.; Klene, M.; Adamo, C.; Cammi, R.; Ochterski, J. W.; Martin, R. L.; Morokuma, K.; Farkas, O.; Foresman, J. B.; Fox, D. J. *Gaussian 16 Rev. B.01*, Wallingford, CT, 2016.

(12) Grimme, S.; Ehrlich, S.; Goerigk, L., Effect of the damping function in dispersion corrected density functional theory. *J. Comput. Chem.* **2011,** *32*, (7), 1456-1465.

(13) Becke, A. D., Density-functional thermochemistry. III. The role of exact exchange. *J. Chem. Phys.* **1993,** *98*, (7), 5648-5652.

(14) Lee, C.; Yang, W.; Parr, R. G., Development of the Colle-Salvetti correlation-energy formula into a functional of the electron density. *Phys. Rev. B.* **1988,** *37*, (2), 785.

(15) Stephens, P.; Devlin, F.; Chabalowski, C.; Frisch, M. J., Ab initio calculation of vibrational absorption and circular dichroism spectra using density functional force fields. *J. Phys. Chem.* **1994,** *98*, (45), 11623-11627.

(16) Vosko, S. H.; Wilk, L.; Nusair, M., Accurate spin-dependent electron liquid correlation energies for local spin density calculations: a critical analysis. *Can. J. Phys.* **1980,** *58*, (8), 1200-1211.

(17) Liu, J.; Van Hoomissen, D. J.; Liu, T.; Maizel, A.; Huo, X.; Fernández, S. R.; Ren, C.; Xiao, X.; Fang, Y.; Schaefer, C. E., Reductive defluorination of branched per-and polyfluoroalkyl substances with cobalt complex catalysts. *Environ. Sci. Technol. Lett.* **2018,** *5*, (5), 289-294.

(18) Marenich, A. V.; Cramer, C. J.; Truhlar, D. G., Universal solvation model based on solute electron density and on a continuum model of the solvent defined by the bulk dielectric constant and atomic surface tensions. *J. Phys. Chem. B* **2009,** *113*, (18), 6378-6396.

(19) Lemal, D. M., Perspective on fluorocarbon chemistry. *J. Org. Chem.* **2004,** *69*, (1), 1-11.

(20) Krafft, M. P.; Riess, J. G., Selected physicochemical aspects of poly-and perfluoroalkylated substances relevant to performance, environment and sustainability—Part one. *Chemosphere.* **2015,** *129*, 4-19.

APPENDIX B: APPENDICES FOR CHAPTER 3

Detailed Information on Materials and Methods

Chemicals and Preparation of PFAS Stock Solutions. All PFAS chemicals were purchased from Alfa-Aesar, Fluoryx Labs, Oakwood Chemicals, and SynQuest Laboratories. Table B.1 summarizes the name, purity, and CAS number of all PFECAs included in this study. All other chemicals and solvents were purchased from Fisher Chemical. Individual PFECAs were dissolved in either deionized (DI, produced by Milli-Q system) water or methanol as 10 mM stock solutions. For acid compounds in water solvent, the addition of 20 mM NaOH effectively facilitated the dissolution of long chain structures and prevented the volatilization of short chain structures. For long chain PFECAs that did not readily dissolve in water, methanol was used as the solvent. Methanol does not interfere with the PFAS defluorination with hydrated electrons. For example, preliminary experiments with 25 μM HFPO-DA introduced with the water stock solution (1.5 mL into 600 mL final volume) and with the methanol stock solution (1.5 mL into 600 mL final volume, resulting in ~62 mM methanol in water) gave the same rate and extent of defluorination. All PFECA stock solutions were wrapped in Parafilm and stored at room temperature (20°C).

Table B.1 Information of PFECAs Used in This Study.

Entry	Chemical Name	*n*	Purity	CAS#
	CF_3CF_2–[CF_2–O–$CF(CF_3)$]$_n$–COOH			
A1	Perfluoro(2-methyl-3-oxahexanoic) acid	1	97%	13252-13-6
A2	Perfluoro(2,5-dimethyl-3,6-dioxanonanoic) acid	2	95%	13252-14-7
A3	Perfluoro(2,5,8-trimethyl-3,6,9-trioxadodecanoic) acid	3	97%	65294-16-8
	CF_3O–[CF_2]$_n$–COOH (or salt)			
B1	Perfluoro(2-methoxyacetate) sodium salt	1	98%	21837-98-9
B2	Perfluoro(3-methoxypropanoic) acid	2	98%	377-73-1
B3	Perfluoro(4-methoxybutanoic) acid	3	–	863090-89-5
	CF_3O–[CF_2CF_2O]$_n$–CF_2–COOH			
C1	Perfluoro(3,6-dioxaheptanoic) acid	1	98%	151772-58-6
C2	Perfluoro(3,6,9-trioxadecanoic) acid	2	98%	151772-59-7
	$CF_3CF_2CF_2CF_2O$–[CF_2CF_2O]$_n$–CF_2–COOH			
D1	Perfluoro(3,6-dioxadecanoic) acid	1	97%	137780-69-9
D2	Perfluoro(3,6,9-trioxatridecanoic) acid	2	98%	330562-41-9
	Special structures			
–	Trifluoropyruvic acid **CF_3–CO–COOH**	–	97%	1081801-99-1
–	2-(trifluoromethoxy)acetic acid **CF_3O–CH_2–COOH**	–	97%	69105-00-6

Measurement of PFAS Parent Compound Decay and Transformation Products.

Quantification of PFAS Parent Compounds. The concentrations of PFAS parent compounds were measured by a high-performance liquid chromatography–triple quadrupole mass spectrometry system (HPLC−MS/MS, Agilent 1200 HPLC, and Sciex 5500 QTRAP MS) as previously described,[1] but with a slight modification. Briefly, a 1-μL sample was loaded onto a Zorbax SB-Aq column (particle size 5μm, 4.6×50 mm, Agilent) and eluted with 350 μL min^{-1} of 10 mM ammonia formate (A) and methanol (B), at a linear gradient as follows: 100% A for 0−1 min, 2% A for 2−15 min, and 100% A for 16−21 min. The mass spectra were obtained from a negative ionization mode. The ion spray voltage was set to −4500 V, the source temperature was set to 450°C, and the curtain gas, ion source gas 1, and ion source gas 2 were 30, 50, and 60, respectively. Multiple reaction monitoring (MRM) was used for quantification, and the MRM transition was listed in Table A2. The limit of quantification (LOQ) for each compound was determined as the lowest concentration with a detection variation <20% (Table B.2).

Transformation Products Identification. To identify the transformation products, samples were first analyzed by liquid chromatography coupled to a high-resolution quadrupole orbitrap mass spectrometer (LC-HRMS/MS) (Q Exactive, Thermo Fisher Scientific). As described in our previous study,[1] the transformation products were detected in full scan negative ionization mode on HRMS at a resolution of 70,000 at m/z 200 and a scan range of m/z 50−750. The software Xcalibur (Thermo Fisher Scientific) was used for data acquisition and analysis. Suspect screening was carried out to identify the transformation products of selected PFASs, which was conducted on software TraceFinder 4.1 EFS (Thermo Fisher Scientific). The transformation product suspect lists were compiled using an automatic product mass prediction script, which considered all possible reactions including both chain shortening and H/F exchange. Plausible transformation products were identified based on the following criteria: (*i*) mass accuracy tolerance < 5 ppm; (*ii*)

isotopic pattern score > 70%; (*iii*) peak area > 10^5; (iv) peak area showing an increasing trend over time, or a first increase then followed by a decrease. For the identified transformation products with the reference compounds available, their concentrations were further determined by the liquid chromatography–triple quadrupole mass spectrometer (HPLC−MS/MS) as above described.

Table B.2 MRM Transition and LOQ.

Entry	Chemical Name	*n*	MRM Transition (m/z)	LOQ (nM)
	CF_3CF_2−[CF_2−O−$CF(CF_3)$]$_n$−COOH			
A1	Perfluoro(2-methyl-3-oxahexanoic) acid	1	329.0/185.0	1
A2	Perfluoro(2,5-dimethyl-3,6-dioxanonanoic) acid	2	495.0/185.0	1
A3	Perfluoro(2,5,8-trimethyl-3,6,9-trioxadodecanoic) acid	3	661.0/185.0	25
	CF_3O−[CF_2]$_n$−COOH (or salt)			
B2	Perfluoro(3-methoxypropanoic) acid	2	229.0/85.0	25
B3	Perfluoro(4-methoxybutanoic) acid	3	279.0/85.0	0.1
	CF_3O−[CF_2CF_2O]$_n$−CF_2−COOH			
C1	Perfluoro(3,6-dioxaheptanoic) acid	1	295.0/135.0	25
C2	Perfluoro(3,6,9-trioxadecanoic) acid	2	411.0/317.0	2
	$CF_3CF_2CF_2CF_2O$−[CF_2CF_2O]$_n$−CF_2−COOH			
D1	Perfluoro(3,6-dioxadecanoic) acid	1	445.0/169.0	2
D2	Perfluoro(3,6,9-trioxatridecanoic) acid	2	561.0/467.0	2

Ion Chromatography Analysis of Small Parent Compounds and Transformation Products. Analysis was performed using a Dionex ICS-5000 ion chromatography system equipped with a conductivity detector and suppressor (AERS 4 mm). Ion separation was executed with an IonPac AS11-HC analytical column (4 × 250 mm) in line with an AG11-HC guard column (4 × 50 mm). The column temperature was maintained at 30°C. The isocratic NaOH mobile phase was provided by a Dionex ICS-6000 EG eluent generator. Specific methods for each target analyte are below:

- Perfluoro(2-methoxy)acetate (***B1***) and oxalate: 20 mM NaOH, 1.0 mL min^{-1};
- 2-(Trifluoromethoxy)acetate ($CF_3{-}O{-}CH_2{-}COOH$): 10 mM NaOH, 1.0 mL min^{-1};
- Trifluoropyruvate (TFPy): 20 mM NaOH, 1.5 mL min^{-1} / 15 mM NaOH, 1.0 mL min^{-1};
- Trifluoroacetic acid (TFA): 10 mM NaOH, 1.0 mL min^{-1}.

Tables B.3 to B.11 Referred in the Main Text

Table B.3 Concentrations and Peak Areas of the Parent Compound and Transformation Product (TP) Suspects from Perfluoro(2-methyl-3-oxahexanoate) [*A1*, HPFO-DA] Degradation.

	HPFO-DA (*A1*)[a]			
Time(h)	[b,c]**$C_6F_{11}O_3^-$**		[c]$C_6F_{10}HO_3^-$	[c]$C_5F_7H_2O_3^-$
0	25.0	1.03E+07	ND	*ND*
1	23.4	9.67E+06	5.34E+05	*ND*
2	20.3	8.32E+06	1.51E+06	*ND*
4	7.2	5.80E+06	3.54E+06	*ND*
8	6.3	2.62E+06	5.36E+06	*ND*
12	3.5	1.44E+06	5.71E+06	*ND*
24	1.2	4.59E+05	5.38E+06	*ND*
48	0.4	1.73E+05	4.02E+06	*ND*

[a]Products with the same chain length are assumed to be H/F and H/CF_3 exchange derivatives from the corresponding branched PFECA.
[b]Quantified by LC-MS/MS with standards (in μM).
[c]Observed by HRMS analysis without standards for quantification (in peak area).

Table B.4 Concentrations and Peak Areas of the Parent Compound and TP Suspects from Perfluoro(2,5-dimethyl-3,6-dioxanonanoate) [*A2*, HFPO-TrA] Degradation.

	HFPO-TrA (*A2*)[a]			**HFPO-DA (*A1*)**[a]		
Time(h)	[c,d]**$C_9F_{17}O_4^-$**	[c]$C_9F_{16}HO_4^-$	[c]$C_8F_{13}H_2O_4^-$	[b]**$C_6F_{11}O_3^-$**	[c]$C_6F_{10}HO_3^-$	[c]$C_5F_7H_2O_3^-$
0	4.05E+05	*ND*	*ND*	2.53	*ND*	*ND*
1	3.10E+05	9.10E+04	*ND*	4.06	6.87E+04	*ND*
2	2.12E+05	1.43E+05	*ND*	4.18	2.79E+05	*ND*
4	1.37E+05	6.63E+05	*ND*	5.95	1.40E+06	*ND*
8	7.18E+04	1.00E+06	3.28E+04	6.57	3.64E+06	*ND*
12	1.27E+05	1.10E+06	8.78E+04	5.58	4.93E+06	*ND*
24	*ND*	1.85E+06	1.09E+05	3.79	7.87E+06	*ND*
48	*ND*	1.85E+06	1.61E+05	2.61	7.98E+06	*ND*

[a]Products with the same chain length are assumed to be H/F and H/CF_3 exchange derivatives from the corresponding branched PFECA.
[b]Quantified by LC-MS/MS with standards (in μM).
[c]Observed by HRMS analysis without standards for quantification (in peak area).
[d]Not stable under the ionization condition used for both MS detection methods. Only the small peak areas by HRMS are shown. Note the significant concentration of HFPO-DA detected in the t = 0 sample.

Table B.5 Concentrations and Peak Areas of the Parent Compound and TP Suspects from Perfluoro(2,5,8-trimethyl-3,6,9-trioxadodecanoate) [*A3*, HFPO-TeA] Degradation.

	HFPO-TeA (*A3*)[a]		**HFPO-TrA (*A2*)[a]**				**HFPO-DA (*A3*)[a]**		
Time(h)	[b,e]**$C_{12}F_{23}O_5^-$**	[c]$C_{10}F_{15}H_4O_5^-$	[b]**$C_9F_{17}O_4^-$**	[c]$C_9F_{16}HO_4^-$	[c]$C_9F_{15}H_2O_4^-$	[c]$C_8F_{13}H_2O_4^-$	[b]**$C_6F_{11}O_3^-$**	[c]$C_6F_{10}HO_3^-$	[c]$C_5F_7H_3O_3^-$
0	25.0	*ND*	0.27	*ND*	*ND*	*ND*	0	*ND*	*ND*
1	23.4	*ND*	2.02	*ND*	*ND*	*ND*	0.04	*ND*	*ND*
2	14.2	*ND*	3.57	*ND*	*ND*	*ND*	0.27	*ND*	*ND*
4	13.0	*ND*	6.45	2.86E+05	4.78E+04	*ND*	1.22	*ND*	*ND*
8	6.9	*ND*	7.93	8.60E+05	1.99E+05	7.13E+04	2.97	2.93E+06	6.61E+05
12	4.9	6.37E+04	7.49	1.13E+06	1.08E+06	5.77E+04	3.71	3.69E+06	4.16E+05
24	3.1	2.42E+05	4.80	1.70E+06	2.61E+06	1.00E+05	3.46	6.71E+06	1.16E+06
48	2.9	4.86E+05	2.17	1.90E+06	4.61E+06	1.09E+05	2.45	7.23E+06	1.06E+06

	PFPrA[d]		
Time(h)	[b]**$C_3F_5O_2^-$**	[b]$C_3F_4HO_2^-$	[b]$C_3F_3H_2O_2^-$
0	*ND*	*ND*	*ND*
1	*ND*	*ND*	*ND*
2	*ND*	0.19	*ND*
4	*ND*	0.47	*ND*
8	0.35	0.81	*ND*
12	0.62	0.93	*ND*
24	0.70	0.96	*ND*
48	0.71	0.80	*ND*

[a]Products with the same chain length are assumed to be H/F and H/CF_3 exchange derivatives from the corresponding branched PFECA.
[b]Quantified by LC-MS/MS with standards (in μM).
[c]Observed by HRMS analysis without standards for quantification (in peak area).
[d]Products with the same chain length are assumed to be H/F exchange derivatives from the corresponding PFCA.
[e]Not stable under the ionization condition used for HRMS detection.

Table B.6 Concentrations and Peak Areas of the Parent Compound and TP Suspects from Perfluoro(3-methoxypropanoate) [*B2*] Degradation.

	Perfluoro(3-methoxypropanoate) (*B2*)[a]				**Perfluoro(2-methoxyacetate)**
Time (h)	[b,c]**$C_4F_7O_3^-$**		[c]$C_4F_6HO_3^-$	[c]$C_4F_5H_2O_3^-$	[c]**$C_3F_5O_3^-$**
0	25.0	7.26E+08	1.15E+06	*ND*	1.02E+05
1	20.3	5.91E+08	3.71E+06	*ND*	4.54E+05
2	15.2	4.42E+08	7.01E+06	*ND*	9.75E+05
4	6.3	1.83E+08	9.23E+06	*ND*	7.14E+05
8	0.6	1.75E+07	6.30E+06	3.74E+04	2.65E+05
12	0.2	6.35E+06	3.99E+06	4.86E+04	1.77E+05
24	0.2	5.61E+06	1.76E+06	1.02E+05	8.92E+04
48	0.1	5.52E+06	1.01E+06	1.39E+05	2.04E+05

[a]Products with the same chain length are assumed to be H/F exchange derivatives from the corresponding linear PFECA.
[b]Quantified by LC-MS/MS with standards (in μM).
[c]Observed by HRMS analysis without standards for quantification (in peak area).

Table B.7 Concentrations and Peak Areas of the Parent Compound and TP Suspects from Perfluoro(4-methoxybutanoate) [*B3*] Degradation.

	Perfluoro(4-methoxybutanoate) (*B3*)[a]				**Perfluoro(3-methoxypropanoate) (*B2*)[a]**		**Perfluorosuccinate**
Time (h)	[b,c]**$C_5F_9O_3^-$**		[c]$C_5F_8HO_3^-$	[c]$C_5F_7H_2O_3^-$	[b]**$C_4F_7O_3^-$**	[c]$C_4F_6HO_3^-$	[b]**$C_4F_4O_4^{2-}$**
0	25.0	6.74E+08	2.23E+06	*ND*	0.23	4.39E+06	*ND*
1	13.9	5.16E+08	4.50E+07	*ND*	0.83	9.08E+06	*ND*
2	8.9	3.44E+08	7.96E+07	1.21E+05	0.81	8.35E+06	0.12
4	2.8	1.71E+08	1.03E+08	3.57E+05	0.40	4.04E+06	0.29
8	0.3	2.89E+07	9.19E+07	8.72E+05	0.08	6.89E+05	0.33
12	*ND*	3.94E+06	7.40E+07	6.12E+05	0.05	4.18E+05	0.37

[a]Products with the same chain length are assumed to be H/F exchange derivatives from the corresponding linear PFECA.
[b]Quantified by LC-MS/MS with standards (in μM).
[c]Observed by HRMS analysis without standards for quantification (in peak area).

Table B.8 Concentrations and Peak Areas of the Parent Compound and TP Suspects from Perfluoro(3,6-dioxaheptanoate) [*C1*] Degradation.

	Perfluoro(3,6-dioxaheptanoate) (*C1*)[a]				**Perfluoro(2-methoxyacetate)**
Time (h)	[b,c]**$C_5F_9O_4^-$**		[c]$C_5F_8HO_4^-$	[c]$C_5F_7H_2O_4^-$	[c]**$C_3F_5O_3^-$**
0	25.6	6.91E+07	2.03E+06	*ND*	*ND*
1	20.7	5.60E+07	1.82E+06	*ND*	2.41E+07
2	17.4	4.69E+07	4.55E+06	*ND*	3.85E+07
4	10.6	2.86E+07	6.63E+06	*ND*	4.37E+07
8	4.4	1.18E+07	5.56E+06	*ND*	3.57E+07
12	2.5	6.75E+06	4.24E+06	*ND*	2.50E+07

[a]Products with the same chain length are assumed to be H/F exchange derivatives from the corresponding linear PFECA.
[b]Quantified by LC-MS/MS with standards (in μM).
[c]Observed by HRMS analysis without standards for quantification (in peak area).

Table B.9 Concentrations and Peak Areas of the Parent Compound and TP Suspects from Perfluoro(3,6,9-trioxadecanoate) [*C2*] Degradation.

	Perfluoro(3,6,9-trioxadecanoate) (*C2*)[a]				**Perfluoro(3,6-dioxaheptanoate) (*C1*)[a]**	
Time (h)	[b,c]**$C_7F_{13}O_5^-$**		[c]$C_7F_{12}HO_5^-$	[c]$C_7F_{11}H_2O_5^-$	[b]**$C_5F_9O_4^-$**	[c]$C_5F_8HO_4^-$
0	25.0	1.26E+07	*ND*	*ND*	*ND*	*ND*
1	23.6	9.17E+06	1.90E+06	*ND*	2.4	2.24E+05
2	20.1	8.14E+06	5.19E+06	7.99E+04	4.6	7.11E+05
4	12.7	5.66E+06	1.01E+07	6.18E+05	6.5	2.55E+06
8	3.8	3.36E+06	9.55E+06	1.82E+06	5.2	4.85E+06
12	1.8	1.98E+06	6.89E+06	2.97E+06	2.9	4.45E+06

[a]Products with the same chain length are assumed to be H/F exchange derivatives from the corresponding linear PFECA.
[b]Quantified by LC-MS/MS with standards (in μM).
[c]Observed by HRMS analysis without standards for quantification (in peak area).

Table B.10 Concentrations and Peak Areas of the Parent Compound and TP Suspects from Perfluoro(3,6-dioxadecanoate) [*D1*] Degradation.

	Perfluoro(3,6-dioxadecanoate) (*D1*)[a]				**Perfluoro(3-oxaheptanoate)[a]**			**PFBA**
Time (h)	[b,c]**$C_8F_{15}O_4^-$**		[c]$C_8F_{14}HO_4^-$	[c]$C_8F_{13}H_2O_4^-$	[c]**$C_6F_{11}O_3^-$**	[c]$C_6F_{10}HO_3^-$	[c,d]$C_5F_6H_3O_3^-$	[b]**$C_4F_7O_2^-$**
0	26.7	6.83E+06	5.73E+05	*ND*	5.39E+06	*ND*	*ND*	*ND*
1	20.6	5.27E+06	3.92E+06	3.50E+04	1.05E+07	5.18E+05	*ND*	0.6
2	20.6	5.28E+06	7.86E+06	1.63E+05	1.32E+07	1.99E+06	5.57E+04	2.4
4	12.7	3.24E+06	1.13E+07	8.99E+05	1.32E+07	4.88E+06	6.77E+05	4.6
8	6.9	1.78E+06	8.14E+06	1.29E+06	8.04E+06	5.58E+06	1.76E+06	3.8
12	3.3	8.36E+05	4.74E+06	1.87E+06	4.87E+06	3.70E+06	2.94E+06	2.0

[a]Products with the same chain length are assumed to be H/F exchange derivatives from the corresponding linear PFECA.
[b]Quantified by LC-MS/MS with standards (in μM).
[c]Observed by HRMS analysis without standards for quantification (in peak area).
[d]Product assigned as the product after *DHEH*.

Table B.11 Concentrations and Peak Areas of the Parent Compound and TP Suspects from Perfluoro(3,6,9-trioxatridecanoate) [*D2*] Degradation.

	Perfluoro(3,6,9-trioxatridecanoate) (*D2*)[a]				**Perfluoro(3,6-dioxadecanoate) (*D1*)[a]**		
Time (h)	[b,c]**$C_{10}F_{19}O_5^-$**		[c]$C_{10}F_{18}HO_5^-$	[c,d]$C_9F_{14}H_3O_5^-$	[b]**$C_8F_{15}O_4^-$**	[c]$C_8F_{14}HO_4^-$	[c]$C_8F_{13}H_2O_4^-$
0	25.0	1.43E+06	3.54E+05	2.22E+05	0.02	*ND*	*ND*
1	22.7	1.44E+06	3.66E+06	2.13E+05	5.0	4.77E+05	*ND*
2	17.9	9.28E+05	7.64E+06	1.00E+06	10.2	1.49E+06	*ND*
4	14.0	8.33E+05	8.96E+06	4.39E+06	14.4	4.16E+06	*ND*
8	7.0	5.09E+05	7.19E+06	1.71E+07	13.2	9.76E+06	1.15E+06
12	3.5	1.64E+05	3.64E+06	2.78E+07	11.0	1.02E+07	9.30E+05

	Perfluoro(3-oxaheptanoate)[a]		**PFBA**
Time (h)	[c]**$C_6F_{11}O_3^-$**	[c]$C_6F_{10}HO_3^-$	[b]**$C_4F_7O_2^-$**
0	1.27E+06	*ND*	*ND*
1	2.48E+06	*ND*	*ND*
2	4.53E+06	2.69E+05	0.1
4	7.24E+06	1.11E+06	0.4
8	1.03E+07	3.85E+06	1.3
12	9.22E+06	4.99E+06	1.4

[a]Products with the same chain length are assumed to be H/F exchange derivatives from the corresponding linear PFECA and PFCA.
[b]Quantified by LC-MS/MS with standards (in μM).
[c]Observed by HRMS analysis without standards for quantification (in peak area).
[d]Product assigned as the product after *DHEH*.

Figures B.1 to B.13 Referred in the Main Text

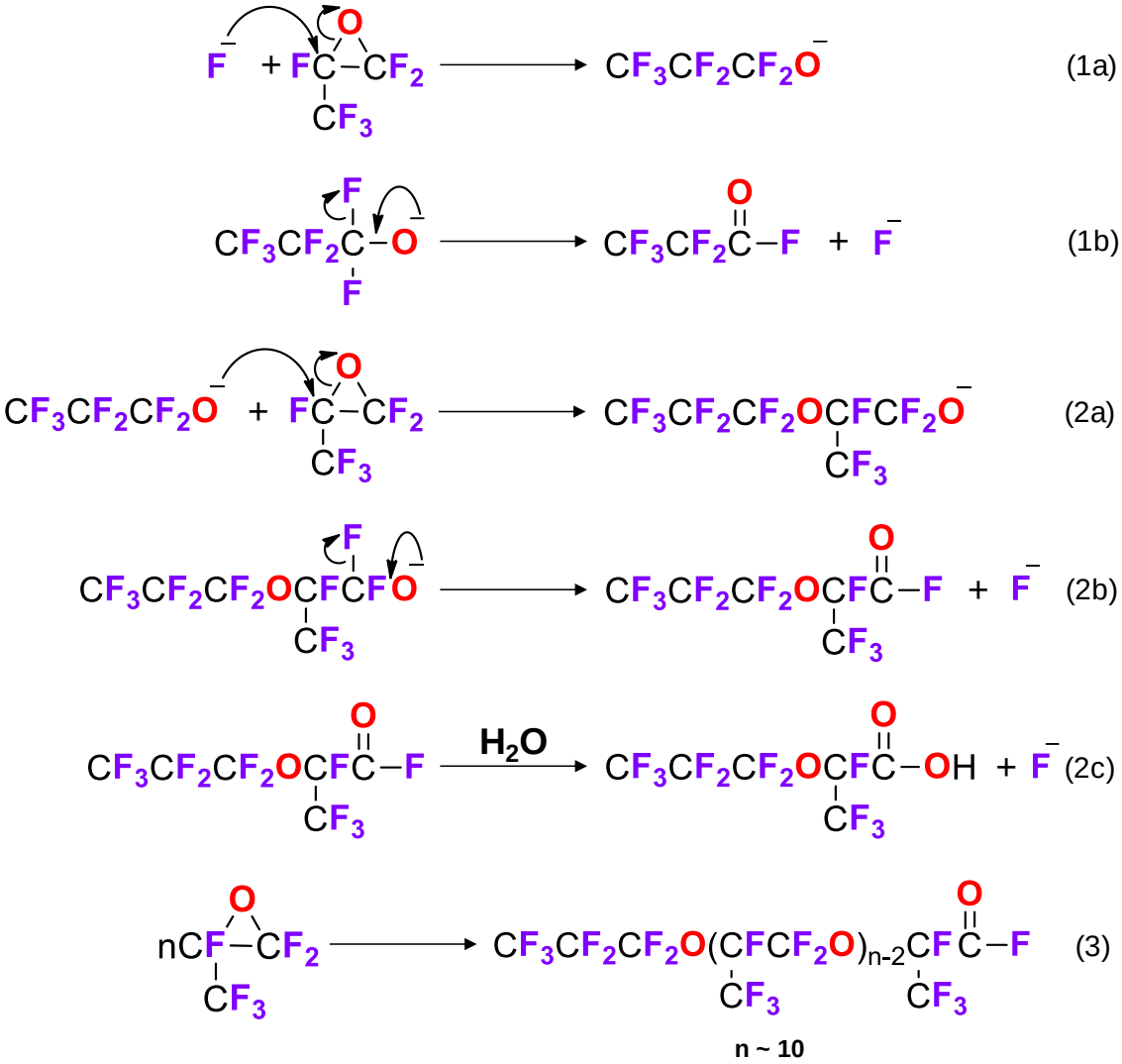

Figure B.1 Polymerization of hexafluoropropylene oxide (HFPO).[2] A fluoride ion opens the epoxide ring to generate *n*-perfluoroalkoxide (1a). This structure can undergo rearrangement to generate perfluoroacyl fluoride (1b). Alternatively, *n*-perfluoroalkoxide can attack another epoxide monomer to generate the branched perfluoroalkoxide dimer (2a). The dimer can undergo rearrangement to form the dimer acyl fluoride (2b). Subsequent hydrolysis yields the carboxylic acid (i.e., HFPO-DA or "GenX" in this example) (2c). Following this reaction scheme, a variety of branched perfluoroalkyl ether oligomers and polymers can be synthesized (3).

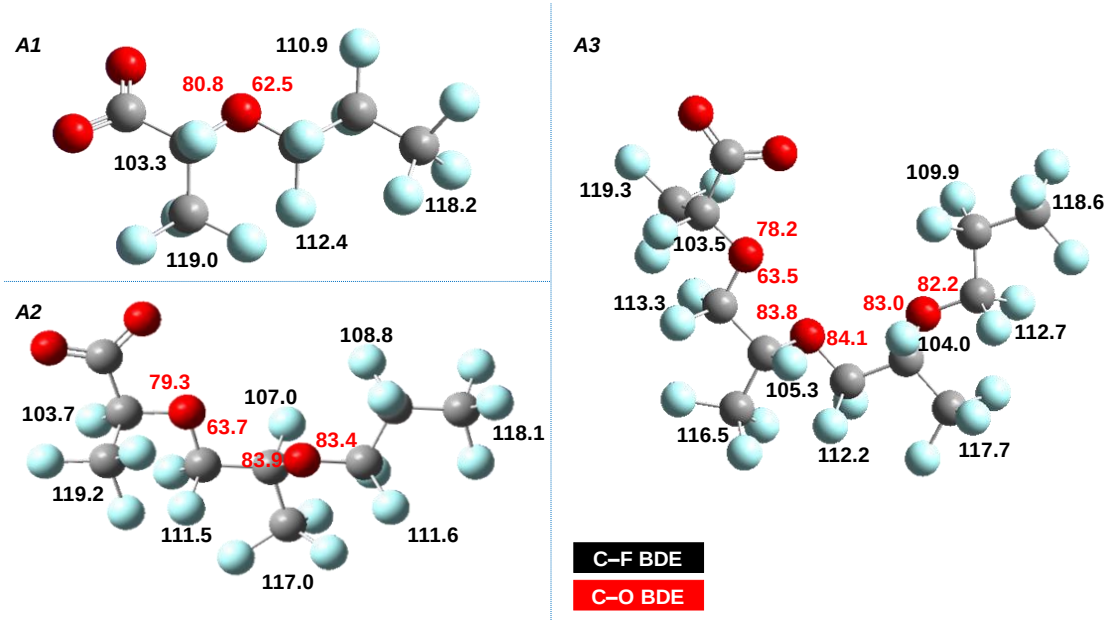

Figure B.2 Calculated C−F and C−O BDEs (kcal mol^{-1}) for branched HFPO oligomers.

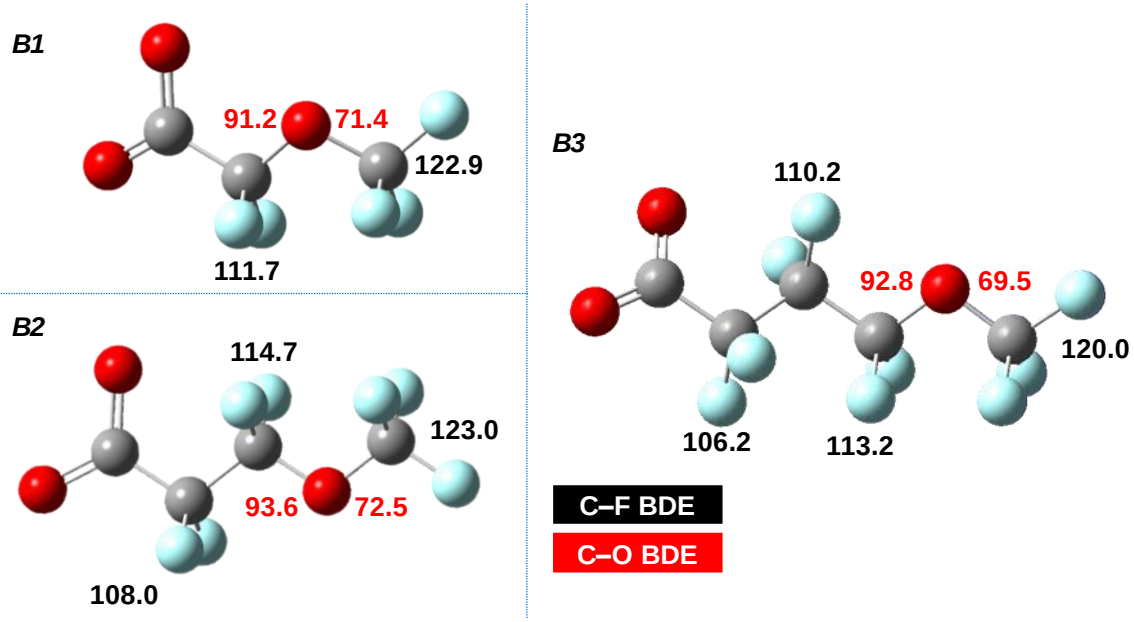

Figure B.3 Calculated C–F and C–O BDEs (kcal mol^{-1}) for mono-ethers with the CF_3O– head group.

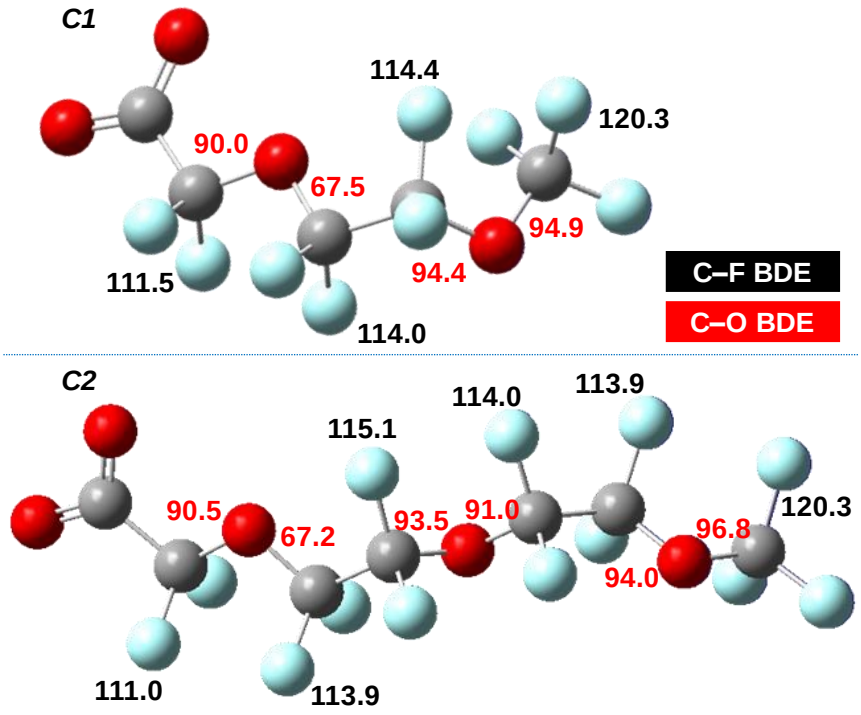

Figure B.4 Calculated C−F and C−O BDEs (kcal mol^{-1}) of TFEO oligomers with the CF_3O– head group.

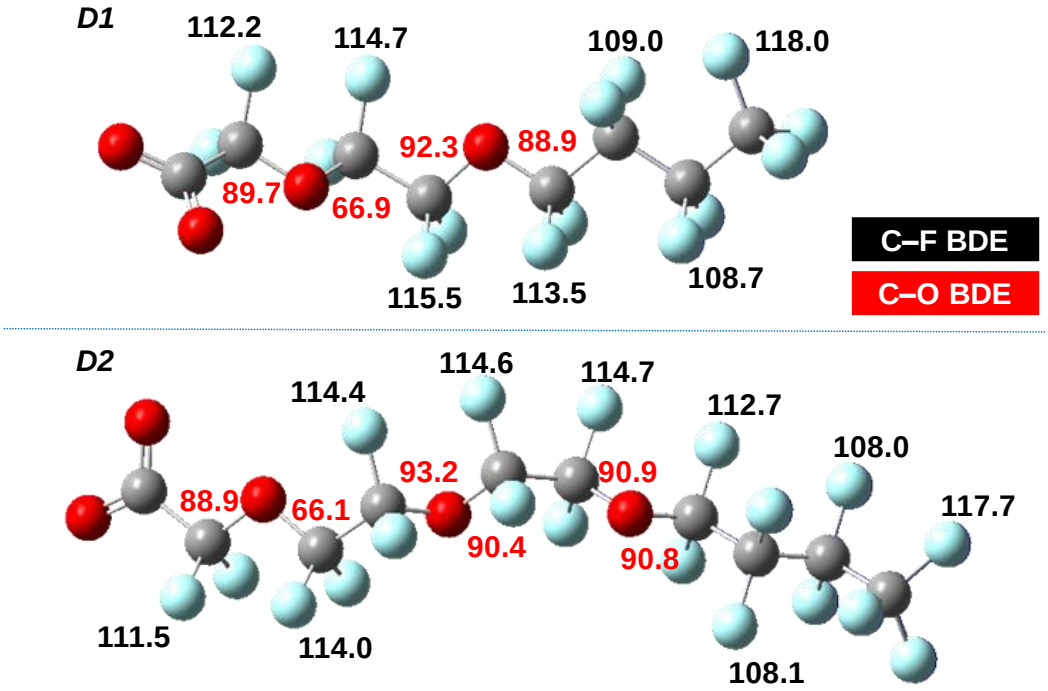

Figure B.5 Calculated C–F and C–O BDEs (kcal mol^{-1}) for TFEO oligomers with the C_4F_9O– head group.

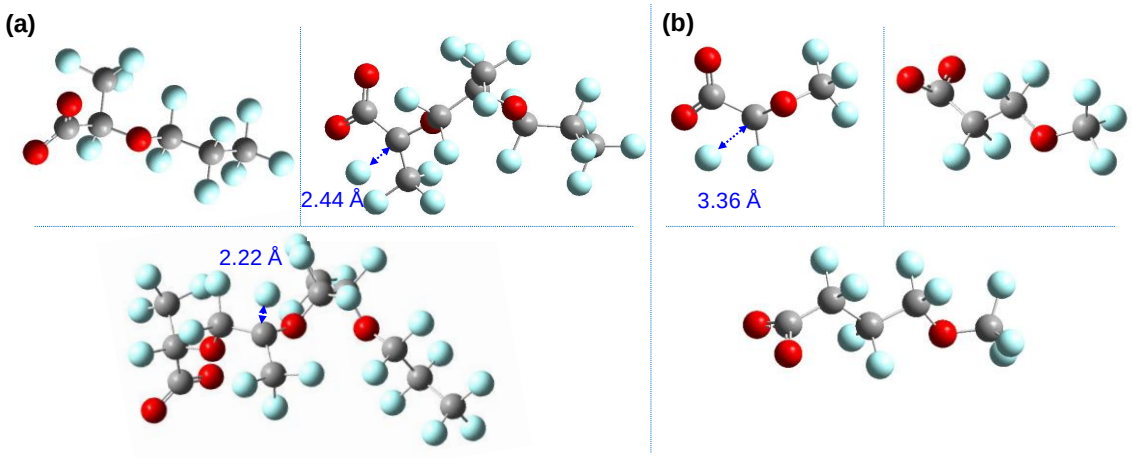

Figure B.6 Geometry-optimized [R_F–COO]$^{\bullet 2-}$ structures from (a) *A1*−*A3* and (b) *B1*−*B3* at the B3LYP-D3(BJ)/6-311+G(2d,2p) level of theory, showing C−F bond stretching.

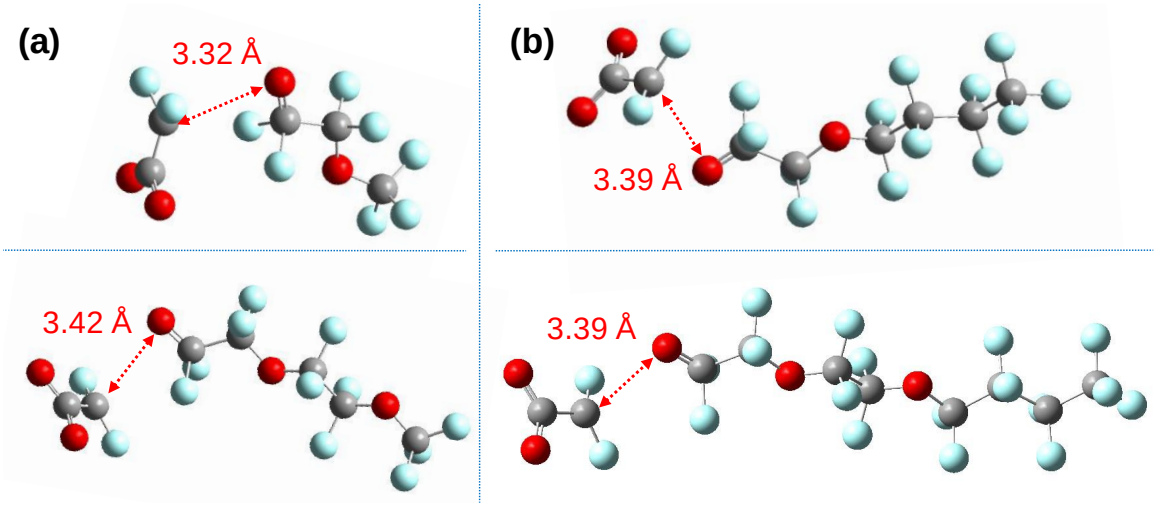

Figure B.7 Geometry-optimized $[R_F\text{–COO}]^{\bullet 2-}$ structures of (a) *C1−C2* and (b) *D1−D2* at the B3LYP-D3(BJ)/6-311+G(2d,2p) level of theory, showing C−O bond stretching.

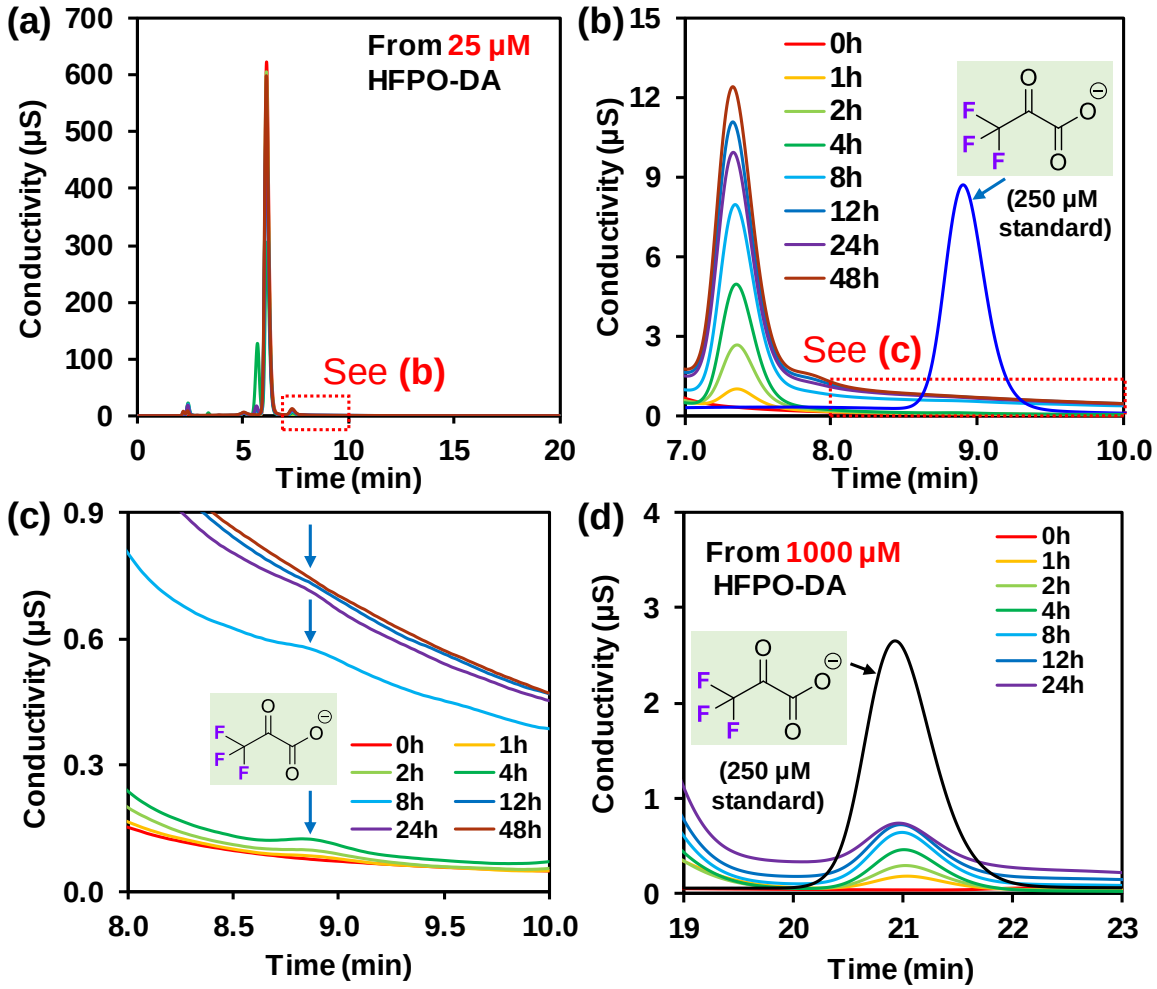

Figure B.8 Ion-chromatography analysis for the generation of trifluoropyruvate (TFPy) from the degradation of HFPO-DA (*A1*). The chromatograph from the reaction mixture (a) is magnified in panels (b) and (c). *Reaction conditions*: *A1* (0.025 mM), Na_2SO_3 (10 mM), carbonate buffer (5 mM, pH adjusted to 9.5), 600 mL solution, 254 nm irradiation (18 W low-pressure Hg lamp) at 20°C. The formation of TFPy was observed in panel (c), but the quantification was difficult due to the interference of another unknown species in a much higher intensity. However, as shown in panel (d), the elevated concentration of *A1* (1 mM) generated more TFPy, and the peak separation was also improved by adjusting the eluent flow rate of the ion chromatography. Separation conditions: AS11-HC column (4 mm × 250 mm, 4μm) with AG-11 guard column at 30°C; isocratic eluent with 20 mM NaOH at a flow rate of 1.5 mL min^{-1} for (a)−(c) and with 15 mM NaOH at a flow rate of 1.0 mL min^{-1} for (d).

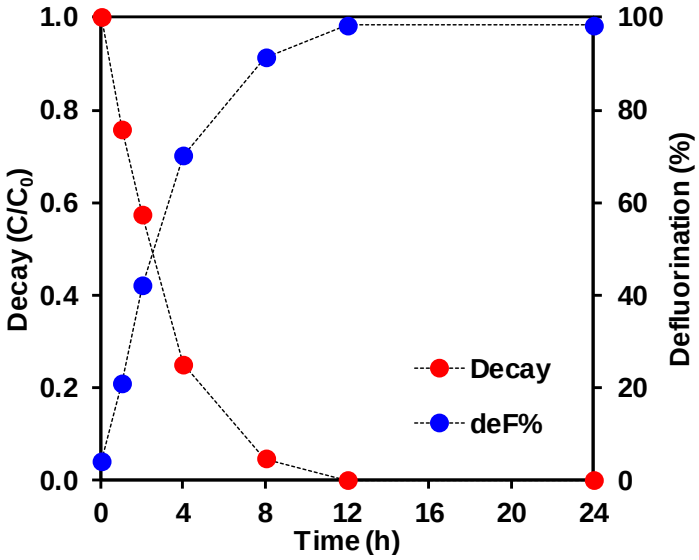

Figure B.9 Time profiles of parent compound decay and defluorination percentage for trifluoropyruvate (TFPy). *Reaction conditions*: $CF_3{-}CO{-}COO^-$ (0.025 mM), Na_2SO_3 (10 mM), carbonate buffer (5 mM, pH adjusted to 9.5), 600 mL solution, 254 nm irradiation (18 W low-pressure Hg lamp for 600 mL solution) at 20°C.

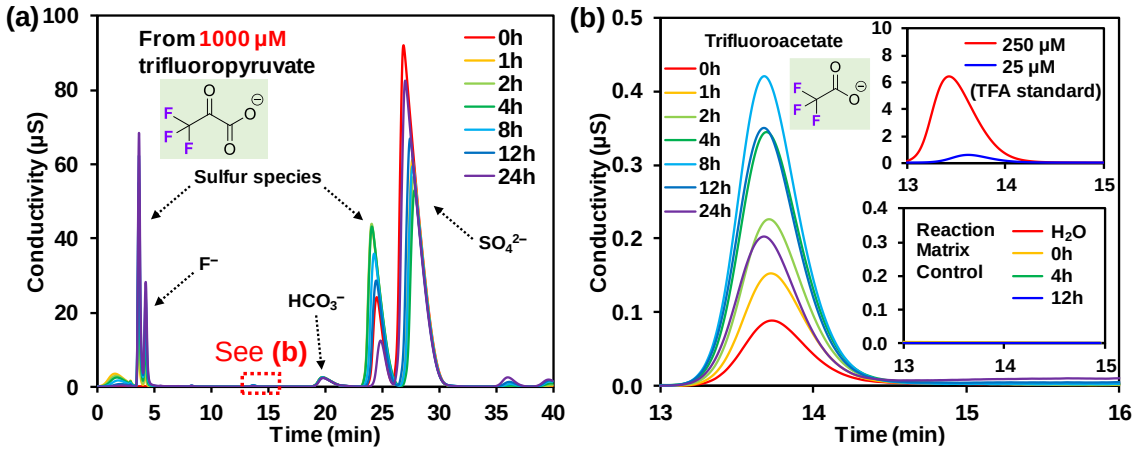

Figure B.10 Ion-chromatography analysis for the generation of trifluoroacetate (TFA) from the degradation of trifluoropyruvate (TFPy). The chromatograph from the reaction mixture (a) is zoomed in panel (b). The top small panel in (b) shows the peaks of two TFA standards. The bottom panel shows the lack of this TFA peak in the reaction matrix control where TFPy was not added. *Reaction conditions*: TFPy (1 mM), Na_2SO_3 (10 mM), carbonate buffer (5 mM, pH adjusted to 9.5), 600 mL solution, 254 nm irradiation (18 W low-pressure Hg lamp) at 20°C. The high concentration of TFPy was used because the amount of TFA generated from 25 µM TFPy was too small (similar to Figure B.8c). The maximum concentration of TFA generated at 8 h was 19 µM (i.e., 1.9% of the initial TFPy). Separation conditions: AS11-HC column (4 mm × 250 mm, 4µm) with AG-11 guard column at 30°C; isocratic eluent with 10 mM NaOH at a flow rate of 1.0 mL min^{-1}.

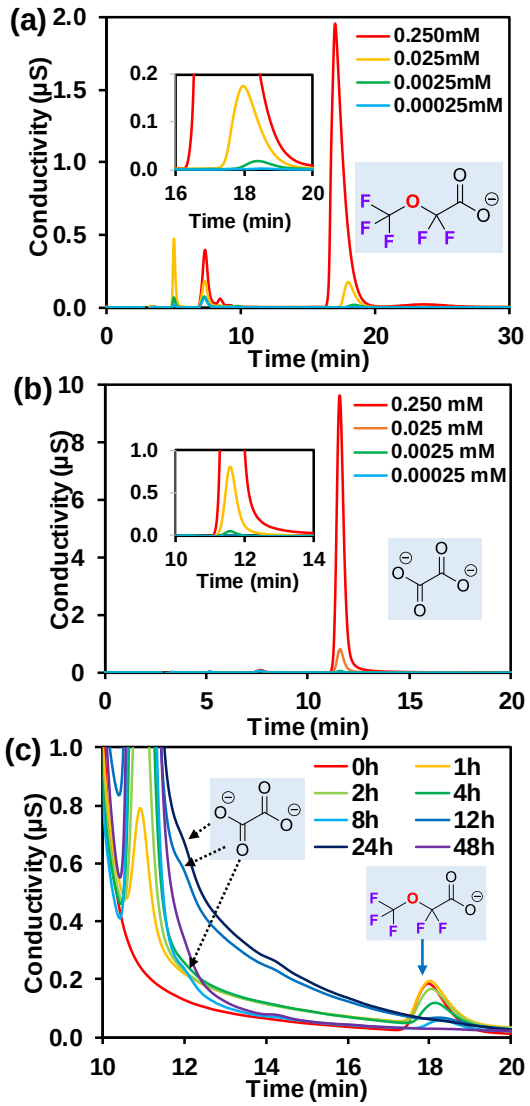

Figure B.11 Ion-chromatography analysis for the generation of oxalate from the degradation of *B1*. The peaks for (a) compound *B1* and (b) oxalate are verified with four standard calibrating concentrations. The zoomed chromatograph for the reaction mixture is shown in panel (c). *Reaction conditions*: *B1* (0.025 mM), Na_2SO_3 (10 mM), carbonate buffer (5 mM, pH adjusted to 9.5), 600 mL solution, 254 nm irradiation (18 W low-pressure Hg lamp) at 20°C. The quantification of oxalate was difficult due to the interference of another unknown species in a much higher intensity. Separation conditions: AS11-HC column (4 mm × 250 mm, 4μm) with AG-11 guard column at 30°C; isocratic eluent with 20 mM NaOH at a flow rate of 1.0 mL min^{-1}.

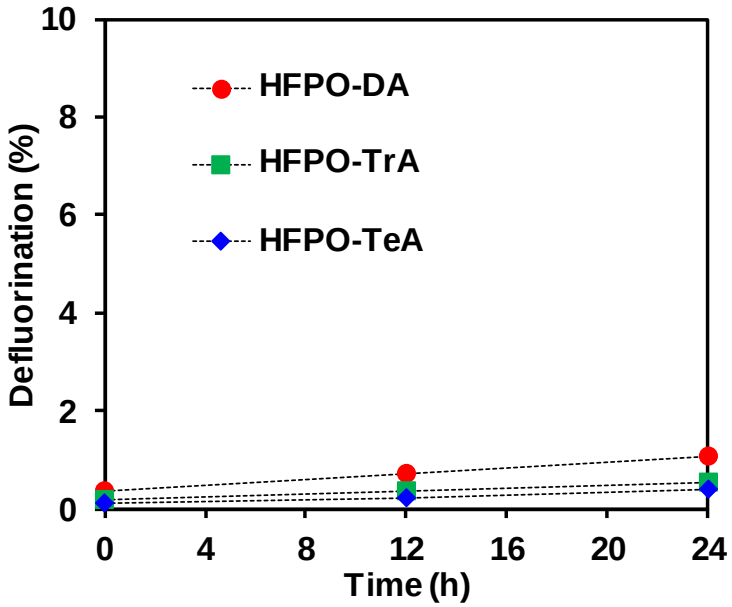

Figure B.12 Defluorination percentages of the three HFPO oligomer acids without adding sulfite. Note that the y-axis range is 0−10%. R*eaction conditions*: individual PFECA (0.025 mM), carbonate buffer (5 mM), 254 nm irradiation (an 18 W low-pressure Hg lamp for 600 mL solution) at pH 9.5 and 20°C.

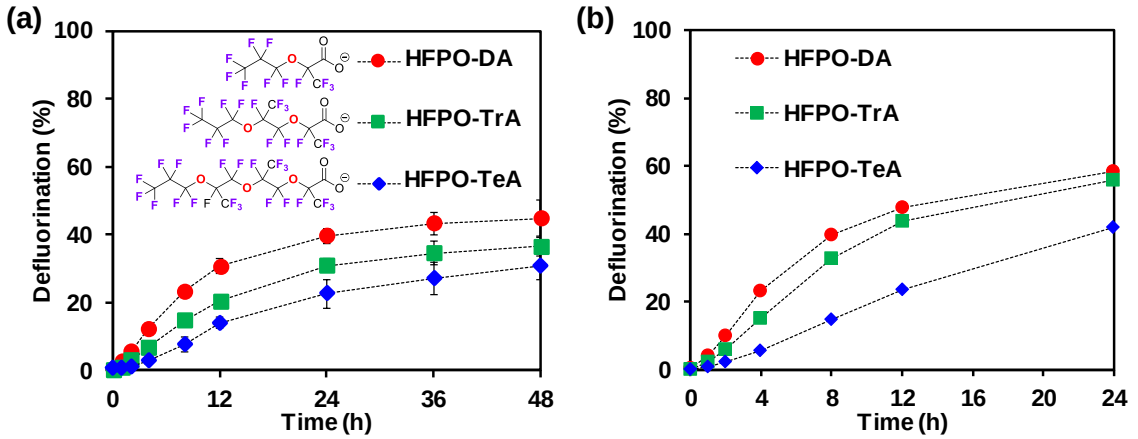

Figure B.13 Comparison of defluorination percentages of the three HFPO oligomer acids with (a) 10 mM Na_2SO_3 at pH 9.5 and (b) 20 mM Na_2SO_3 at pH 10.0. *Common reaction conditions*: individual PFECA (0.025 mM), carbonate buffer (5 mM), 254 nm irradiation (an 18 W low-pressure Hg lamp for 600 mL solution) at 20°C.

Schemes B.1 to B.10 Referred in the Main Text

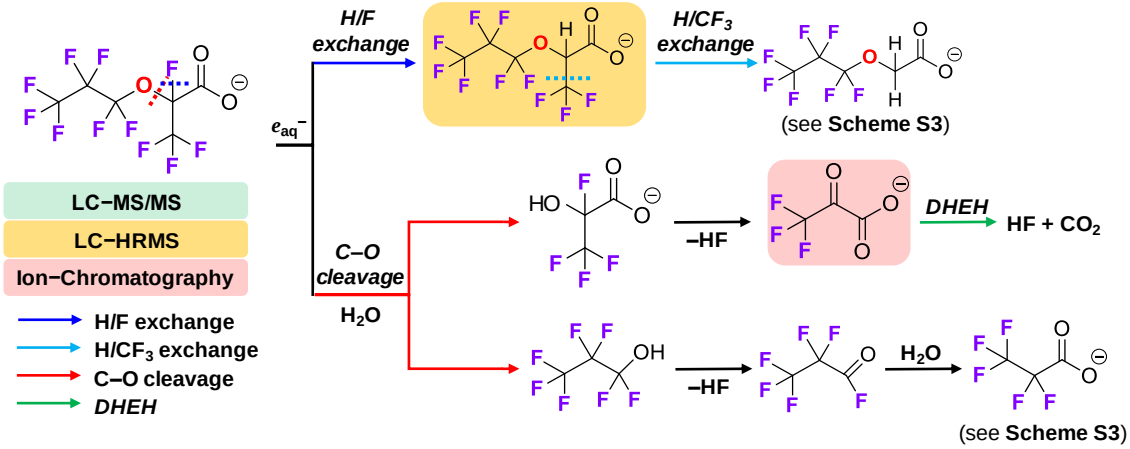

Scheme B.1 Proposed degradation mechanism for perfluoro(2-methyl-3-oxahexanoate) [*A1*, HPFO-DA].

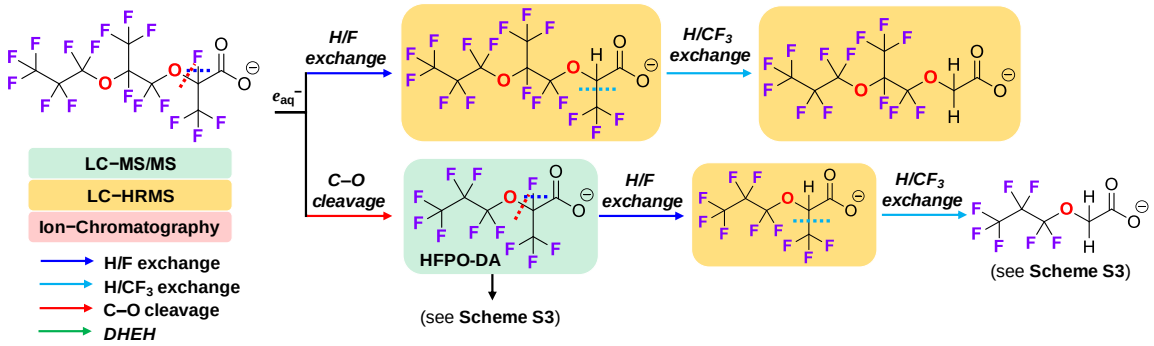

Scheme B.2 Proposed degradation mechanism for perfluoro(2,5-dimethyl-3,6-dioxanonanoate) [*A2*, HFPO-TrA].

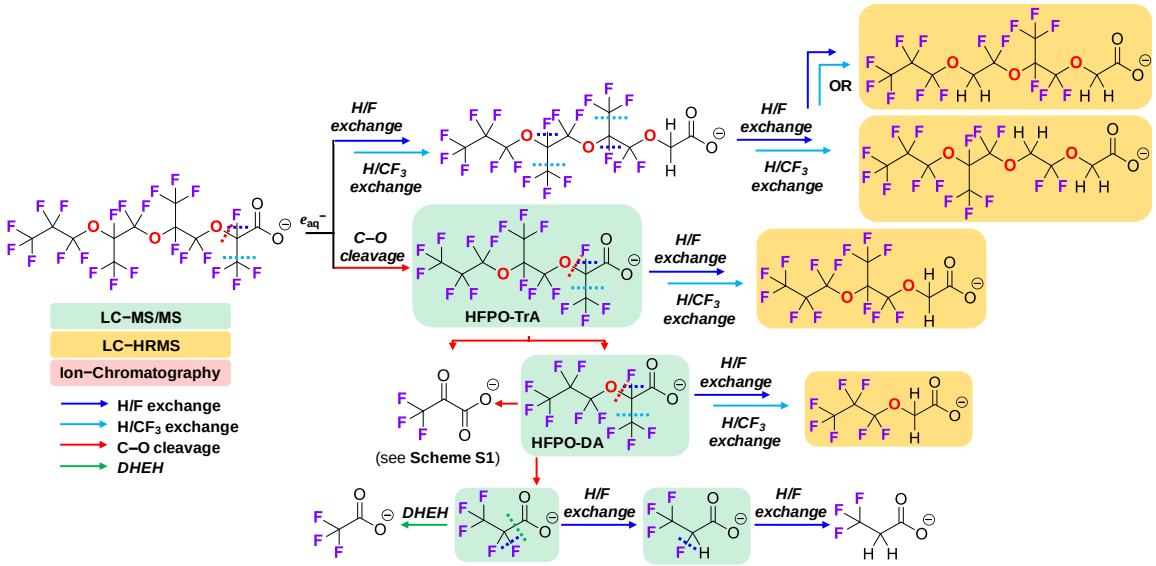

Scheme B.3 Proposed degradation mechanism for perfluoro(2,5,8-trimethyl-3,6,9-trioxa dodecanoate) [*A3*, HFPO-TeA].

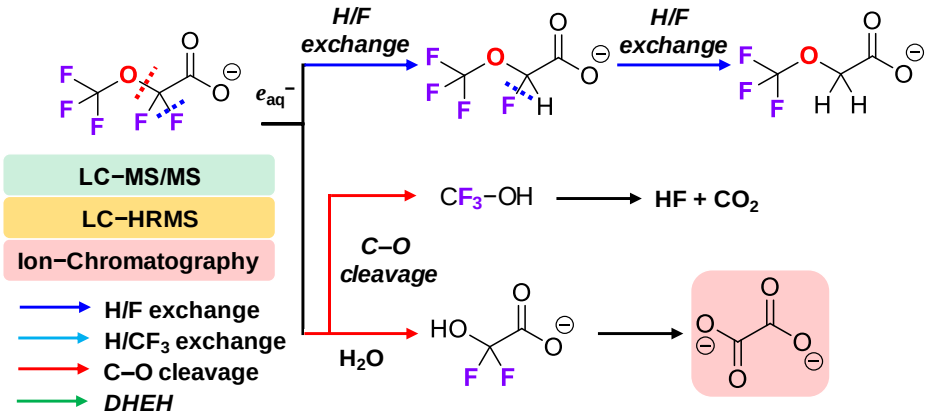

Scheme B.4 Proposed degradation mechanism for perfluoro(2-methoxyacetate) [*B1*].

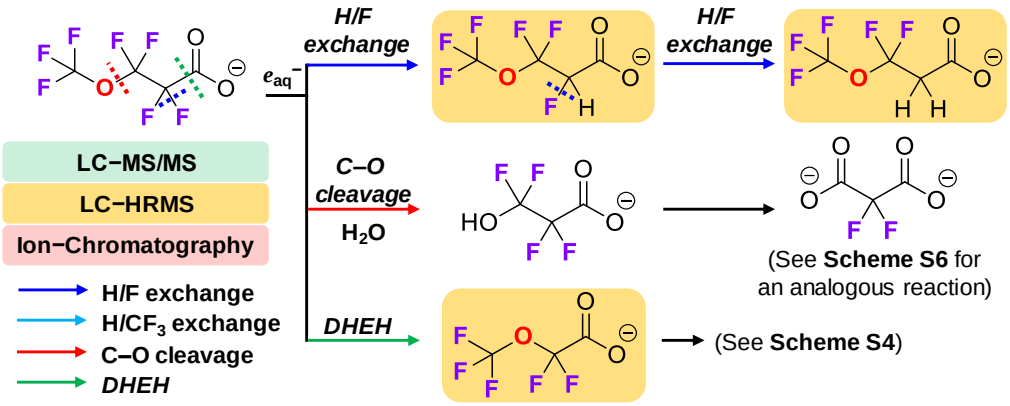

Scheme B.5 Proposed degradation mechanism for perfluoro(3-methoxypropanoate) [*B2*].

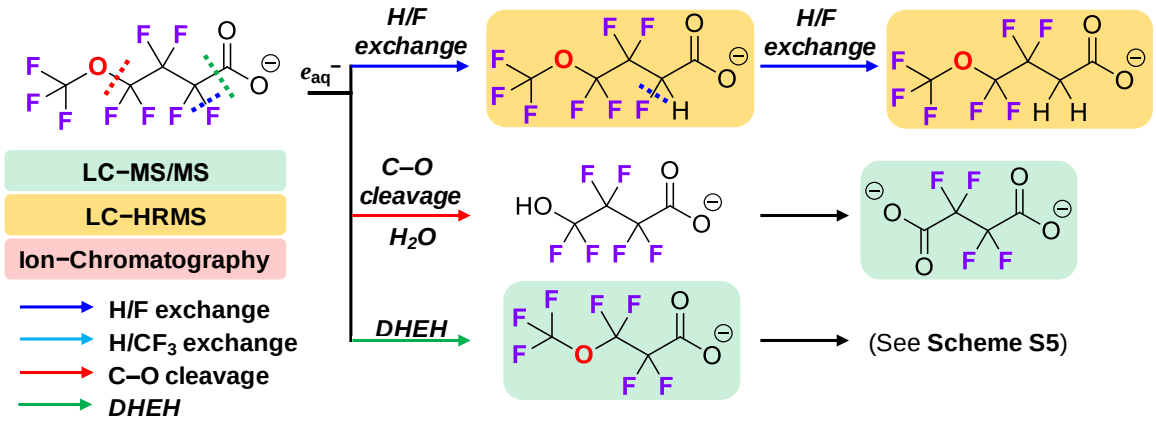

Scheme B.6 Proposed degradation mechanism for perfluoro(4-methoxybutanoate) [*B3*].

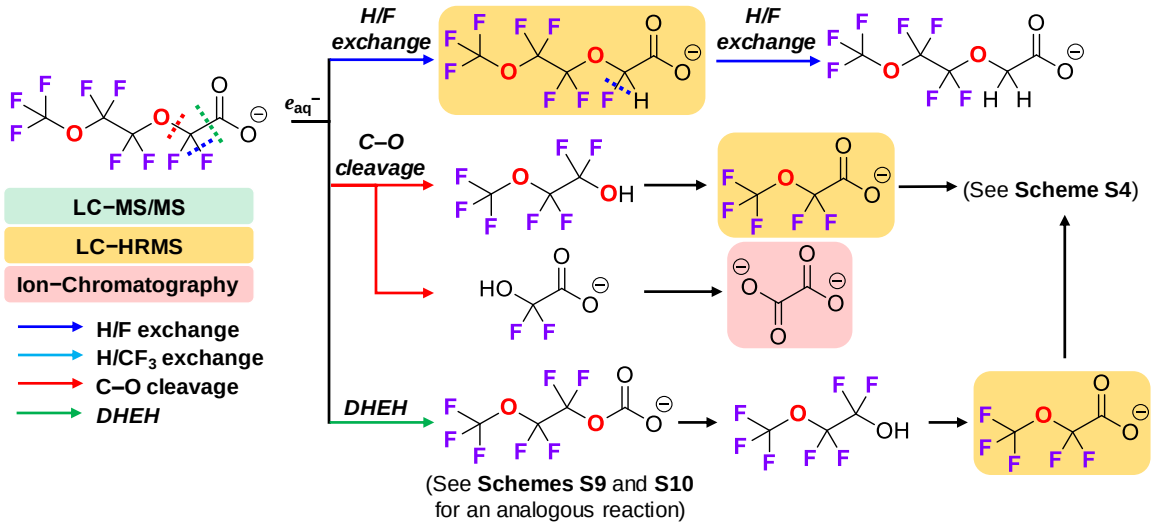

Scheme B.7 Proposed degradation mechanism for perfluoro(3,6-dioxaheptanoate) [*C1*].

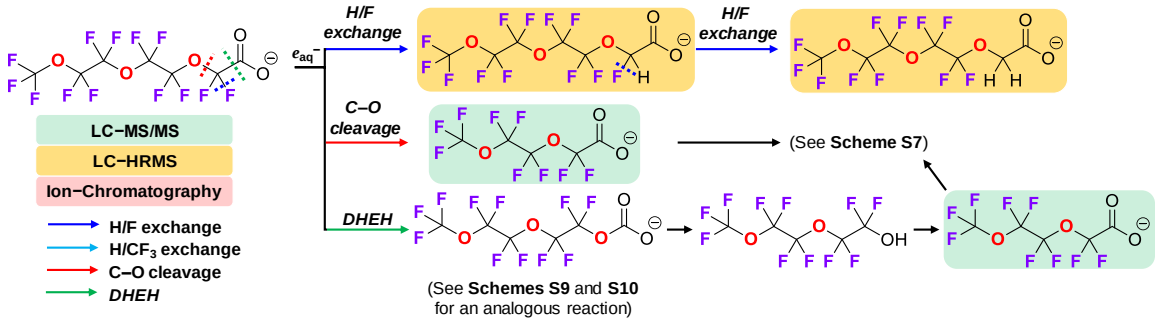

Scheme B.8 Proposed degradation mechanism for perfluoro(3,6,9-trioxadecanoate) [*C2*].

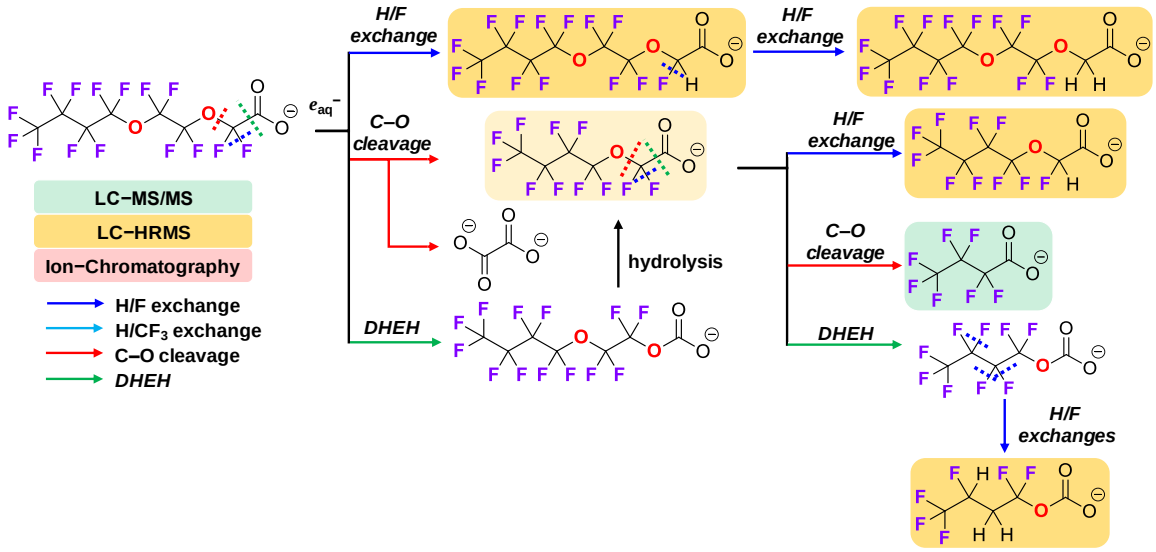

Scheme B.9 Proposed degradation mechanism for perfluoro(3,6-dioxadecanoate) [*D1*].

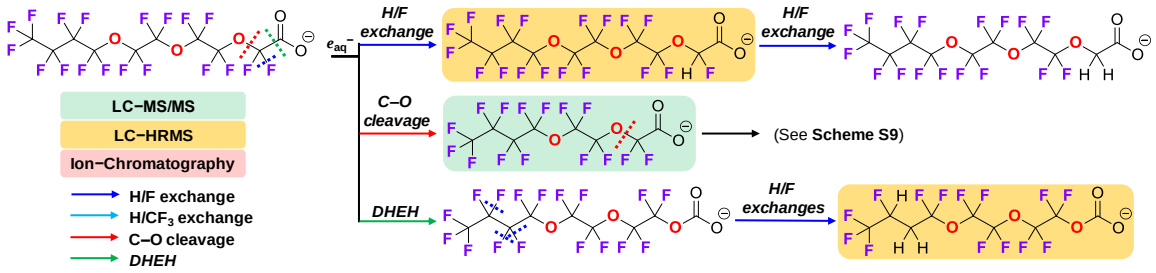

Scheme B.10 Proposed degradation mechanism for perfluoro(3,6,9-trioxatridecanoate) [*D2*].

REFERENCES

(1) Bentel, M. J.; Yu, Y.; Xu, L.; Li, Z.; Wong, B. M.; Men, Y.; Liu, J., Defluorination of per- and polyfluoroalkyl substances (PFASs) with hydrated electrons: Structural dependence and implications to PFAS remediation and management. *Environ. Sci. Technol.* **2019,** *53* (7), 3718-3728.

(2) Hill, J. T., Polymers from hexafluoropropylene oxide (HFPO). *J. Macromol. Sci. Chem.* **1974,** *8* (3), 499-520.

APPENDIX C: APPENDICES FOR CHAPTER 4

Detailed Information on Materials and Methods

Chemicals and the Preparation of PFCA Stock Solutions. Per- and polyfluorinated carboxylates (PFCAs) were purchased from Acros Organics, Alfa-Aesar, MP Biomedicals, Oakwood Chemicals, Sigma-Aldrich, and SynQuest Laboratories. Table C1 summarizes the name, purity, and CAS number of all PFCAs included in this study. All other chemicals and solvents were purchased from Fisher Chemical. Individual PFCAs were dissolved in deionized water (produced by a Milli-Q system) as 10 mM stock solutions by the addition of 20 mM NaOH to facilitate the dissolution of long-chain structures in water and prevent the volatilization of short-chain structures. All PFCA stock solutions were stored on benchtop at room temperature (20°C).

Table C.1 Information of PFCAs Used in This Study.

Entry	Chemical Name	Fluoroalkyl Length (n)	Purity	CAS#
	$F(CF_2)_n$−COOH (or salt)			
1	Sodium trifluoroacetate	1	98%	2923-18-4
2	Perfluoropropionic acid	2	97%	422-64-0
3	Perfluorobutyric acid	3	98%	375-22-4
4	Perfluoropentanoic acid	4	97%	2706-90-3
5	Perfluorohexanoic acid	5	97%	307-24-4
6	Perfluoroheptanoic acid	6	98%	375-85-9
7	Perfluorooctanoic acid	7	96%	335-67-1
8	Perfluorononanoic acid	8	97%	375-95-1
	Polyfluorinated propanoate			
9	3,3,3-trifluoropropionic acid		97%	2516-99-6
10	2,3,3,3-tetrafluoropropionic acid		97%	359-49-9
11	2,2,3,3-tetrafluoropropionic acid		97%	756-09-2
	Polyfluorinated acetate			
12	Difluoroacetic acid		98%	381-73-7
13	Sodium monofluoroacetate		95%	62-74-8

Measurement of PFCA Parent Compound Decay and Transformation Products.

Quantification of short-chain PFCAs and sulfite. Concentrations of anions were analyzed by a Dionex ICS-5000 ion chromatography (IC) system equipped with a conductivity detector and suppressor (AERS 4 mm) and a Dionex ICS-6000 EG eluent generator using an EGC 500 KOH cartridge. The separation of organic and fluoroorganic anions used an IonPac AS11-HC analytical column (4 × 250 mm) in line with an AG11-HC guard column (4 × 50 mm). The separation of sulfite used an IonPac AS25 analytical column (4 × 250 mm) in line with an AG25 guard column (4 × 50 mm). Specific methods for each analyte are below:

- TFA and DFA: Isocratic, 1.0 mL min^{-1}, 10 mM KOH, 17°C, 30 minutes;
- MFA and acetate: Gradient, 1.0 mL min^{-1}, 1−20 mM KOH, 30°C, 50 minutes;
- PFPrA: Isocratic, 1.5 mL min^{-1}, 20 mM KOH, 30°C, 20 minutes;
- Polyfluorinated propanoates: Gradient, 1.0 mL min^{-1}, 1−26 mM KOH, 30°C, 33 minutes;
- Sulfite (SO_3^{2-}): Isocratic, 20 mM NaOH, 1.0 mL min^{-1}.

The separation chromatographs and calibration curves are shown in Figure C1.

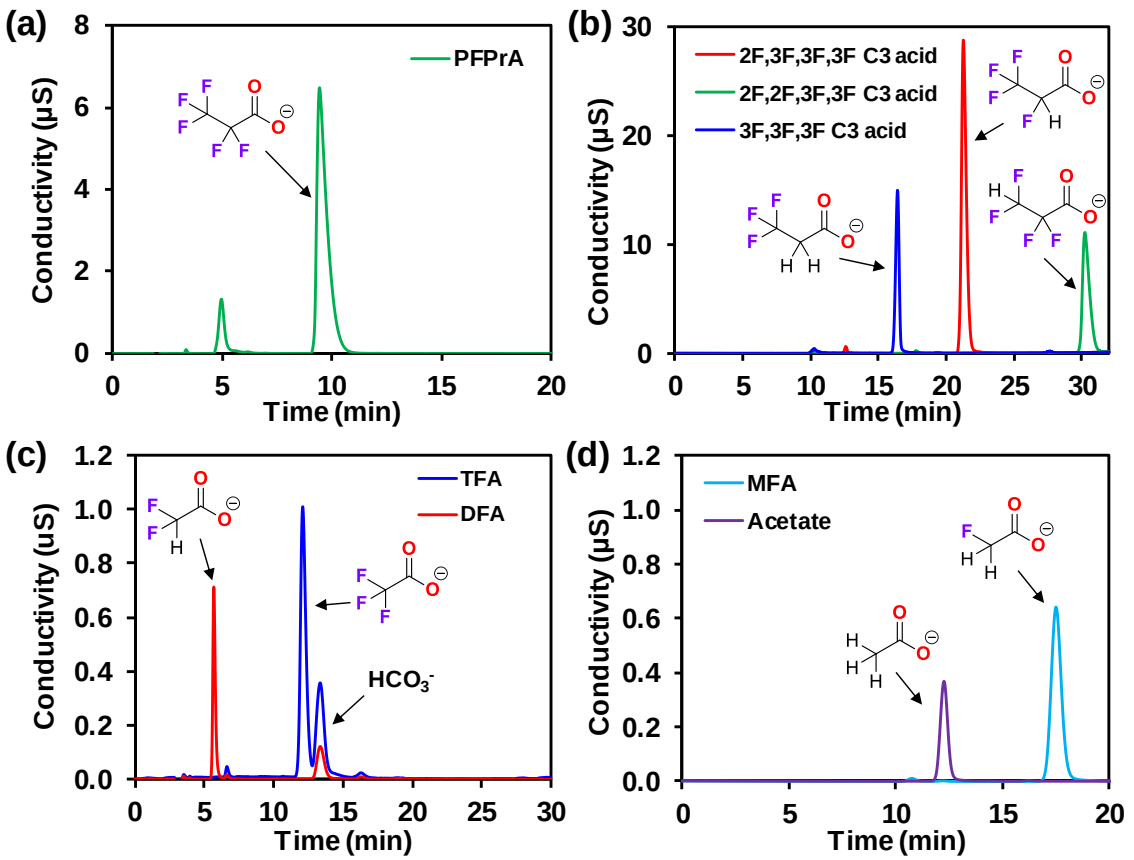

Figure C.1 IC chromatographs of (a) PFPrA, (b) polyfluorinated propanoates, (c) TFA/DFA, and (d) MFA/acetate.

Quantification of long-chain PFASs and transformation products. For C4 PFBA and longer PFCAs, the parent compounds were analyzed by liquid chromatography equipped with a high-resolution quadrupole orbitrap mass spectrometer (LC−HRMS/MS) (Q Exactive, Thermo Fisher Scientific). For the LC separation, a 10-μL sample was loaded onto a Zorbax SB-Aq column (particle size 5μm, 4.6×50 mm, Agilent) and eluted at a flow rate of 350 μL min^{-1} with 10 mM ammonia formate (A) and methanol (B), at the gradient as follows: 100% A for 0−1 min, 2% A for 2−15 min, and 100% A for 16−21 min. Both parent compounds and transformation products were detected in full scan negative ionization mode on HRMS at a resolution of 70,000 at m/z 200 and a scan range of m/z 50−750. The software Xcalibur (Thermo Fisher Scientific) was used for data acquisition and analysis. The limit of quantification (LOQ) for PFCAs was determined as the lowest concentration with a detection variation < 20% (Table C.2).

Table C.2 LOQ of Long-Chain PFCAs.

Entry	Chemical Name	Chain Length (n)	LOQ(nM)
	$F(CF2)_n$−COOH		
1	Perfluorobutyric acid	3	10
2	Perfluoropentanoic acid	4	10
5	Perfluorohexanoic acid	5	10
4	Perfluoroheptanoic acid	6	10
5	Perfluorooctanoic acid	7	10
6	Perfluorononanoic acid	8	10

The suspect screening was carried out to identify transformation products (TPs) as described in our previous study.[1, 2] Briefly, TraceFinder 4.1 EFS (Thermo Fisher Scientific) was used for the acquisition. The TP suspect lists were generated by a self-written automatic product mass prediction script, which includes all possible products from the mechanisms of both *DHEH* chain-shortening and H/F exchange. Plausible TPs were identified based on the following criteria: (*i*) mass tolerance < 5 ppm; (*ii*) isotopic pattern score > 70%; (*iii*) peak area > 10^5; (*iv*) peak area showing either an increasing trend or first showing an increasing trend then followed by a decreasing trend over time.

Quality Assurance and Quality Control (QA/QC). For QA/QC, a mass calibration was performed before each analytical run. We prepared the calibration standards with a PFCA-free solution, which contained all other chemicals (i.e., sulfite and carbonate added at the same concentrations and the same pH) and was treated under the same UV irradiation. This procedure takes into consideration of the matrix effect on LC−MS quantification. The matrix-match standard series included nine concentration points ranging from 1 nM to 5 μM. No PFASs were detected in the Milli-Q water and matrix-match blank controls. Milli-Q water blanks were also run between each group of batch experiment samples and checked for PFAS detection, to avoid any PFAS carry over. All samples were stored at 4°C before measurement. The storage time for all samples was less than three weeks.

Fluoride Analysis. All reactions were monitored for fluoride ion (F^-) release using an ion-selective electrode (ISE, Fisherbrand Accumet) with a Thermo Scientific Orion Versa Star Pro meter. Prior to analysis, each sample (2 mL) was added with an equal volume of the total ionic strength adjustment buffer (TISAB for fluoride electrode, Thermo Scientific). The accuracy of F^- measurement by ISE was validated by IC in our previous work.[1]

Thermodynamic Estimation of the Effect of pH.

In aqueous solutions, e_{aq}^- can be rapidly quenched by H^+:[3]

$$H^+ + e_{aq}^- \rightarrow 0.5\ H_2$$

This reaction is considered as the combination of two half reactions:

$$H^+ + e^- \rightarrow 0.5\ H_2\ (E^0_{cathode} = 0.00\ V)$$

$$e^- \rightarrow e_{aq}^-\ (E^0_{anode} = -2.87\ V)^4$$

The overall reaction potential is:

$$E^0 = E^0_{cathode} - E^0_{anode} = 0.0 - (-2.87) = +2.87\ V$$

Assuming $P_{H2} = 1$ atm and $[e_{aq}^-] = 1$ M,

$$Q = (P_{H2})^{0.5}/[H^+][e_{aq}^-] = 1/[H^+]$$

$$E = E^0 - 0.059 \times \log Q = 2.87 - 0.059\ pH$$

Therefore, $E_{pH\ 9.5} = 2.31$ V and $E_{pH\ 12} = 2.16$ V. From pH 9.5 to pH 12, $\Delta E = -0.15$ V and $\Delta\Delta G = 14.47$ kJ mol^{-1} or 3.46 kcal mol^{-1}.

The positive E values at both pH indicate that the quenching of e_{aq}^- by H^+ is highly favorable. However, the positive $\Delta\Delta G$ from pH 9.5 to pH 12 shows that the quenching becomes less favorable at high pH. The saved Gibbs free energy of 3.46 kcal mol^{-1} may be correlated to the cleavage of more recalcitrant C–F bonds. For example, the relatively strong C–F in TFA (116.8 kcal mol^{-1}) can be directly cleaved at pH 12 but not at pH 9.5. Based on our previous results using pH 9.5,[1, 2] the e_{aq}^- could directly cleave the C–F bond of up to 111.7 kcal mol^{-1} for H/F exchange.

The general reaction for H/F exchange can be written as:

$$C{-}F + H^+ + 2e_{aq}^- \rightarrow C{-}H + F^-$$

This equation can be further modified into:

$$C{-}F + 2H^+ + 2e_{aq}^- + H_2 \rightarrow C{-}H + F^- + H^+ + H_2$$

So that the new equation can be de-coupled into two reactions:

$$2H^+ + 2e_{aq}^- \rightarrow H_2 \qquad (1)$$

$$C{-}F + H_2 \rightarrow C{-}H + F^- + H^+ \qquad (2)$$

Due to the lack of thermodynamic data (e.g., $\Delta_f G^0$) for individual PFAS molecules and defluorination products, for rough estimation, we assume that except for the various C−F bonds, all other species in Equation (2) have the same $\Delta_f G^0$. Thus, from pH 9.5 to pH 12, the saved Gibbs free energy from Equation (1) may partially compensate for the energy needed to break the relatively strong C−F bond in Equation (2).

It must be pointed out that this simplified approach does not consider the potentially elevated concentration of e_{aq}^- and enhanced kinetic factors at pH 12. Substantial future efforts will be necessary to measure those parameters and elucidate detailed mechanisms.

Tables C.3 to C.10 Referred in the Main Text

Table C.3 Quantification of Transformation Products (TPs) from Perfluoropropanoate (PFPrA) Degradation at pH 12 and pH 9.5.

pH 12		**PFPrA**		**TFA**
Time (h)	**$C_3F_5O_2^-$**	$C_3HF_4O_2^-$	$C_3H_2F_3O_2^-$	**$C_2F_3O_2^-$**
0	265.3 µM	2.9 µM[a]	ND	2.9 µM[a]
1	3.6 µM	22.9 µM	11.5 µM	4.3 µM
2	ND	10.5 µM	21.3 µM	5.1 µM
4	ND	4.9 µM	29.6 µM	5.0 µM
8	ND	3.2 µM	33.2 µM	4.5 µM
12	ND	3.1 µM	33.2 µM	5.5 µM
24	ND	3.0 µM	33.6 µM	5.8 µM

pH 9.5		**PFPrA**		**TFA**
Time (h)	**$C_3F_5O_2^-$**	$C_3HF_4O_2^-$	$C_3H_2F_3O_2^-$	**$C_2F_3O_2^-$**
0	264.2 µM	2.9 µM[a]	ND	2.8 µM[a]
1	162.3 µM	11.1 µM	2.4 µM	3.1 µM
2	96.1 µM	18.9 µM	3.1 µM	3.2 µM
4	33.2 µM	27.3 µM	6.2 µM	3.2 µM
8	7.8 µM	26.4 µM	16.1 µM	3.0 µM
12	ND	22.0 µM	24.9 µM	2.9 µM
24	ND	15.5 µM	41.0 µM	2.8 µM

[a]The positive concentrations detected in $t = 0$ samples indicate the presence of these structures as impurities. However, an increased level of these species at the following time intervals suggests the formation of these structures as TPs.

Table C.4 The Maximal Concentrations of the Daughter PFCA and the Ratios to the Parent PFCA (25 μM) at pH 9.5 and pH 12.

PFCA $C_nF_{2n+1}COO^-$	Daughter PFCA $C_{n-1}F_{2n-1}COO^-$	pH 9.5			pH 12			Fold of Enhanced Ratios
		Max. Conc.	Time Observed	Ratio	Max. Conc.	Time Observed	Ratio	
PFHxA	PFPeA	0.113 μM	1 h	0.45%	0.774 μM	1 h	3.1%	6.9
PFHpA	PFHxA	0.192 μM [a]	2 h	0.77%	1.12 μM	1 h	4.5%	5.8
PFOA	PFHpA	0.141 μM [a]	1 h	0.57%	1.42 μM	1 h	5.7%	10
PFNA	PFOA	0.167 μM [a]	1 h	0.67%	1.30 μM	1 h	5.2%	7.8
PFDA	PFNA	0.243 μM [a]	4 h	0.97%	1.41 μM	1 h	5.6%	5.8

[a]The values are 53−75% of those in the previous report[1] due to the modified calibration.

Table C.5 Quantification or Peak Areas of TPs from Perfluorodecanoate (PFDA) Degradation at pH 12.

Note: (*i*) only the perfluorocarboxylates that have pure chemicals as the calibration standard are quantified into molar concentrations; (*ii*) TPs with the same chain length are assumed to be H/F exchange products from the corresponding PFCA.

pH 12	**PFDA**						
Time (h)	**$C_{10}F_{19}O_2^-$**	$C_{10}HF_{18}O_2^-$	$C_{10}H_2F_{17}O_2^-$	$C_{10}H_4F_{15}O_2^-$	$C_{10}H_5F_{14}O_2^-$	$C_{10}H_6F_{13}O_2^-$	$C_{10}H_8F_{11}O_2^-$
0	25 µM	*ND*	*ND*	*ND*	*ND*	*ND*	*ND*
1	0.105 µM	1.33E+07	6.96E+05	1.49E+06	1.77E+05	4.24E+05	*ND*
2	*ND*	3.12E+06	*ND*	3.18E+05	1.79E+05	7.38E+05	*ND*
4	*ND*	9.59E+05	*ND*	*ND*	*ND*	1.08E+06	*ND*
8	*ND*	*ND*	*ND*	*ND*	*ND*	9.56E+05	1.25E+05
12	*ND*	*ND*	*ND*	*ND*	*ND*	7.42E+05	1.42E+05
24	*ND*	*ND*	*ND*	*ND*	*ND*	4.14E+05	*ND*

pH 12	**PFNA (product)**	
Time (h)	**$C_9F_{17}O_2^-$**	$C_9HF_{16}O_2^-$
0	0.018 µM	*ND*
1	1.41 µM	4.88E+05
2	0.900 µM	2.47E+05
4	0.499 µM	1.52E+05
8	0.062 µM	*ND*
12	0.014 µM	*ND*
24	*ND*	*ND*

Table C.6 Quantification or Peak Areas of TPs from Perfluorononanoate (PFNA) Degradation at pH 12.

pH 12	**PFNA**							
Time (h)	**$C_9F_{17}O_2^-$**	$C_9HF_{16}O_2^-$	$C_9H_2F_{15}O_2^-$	$C_9H_3F_{14}O_2^-$	$C_9H_4F_{13}O_2^-$	$C_9H_5F_{12}O_2^-$	$C_9H_6F_{11}O_2^-$	$C_9H_8F_9O_2^-$
0	25 µM	6.27E+06	*ND*	*ND*	*ND*	*ND*	*ND*	*ND*
1	0.277 µM	2.32E+07	1.05E+06	*ND*	1.98E+06	2.77E+05	3.54E+05	*ND*
2	<LOQ	1.00E+07	6.12E+05	*ND*	8.74E+05	2.90E+05	7.21E+05	*ND*
4	*ND*	3.42E+06	*ND*	*ND*	3.68E+05	2.52E+05	1.21E+06	7.96E+04
8	*ND*	6.35E+05	*ND*	*ND*	1.25E+05	1.98E+05	1.60E+06	1.48E+05
12	*ND*	1.15E+05	*ND*	*ND*	1.24E+05	1.75E+05	1.54E+06	1.51E+05
24	*ND*	*ND*	*ND*	*ND*	*ND*	6.73E+04	1.48E+06	1.61E+05

pH 12	**PFOA (product)**	
Time (h)	**$C_8F_{15}O_2^-$**	$C_8HF_{14}O_2^-$
0	0.014 µM	2.34E+05
1	1.30 µM	3.62E+05
2	1.13 µM	3.15E+05
4	0.736 µM	2.51E+05
8	0.201 µM	1.79E+05
12	0.051 µM	1.11E+05
24	<LOQ	1.20E+05

Table C.7 Quantification or Peak Areas of TPs from Perfluorooctanoate (PFOA) Degradation at pH 12.

pH 12	**PFOA**							
Time (h)	**$C_8F_{15}O_2^-$**	$C_8HF_{14}O_2^-$	$C_8H_2F_{13}O_2^-$	$C_8H_3F_{12}O_2^-$	$C_8H_4F_{11}O_2^-$	$C_8H_6F_9O_2^-$	$C_8H_7F_8O_2^-$	$C_8H_8F_7O_2^-$
0	25 µM	2.66E+05	*ND*	*ND*	*ND*	*ND*	*ND*	*ND*
1	0.132 µM	1.47E+07	1.51E+05	1.29E+06	2.00E+05	*ND*	*ND*	*ND*
2	<LOQ	9.33E+06	*ND*	3.27E+05	1.95E+05	4.37E+05	6.95E+04	4.19E+04
4	<LOQ	3.79E+04	*ND*	4.98E+04	1.90E+05	7.55E+05	1.56E+05	3.26E+05
8	<LOQ	5.81E+04	*ND*	*ND*	9.36E+04	8.29E+05	2.38E+05	8.39E+04
12	<LOQ	*ND*	*ND*	*ND*	6.67E+04	9.62E+05	2.69E+05	1.33E+05
24	<LOQ	4.75E+04	*ND*	*ND*	*ND*	8.03E+05	2.12E+05	2.32E+05

pH 12	**PFHpA (product)**	
Time (h)	**$C_7F_{13}O_2^-$**	$C_7HF_{12}O_2^-$
0	0.099 µM	7.27E+04
1	1.42 µM	2.05E+05
2	0.714 µM	1.82E+05
4	0.081 µM	6.64E+04
8	<LOQ	5.72E+04
12	*ND*	4.96E+04
24	*ND*	4.58E+04

Table C.8 Quantification or Peak Areas of TPs from Perfluoroheptanoate (PFHpA) Degradation at pH 12.

pH 12	**PFHpA**						
Time (h)	**$C_7F_{13}O_2^-$**	$C_7HF_{12}O_2^-$	$C_7H_2F_{11}O_2^-$	$C_7H_3F_{10}O_2^-$	$C_7H_5F_8O_2^-$	$C_7H_6F_7O_2^-$	$C_7H_8F_5O_2^-$
0	25 µM	*ND*	*ND*	*ND*	*ND*	*ND*	*ND*
1	0.031 µM	*ND*	*ND*	*ND*	1.16E+05	1.28E+05	1.40E+05
2	<LOQ	*ND*	*ND*	*ND*	1.50E+05	3.20E+05	1.95E+05
4	0.012 µM	*ND*	*ND*	*ND*	1.22E+05	4.48E+05	1.77E+05
8	<LOQ	*ND*	*ND*	*ND*	4.55E+04	5.14E+05	1.89E+05
12	<LOQ	*ND*	*ND*	*ND*	*ND*	5.34E+05	1.47E+05
24	<LOQ	*ND*	*ND*	*ND*	*ND*	4.97E+05	*ND*

pH 12	**PFHxA (product)**	
Time (h)	**$C_6F_{11}O_2^-$**	$C_6HF_{10}O_2^-$
0	0.018 µM	*ND*
1	1.12 µM	*ND*
2	0.646 µM	*ND*
4	0.288 µM	*ND*
8	0.019 µM	*ND*
12	<LOQ	*ND*
24	<LOQ	*ND*

Table C.9 Quantification or Peak Areas of TPs from Perfluorohexanoate (PFHxA) Degradation at pH 12.

pH 12	**PFHxA**				**PFPeA (product)**		
Time (h)	**$C_6F_{11}O_2^-$**	$C_6HF_{10}O_2^-$	$C_6H_2F_9O_2^-$	$C_6H_6F_5O_2^-$	**$C_5F_9O_2^-$**	$C_5HF_8O_2^-$	$C_5H_4F_5O_2^-$
0	25 µM	3.72E+06	*ND*	*ND*	0.016 µM	*ND*	*ND*
1	<LOQ	1.73E+05	*ND*	1.38E+05	0.774 µM	*ND*	*ND*
2	<LOQ	*ND*	*ND*	2.48E+05	0.544 µM	*ND*	1.07E+05
4	<LOQ	1.02E+05	*ND*	3.38E+05	0.082 µM	*ND*	9.33E+04
8	<LOQ	9.02E+04	*ND*	4.13E+05	0.018 µM	*ND*	9.47E+04
12	<LOQ	*ND*	*ND*	3.78E+05	<LOQ	*ND*	1.23E+05
24	<LOQ	8.41E+04	*ND*	3.56E+05	<LOQ	*ND*	8.40E+04

Table C.10 Quantification of Perfluoropentanoate (PFPeA) and Perfluorobutanoate (PFBA) Degradation at pH 12.

Note: Product analysis of these two relatively short PFCAs on the LC−HRMS was challenging.

pH 12	**PFPeA**	**PFBA**
Time (h)	**$C_5F_9O_2^-$**	**$C_4F_7O_2^-$**
0	25 µM	25 µM
1	0.113 µM	<LOQ
2	0.032 µM	*ND*
4	<LOQ	*ND*
8	<LOQ	*ND*
12	<LOQ	*ND*
24	<LOQ	*ND*

Figures C.2 to C.6 Referred in the Main Text

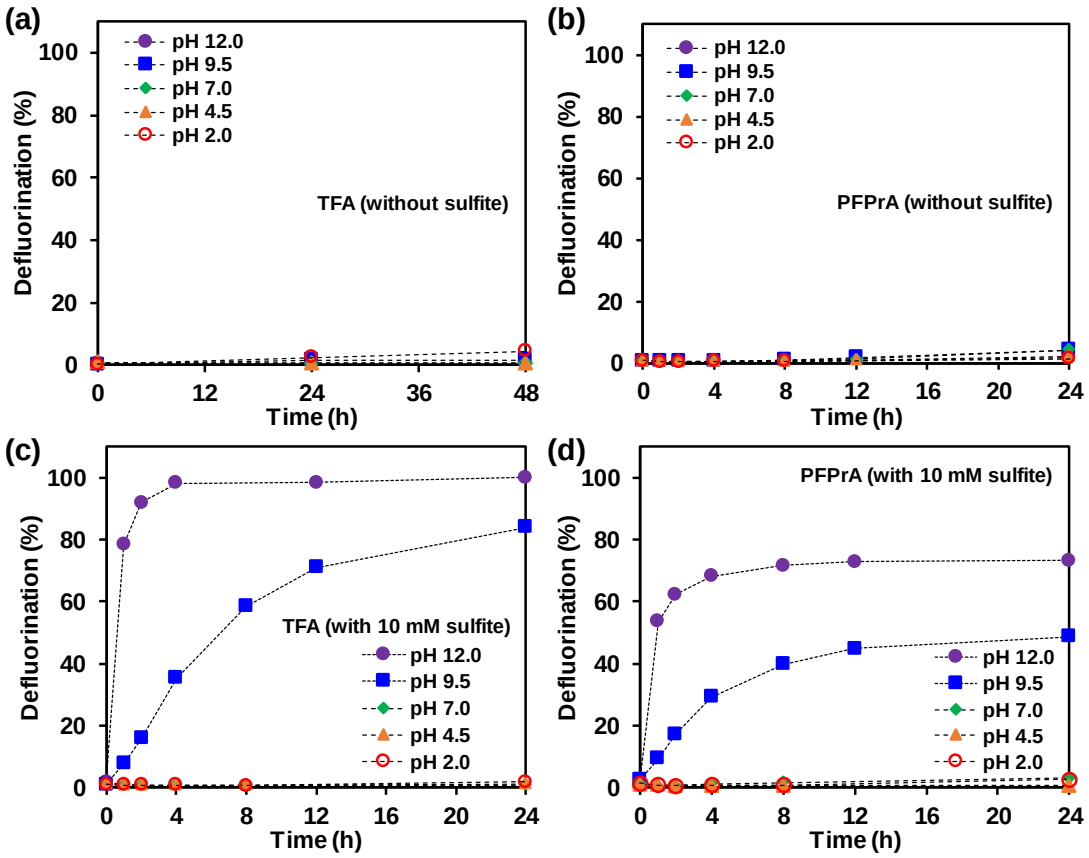

Figure C.2 Defluorination of n = 1 TFA and n = 2 PFPrA at various solution pH with and without sulfite addition. *Reaction conditions*: individual PFCA (0.025 mM), carbonate buffer (5 mM), 254 nm irradiation (an 18 W low-pressure Hg lamp for 600 mL solution) and 20 °C.

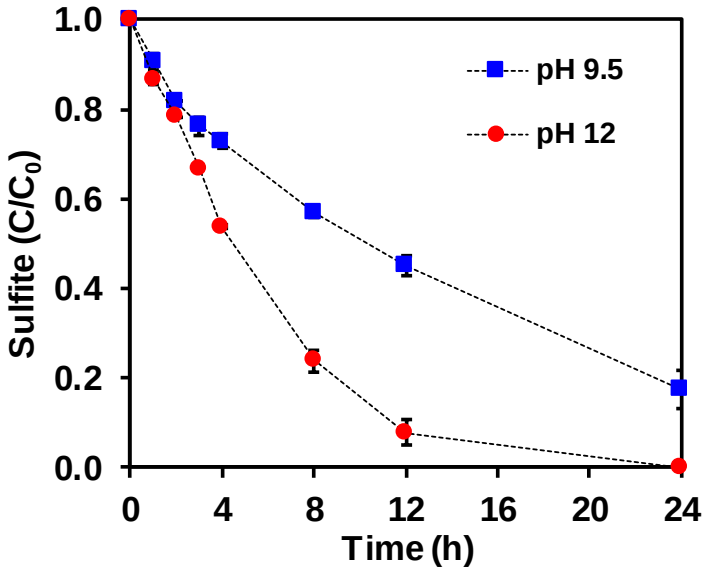

Figure C.3 The decay of SO_3^{2-} at pH 9.5 and pH 12. *Reaction conditions*: Na_2SO_3 (10 mM), carbonate buffer (5 mM), 254 nm irradiation (an 18 W low-pressure Hg lamp for 600 mL solution) and 20 °C.

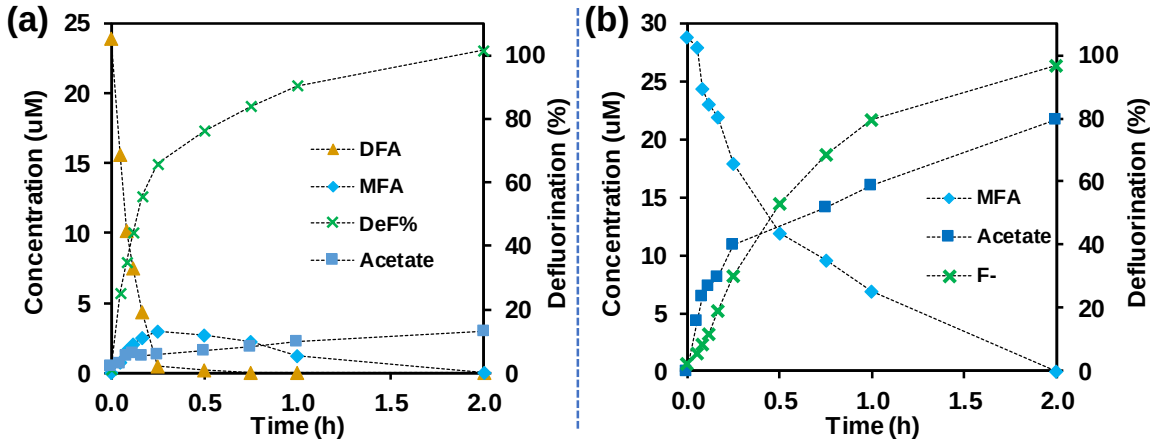

Figure C.4 The degradation, defluorination, and transformation product formation for (a) DFA and (b) MFA. *Reaction conditions*: PFAS (0.025 mM), Na_2SO_3 (10 mM), carbonate buffer (5 mM), 254 nm irradiation (18 W low-pressure Hg lamp), pH 12 and 20 °C.

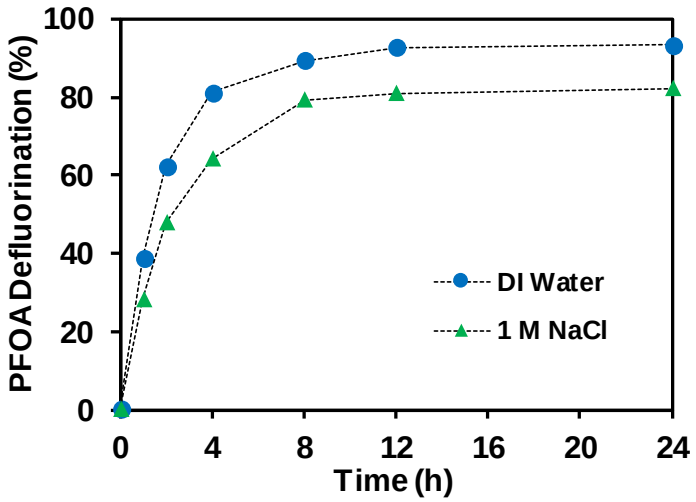

Figure C.5 PFOA degradation in DI water and in 1 M NaCl brine at pH 12. *Reaction conditions*: PFOA (0.025 mM), carbonate buffer (5 mM), 254 nm irradiation (18 W low-pressure Hg lamp) and 20 °C.

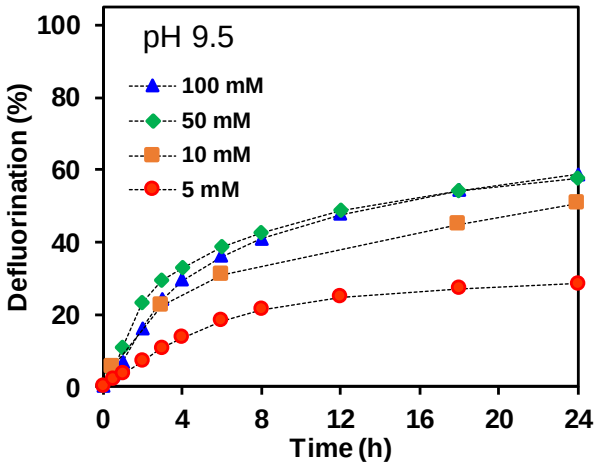

Figure C.6 PFOA degradation with various sulfite concentrations at pH 9.5. *Reaction conditions*: PFOA (0.025 mM), carbonate buffer (5 mM), 254 nm irradiation (18 W low-pressure Hg lamp) and 20 °C.

REFERENCES

(1) Bentel, M. J.; Yu, Y.; Xu, L.; Li, Z.; Wong, B. M.; Men, Y.; Liu, J., Defluorination of per- and polyfluoroalkyl substances (PFASs) with hydrated electrons: Structural dependence and implications to PFAS remediation and management. *Environ. Sci. Technol.* **2019,** *53*, 3718-3728.

(2) Bentel, M. J.; Yu, Y.; Xu, L.; Kwon, H.; Li, Z.; Wong, B. M.; Men, Y.; Liu, J., Degradation of perfluoroalkyl ether carboxylic acids with hydrated electrons: Structure–reactivity relationships and environmental implications. *Environ. Sci. Technol.* **2020,** *54*, 2489-2499.

(3) Jortner, J.; Noyes, R. M., Some thermodynamic properties of the hydrated electron. *J. Phys. Chem.* **1966,** *70*, 770-774.

(4) Schwarz, H. A., Free radicals generated by radiolysis of aqueous solutions. *J. Chem. Educ.* **1981**, *58*, 101-105.

APPENDIX D: APPENDICES FOR CHAPTER 5

Detailed Information on Materials and Methods

Chemicals and the Preparation of PFCAm Stock Solutions. Per- and polyfluorinated carboxamides (PFCAms) and carboxylic acids (PFCAs) were purchased from Acros Organics, Alfa-Aesar, MP Biomedicals, Oakwood Chemicals, Sigma-Aldrich, and SynQuest Laboratories. **Table A1** summarizes the name, purity, and CAS number of all PFCAms included in this study. All other chemicals and solvents were purchased from Fisher Chemical. Individual PFCAms were dissolved in methonal as 10-50 mM stock solutions. All PFCAms stock solutions were wrapped in parafilm and stored on the benchtop at room temperature (20°C).

Table D.1 Information of PFCAms Used in This Study.

Entry	Chemical Name	Fluoroalkyl Length (n)	Purity	CAS#
	$F(CF_2)_n-CONH_2$			
1	Trifluoroamide	1	98	354-38-1
2	Perfluoropropanamide	2	97	354-76-7
3	Perfluorobutanamide	3	98	662-50-0
4	Perfluoropentanamide	4	N/A	13485-61-5
5	Perfluorohexanamide	5	97	335-54-6
6	Perfluorooctanamide	7	97	423-54-1
7	Perfluorodecanamide	9	97	307-40-4
	$H_2NOC-(CF_2)_n-CONH_2$			
8	2,2-difluoromalonamide	1	90	425-99-0
9	Tetrafluorosuccinamide	2	98	377-37-7
10	Hexafluoroglutaramide	3	97	507-68-6
11	Octafluoroadipamide	4	97	355-66-8
	Polyfluorinated amide			
12	2,2-difluoroacetamide		97	359-38-6
13	2,2-difluoropropanamide		97	49781-48-8
14	3,3,3-trifluoropropanmide		97	460-75-3
	$F(CF_2)_n-CONR_2$			
15	Perfluorooctaneamido ammonium salt	7	97	45305-66-6

Measurement of PFCA Parent Compound Decay and Transformation Products.

Quantification of short-chain transformation products. Concentrations of organic and inorganic anions were analyzed by a Dionex ICS-5000 ion chromatography (IC) system equipped with a conductivity detector and suppressor (AERS 4 mm) and a Dionex ICS-6000 EG eluent generator using an EGC 500 KOH cartridge. The separation of organic, fluoro-organic, and inorganic anions used an IonPac AS11-HC analytical column (4 × 250 mm) in line with an AG11-HC guard column (4 × 50 mm).

Table D.2 Summary of IC instrument methods.

PFPrA method	
Flowrate	1.5 mL min^{-1}
Concentration	20 mM KOH
Column Temperature	30°C
Analyte(s)	Perfluoropropanoate

TFA method	
Flowrate	1.0 mL min^{-1}
Concentration	10 mM KOH
Column Temperature	17°C
Analyte(s)	Trifluoroacetate

Small−molecule method	
Flowrate	1.0 mL min^{-1}
Concentration	Gradient
0−5 min	1 mM KOH
5−21 min	8 mM KOH
21−27 min	14 mM KOH
27−33 min	26 mM KOH
33−43 min	45 mM KOH
43−60 min	1 mM KOH
Column Temperature	30°C
Analyte(s)	
Organic	*Fluoro-organic*
Formate	Monofluoroacetate
Acetate	Difluoroacetate
Propanoate	2-monofluoropropanoate
	2,2-difluoropropanoate
	3,3,3-trifluoropropanoate
	2,3,3,3-tetrafluoropropanoate

Quantification of PFAS parent compound and transformation products. High-performance liquid chromatography coupled to high-resolution tandem mass spectrometry (HPLC-HRMS/MS) analysis. Concentrations of the parent compound and transformation products were analyzed by high-performance liquid chromatography coupled to a high-resolution quadrupole orbitrap mass spectrometer (HPLC-HRMS/MS, Q Exactive, Thermo Fisher Scientific). For HPLC analysis, a 2 μL sample was loaded onto a Hypersil GOLD column (particle size 1.9 μm, 100×2.1 mm, Thermo Fisher Scientific), and eluted at a flow rate of 300 μL/min with nano-pure water (A) and methanol (B) (both amended with 10 mM ammonium acetate). The linear gradient for LC separation was set as follows: 95% A:0−1 min, 95%−5% A:1−6 min, 5% A: 6−8 min, and 95% A: 8−10 min. For HRMS, mass spectra were acquired in full scan mode at a resolution of 70,000 at m/z 200 and a scan range of m/z 50 − 750 under negative/positive switch ionization (ESI) mode. For data-dependent MS^2 acquisition, MS^2 fragments were obtained at a resolution of 17,500 with stepped normalized collision energy at 15, 26, and 35. The Xcalibur 4.0 and TraceFinder 4.1 EFS (Thermo Fisher Scientific) were used for data acquisition and analysis as described in our previous publications.[1–3] The limit of quantification (LOQ) for PFCAs was determined as the lowest concentration with a detection variation < 20% (**Table D.3**).

Table D.3 LOQ of PFCAs.

Entry	Chemical Name	Chain Length (n)	LOQ (nM)
	$F(CF_2)_n$−COOH		
1	Trifluoroacetic acid	1	50
2	Perfluoropropionic acid	2	100
5	Perfluorobutyric acid	3	25
4	Perfluoropentanoic acid	4	50
5	Perfluorohexanoic acid	5	25
6	Perfluoroheptanoic acid	6	25
7	Perfluorooctanoic acid	7	25
8	Perfluorononanoic acid	8	10

Transformation products (TPs) were identified by suspect screening as described in our previous study.[1, 2] Briefly, TraceFinder 4.1 EFS (Thermo Fisher Scientific) was used for the screening. The TP suspect lists were generated by a self−written automatic product mass prediction script, which includes all possible products from the mechanisms of both *DHEH* chain−shortening and H/F exchange. Plausible TPs were identified based on the following criteria: (*i*) mass tolerance < 5 ppm; (*ii*) isotopic pattern score > 70%; (*iii*) peak area > 10^5; (*iv*) peak area showing either an increasing trend or first showing an increasing trend then followed by a decreasing trend over time.

Quality Assurance and Quality Control (QA/QC). For QA/QC, the mass detector was calibrated using Pierce ESI Positive/Negative Ion Calibration Solutions (Thermo Scientific) every time before each analytical run. For samples quantification, PFCA standards was prepared in a PFCA−free solution, which contained all other chemicals (i.e., sulfite and carbonate added at the same concentrations and the same pH) and was treated under the same UV irradiation. This procedure takes into consideration of the matrix effect on LC−MS quantification. The matrix−match standard series included eleven concentration points ranging from 10 nM to 2 μM. No PFASs were detected in the Milli−Q water, pure methanol, and matrix−match blank controls. One Milli−Q water and one methanol blanks were also run between each group of batch experiment samples and checked for PFAS detection, to avoid any PFAS carry over. The storage time for all samples was less than three weeks before measurement.

Fluoride Analysis. All reactions were monitored for fluoride ion (F^-) release using an ion−selective electrode (ISE, Fisherbrand Accumet) with a Thermo Scientific Orion Versa Star Pro meter. Prior to analysis, each sample (2 mL) was added with an equal volume of total ionic strength adjustment buffer (TISAB for fluoride electrode, Thermo Scientific). The accuracy of F^- measurement by ISE was validated by IC in our previous work.[1]

Ammonia Analysis. All PFCAm structures were prepared in Milli−Q water and free ammonia (NH_3) was quantified by using an ammonium test (Ammonium LR with Vario Vial Test, 0.02−2.5 mg/L N, Lovibond) and measuring the absorbance at 655 nm (Hach DR3900 spectrophotometer). Prior to analysis, PFCAm methanol solution was diluted in water to 25 μM and subsequently added to an ammonium test vial (2 mL). Following the salicylate method, immediately after addition to vial, reagent packets were added to the vial and mixed until dissolution. Briefly, the salicylate method is a two−step procedure:

(1) ammonia is reacted with hypochlorite to form monochloroamine (a) which reacts with salicylate to form 5−aminosalicylate (b);

(a) 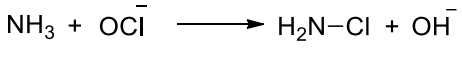

(b) 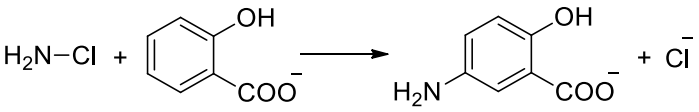

(2) oxidation of 5−aminosalicylate in the presence of a catalyst forming indosalicylate, a blue−colored compound.

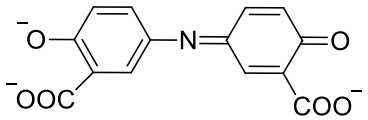

After the reaction is complete (20 minutes), the absorbance was measured and the concentration calculated based on a six−point calibration. This procedure relies on basic conditions (pH >12), therefore the measured ammonia is due to the base−hydrolysis of PFCAms within 20 minutes.

Tables D.4 to D.10 Referred in the Main Text

Table D.4 Quantification by LC–HRMS of PFAS Reactants and Products from Perfluorooctamide (PFOAm) Degradation.

LC–ESI–HRMS	**n=7 PFOA**	**n=6 PFHpA**	**n=5 PFHxA**	**n=4 PFPeA**	**n=3 PFBA**	**n=2 PFPrA**
Time (h)	$C_8F_{15}O_2^-$	$C_7F_{13}O_2^-$	$C_6F_{11}O_2^-$	$C_5F_9O_2^-$	$C_4F_7O_2^-$	$C_3F_5O_2^-$
0	21.85 µM	0.204 µM	ND	*ND*	*ND*	*ND*
0.08 (5 min)	20.36 µM	0.194 µM	0.061 µM	0.064 µM	*ND*	0.089 µM
0.17 (10 min)	17.13 µM	0.169 µM	0.107 µM	0.090 µM	*ND*	0.075 µM
0.25 (15 min)	12.75 µM	0.180 µM	0.146 µM	0.081 µM	0.068 µM	0.131 µM
0.50 (30 min)	8.79 µM	0.193 µM	0.185 µM	0.094 µM	0.084 µM	0.133 µM
0.75 (45 min)	3.19 µM	0.153 µM	0.206µM	0.093 µM	0.084 µM	0.148 µM
1	1.23 µM	0.125 µM	0.159µM	0.050 µM	*ND*	0.192 µM
2	0.77 µM	0.139 µM	0.074 µM	0.026 µM	*ND*	0.051 µM
4	0.45 µM	0.127 µM	*ND*	*ND*	*ND*	*ND*
8	0.29 µM	0.102 µM	*ND*	*ND*	*ND*	*ND*
12	*ND*	0.075 µM	*ND*	*ND*	*ND*	*ND*

LC–ESI–HRMS	**n=1 TFA**	**3F,3F,3F C3 COOH**
Time (h)	$C_2F_3O_2^-$	$C_3H_2F_3O_2^-$
0	*ND*	16.28 µM
0.08 (5 min)	0.234 µM	17.94 µM
0.17 (10 min)	0.375 µM	16.53 µM
0.25 (15 min)	0.324 µM	13.91 µM
0.50 (30 min)	0.313 µM	20.47 µM
0.75 (45 min)	0.569 µM	17.53 µM
1	0.433 µM	16.92 µM
2	0.286 µM	23.41 µM
4	0.205 µM	26.02 µM
8	*ND*	27.38 µM
12	*ND*	22.95 µM

Table D.5 Quantification by LC–ESI–HRMS of PFAS Reactants and Products from Perfluorooctamide Ammonium Salt (PFOAAmS) Degradation.

LC–ESI–HRMS	**n=7 PFOA**	**n=6 PFHpA**	**n=5 PFHxA**	**n=4 PFPeA**	**n=3 PFBA**	**n=2 PFPrA**
Time (h)	$C_8F_{15}O_2^-$	$C_7F_{13}O_2^-$	$C_6F_{11}O_2^-$	$C_5F_9O_2^-$	$C_4F_7O_2^-$	$C_3F_5O_2^-$
0	15.18 µM	0.073 µM	*ND*	*ND*	*ND*	*ND*
0.02 (1 min)	11.97 µM	0.037 µM	*ND*	*ND*	*ND*	0.042 µM
0.03 (2 min)	7.91 µM	0.079 µM	0.091 µM	*ND*	*ND*	0.181 µM
0.05 (3 min)	4.37 µM	0.072 µM	0.171 µM	*ND*	0.056 µM	*ND*
0.07 (4 min)	1.85 µM	0.080 µM	0.198 µM	*ND*	0.102 µM	0.242 µM
0.08 (5 min)	1.23 µM	0.092 µM	0.203 µM	0.041 µM	0.123 µM	0.089 µM
0.25 (15 min)	*ND*	0.109 µM	0.202 µM	0.061 µM	0.085 µM	0.039 µM
0.50 (30 min)	*ND*	0.153 µM	0.146 µM	0.065 µM	0.086 µM	0.251 µM
1	*ND*	0.154 µM	0.142 µM	0.035 µM	0.060 µM	0.084 µM
2	*ND*	0.211 µM	0.096 µM	*ND*	0.090 µM	0.105 µM
4	*ND*	0.068 µM	0.062 µM	*ND*	0.042 µM	0.049 µM
8	*ND*	*ND*	*ND*	*ND*	*ND*	*ND*
12	*ND*	*ND*	*ND*	*ND*	*ND*	*ND*

LC–ESI–HRMS	**n=1 TFA**	**3F,3F,3F C3 COOH**
Time (h)	$C_2F_3O_2^-$	$C_3H_2F_3O_2^-$
0	*ND*	13.42 µM
0.02 (1 min)	*ND*	11.16 µM
0.03 (2 min)	0.344 µM	11.59 µM
0.05 (3 min)	0.423 µM	16.72 µM
0.07 (4 min)	0.512 µM	16.91 µM
0.08 (5 min)	0.602 µM	13.05 µM
0.25 (15 min)	0.627 µM	14.19 µM
0.50 (30 min)	0.572 µM	16.08 µM
1	0.330 µM	14.24 µM
2	0.257 µM	15.82 µM
4	0.204 µM	22.41 µM
8	*ND*	26.93 µM
12	*ND*	28.64 µM

Table D.6 Quantification by LC–ESI–HRMS of PFAS Reactants and Products from Perfluorohexamide (PFHxAm) Degradation.

LC–ESI–HRMS	**n=5 PFHxA**	**n=4 PFPeA**	**n=3 PFBA**	**n=2 PFPrA**	**n=1 TFA**	**3F,3F,3F C3 COOH**
Time (h)	$C_6F_{11}O_2^-$	$C_5F_9O_2^-$	$C_4F_7O_2^-$	$C_3F_5O_2^-$	$C_2F_3O_2^-$	$C_3H_2F_3O_2^-$
0	24.31 μM	*ND*	*ND*	*ND*	*ND*	15.00 μM
0.08 (5 min)	4.70 μM	0.099 μM	0.155 μM	0.743 μM	0.479 μM	9.57 μM
0.17 (10 min)	4.28 μM	*ND*	0.098 μM	0.479 μM	0.465 μM	14.42 μM
0.25 (15 min)	2.67 μM	0.103 μM	0.053 μM	0.183 μM	0.441 μM	8.12 μM
0.50 (30 min)	4.11 μM	0.072 μM	0.070 μM	0.093 μM	0.389 μM	13.44 μM
0.75 (45 min)	2.72 μM	0.021 μM	0.054 μM	0.058 μM	0.293 μM	13.09 μM
1	3.58 μM	0.026 μM	0.053 μM	0.065 μM	0.334 μM	14.78 μM
2	0.82 μM	0.037 μM	*ND*	*ND*	0.234 μM	17.64 μM
4	0.48 μM	0.042 μM	*ND*	*ND*	*ND*	18.50 μM
8	*ND*	*ND*	*ND*	*ND*	*ND*	19.94 μM
12	*ND*	*ND*	*ND*	*ND*	*ND*	19.43 μM

Table D.7 Quantification by LC–ESI–HRMS of PFAS Reactants and Products from Perfluoropentamide (PFPeAm) Degradation.

LC–ESI–HRMS	**n=4 PFPeA**	**n=3 PFBA**	**n=2 PFPrA**	**n=1 TFA**	**3F,3F,3F C3 COOH**
Time (h)	$C_5F_9O_2^-$	$C_4F_7O_2^-$	$C_3F_5O_2^-$	$C_2F_3O_2^-$	$C_3H_2F_3O_2^-$
0	27.51 μM	*ND*	*ND*	*ND*	12.68 μM
0.08 (5 min)	2.87 μM	0.106 μM	0.161 μM	1.154 μM	13.58 μM
0.17 (10 min)	0.71 μM	0.128 μM	0.136 μM	0.765 μM	11.77 μM
0.25 (15 min)	0.68 μM	0.049 μM	ND	0.461 μM	10.33 μM
0.50 (30 min)	0.68 μM	0.124 μM	0.120 μM	0.279 μM	12.56 μM
0.75 (45 min)	0.53 μM	0.178 μM	0.086 μM	0.309 μM	8.92 μM
1	0.33 μM	0.132 μM	0.108 μM	0.213 μM	14.95 μM
2	*ND*	0.125 μM	0.039 μM	*ND*	15.18 μM
4	*ND*	*ND*	*ND*	*ND*	23.93 μM
8	*ND*	*ND*	*ND*	*ND*	24.64 μM
12	*ND*	*ND*	*ND*	*ND*	22.45 μM

Table D.8 Quantification by LC–ESI–HRMS of PFAS Reactants and Products from Perfluorobutamide (PFBAm) Degradation.

LC–ESI–HRMS	**n=3 PFBA**	**n=2 PFPrA**	**n=1 TFA**	**2F,3F,3F,3F C3 COOH**	**3F,3F,3F C3 COOH**
Time (h)	$C_4F_7O_2^-$	$C_3F_5O_2^-$	$C_2F_3O_2^-$	$C_3HF_4O_2^-$	$C_3H_2F_3O_2^-$
0	21.90 μM	*ND*	*ND*	0.062 μM	9.59 μM
0.08 (5 min)	4.83 μM	*ND*	1.72 μM	0.061 μM	11.89 μM
0.17 (10 min)	1.79 μM	0.072 μM	0.33 μM	*ND*	14.70 μM
0.25 (15 min)	1.75 μM	0.113 μM	0.20 μM	0.093 μM	15.66 μM
0.50 (30 min)	2.05 μM	*ND*	*ND*	*ND*	12.88 μM
0.75 (45 min)	1.49 μM	0.042 μM	*ND*	*ND*	14.77 μM
1	1.30 μM	0.104 μM	*ND*	*ND*	10.70 μM
2	0.86 μM	*ND*	*ND*	0.056 μM	16.94 μM
4	0.27 μM	*ND*	*ND*	0.044 μM	20.32 μM
8	*ND*	*ND*	*ND*	*ND*	21.88 μM
12	*ND*	*ND*	*ND*	*ND*	21.41 μM

Table D.9 Quantification by IC and LC–ESI–HRMS of PFAS Reactants and Products from Perfluoropropanamide (PFPrAm) Degradation.

IC	n=2 PFPrA	2F,3F,3F,3F C3 COOH	3F,3F,3F C3 COOH
Time (min)	$C_3F_5O_2^-$	$C_3HF_4O_2^-$	$C_3H_2F_3O_2^-$
0	25.1 µM	*ND*	*ND*
5	8.22 µM	8.67 µM	*ND*
10	8.67 µM	2.67 µM	3.95 µM
15	8.44 µM	*ND*	7.91 µM
30	8.22 µM	*ND*	14.88 µM
45	8.00 µM	*ND*	16.51 µM
60	6.00 µM	*ND*	16.51 µM
120	4.00 µM	*ND*	17.21 µM
240	0.67 µM	*ND*	16.74 µM
480	*ND*	*DNM*	*DNM*
720	*ND*	*DNM*	*DNM*

Table D.10 Quantification by IC and LC–ESI–HRMS of PFAS Reactants and Products from Trifluoroacetamide (TFAm) Degradation.

	n=1
IC	**TFA**
Time (min)	$C_2F_3O_2^-$
0	24.1 ± 1.8 μM
5	14.3 ± 0.0 μM
10	12.7 ± 0.0 μM
15	9.2 ± 0.8 μM
30	8.3 ± 0.6 μM
45	8.5 ± 0.2 μM
60	8.0 ± 0.3 μM
120	6.6 ± 0.8 μM
240	4.3 ± 0.2 μM

Figures D.1 to D.17 Referred in the Main Text

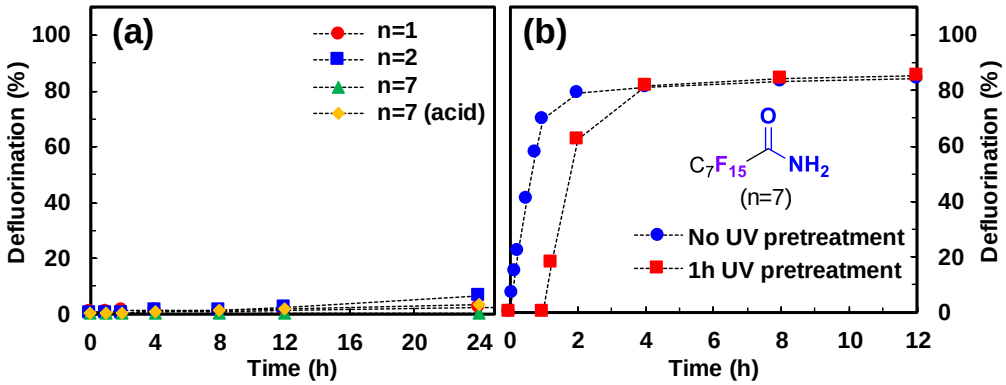

Figure 0.1 (a) Defluorination from UV control experiments (i.e., no sulfite) for PFCAms (*n*=1 TFAm, *n*=2 PFPrAm, and *n*=7 PFOAm) and PFCA (*n*=7 PFOA); (b) defluorination comparison of *n*=7 PFOAm with 10 mM sulfite addition at 0 h and at 1 h (i.e., PFOAm subjected to "1 h UV pretreatment"). *Reaction conditions*: PFCA(m) (0.025 mM), carbonate buffer (5 mM), 254 nm irradiation (an 18 W low-pressure Hg lamp for 600 mL solution), pH 9.5 and 20 °C.

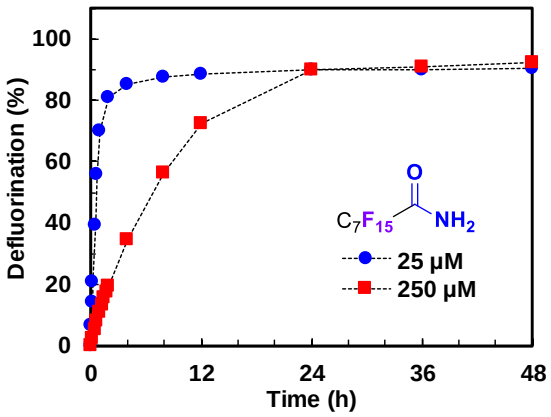

Figure D.2 Defluorination profile for the treatment of 25 µM and 250 µM perfluorooctamide (PFOAm). *Reaction conditions*: Na_2SO_3 (10 mM), carbonate buffer (5 mM), 254 nm irradiation (an 18 W low-pressure Hg lamp for 600 mL solution), pH 9.5 and 20 °C.

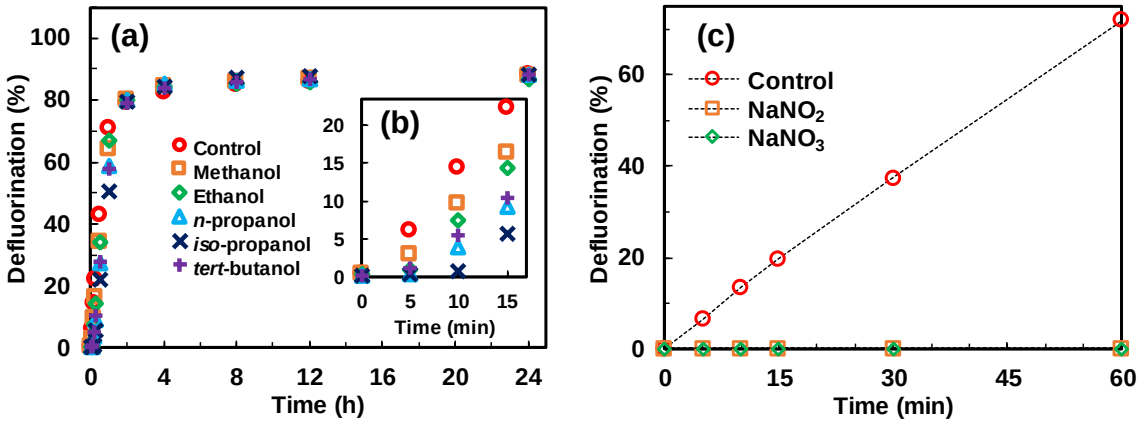

Figure D.3 Defluorination profile for PFOAm with (a) oxidant radical scavengers (100 mM), (b) inset of (a); and (c) hydrated electron (e_{aq}^-) scavengers ($NaNO_2$=10 mM; $NaNO_3$=10 mM). *Reaction conditions*: PFOAm (25 μM), Na_2SO_3 (10 mM), carbonate buffer (5 mM), 254 nm irradiation (an 18 W low-pressure Hg lamp for 600 mL solution), pH 9.5 and 20 °C.

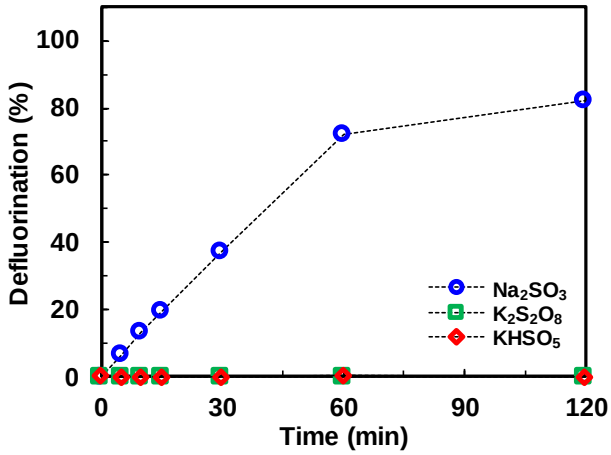

Figure D.4 Defluorination profile for PFOAm treated with various photochemically active sulfur oxyanions, including sodium sulfite (Na_2SO_3), potassium persulfate ($K_2S_2O_8$), and potassium peroxymonosulfate ($KHSO_5$). *Reaction conditions*: PFOAm (25 μM), sulfur oxyanion (10 mM), carbonate buffer (5 mM), 254 nm irradiation (an 18 W low−pressure Hg lamp for 600 mL solution), pH 9.5 and 20 °C.

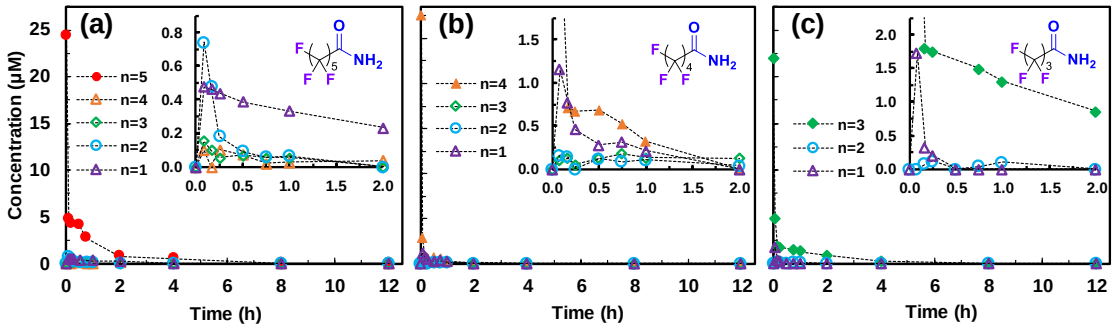

Figure D.5 LC–ESI–HRMS results for decay and product generation of (a) *n*=5 PFHxAm, (b) *n*=4 PFPeAm, and (c) *n*=3 PFBAm *Reaction conditions*: PFCAm (0.025 mM), Na_2SO_3 (10 mM), carbonate buffer (5 mM), 254 nm irradiation (an 18 W low−pressure Hg lamp for 600 mL solution), pH 9.5 and 20 °C.

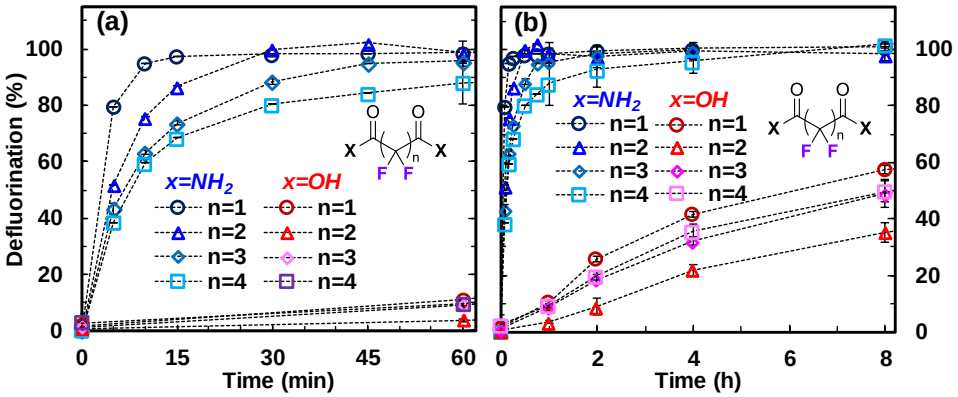

Figure D.6 Defluorination profiles for perfluoroalkylated dicarboxamides [$H_2N{-}(CF_2)_n{-}NH_2$] and dicarboxylates [$^{-}OOC{-}(CF_2)_n{-}COO^{-}$]. *Reaction conditions*: PF*di*CA(m) (0.025 mM), Na_2SO_3 (10 mM), carbonate buffer (5 mM), 254 nm irradiation (an 18 W low-pressure Hg lamp for 600 mL solution), pH 9.5 and 20 °C.

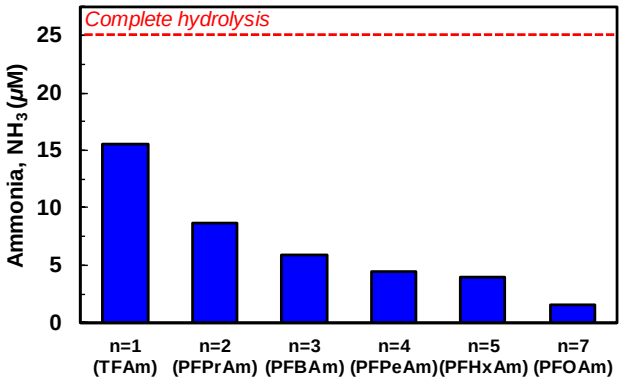

Figure D.7 Ammonia release due to hydrolysis from PFCAms. *Reaction conditions*: PFCAm (0.025 mM), Na_2SO_3 (10 mM), carbonate buffer (5 mM).

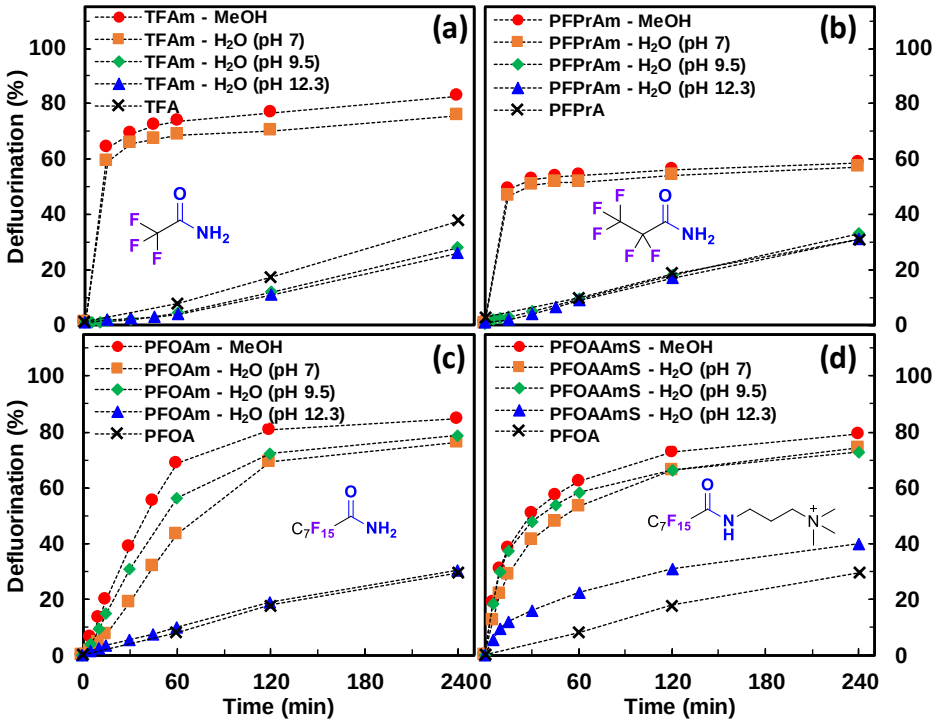

Figure D.8 Defluorination profiles for PFCAm stability studies in different solvents and solution pH for (a) *n*=1 TFAm, (b) *n*=2 PFPrAm, (c) *n*=7 PFOAm, and (d) *n*=7 PFOAAmS. *Reaction conditions*: PFCAm (0.025 mM), Na_2SO_3 (10 mM), carbonate buffer (5 mM), 254 nm irradiation (an 18 W low-pressure Hg lamp for 600 mL solution), pH 9.5 and 20 °C.

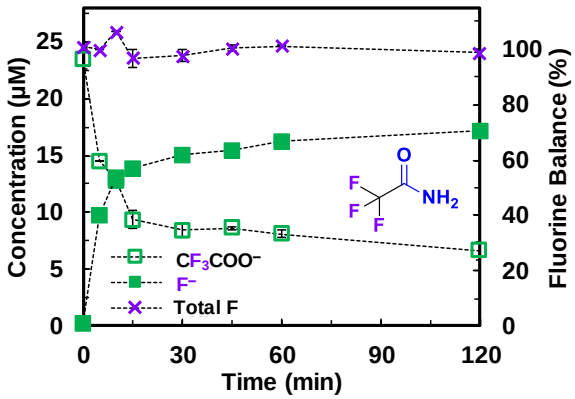

Figure D.9 IC results for decay and product generation of *n*=1 TFAm. *Reaction conditions*: TFAm (0.025 mM), Na_2SO_3 (10 mM), carbonate buffer (5 mM), 254 nm irradiation (an 18 W low-pressure Hg lamp for 600 mL solution), pH 9.5 and 20 °C.

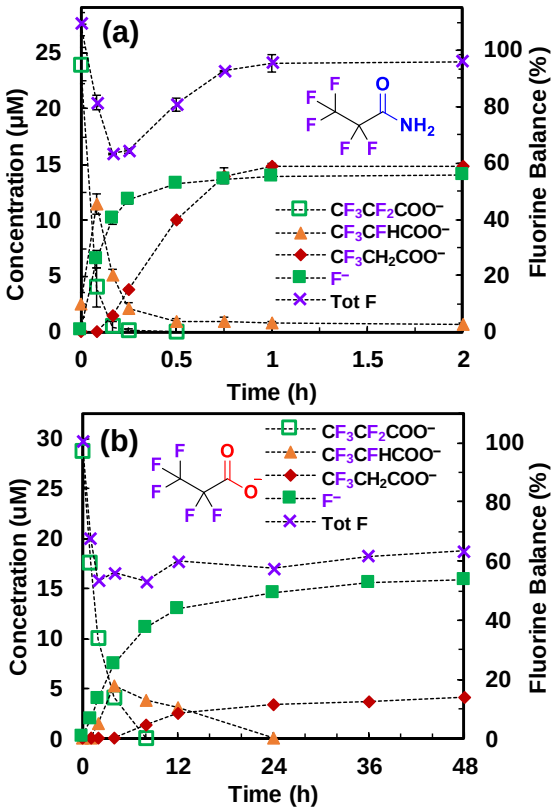

Figure D.10 IC results for decay and product generation of (a) *n* = 2 PFPrAm and (b) *n*=2 perfluoropropanoate (PFPrA). *Reaction conditions*: PFCA(m) (0.025 mM), Na_2SO_3 (10 mM), carbonate buffer (5 mM), 254 nm irradiation (an 18 W low-pressure Hg lamp for 600 mL solution), pH 9.5 and 20 °C.

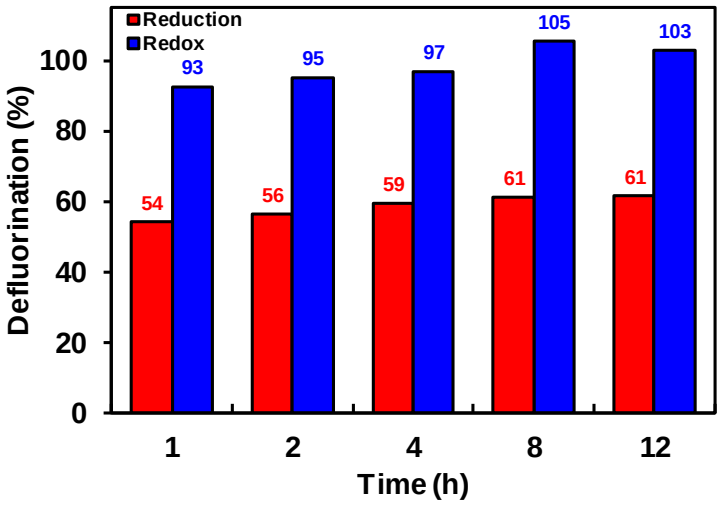

Figure D.11 Fluoride recovery from combined reduction−oxidation for *n*=2 PFPrAm. *Reduction reaction conditions*: PFPrAm (0.025 mM), Na_2SO_3 (10 mM), carbonate buffer (5 mM), 254 nm irradiation (an 18 W low-pressure Hg lamp for 600 mL solution), pH 9.5 and 20 °C. *Oxidation reaction conditions*: reduction sample time point (3 mL), potassium persulfate (2.5 mM), pH 12 and 120 °C, 40 minutes.

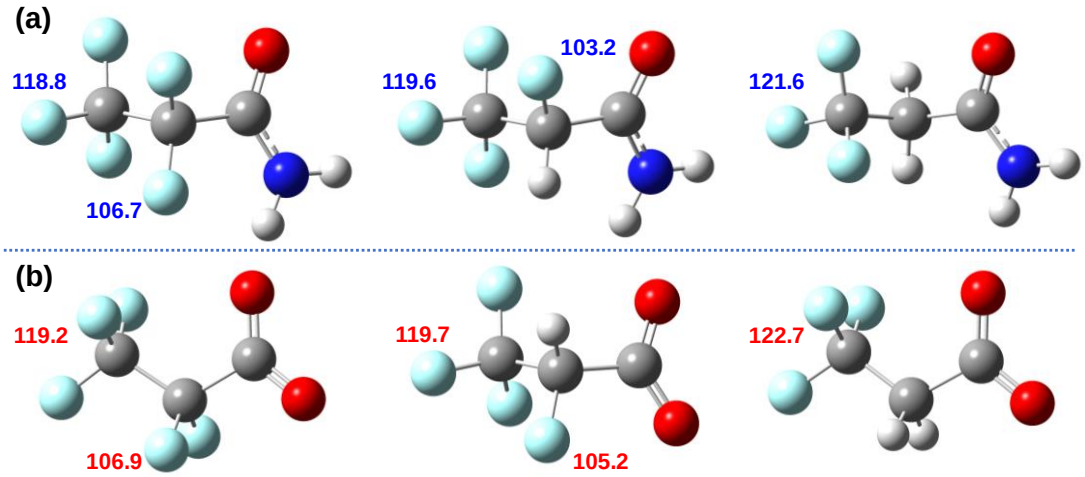

Figure D.12 Calculated C−F bond dissociation energies (kcal mol^{-1}) of CF_3−CF_2−*FG*, CF_3−CFH−*FG*, and CF_3−CH_2−*FG* for *FG* = (a) −$CONH_2$ and (b) −COO^-.

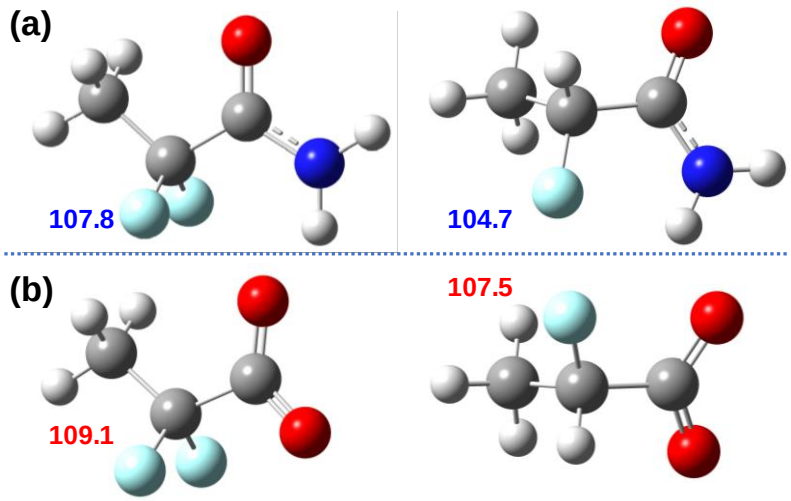

Figure D.13 Calculated C−F bond dissociation energies (kcal mol^{-1}) of CH_3−CF_2−*FG* and CH_3−CFH−*FG* for *FG* = (a) −$CONH_2$ and (b) −COO^-.

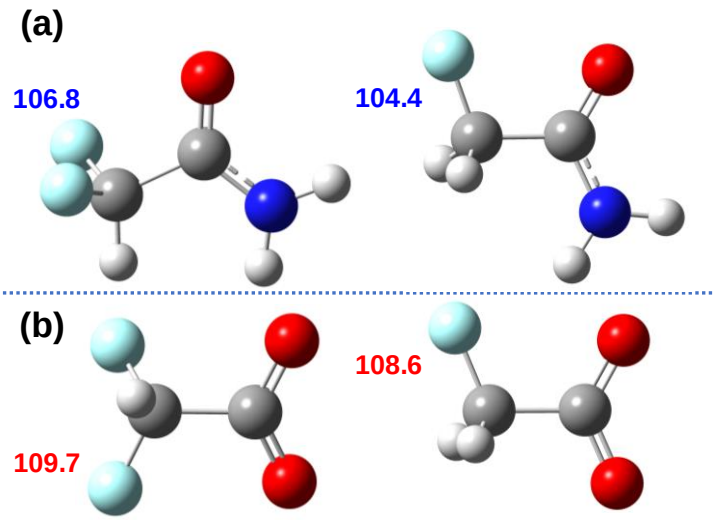

Figure D.14 Calculated C−F bond dissociation energies (kcal mol^{-1}) of H−CF_2−*FG* and H−CFH−*FG* for *FG* = (a) −$CONH_2$ and (b) −COO^-.

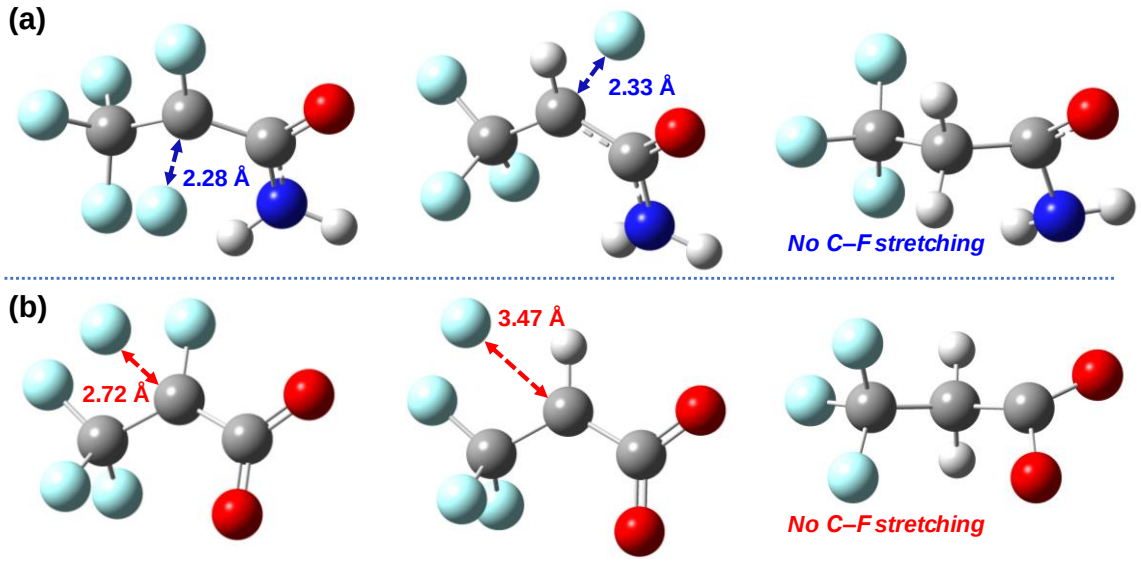

Figure D.15 Geometry−optimized structures for $[CF_3{-}CF_2{-}FG]^{\bullet-}$, $[CF_3{-}CFH{-}FG]^{\bullet-}$, and $[CF_3{-}CH_2{-}FG]^{\bullet-}$ at the B3LYP−D3(BJ)/6−311+G(2d,2p) level of theory showing C−F bond stretching, where *FG* = (a) $-CONH_2$ and (b) $-COO^-$.

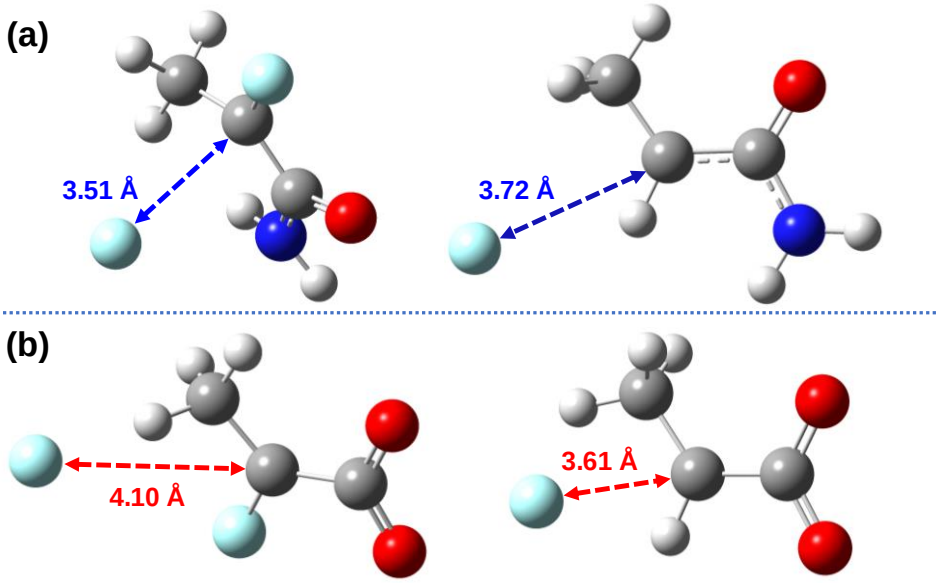

Figure D.16 Geometry−optimized structures for $[CH_3{-}CF_2{-}FG]^{\bullet-}$ and $[CH_3{-}CFH{-}FG]^{\bullet-}$ at the B3LYP−D3(BJ)/6−311+G(2d,2p) level of theory showing C−F bond stretching, where *FG* = (a) $-CONH_2$ and (b) $-COO^-$.

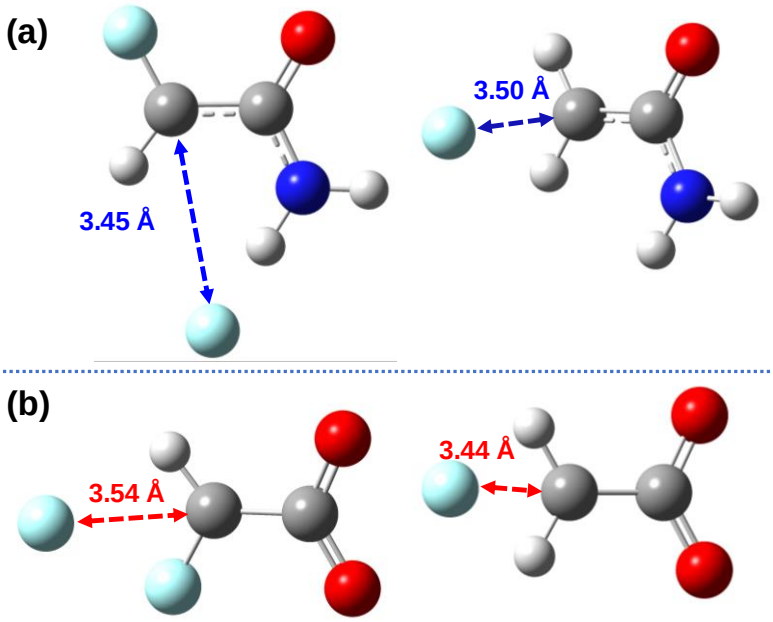

Figure D.17 Geometry−optimized structures for [H−CF_2−*FG*]$^{\bullet-}$ and [H−CFH−*FG*]$^{\bullet-}$ at the B3LYP−D3(BJ)/6−311+G(2d,2p) level of theory showing C−F bond stretching, where *FG* = (a) −$CONH_2$ and (b) −COO^-.

REFERENCES

(1) Bentel, M. J.; Yu, Y.; Xu, L.; Li, Z.; Wong, B. M.; Men, Y.; Liu, J. Defluorination of Per- and Polyfluoroalkyl Substances (PFASs) with Hydrated Electrons: Structural Dependence and Implications to PFAS Remediation and Management. *Environ. Sci. Technol.* **2019**, *53* (7), 3718–3728.

(2) Bentel, M. J.; Yu, Y.; Xu, L.; Kwon, H.; Li, Z.; Wong, B. M.; Men, Y.; Liu, J. Degradation of Perfluoroalkyl Ether Carboxylic Acids with Hydrated Electrons: Structure–Reactivity Relationships and Environmental Implications. *Environ. Sci. Technol.* **2020**, *54* (4), 2489–2499.

(3) Bentel, M. J.; Liu, Z.; Yu, Y.; Gao, J.; Men, Y.; Liu, J. Enhanced Degradation of Perfluorocarboxylic Acids (PFCAs) by UV/Sulfite Treatment: Reaction Mechanisms and System Efficiencies at PH 12. *Environ. Sci. Technol. Lett.* **2020**, *7* (5), 351–357. https://doi.org/10.1021/acs.estlett.0c00236.